Theory and Optimisation of Double Conversion Heterodyne Photoparametric Amplifier

By

Hussam Amin Alhagagi

A thesis submitted in partial fulfilment of the requirements for the degree of

Doctor of Philosophy

School of Engineering

THE UNIVERSITY OF
WARWICK

June 2012

For my Family

Table of Contents

List of Figures

List of Tables

List of Abbreviations

AC–Alternating Current

ACTS–Advanced Communications Technologies and Services

AM–Amplitude Modulation

AMPS–Advanced Mobile Phone Services

BER–Bit Error Rate

BPF–Bandpass Filter

CV–Capacitance Voltage characteristics

CNR–Carrier to Noise Ratio

DBM–Double Balanced Mixer

DC–Direct Current

DCHPPA–Double Conversion Heterodyne Photoparametric Amplifier

DR–Dynamic Range

DD/IM–Direct Detection / Intensity Modulation

EIN–Equivalent Input Noise

ETSI–European Telecommunications Standards Institute

F–Noise Factor

FOV–Field Of View

FM–Frequency Modulation

FSO–Free Space Optical

GBP–Gain Bandwidth Product

GSM–Global System for Mobile Communication

HB–Harmonic Balance

IF–Intermediate Frequency

ISDN–Integrated Service Digital Network

IV–Current Voltage characteristics

IMD–Inter Modulation Distortion

IR–Infra Red

IrDA–Infrared Data Association

ITU–International Telecommunications Union

LAN–Local Area Network

LC–BPF – Inductor Capacitance- BandPass Filter

LD–Laser Diode

LED–Light Emitter Diode

LNA–Low Noise Amplifier

LO–Local Oscillator

LOS–Line-Of-Sight

MWO–Microwave Office

NEB–Noise Equivalent Bandwidth

NF–Noise Figure

OMI–Optical Modulation Index

PA–Parametric Amplifier

PCB–Printed Circuit Board

PD–Photo Diode

PPA–PhotoParametric Amplifier

PIN–Positive Intrinsic Negative

QoS–Quality of Service

OCD–Optical Coherent Detection

OEIHD–Optical Electrical Incoherent Heterodyne Detection

OW–Optical Wireless

RF–Radio Frequency

RIN–Relative Intensity Noise

SAW–Surface Acoustic Wave

SCM–Sub Carrier Multiplex

SNR–Signal to Noise Ratio

UMTS–Universal Mobile Telecommunications System

UHF–Ultra High Frequency

VHF–Very High Frequency

WAN–Wide Area Network

WDM–Wavelength Division Multiplexing

Acknowledgments

First of all, I would like to thank God and the many people that have helped me to make this study and thesis possible. I am indebted to my supervisor, Prof. Roger J. Green, for his guidance, patience and encouragement throughout this work, without which it would not have reached this stage. It has been a privilege to work with him, and I wish to thank him with sincere gratitude. I also acknowledge the contribution of my second supervisor, Prof. Evor Hines.

I wish to express my gratitude to the Ministry of High Education in Libya for their financial support for this study. I would also like to express my thanks to all the staff of the University of Warwick who have directly or indirectly contributed to the project. Also acknowledged are the facilities of the Warwick Communication Systems Laboratory, and the technical support facilities and staff of the School of Engineering, Ian for his technical support, and my colleagues in the Communications Research Group. I would like to acknowledge the AWR Corporation, which has provided the Microwave Office simulation tools free of charge.

Last but not least, thanks go to all my family, with extra mention of my mother, my special thanks go to a remarkable wife. I could not have completed this work without her; therefore, I dedicate this work to her, and to my children.

Declaration

This thesis is submitted in partial fulfilment for the degree of Doctor of Philosophy under the regulations set out by the Graduate School at the University of Warwick. This thesis is solely composed of research completed by Hussam Alhagagi, except where stated, under the supervision of Prof. Roger Green between the dates of 2008 and 2012. No part of this work has been previously submitted to any institution for admission to a higher degree.

Hussam Alhagagi
June 2012

Abstract

An optical wireless transmission technique represents an attractive choice for many indoor and outdoors applications within fixed and mobile networks. It has the advantage of providing a wide bandwidth that is unregulated worldwide, with availability to use it in a very dense fashion, and potentially very low cost. Due to the high attenuation suffered by Infrared radiation through the air, operating low power transmission sources, and generally adverse signal to the noise environment found by ambient background light, where the optical signal is typically at it is minimum power level when detected. A high sensitivity and high selectivity receiver will be imperative for such applications as subcarrier multiplex systems, millimetre-wave radio over fibre and other wireless optical system applications.

The thesis details the research, design, and optimisation of a novel, low-noise front-end optical receiver concept using a photoparametric amplifier (PPA) technique, in which the detected optical baseband signal is electrically amplified and up-converted to upper-side frequency, based on the nonlinear characteristic of the *pin* photodiode junction; the desired signal passes through a further signal processing stage, and the original baseband signal is recovered again, using the concept of the superheterodyne principle. The designed DCHPPA receiver acts in a parallel manner to a conventional double superheterodyne detector system, but without the noise penalty normally incurred in the first stage. The PPA is used instead of a resistive/transistor based mixer at the first stage. DCHPPAs have the properties to provide very high gain, with high selectivity, combined with a very low noise operation.

The research is conducted from three aspects: theoretical analysis, modelling and simulation, and practical implementation and result analysis. The three approaches followed the same trend shown, and the results correspond closely with each other. Theoretically, a new non-degenerate PPA mode of operation is discussed, in which the applied *dc* bias to the *pin* photodetector is replaced by the applied *ac* pump signal. This is shown to be advantageous in terms of the desirable characteristics for PPA operation, leading to improved conversion efficiency and the potential for low noise operation. PPA was shown to behave more optimally with load resistance which was much lower than normally used in the common optical wireless receiver-amplifiers. A new PPA gain theory was derived and optimised accordance with the original gain theory, PPA input/output admittance power was analysed for optimum power transfer. More accurate DCHPPA circuit configurations were modelled and simulated using nonlinear simulator tools (*AWR*) which help to understand and optimise system performance, particularly device parameters and characteristics. The full DCHPPA system was implemented practically, and tested in VHF and UHF as a sequel to the simulation configuration, which subsequently exhibited a 34.9dB baseband signal over the modulated optical signal; by employing a chain gain DCHPPA cascaded configuration, 56.3 dB baseband signal gain was achieved. The PPA noise was also measured and analysed, which satisfied the tough front-end optical system requirements.

Publication Associated with this Research Work

The following conference papers have been published as a result of the work contained within this thesis.

H. A. Alhagagi, R. J. Green, "Load analysis with gain enhancement for the PhotoParametric Amplifier (PPA)," in *14*th *Anniversary International Conference on International Transparent Optical Networks, IEEE, ICTON 2012*, Warwick, U.K, July 2012.

H. A. Alhagagi, R. J. Green, M. S. Leeson, E. L. Hines, "New mode of operation of the photoparametric amplifier for automotive application," in *13*th *Anniversary International Conference on International Transparent Optical Networks, IEEE, ICTON 2011*, Stockholm, Sweden, June 2011.

R. J. Green, H. A. Alhagagi, E. L. Hines, " Double conversion heterodyne photoparametric amplifier," in *12*th *Anniversary International Conference on International Transparent Optical Networks, IEEE, ICTON 2010*, Munich, Germany, June 2010.

Chapter 1

1. Introduction

This chapter present an overview of optical wireless communication systems and describes the challenges and the key motivations of infrared communication in the design of high sensitivity front-end optical receivers. It focuses on the concept of a photo-parametric amplification techniques using up-converter optoelectronic mixing that provides low noise photo-detection, amplification and frequency conversion, with the aim of recovering the baseband electrical signal at high gain with better signal to noise performance. At the end of the chapter, the organization of the thesis is given.

1.1 Overview

In recent years, interest in optical wireless communication (OW) has increased. Since data rate has reached over 155Mbits/s when operate in a line of sight (LOS) mode [1]. The techniques and applications found within OW communication have become more advanced and interesting, and are a strong candidate for high speed indoor/outdoors optical communication [2-7]. Moreover, it has much promise as an access technology, because of offering flexibility, mobility, and cost-effectiveness [8, 9]. Recently, there has been a strong need for high bandwidth with high data rate communications (i.e. Gbits/s) particularly with the increase in demand for real-time and multimedia applications in both communication and computing. This may provide a method of achieving a high quality of service (QoS) with a larger growth in user density. Light, as a medium of communication, offers unequalled channel bandwidth, and is capable of data rates in the terabits per second range (Tbits/s) whether travelling through optical fibre, or potentially by OW.

OW communication can be classified into two main categories: visible light communication (VLC) and infra-red communication (IRC). Indoor IR optical wireless communication was first proposed in 1979 [10] and has found use in homes and offices with devices ranging from TV remote control to the Infrared Data Association (IrDA) port [11] on portable devices which are likely to proliferate in the future to become the leading serial port alternative to USB and IEEE1394 connectivity. One way of achieving high speed indoor optical communication is by using infrared radiation [7, 12] particularly at the longer NIR wavelengths (1550nm). However, operating in a near-visible IR spectral region (780nm to 850nm) principally makes use of very low cost optoelectronic components, due to the available commercial infrastructure and the availability of efficient and reliable direct semiconductor diode-based detectors at these wavelengths (i.e. silicon material). In addition to achieving comparable quantum efficiencies, particularly when operating at a

higher wavelength. Therefore, high speed and better receiver sensitivity can be achieved due to the lower energy per photon implied.

OW offers many advantages, over other RF communication networks (i.e. LAN,WAN and MANs) and can be seen as a complementary scheme to RF systems. Advantages can be summarised as follows:

- It does not require expensive licences in order to use spectrum.
- It can provide a high fibre-like bandwidth [13, 14].
- Low cost and ease of implementation, as it offers the lowest cost per bit of any other access technology (i.e. RF spectrum licenses are expensive, and there are bandwidth restrictions for unlicensed spectrum).
- Freedom from interference, particularly in indoor applications.
- Small, secure, and consume little power (i.e. very important for mobile terminal system).
- OW is able to add communication to illumination with little extra cost (i.e. send information via room illumination, traffic lights and signboards) and provide other functions that can be useful for many applications such as the last mile access, CATV, infofuelling and teleconferences (see table 1.1 for a brief comparison of RF and IR Properties).

The bandwidth of OW is about 10,000 times higher than the highest frequency used by RF technology. Also more than 1000 independent data channels can be grouped into the air on a single optical beam, using wavelength division multiplexing (WDM) and sub carrier multiplexing (SCM), thus providing a potential bandwidth ten million times that of any RF solution [15]. It also offers high data rates via low dispersion at operational wavelength[16]. Recently, fibre optic networks have become widely available to homes,

industry and commercial buildings, resulting in a real need for cost-effective indoor OW devices (i.e. like-fibre) to benefit from the high capacity provided by fibre communication (i.e. FTTH). Comparatively speaking, IR-OW systems with low implementation complexity, a license free spectrum access technique and better sensitivity/selectivity could be an attractive alternative when fibre deployment is difficult or due to the rapid deployment required to connect point-to-point FSO networks (i.e. time and cost effect). An analogue IR-OW system could be a candidate for a practical solution for millimetre wave radio over fibre and using a SCM/WDM system, which potentially could combine high bandwidth availability in optical communications, with the mobility found in RF communication systems.

Table 1.1 comparisons of RF and IR properties for wireless communication

Property	RF	IR
Spectrum license	Expensive	Free
RF interference	Yes	No
Path loss	High	High
Multi-path fading	Yes	No
Multi-path dispersion	Yes	Yes
Coverage	Medium	Low
Technology cost (Transceiver)	Variable	Potentially low
Input represent	Signal amplitude	Signal power
Mobility	Yes	Some configuration
Transmission ranges	Long range	Short range
Dominate noise	Interference	Ambient light
Wall penetration	Yes	No
Security	low	High
Bandwidth limitation	Regulatory, Radio Communication Agency RCA-UK	Photo-detector/Preamplifier, Diffuse channel

1.2 Challenge and Motivation

In spite of the advantages of IR presented in the previous section, there are some challenges in employing IR-OW systems in our daily lives. The greatest challenges in outdoor systems is atmospheric attenuation due to fog, rainfall, snow and mist, and hence

high power transmission is required. Other challenges include eye safety, particularly if a laser diode (LD) is employed indoors, so the emitted optical power has to be strictly restricted according to the Maximum Power Exposure (MPE) value limit defined by [17] to be 1 mW for a typical beam, (or 5.7 Wm^{-2}), depending on the wavelength of the light. However, light emitted diode (LED) with low power and low wavelength transmission are preferable for indoor applications. The dominating noise source in IR-OW comes from background interference sources; ambient light which is a combination of incandescent light, fluorescent light and sunlight can raise the level of photonic noise in the receiver, and hence, can impair performance with respect to signal to noise ratio (SNR). Using optical filters helps to diminish this ambient light [18]. The power spectral densities of background lights sources with the sensitivity of photodiodes (PD) are shown in figure 1.1[19].

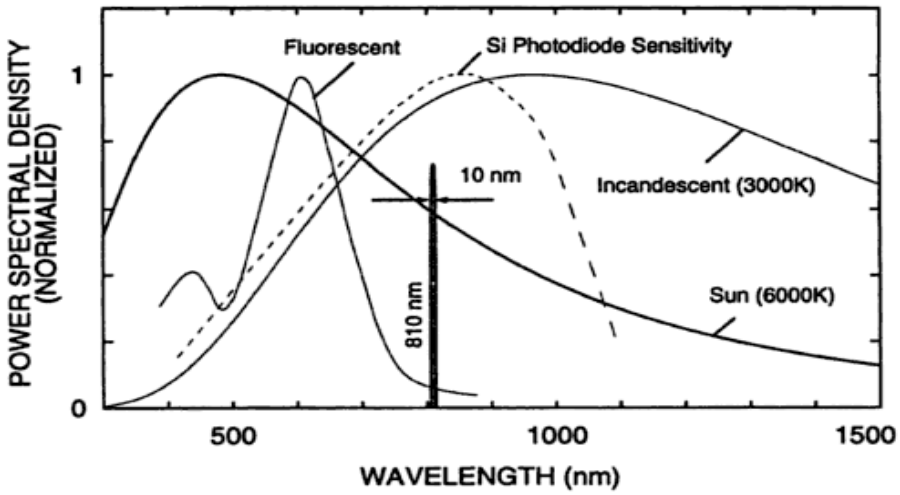

Figure 1.1 Coincidence of background radiation vs. photodiode sensitivity

Other indoor challenges are the network transmission topologies, which are classified according to the degree of directionality of the transmitter and receiver, IR links can be classified as line-of-sight (LOS) and non-line-of-sight (i.e. diffused configuration) [19, 20], each topology having advantages and disadvantages [15, 21]. The direct LOS, with careful straight alignment, can minimize the multi-path distortion, and provide better

power efficiency, as shown in figure 1.2 [22]. This is because the emitted energy is concentrated into a narrow beam (i.e. more power per unit area) and therefore, high gain can be achieved, which leads to an increase in receiver signal. In the diffused configuration approach, straight alignment is not required if a wide field of view (FOV) is provided for both transmitter and receiver. This means a large area of detection is required for the photodetector to have more power per unit area. The issue is that large capacitance is required which is not favourable for high frequency response and receiver bandwidths according to the 3dB corner frequency expression. Moreover, it presents maximum multi-path distortion that can raise inter-symbol interference (ISI) which becomes critical at higher data rates. Hence such a configuration can have low gain and poor receiver sensitivity.

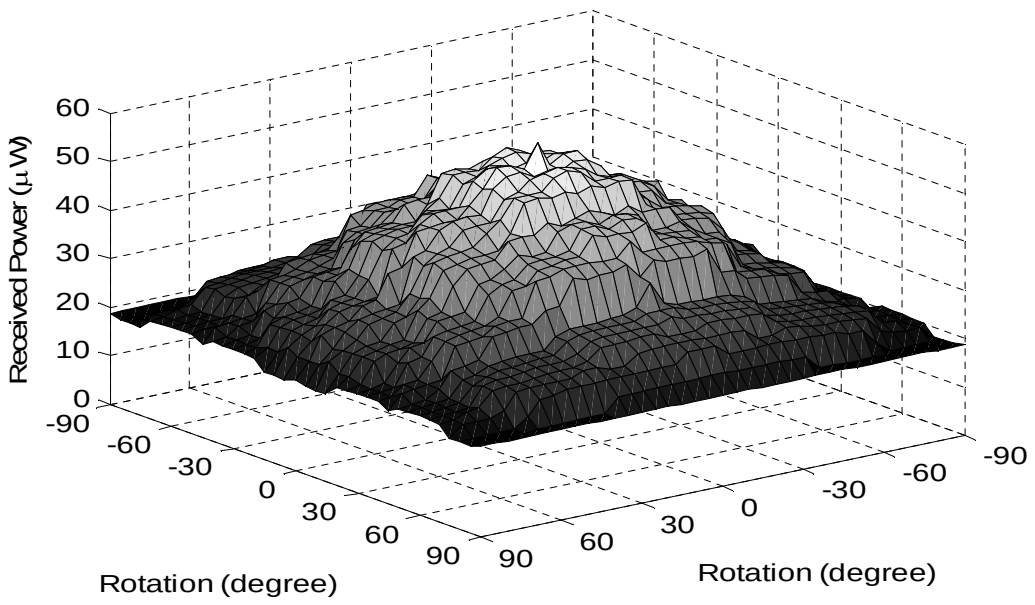

Figure 1.2 The received power within an empty environment as function of orientation

As mentioned earlier, undesired background noise sources induce noise currents (i.e. a steady state DC current). Also, due to optoelectronic conversion, additional shot noise (i.e. dark current and bias current) and other resistor thermal noise (i.e. bias, bulk

and shunt resistor) are present. These noise sources induce additional noise currents in a single photodetector receiver, which will significantly degrade receiver performance.

For all short range, indoor applications, intensity modulation direct detection (IM/DD) is the only practical transmission technique [23], and the attenuation can be low for short link transmission. Amplification of weak received signals is necessary because of several factors. Firstly, mobility implies a lack of alignment between transmitters and receivers, resulting in poor SNR. Secondly, the issues of IR handover can result in problems of signal level. Thirdly, the channel impulse response for a given source and receiver can affect signal levels and hence SNR. Fourthly, eye safety constraints restrict signal level as well. Therefore a highly sensitive receiver is required, especially if the configuration is diffuse, or quasi-diffuse, which also limits the bandwidth and therefore data rate [5].

Designing a high sensitivity receiver is a crucial component, and is not straightforward, as the issue is a matter of dealing with the conflicting requirements of gain and bandwidth. Another very important consideration is noise performance which interacts with the previous two requirements adversel; some techniques have been devoted to this issue, such as those presented for Analogue/digital systems [1, 5, 8, 24-27]. Different optical detector interface techniques are presented in different application areas, with most of them being based on photodetection devices, followed by front-end amplifiers, and consequent demodulation within the limit of the acceptable bit error rate (BER), as shown in figure 1.3. Examples of these amplifiers are: the High-impedance front-end amplifier, and the Tran-impedance front-end amplifier configuration [21, 22], as shown in figure 1.4.

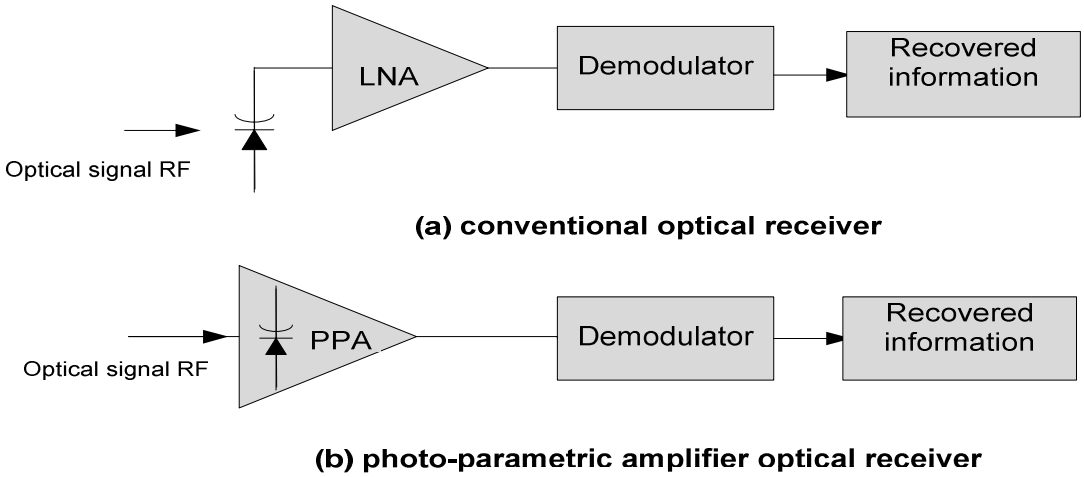

Figure 1.3 Block diagram of front-end optical receiver system

These approaches afford a good compromise between bandwidth and noise, in which bandwidth is influenced by the capacitance of the PD and the majority of noise in these amplifiers is due to the effective load resistance (i.e. the load resistance in first approach represents the input impedance of the amplifier in parallel with the bias resistor, whereas the load resistance in the second approach represents the amplifier feedback resistor); yet sensitivity improvement has led to a bandwidth trade-off.

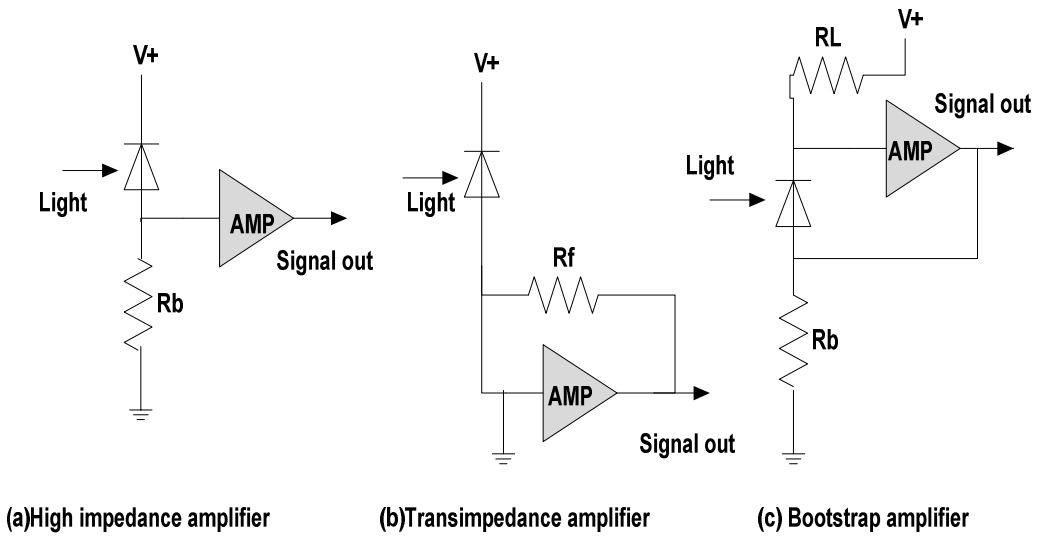

Figure 1.4 Different basic amplifiers configuration

An approach to improve interfacing effectively and maintaine bandwidth at low noise penalty is that of combining the transimpedance approach with bootstrapping amplifiers [28], the latter reduces the effective capacitance of the PD, which in turn allows a relatively high feedback impedance to be used; this can reduce noise and increase sensitivity. Measurement performance of these receivers using PIN and avalanche photodiodes (APDs) for different dimensions are presented in [5]. The APD gives a sensitivity advantage over PIN receivers [20] because it exhibit current multiplication inside the detection junction. However, it is more costly, and requires high operating voltages (typically 200-400volts) [29], and hence, is predominantly used in specialist systems where performance is key, this made them unattractive for use in terminal equipment. Where low-cost is a priority, PIN receivers are preferred which require low power to operate and more suitable for most indoor applications.

Although the above approaches can offer bandwidth and sensitivity enhancement, this is not the optimum situation for the front-end amplifier in terms of noise figure, as the total noise figure of the receiver is a consequence of the Friis formula:

$$F_r = F_1 + \frac{F_2 - 1}{G_1} + \frac{F_3 - 1}{G_1 G_2} + \text{.....} \quad . \qquad (1.1)$$

Where F_r is the overall noise figure of the receiver, F_1 is the noise figure of stage 1 (i.e. photodiode), and G_1 is the gain of stage 1, F_2 is the noise figure of stage 2 (i.e. pre-amplifier LNA) and so on as shown in figure 1.5. Ideally, of course, G_1 should be set to as high a value as possible to minimise the effect of F_2, and this therefore makes the first stage crucial. In contrast, the high gain at early stages is the better with respect to the receiver noise figure. Other important considerations in this research is to set a high G_2 which can minimise the effect of later stage as well as help to increase the overall receiver

noise figure, and hence increase the receiver's overall gain and so on. The main consideration is that the dominate noise source is receiver pre-amplifier noise.

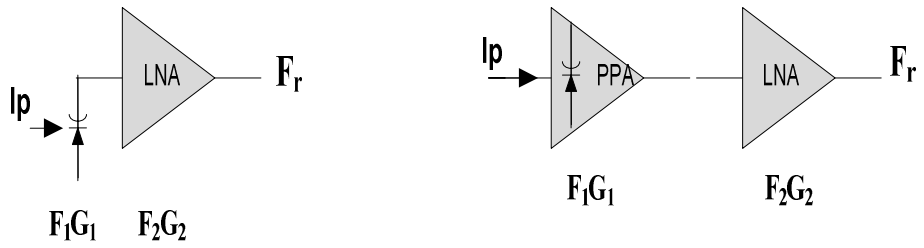

(a) Conventional optical receiver- noise figure (b) Photoparametric Amp. optical receiver- noise figure

Figure 1.5 Front-end optical receiver with noise figure

Another important issue with the front-end optical receiver design is the frequency selectivity feature, which is as important as sensitivity when considering Sub-carrier Multiplex Systems (SCM), millimetre wave radio over fibre, and other wireless optical system applications. In contrast, an optical wireless typically uses simple baseband modulation schemes that require very limited signal processing and have low latency [13]. Moreover, the ability of up/down conversion flexibility, in such a system, provides great utility to OW and FSO links that are to operate outside of any specific cyclostationary noise [10] or bandwidth constraints imposed by multi-path dispersion[30]. In other words the separation of the input and output signal can be seen as an issue for direct baseband amplification. According to the above and previous challenges, the issue is a matter of dealing with the conflicting requirements of gain, bandwidth, frequency selectivity, power effective, cost effectiveness, circuit complication, delay, signal interfacing. In addition, another very important consideration is system sensitivity (i.e. noise, SNR), which needs to interact with the previous requirements non-adversely. However, the ultimate measurement of the value of any communication system (i.e. RF or Optical) is whether it can cost

effectively transmit broadband data across the medium link with an acceptable bit error rate BER (typically taken as 10^{-9} or better) [31].

There are ways to combat the issues and the challenges been discussed above, namely to make better use of the photodetector devices at stage-1 (i.e. photodiode) if the requirements for high bandwidth are not too stringent. However, high bandwidth in analogue transmission applications is not always preferable if narrow band applications are required; this can be explained if the bandwidth of the system is much higher than the data rate. This broadening will be insignificant, but the system noise will be an issue. A concept called the photoparametric amplifier (PPA) may be employed. This configuration takes advantage of the phenomenon of parametric amplification which has been exploited in RF microwave (MW) communication systems [32, 33], but only relatively recently in optical communications as illustrated in the next chapter.

1.3 Photoparametric Amplification Approach

The term photoparametric amplifier (PPA) is used to describe a system in which photodetection, amplification, frequency changing or harmonic generation can be achieved by varying parameters within a single photodetector device. The PPA can be seen as one of the attractive approaches to achieving very low noise amplification by using a purely reactive amplifier (almost exclusively variable capacitance). In the PPA, the photodiode converts modulated optical input into a photocurrent, which is then parametrically amplified. A pump modulates the junction capacitance, producing parametric amplification at low noise. The main advantage of the PPA is that it combines optical detection with very low noise amplification; this is because a pure reactance is being used as the amplifying mechanism. Imperfections in the device, such as bulk resistance and stray capacitance, lead to non-optimal performance. Theoretically and ideally, the PPA can be considered as

having a zero dB noise figure. The unique frequency selectivity features seem to be particularly attractive for Subcarrier Multiplex Systems (SCM), millimetre wave radio over fibre, and wireless optical system applications [34]. Also, it has become much more relevant due to an increase in interest in Wavelength Division Multiplexing (WDM) and SCM, in which many forms of signals are transmitted and bandwidth can be up to a few GHz wide, since sub-carriers are independent of each other, and there is great flexibility to deliver a variety of services to the subscribers.

In the PPA, the amplification depends on pumping the nonlinear capacitance of a diode, which is similar to electrical Parametric Amplifiers (PA), with the distinction that PPAs use a photodiode instead of a varactor diode to perform photodetection and parametric amplification simultaneously. The theory of all parametric amplifiers is well established and mature [35] .The main advantage of this type of amplifier is the ultra low noise performance and the unique amplification technique that can increase the sensitivity of the receiver, with the potential to reduce the cost and the complexity of an optical receiver circuit [36] Also it can improve the performance of the system as a whole to be less noisy [37]. Although photoparametric amplification at microwave frequencies has been analysed [38] and demonstrated experimentally [39, 40], it seems to have received little attention in the literature since 1965. On the other hand, the basic technique has been applied using an optical pump (i.e. coherent amplifier) [41, 42]. This type of amplifier cannot be used in free space terrestrial links, due to cost and the polarisation issue (i.e. signal and local oscillator source (LO) need to be coplanar) [34].

The PPA with local oscillator (LO) has been shown to work in several configurations [36-40], in both non-degenerate and degenerate-mode. In non-degenerate mode, the photodiode (PD) is pumped with RF energy and a photo-detected current can be up- or down converted with an output signal at idler frequencies $\omega_i = \omega_p \pm \omega_s$. A typical PPA

configuration is shown in figure 1.6; the optoelectronic mixing occurring between the two input frequency components, one being the modulated optical signal at ω_s, and the electronic pump at ω_p , in such a nonlinear element, such that there is energy transfer from the strong pump to the output idler frequency.

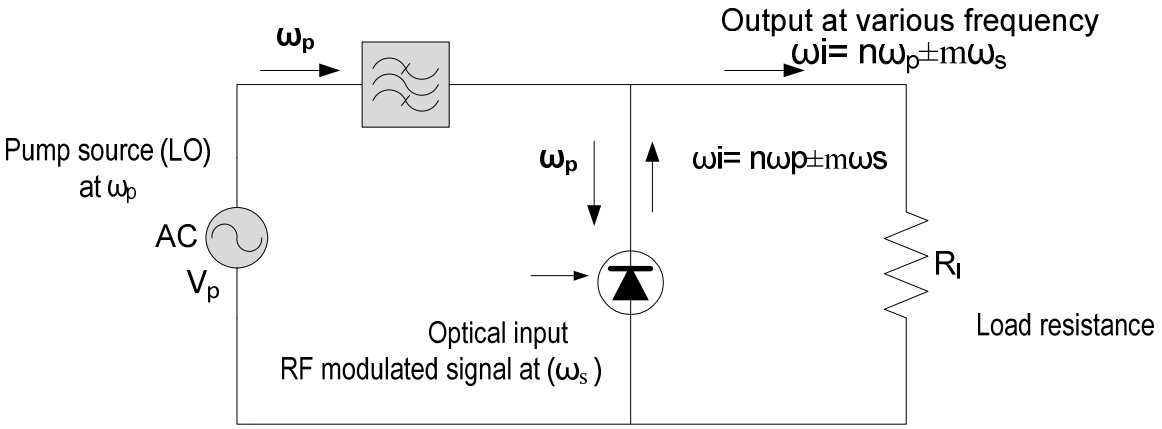

Figure 1.6 Photoparametric amplifier circuit configurations

In the degenerate mode, the PPA operates with the same input and output frequencies based on the application. However, the amplifier can be more susceptible to potential instability due to the need to operate as a negative resistance [37]. Investigative work suggests that PPAs offer potential advantages over conventional optical receivers (PD followed by preamplifier) with respect to frequency tunability [36] and noise performance [39, 43]. Moreover, it has been shown that the PPA is capable of improving sensitivity in exchange for very little penalty in terms of circuit complexity [44].

The requirement for optimum photoparametric amplification is that the photodiode should have low bulk resistance, and a high ratio of maximum to minimum capacitance at applied voltage, in order to optimise tunability. In addition, it should exhibit efficient optical detection and good responsitivity. Based on the proceeding requirements, a *pin* structure is more desirable than a *pn* photodiode. This may at first not seem appropriate, as

the CV characteristic of a *pin* diode can be less dependent on bias. Nevertheless, in reality this has not been found to be the case.

In this research, the aim of this work is to optimise the front-end optical wireless receiver concept using the photo-parametric technique in which the detected baseband signal will be up converted to upper-side frequency, and then recovered again using the concept of the super-heterodyne technique, and hence, improve sensitivity/selectivity at low cost. Ideally, this approach should provide low noise across the band to maximize the sensitivity of all the received channels and have good gain flatness across the band of each channel, which helps to preserve channel content. A new approach to the design of a front end optical receiver is based on the non-degenerate up-converter photoparametric amplification approach at the first stage, instead of a resistive/transistor based mixer. The problem of signal interfacing is avoided, and the benefit of this, optoelectronic, frequency conversion and amplification are performed in pure variable reactance impedance (i.e. less noise). The challenge to obtain high gain, a low noise figure and optimum power transfer were considered at the outset in the design of stage-1 for the front-end receiver. This is by operating the varactor PD at no external bias voltage, in which the degree of nonlinearity of CV characteristics is higher, leading to improved conversion efficiency (i.e. greater conversion gain) and the potential for low noise operation (i.e. better sensitivity); and better power efficiency (i.e. desirable for mobile devices).

In this approach, the input, as designated, is an optical signal modulated at some baseband frequency, then up-converted when detected in the PPA approach (i.e. stage1) and then passed to the intermediate frequency (IF) signal processing unit (stage-2) which help to utilise the IF signal to full advantage by boosting the selected IF signal to a useful power level and offering additional gain at low cost with the careful consideration of component choice. The output of the IF signal unit is passed along to the conventional

mixer (stage-3), using the same local oscillator as was the case for the PPA stage-1 for its local pump source, and then the output of the mixer is channelled through a low pass filter, from which the baseband modulation can be recovered intact, as shown in figure 1.7.

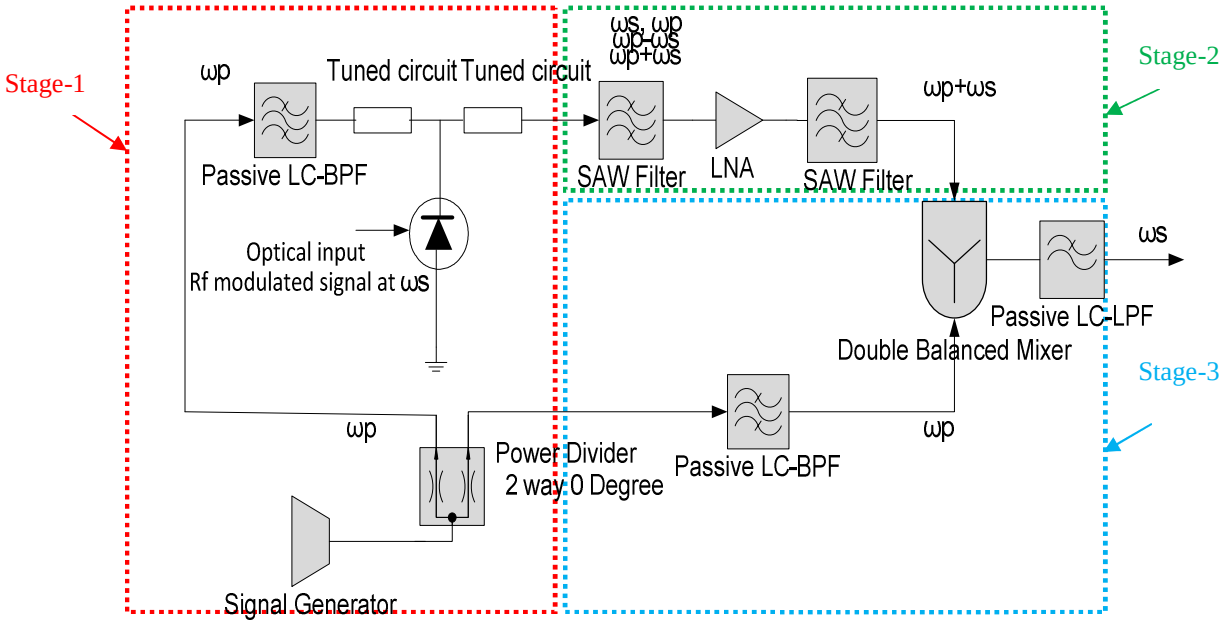

Figure 1.7 DCHPPA circuit configuration

This technique is called a double conversion super-heterodyne photo-parametric amplifier (DCHPPA); this sophisticated arrangement leads to certain matching requirements, yet a beneficial overall signal gain at low noise penalty can be achieved with a passive mixer, as found in the SCM optical front-end receiver.

This approach permits a direct detection of the DD baseband signal with more sensitivity than a basic PD detector alone or followed by pre-amplifier. This is particularly beneficial in analogue optical wireless configurations, due to the generally adverse signal to noise environment found there. Moreover, the particular merits of this approach can be quite similar to that of the superheterodyne configuration in the RF system, as it has been shown to be very useful in obtaining selectivity and sensitivity. This approach is designed

to be cost- and power effective, and has the aim of increasing the compactness and the reduction of parasitic effect that lead to economies of scale facilitating the mass production of, say, the front end optical receive at a very low price, offering substantial yet affordable benefits in access networks. The technique is thus quite versatile, offering the prospect of significant benefits to OW and FSO, and aiding their widespread implementation, as well as offering improved performance in fibre access network that can be used for optical-to-RF interface systems using RF, optical fibre and optical wireless links (i.e. fibre hub, optical fibre termination, optical wireless spot, etc) as demonstrated in [45].

1.4 Organization of the Thesis

The thesis is organized into seven chapters and two appendixes, with the following chapters are organised thus:

- Chapter 2 provides the necessary background related to this research followed by a review of a conventional PA technique. A comprehensive review of prior important work on the development of PPA is presented.
- Chapter 3 provides a new PPA mode of operation, followed by a theoretical analysis of PPA operation with respect to the amplifier gain expression, maximum input/output admittance power transfer and general load analysis.
- Chapter 4 presents a versatile model of the DCHPPA circuit, and the result obtained from employing nonlinear simulation tools that help to provide good realistic assessment and better performance optimisation.
- Chapter 5 describes in details the experimental arrangement and circuit configurations with the result obtained from the practical implementation of the system as a sequel to the simulation configuration.

- Chapter 6 presents a brief performance analysis that helps to compare the theoretical analysis results and verify them with both simulation and practical results, followed by noise analysis.
- Chapter 7 presents the conclusions of the thesis by summarizing major research achievements and making suggestion for future work.

Chapter 2

2. Background and Literature Review

This chapter presents an overview of optical communication detection techniques, and briefly describes the properties of each technique. This is followed by a review of the conventional parametric amplifier technique, with a brief discussion of the established Manley and Rowe nonlinear device theory with respect to the three and four frequency parametric amplifier. A comprehensive review of prior important work relating to the development of the photoparametric amplifier theory of operation, signal analysis and practical implementation is presented, followed by the chapter conclusion.

2.1 Background

Wireless optical communication systems have attracted many researchers since the early 1960s, when the optical communications ‘explosion’ effectively began. Recently, with the rapid development of optical systems such as radio over fibre, that operate at millimetre-wave frequencies, passive optical networks and SCM systems also seem to be potential technologies for large scale implementation. The interest in this technology has increased again, and become very important as we move towards being “always on” and “always connected”. Optical communication systems use different optical detection techniques; these techniques are used to convert the received optical signal into a signal in the electronic domain, since this is the most appropriate domain for further signal processing.

Optical detection can be classified according to two main techniques known as Direct Detection Intensity Modulation (DD/IM) and Coherent Detection (CD). In DD/IM, the term DD indicates that the receiver measures the optical power of the input signal, where ‘intensity’ refers to optical power and ‘modulation’ refers to the electro-optical conversion process. DD is easily obtained because the photodetector generates a current proportional to the received optical power, as shown in figure 2.1a. Simply put, it is a photon counting process where each detected photon may be converted into an electron-hole pair. The DD receiver responds only to fluctuations in the power in the received field, where the phase, frequency and polarization information are ignored; unless other optical signal processing elements are employed, ahead of the photodetector device, such as an interferometer or polarizers that makes the DD receiver more sensitive to the optical phase, frequency or polarization, as well as the intensity.

The Coherent Detection (CD) technique, which may potentially improve receiver sensitivity, together with wavelength selectivity, compared with the DD technique, generally limited by noise generated in the detector and pre-amplifier except at very high SNR. Optical Coherent Detection (OCD) is based on the mixing of two optical waves prior to the detecting with the implication to use a phase synchronous local oscillator, as shown in figure 2.b; the weak incoming optical signal field is mixed with the strong local laser signal (i.e. Local Oscillator LO), a third signal is generated at their frequency difference, called intermediate frequency (IF), The photodetector responds as a square-law detector for the electrical field, and generates a photocurrent; the resulting photocurrent is a replica of the original signal, which is translated up or down in frequency from the optical domain to the electrical domain for further signal processing and demodulation; this technique showed an improvement in receiver sensitivity with more than a 20dB over DD[46]. This technique was shown to work well in both free space optical communication and optical fibre communication, and provided an increase in repeater spacing, improved sensitivity/selectivity, increased the power budget and provided high transmission rates over the existing route. The theory and coherence properties of signal detection by optical mixing has been studied in detail in [47-49]; the EDFA is an example of this technique.

The Optical-Electrical Incoherent Heterodyne Detection (OEIHD) technique is based on mixing the weak optical received signal (incident field) with a strong local electrical signal (i.e. electrical local oscillator LO). This technique shares both the properties of the DD and OCD techniques; the OEIHD receiver responds only to fluctuations in the power in the received field as DD, which at the same time shares the advantages of OCD with respect to frequency mixing and power flow transfer, as shown in figure 2.1c. Photoparametric amplification is an example of this system. Although optical coherent detection (OCD) can essentially improve receiver sensitivity, its applicability in

optical wireless mobile systems is limited because of the required matching of the wavefronts of the signal and local laser [50]. Conversely, OEIHD seems to be more applicable to optical wireless communication, particularly for mobile terminal devices, as its does not suffer from the matching issue.

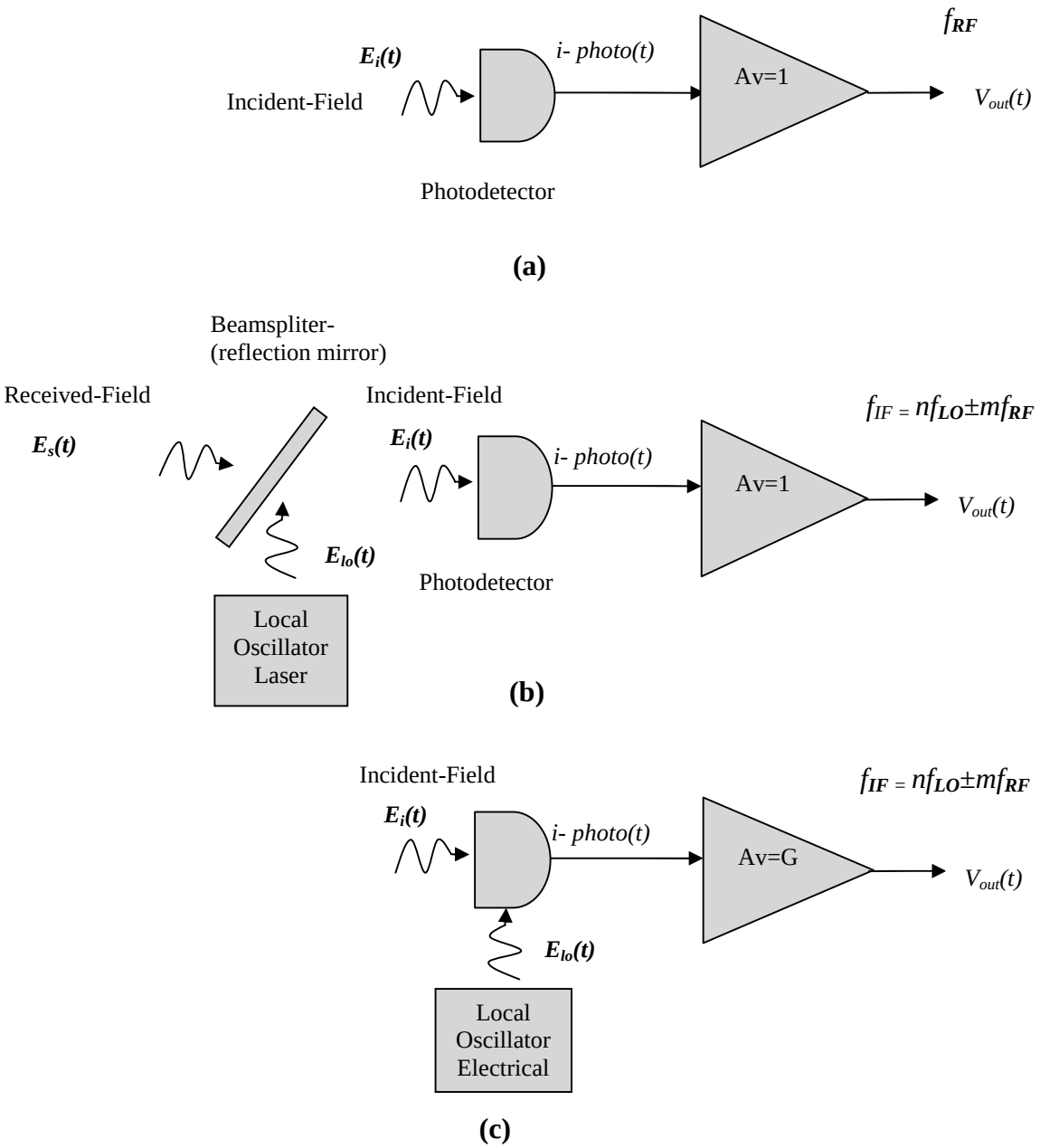

Figure 2.1 *Optical detection techniques of (a) Direct Detection (DD); (b) Optical Coherent Detection (OCD), (c) Optical/Electrical Incoherent Detection (OEIHD-PPA)*

As mentioned in the previous chapter, the photo-detectors used in optical communications that perform the best are *PIN* and *APD*. Although an electrically-pumped APD with down-conversion optoelectronic mixing was practically demonstrated in [51, 52], the main drawback in the use of an APD is the very high reverse bias needed, as it is shown to operate under 100 and 160 volts respectively (i.e. not suitable for mobile devices). Therefore, a photoparametric amplification technique (i.e. OEIHD) based on the *pn/pin* structure was chosen for further investigation.

A basic requirement in the design of a baseband optical wireless receiver is the achievement of high sensitivity/selectivity, as well as a wide-bandwidth; a parametric amplification (PA) technique was shown to work well in handling a low level received signal with minimum degradation of SNR with a substantial conversion gain and frequency conversion at the same time. A very low noise optical detection may be implemented at the same time as frequency selectivity in a single junction PD, creating a new definition known as the PPA. The concept of the PPA was inherited from the conventional electronic PA, as mentioned before; both the amplifiers can be considered to be mixers (modulators), in that the input signal causes variation in the energy flowing from the amplifier's energy source. The mixer must deliver more power to the output load than the input signal delivers to the mixer if it is to provide useful gain. Both techniques are based on *parametric* effect devices (i.e , capacitance or inductor) which use a nonlinear reactance impedance (i.e. modulator) for amplification, frequency conversion, oscillations or harmonic generation at MW frequencies [53-59]. It is necessary to review the microwave PA technique with a brief discussion of the established Manley and Rowe theory. This can help to facilitate comparisons of the PPA mechanism with the conventional PA used in microwave systems.

Considerable work has been undertaken to investigate the theory and practice of parametric amplification (PA). In particular, a definitive reference textbook was published

by Howson and Smith [32] (i.e. considered as PA “Bible”). Parametric amplification has been incorporated in many amplifier configurations, such as up-converters, down-converters, or travelling-wave PAs. These amplifiers are based on nonlinear capacitance (pure reactance), and not on nonlinear resistance, therefore avoids Johnson noise, resulting in low noise amplifiers [60]. This low noise amplification technique has been widely used as a front-end preamplifier for microwave ground receivers in the satellite link, and in many radar applications, particularly with the new improvement in varactor diode fabrication that leads to better receiver performance.

In later years, with the development of more powerful satellite transmitter and beam forming techniques, the need for ultra-low noise-cooled parametric amplifiers has diminished substantially [37]. Except in scientific and some radar applications, the demise of PA in microwave receiver systems was assisted by an improvement in low noise GaAs FET technology, such as MESFETs and HEMETs, that are adequate for these applications. The complexity of the PA configuration contrasted sharply with the simplicity of the GaAs FET approach (i.e. less complicated and required less maintenance).

In parallel with the idea of the GaAs FET technique, the application of three-terminal transistor-based preamplifiers has been adapted to low-noise optical fibre receiver amplifiers; many techniques have been developed with respect to bandwidth, gain and sensitivity as mentioned in the previous chapter. However, when large bandwidths in such applications as multiple channel television and broad-band ISDN, are considered, and also, due to increased interest in optical and broadband wireless services, BISDIN and video in demand (VOD), there is a real need for a suitable front-end receiver technique that considers both selectivity and sensitivity. In contrast, most of the existing front-end optical fibre receivers use a double-balanced heterodyne approach (as found for an SCM receiver), which exhibits a considerably large noise figure in the receiver as a whole, as the

amplification occurrs at a second stage (pre-amplifier), as well as the signal selectivity, based on the resistive/transistor based mixer (i.e. interface issues). Reverse biased *pin* PDs are mostly widely used as photo-detectors in broad-band receivers, as they reach few PF under high reverse bias, and are capable of better optical efficiency and a better frequency response; hence, it is interesting to investigate the performance of photoparametric amplification based on *pin* structures. The two main sources of noise in the OW receiver: are background noise (i.e. ambient light as in optical domain), and preamplifier noise (i.e. thermal noise as in electrical domain); hence, photoparametric amplification seems to be potentially attractive to simplify the optical front-end receiver using the parametric amplification. The next section will review the conventional parametric amplifier technique prior to the photoparametric technique.

2.2 Electronic Parametric Amplifier

The first interest in such an amplifier dates back to 1936. Hartley describes experiments in which a time-varying capacitance was used; in 1948, van der Ziel pointed out that amplification which could be achieved using an almost purely reactive element would be accompanied by low noise. Following this, a classic development of the theory of parametric amplification was undertaken by Manley and Rowe in 1956, who presented an exhaustive analysis of the mixing properties of non-linear reactance[61, 62]. Both inductive and capacitive parametric amplifiers have been investigated experimentally and theoretically, and inductive types of amplifier that employ the nonlinear properties of certain ferrites do not have low-noise properties (i.e. impractical). However, a capacitive parametric amplifier is based on nonlinear capacitance-voltage characteristics of the junction diodes (i.e. varactor diode) do have low noise properties [32].

In a conventional *ac* power amplifier no frequency translation occurs, and the power gain is achieved by conversion from *dc* power. There are other possible gain configurations, and these can be classified as: 1) *Parametric amplifier,*: if power amplification is achieved by conversion from power at independent frequency (i.e. pump frequency), with no frequency translation; 2) *frequency changer*, the output power is at a frequency that is different from the input power, such that this device produces such a modulation product, usually termed a mixer, as the output power is an upper sideband or a lower sideband; 3) *parametric converter*: in which the power amplification can be achieved by conversion from *dc* power or, alternatively, by conversion from power at an independent frequency (i.e. LO); 4) *harmonic generator*, in which the output power is at a harmonic frequency of the input signal, and is usually called a frequency-multiplier.

A classical development of the theory of parametric amplification was achieved by Manley and Rowe; the power flow derived equation can be applied to both the nonlinear capacitive and inductive energy storage system, as the reactances are characterised by their energy-storage or memory properties, and the energy for nonlinear capacitance may be defined as the area under the *v-q* curve. In referring to figure 2.2, signal energy at source frequency (ω_s) is coupled via the tuned circuit to the non-linear capacitance (i.e. varactor), which is pumped by other independent frequencies with energy at (ω_p). This pumped capacitance is assumed to be loss-free. The pump modulates the variable capacitance in such a way that the signal power is amplified by the energy transfer from the pump signal; the output signal with gained energy can be at the same frequency as the source frequency, known as degenerate mode, or the output energy can be collected from a chosen upper/down sideband known as idler frequencies (ωi), which is $\omega_i = n\omega_p \pm m\omega_s$ where m and n are any integers from zero to infinity.

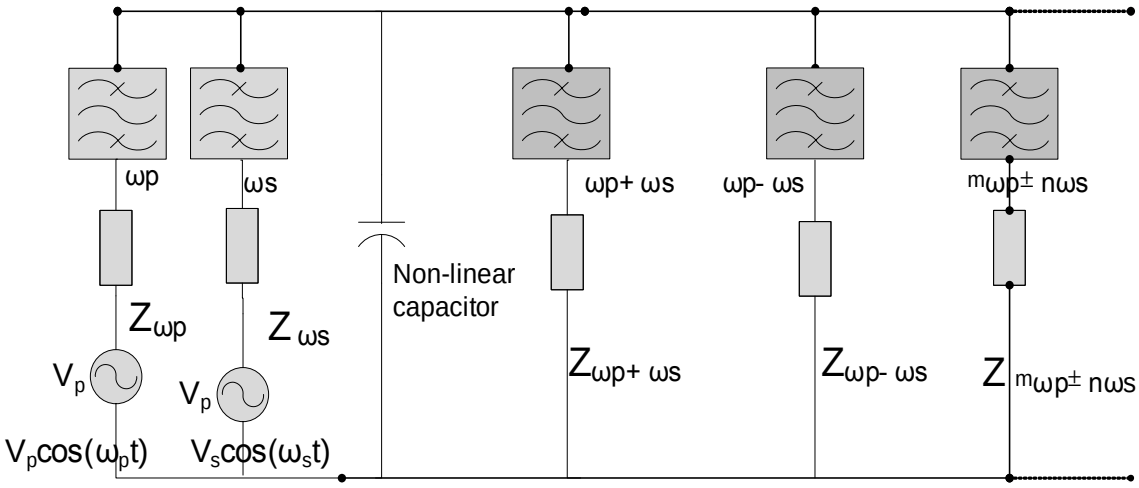

Figure 2.2 Idealized conventional parametric amplifier configuration

The general relationships developed by Manley and Rowe are based on three essential points: the reactance is an energy-storage element; the reactance is lossless; the pump frequency (ω_p) and the signal frequency (ω_s) are independent [32]. The Manley and Rowe equations to describe power flow in the circuit are:

$$\sum_{m=0}^{\infty}\sum_{n=-\infty}^{\infty}\frac{mP_{m,n}}{m\omega_s + n\omega_p} = 0 \qquad (2.1)$$

$$\sum_{n=0}^{\infty}\sum_{m=-\infty}^{\infty}\frac{nP_{m,n}}{m\omega_s + n\omega_p} = 0 \qquad (2.2)$$

$P_{m,n}$ represents the power at frequency ($m\omega_s+n\omega_p$). This derived relationship states that the total power in the amplifier circuit remains constant, and that the frequencies at which they are distributed depends on the interrelationships between frequencies that are allowed to flow by the filters.

For three frequency parametric amplifier (*i.e. parametric converter*), the above relationships can be applied to analyse three–frequencies in which ω_s, ω_p and the general idler frequency ($\omega_r=\omega_s +r\ \omega_p$) are the only frequencies at which the power flows. In this restricted case, the Manley and Rowe equations become:

$$\frac{P_{1,0}}{\omega_s} + \frac{P_{1,r}}{\omega_r} = 0 \qquad (2.3)$$

and

$$\frac{P_{0,1}}{\omega_p} + \frac{rP_{1,r}}{\omega_r} = 0 \qquad (2.4)$$

In the adopted convention, power absorbed by the nonlinear capacitance is positive, and the power given by the capacitor is negative. Operating the amplifier circuit as an upper-sideband converter, r>0 and ω_r is positive; writing equation (2.3) as:

$$\frac{P_{1,r}}{P_{1,0}} = -\frac{\omega_r}{\omega_s} \qquad (2.5)$$

The above equation shows that the power $P_{1,0}$, absorbed by the capacitor at input frequency ω_s results in power given out at frequency ω_r since $P_{1,r}$ must then be negative. Further, the power gain is equal to the ratio of output frequency to the input frequency ($Av = \omega_r / \omega_s$).

Note that the above results apply to a pumped capacitor, which is also driven by a signal source of real, finite impedance. The equivalent circuit for the three frequency parametric amplifier (the most common form) is shown in figure 2.3.

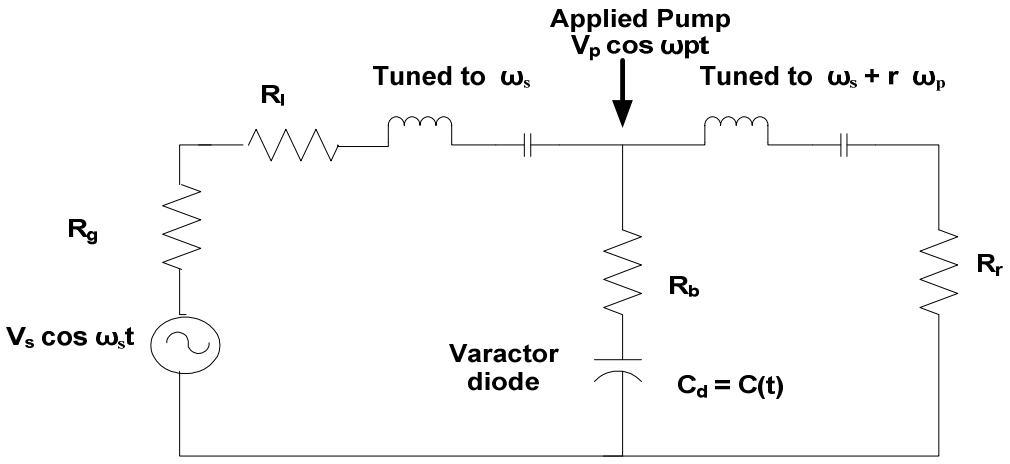

Figure 2.3 Equivalent circuit for three-frequency parametric amplifier

As seen from the above circuit, two series tuned circuits are connected to the varactor, at signal and at general idler frequencies, limiting the current flow through the varactor to

components at these frequencies. The pumped circuit is omitted for clarity. The transducer gain is given by:

$$G_T = 10\log_{10}\left(\frac{output\ power}{available\ input\ power}\right) \tag{2.6}$$

Where the available input power is taken to mean the input power if source impedance and the input impedance of the device were conjugately matched, the gain of the PA circuit configuration is given by:

$$G_T = 10\log_{10}\frac{4R_g R_L}{(Rg + R_L + R_b - R)^2} \quad [32] \tag{2.7}$$

Where

$$R = -\frac{1}{4\omega_g \omega_r C_r^2 (R_r + R_b)} \tag{2.8}$$

The three-frequency up-converter has few of the disadvantages of the negative-resistance amplifier (i.e. susceptible to potential instability), has been little used. ; For high gain, the frequency ratio must be large [32]. To circumvent some of the disadvantages of three-frequency devices that have been outlined, a complex device was proposed, named as a four frequency device, in which there is pump frequency (ω_p), signal frequency (ω_s), idler frequency ($\omega_p + \omega_s$) and an additional second idler frequency ($\omega_p - \omega_s$). The power relation is given by:

$$\frac{P_{1,1}}{P_{1,0}} = \frac{\omega_s + \omega_p}{\omega_s} \tag{2.9}$$

Hence, very large gain can be obtained by operating this device as an up converter, without the need for negative input resistance, if it is possible to match the variable capacitance into the associated input and output circuit [63].

According to the above parametric amplifier (PA) analysis, it may be seen that a problem now occurs in the employment of this well-established theory in the case of the photoparametric amplifier, as the PPA, by comparison, has no direct electronic coupling

between the input path and load circuit, as the input is optically coupled, and this does not lend itself to the PA approach outlined above, and particularly to the equivalent term to source impedance (*Rg*) is an infinite resistance, which would imply a G_T (equation 2.7) found in PA. Therefore Manely and Rowe's expressions do not seem to be readily applicable. However, Khanifar and Green have reported a different approach [40] to deriving the gain equations that allow the signal energy to be externally coupled by the incident light directly into the varactor-PD, as discussed in next section.

2.3 Photoparametric Amplifiers Review

The use of photodiodes for photoparametric operation was first predicted by Ahlstrom et al in 1959 [64], and was first demonstrated by Saito and his co-workers in 1962 [65]. Shortly thereafter, Sawyer reported the successful operation of a negative resistance photoparametric amplifier in 1963 [66] and showed an anticipated increase in detectivity using the parametric operation. He also advised that the diode be cooled to reduce the internal thermally generated noise sources, so as to allow the signal to be greater than the background noise, and hence achieve a better SNR. Shortly after, the noise performance of photodiodes in parametric amplifiers was analysed by Garbrecht and Heinlein in 1964 [67]. Their analysis showed that the PPA arrangement has a poorer sensitivity than a photodiode followed by separate pre-amplifier. Their analysis stated that the shot noise at idler frequency is additionally transformed into the signal circuit, which increases the total noise power and hence degrades the SNR of the parametric receiver, whereas the contribution of the shot noise to the SNR is always less in case of a PD followed by a pre-amplifier.

A detailed analysis of the noise performance of the photoparametric amplifier was then carried out separately by Saito and Fujii in 1964 [43], and Penfield and Sawyer in

1965 [38]. Their analysis corrected the concept finding on [67] with respect to the PPA's poor sensitivity as compared to PD, followed by pre-amplifier, in different ways. First, the authors used an insufficient equivalent circuit of the PD when the pumping voltage was applied; and the proper design of photodetector should maximise the SNR at the signal frequency. They also made an incorrect Thevenin transformation by failing to take into account that the nonlinear capacitance involved is time varying. Second, the shot noise at the signal frequency for most microwave PDs is smaller than the thermal noise, and hence, the shot noise at idler frequency can be properly neglected. The choice of fairly small values for (ω_s/ω_i) to reduce SNR degradation from series resistance (r_s) will cause a large reduction in shot noise at the idler frequency. Furthermore, the maximisation of the SNR is performed by selecting an optimum depletion field width to minimize the combination of the effect of the junction capacitance and transit-time signal reduction. Also, by employing the PD followed by the varactor parametric amplifier, as shown in [38], the principle noise limitation on both PD and the varactor parametric amplifier is the parasitic series resistance of the diodes, and if both operations took place in a single junction, the noise would be reduced, because the signal would not have to travel through both series resistances to get from the detector to the parametric amplifier. Their analysis shows that the best SNR is obtained from PPA rather than from a PD followed by separated PA. Moreover, the gain and noise properties of the photoparametric diode are expressed in terms of the gain and noise of a hypothetical amplifier coupled with a simple non-parametric photodiode. One advantage of operation as PPA is that a circulator is not needed, and it is not necessary to pump the diode hard to get gain.

In contrast, Penfield and Sawyer predicted that if high-Q photodiodes (i.e. figures of merit) are employed, the photoparametric amplifier should provide an amplified output with an SNR of nearly equal to that of the un-amplified output of the same photodiode.

This prediction was experimentally confirmed in 1966 by Grace and Sawyer [68], who utilised a specially fabricated silicon (Si) device with a *p-v-n-n*$^{+}$ construction design for excellent photo detection properties, but also retained a high Q for (a) good parametric operation; their measurement involved a degenerate mode of operation at UHF (i.e. 690MHz) for the case of (ω_s/ω_i=1) and confirms the low-noise features predicted. The measured noise figure (F_t) of the whole receiver was 13.5dB, and the computed value of the noise figure (F_{ppa}) of the PPA was 3.4 dB. The value agrees, within experimental error, with the 3.0 dB value calculated in [38]. A more specific object is to provide a photoparametric amplifier semiconductor device, in which amplification is achieved without any degradation of photodetection capability.

In 1964, Roulston [69] made a similar theoretical analysis for the Photoparametric up converter and the PD, followed by a parametric amplifier, with respect to SNR, the performance being comparable to typical photomultipliers (efficiency of a few per cent) are obtainable, and the sensitivity of the PD relatively to the photomultiplier is improved if compared on the basis of SNR greater than unity. Also shown in photo-parametric up-converter circuit analysis, if the shot noise contribution is less than 10^{-8}A, it introduces negligible noise. In addition, the reverse current must be reduced to 10^{-10}A, otherwise slight cooling is required.

Roulston again reported a similar analysis for the photoparametric up-converter system in 1968 [39], which consisted of a single triplate line with one coaxial output connected to a circulator, through which the pump is applied, as this can provides a convenient method for applying the pump to the diode and extracting the up converted signal, while at the same time isolating the load from the up-converter. The output was fed to a classic mixer via a suitable attenuator and phase adjusted, and the output from the mixer was then at the original baseband. Experimentally, the light was modulated from a

few hertz to an upper limit of about 10MHz (i.e. the determined bandwidth of the triplate circuit). The results were compared with other optical detectors which can be summarised as follows: the photoparametric up-converter is a potentially useful system for optical communications, and can give results that are superior to those of a photomultiplier. Furthermore, the system is optimum from the point of view of SNR for a given optical power and signal bandwidth. Moreover, in terms of the practical value of SNR, e.g., as required for communication system with a threshold of 12dB, the up-converter would be about six times better than a photomultiplier. The sensitivity factor, F, was measured in two bands (i.e. IF bandwidth), 1 MHz and 7MHz, with results of $1.3*10^{-3}$ and $4.4*10^{-4}$ respectively. The junction which can be used for optimum photo parametric amplification should have values of 1-pF capacitance and 7-ohm series resistance. The author did not clearly define or measure conversion gain in his analysis.

Other theoretical analyses were reported by Tandon and Roulston [70] in 1973, who compared the performance of the APD and the photoparametric up-converter (PPUC) with respect to SNR. The APD and PPUC were compared for modulation frequency below the diode transit-time cut-off frequency. The PPUC results in an SNR that is better than the SNR of an APD at low bandwidth (i.e. 1MHz); it also shows lower noise equivalent power (NEP) for 1 MHz bandwidth, but for 100 MHz, the APD has lower NEP and better SNR. Furthermore, additional analysis was carried out to analyse the effect of base parameters on SNR in silicon P^+-N-N^+ PPUC diodes [71]. It was found that the choice of base region parameters resulting in the maximum SNR showed that, for small bandwidths, the shot noise dominates and results in the best SNR. For thermal noise limited case, the optimum base parameters were found for different wavelengths of incident radiation and for large bandwidths, and that thermal noise limits the value of SNR. A similar result was reported by Roulston in [72], who compared the avalanche photodiode

systems (APD) and a photo-detector system consisting of *pin* photodiodes, followed by a base-band parametric up-converter. The overall noise performance was shown to be potentially better than that of existing APD at a bandwidth of less than or equal to 100 MHz, and the NEP is much lower, but at a bandwidth of over 100 MHz, APD starts to perform better.

Mears and Bachman [73] presented a theoretical and comparison study for low noise amplification for wide-band optical and IR heterodyne receivers, based on two detection methods, a pre-amplifier and PPA. They showed that the preamplifier technique only satisfied the noise performance or bandwidth performance, but not both. However, low noise and low bandwidth were easily achievable using the PPA, but a wide-bandwidth is harder to achieve. A similar noise analysis was reported by Korneichuk [74], who showed numerically that the sensitivity in the PPA is much better for an APD receiver for bands of up to 320MHZ, but for very broad pass bands (i.e. >100MHz), an APD is better.

Most of the research works listed above were undertaken in an attempt to evaluate the potential of such photoparametric receivers, compared with widely accepted techniques at both UHF and MW frequencies, where a photodetector or an APD is followed by a separate low noise amplifier. It seems that the PPA has received little attention since the 1960s, and, by and large, the *pin*-FET structure has been favoured for receiver implementation in optical communication applications. As mentioned earlier, the recent interest in optical and broadband wireless services, such as SCM and WDM, has renewed interest in the simplification of receiver systems, as the sub-carriers are independent of each other. This provides flexibility for configuring the system to deliver a variety of services [75].

Khanifar and Green renewed interest in the photo parametric low noise amplification PPA in 1992 by publishing a number of papers including theoretical analysis, findings and experiments involving the PPA. Their small signal time-varying analysis [40, 76] showed that the gain for non degenerate mode is proportional to the ratio of an upper side band to the signal frequency (ω_i/ω_s), which is consistent with the Manley and Rowe, by introducing a new correction factor called (β), added to the conventional gain equation. This correction factor is related to the device structure and the operating point, and β is derived from the pump voltage (V_p), built in potential voltage (V_x) and applied bias voltage (V_b). The practical system operates with high frequency, which requires a MW structure. A circulator was used to pump the PD (ω_p=930MHz) and extracted the upper side frequency (ω_i= 933MHz), as shown in figure 2.4 [40]. The investigation resulted in an 11dB up converter gain over the baseband signal received from the commercial laser diode. They reported further practical work using a waveguide setup at X-band (i.e. 8GHz). The circuit was operated under non optimum conditions (i.e. noisy pump). 0.1MHz and 7.998GHz frequencies are used for signal frequency and pump frequency respectively, the practical measurement demonstrated a 22dB up converter gain and a 9dB signal to noise improvement. Further more, they reported a direct baseband circuit layout, the upper and lower side-bands (idlers) generated across the junction were short circuited and phase adjusted to be reflected back; the sidebands across the diode were parametrically down converted to the baseband, giving their energy to a baseband signal.

Khanifar et al [36] reported results achieved by operating the PPA in the degenerate mode; the practical measurement was based on a fabricated semi-insulating GaAs *pn* and *pin* junctions, which indicated that the amplifier gain improvement was observed in comparison to a commercial junction device, but the quantum efficiency appears to be somewhat lower than that of the commercial diodes. They also stated that amplification in

the degenerate mode is possible, but at the expense of bandwidth, and the stability of amplifier has to be ensured. Also, a *pn* junction, with a hyper-abrupt impurity profile, had the best *CV* characteristics for the purposes of parametric amplification, but did not show their comparison results, nor the obtained amplifier gain.

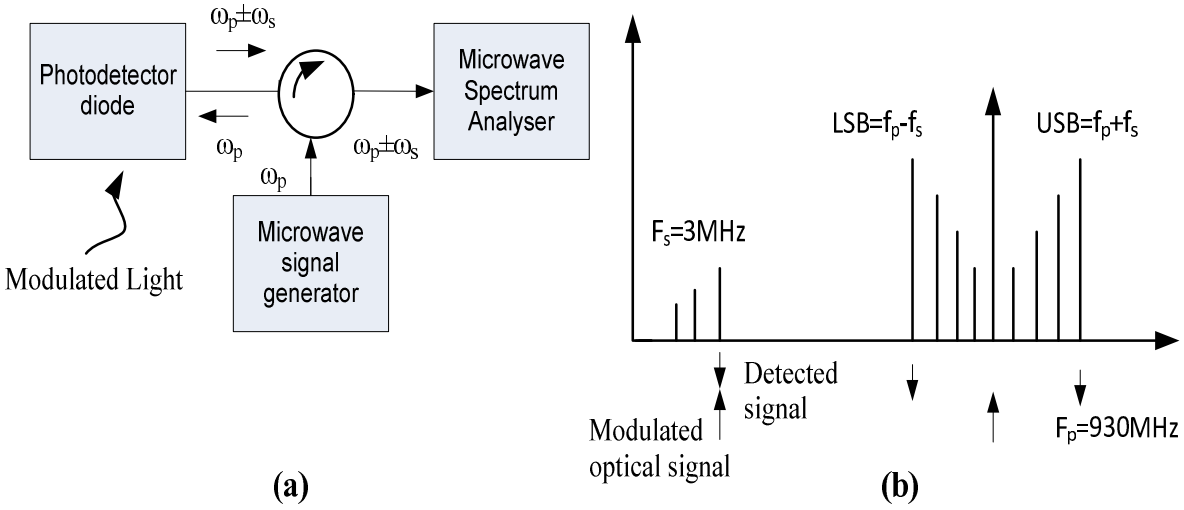

Figure 2.4(a) the experimental setup and (b) the spectrum of signals across the PD

However, the measured results using the fabricated *pn* diodes in direct detection and up-conversion mode were indicated in [77]. The experimental amplifier circuit consists of a bias-tee to supply the bias voltage and a three-stub tuner, used as a convenient method to pump the junction and extract the output signal at idler frequencies. The configuration was successfully tested using an optical fibre link. The experiment was conducted in the MW frequency range, and the optical signal was modulated at 5 MHz (ω_s). 900MHz (ω_P) was used as a pump frequency; the PPA up-converter circuit exhibited 16.55db gain at a frequency of 905MHz (ω_{p+s}). Their work was also carried out to measure the performance of the amplifier in down conversion mode, where ω_P was set to 1890MHz and ω_s to 990MHz. The down conversion gain measured at 900MHz was somewhat lower than the

theoretically predicted value from numerical analysis (i.e. almost less that 1 dB conversion gain) and the issue was related to the experiment setup.

Green and Khanifar [78] examined the PD junction structure for parametric amplification, their experiment being based on the fabricated junction found in [77]. The designed PD aimed to be more suitable for a photo parametric mode of operation with good optical conversion efficiency and high nonlinear capacitance-voltage (cv) dependence. It exhibited nearly a 10 times lower optical conversion efficiency than the commercial junction, but in terms of up conversion, photo parametric amplification outperforms it. For up conversion from 10 MHz to 1 GHz, the designed junction offered 17dB of gain, in comparison to 12dB of gain by the commercial junction diode. Their analysis in [79] estimated that a variation of the nonlinear capacitance C_{max}/C_{min} of greater than 10 is needed for efficient parametric operation. Also, it was reported that the PPA offers better noise performance than direct detection. Their most recent work was published in 1999 [37], in which they presented a simulation and practical measurement that helped to investigates the performance of various modes of operation (up converted and down converter). Their numerical analysis was based on HP simulator MDS, which exhibited a power gain of 17 db in a degenerated mode over a bandwidth of 25MHz, with a 1.1dB noise figure (i.e. 5 ohms series resistance) being predicted as reported in [79]. However, very low power gain was achieved in the practical configuration, which verified their results reported in[77]. There was an observable difference between theory and practice, due to using a different applied frequency and circuit entities in each case.

Idrus and Green have undertaken the most recent investigation of the PPA [80-83]. Their work includes the modelling and practical implementation of the PPA. Their noise analysis shows that, by taking a typical PPA gain of 20dB, and both the series and load resistances to be 50 ohms; the PPA noise factor (F) will be 1.05dB, so that, the PPA thus

does not change the SNR very much if the gain is A>1. If the gain is unity, the PPA only acts as a zero loss mixer, resulting in F=3 to the system. They carried out a measurement of the performance of the amplifier in the up-converter mode. Experimentally, the amplifier was configured to detect a laser optical signal via a *pn* junction, and the source signal (ω_s) was modulated at 1MHz. A pump frequency (ω_p) of 89MHz was used, with the designed up converter circuit offering 7dB gain at a frequency of 90MHz (ω_{p+s}). The Amplifier heterodyne circuit consisted of a commercial crystal filter, connected to the *pn* PD, through which the pump was applied. An output crystal filter was used to extract the up converted signal. The output was fed to the active mixer via a suitable attenuator and phase adjusted, and the output from the mixer was then at the original baseband. Although the system resulted in a 7.4dB gain over the original baseband, the amplifier circuit configuration seemed to have many drawbacks, such as the fact that the crystal filters being used did not provide any isolation; second, the crystal filter had a maximum input power level of 0 dBm. Hence, any pump signal over 0dBm lead to unstable conditions for both input and output crystal filters; third, an active mixer required low oscillator input power and additional dc power supply; fourth, the system did not provide any isolation to prevent the returned back signal from the active mixer, as the PPA was very susceptible to any other non-required signal that may be involved in optoelectronic mixing. The PPA is also susceptible to any shunted reactance impedance, and therefore isolation is essential for low signal parametric amplification.

A further literature review on the simulation and modelling of photoparametric amplifiers will be presented in chapter 4, which helps to give a more complete picture of the main advantages and drawbacks of each reported work.

2.4 Summary

It may be summarised that there is much scope for further research on device and amplifier circuit optimisation, and this is expected to enhance the performance of the amplifier. The OEIHD technique is more suitable for optical wireless communications. Thus far, most of the reviewed work did not consider the figure of merit of the varactor photodiode with respect to its nonlinearity characteristics and its the operational range under the parametric amplification concept (i.e. the PD operates in conductive mode, and has biased in the range of -0.5 to -10 Volts). Most of the experimental and simulation works reported were based on a photodetector with a *pn* junction structure, as it was found to be more suitable for parametric amplification, as it performed much better than the *pin* structure, whereas the latter can be almost constant with bias-voltage variation, due to the large intrinsic layer. However, the reversed *pin* photo detectors are shown to perform well in broad-band receivers which, open up the possibility of further investigation into the employment of this structure for photo parametric amplifications. Reported test-bed works were only demonstrated which were based on a laser wireless transmission link or optical fibre link. Furthermore, there are some parameters, as well as the amplifier circuit configuration, that must be taken into account to develop a more accurate gain formula. The gain equation, founded by Green and Khanifar, needs further investigation and optimisation. Furthermore, according to the PPA review, there is no work that considers the input/output admittance power analysis of the amplifier, nor the analysis of the PPA general load impedance, and the optimisation of the receiver with respect to power efficiency and cost-effectiveness are neglected in most of the reported works. Therefore, the next chapters cover the PPA input/output admittance power analysis, general load analysis and receiver optimisation with respect to power efficiency and cost-effectiveness.

Chapter 3

3. Photoparametric Mode of Operation and Further Theoretical Analysis

The main concern in this chapter is to provide a further theoretical analysis for the photo parametric amplifier operation, particularly in a non degenerate mode of operation. A new PPA mode of operation is presented in which the applied *dc* bias to the photo detector is minimised to maximise the sensitivity for such an application. Input and output power admittance is analysed in which optimal power transfer can be achieved by matching the input pump signal and the nonlinear reactance impedance itself, and between the reactance impedance and the output load impedance that lead to potentially better conversion gain. A new estimated gain expression has been derived, which provides more accurate gain theory analysis with respect to PPA circuit configuration, photo detector characteristics and applied pump signal. PPA load impedance has been analysed, which leads to maximising the PPA output signal at load impedance.

3.1 Photoparametric Mode of Operation

The photodiode may operate with or without an external applied voltage depending on the application; these modes are referred to as photoconductive (reverse biased) and photovoltaic (unbiased) modes. In the photoconductive mode, the PD is often a reversed bias with a *dc* source, which can greatly improve the speed of response, optical detection efficiency and the linearity of the PD. This is due to an increase in the depletion region and consequently, decreases the junction capacitance and reduces the rise time, while operating in high reverse bias has the accompanying disadvantage of increasing both the dark and noise currents (reverse bias leakage current and thermal noise due to bulk and bias resistors), thereby reducing the SNR. In the photovoltaic mode, the generated photocurrent flows through the shunt resistor, causing a voltage across the diode. This voltage opposes the band gap potential of the photodiode junction, forward biasing it. The photovoltaic mode of operation is preferred when a PD is used at low frequencies and low light levels, particularly when employing a *pn* junction; however using a *pin* photodiode junction with an insulating layer makes the depletion region much wider, which has several advantages over a regular *pn* junction, such as reduction in junction capacitance, increase in frequency response, and optical conversion efficiency.

However, in this approach the concern is mainly with the nonlinearity utilization of the junction which is beneficial for parametric amplification. In this mode of operation, the *ac* pump signal (ω_p) is used to modulate the junction capacitance of the photodiode at equilibrium conditions (i.e. zero *dc* bias), where the *CV* characteristics are highly nonlinear and can lead to optimal performance with respect to frequency and gain conversion. In this mode, the LO will bias the junction capacitance, which has nonlinear charge-voltage characteristics due to voltage-dependent capacitance, and the junction capacitance varies with the applied voltage according to equation (3.1). It would be desirable to have good

tunability, which is the ratio of (C_{max}/C_{min}), to be as high as possible, in order to have optimal parametric amplification. Although this is no longer strictly accurate, as we shall see later in chapter 4 and 5, it is nevertheless desirable to have greater capacitance change for the given applied voltage (v_a) changes across junction PD (Gain A α dc/dv_a). Moreover, the pump frequency should be much higher than optical modulation frequency ($\omega_p >> \omega_s$) according to the PPA gain definition reported in [40]. In addition, the parasitic series resistance (r_s) should be smaller, so it can limit its noise figure contribution within the PPA, and also minimise the voltage drop it produces, so as to maximise the voltage across the capacitance and the voltage variations across it (r_s *is series with* c_j). In addition, the input/output admittance power must be considered as shown in the next section, which aims to provide optimum power transfer. An equivalent circuit for a non-degenerate mode (up-converter PPA) at equilibrium mode is shown in figure 3.1.

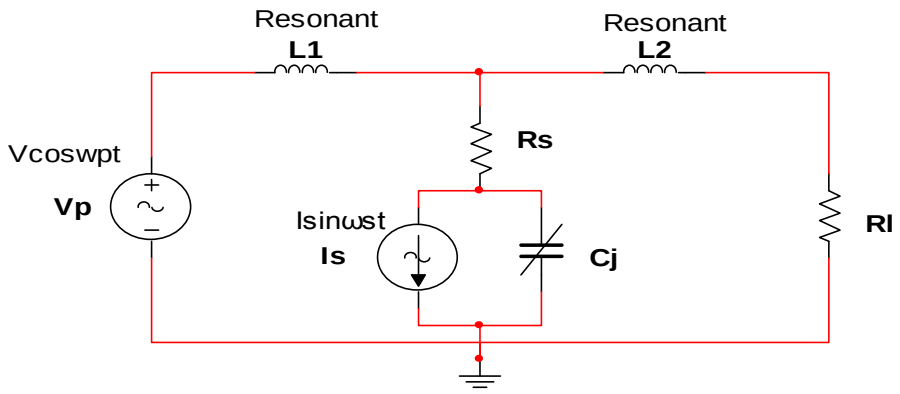

Figure 3.1 PPA up-converter equivalent circuit

There are many advantages to be gained by pumping the junction diode at zero *dc* bias in such a receiver, for example: 1) the junction capacitance is highly nonlinear at zero dc bias mode, as shown in figure 3.2 and the ratio of dc/dv_a can be as high as possible, which is more desirable for parametric amplification; 2) moreover, there is a smaller shot noise due to the low dark current under equilibrium conditions; 3) there is no reverse bias

leakage current; 4) better thermal noise due to no bias resistor. On the other hand, too much pump power can cause the forward current to flow through the PD and increase noise. The aim of this approach is to achieve high conversion gain in an up-converter stage, and then any recovery technique can be used to recover the baseband components at source frequency (ω_s), *Photodiode parameters (m=0.45, Rs=6.5, Cj=72pF, Vx=0.554).*

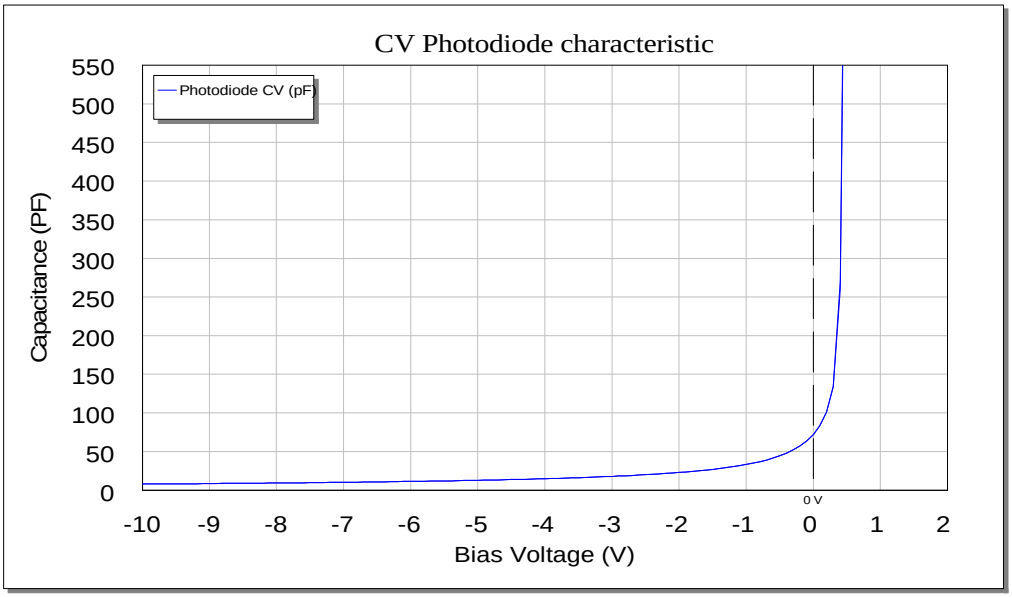

Figure 3.2 Measured photodiode characteristics CV relationship

The PPA operation in non degenerated mode can be illustrated in figure 3.3. The *ac* pump signal (ω_p) serves to modulate the PD variable capacitance in such way that the optical received signal at source frequency (ω_s) is amplified by energy transfer from the large pump signal resulting in Idler frequencies ($\omega_i=\omega_p\pm\omega_s$) with parametric amplification. The PD is mainly biased by the *ac* pump source (i.e. sinewave signal) which sweeps the junction in both photo-conductive (i.e –V, reverse bias) and photovoltaic modes (i.e +V, forward mode), where the *CV* characteristics are shown to be highly nonlinear and the capacitance variation can be driven to a maximum and minimum value of capacitance, according to the pump signal (i.e. C_{max} and C_{min}), as shown in the following graph.

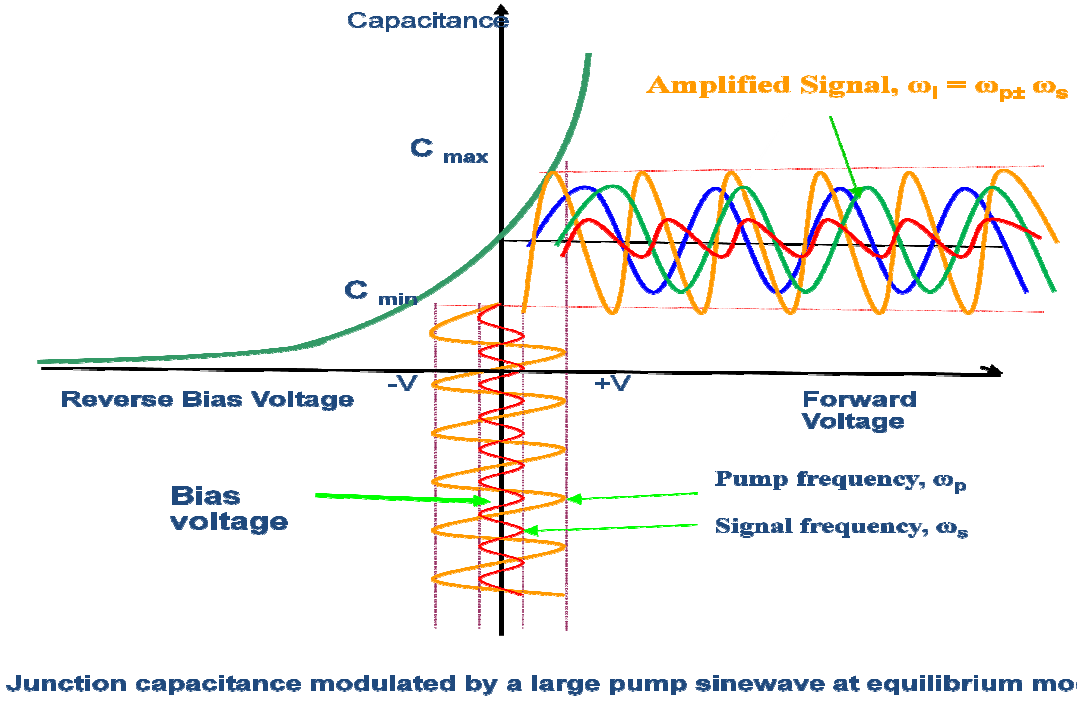

Figure 3.3 PPA junction operation at equilibrium mode

3.1.1 Principle of Operation and Consideration

One of the main considerations for optimal power transfer for the PPA is to study both input and output power admittance. Optimum reactance power transfer will thus require source and load impedance to match with the time varying capacitance. Hence, the input and output admittance should be proportional to the mean value of the variable capacitance (C_{mean}); conversely, the author in [84] states that the input and output admittance should be proportional to the minimum value of the capacitance (C_{min}). In this approach a simple series inductive reactance circuit was used to match both the input and output of the photodiode, as shown in figure 3.1. These reactance circuits (inductors) aim to deliver maximum power from the *ac* pump source to the variable junction at pump frequency (ω_p), where the output inductive reactance circuit aims to dissipate and withdraw as much reactive power to the load impedance at the idler frequency ($\omega_p+\omega_s$). By using

equal and opposite phase angles, the two parts of the circuit are brought into resonance to ensure maximum transfer power ($X_L = -X_{Cmean}$), as shown in figure 3.1. $X_{L1}=2\pi f_p L_1$ and $X_{L2}=2\pi f_{p+s} L_2$. The mean value of *pn* junction capacitance (C_{mean}) can be calculated as follows: The capacitance versus applied voltage is, by definition, the change in charge for a change in applied voltage:

$$C_j = \left| \frac{dQ}{d(V_x - V_a)} \right| = \frac{A}{2} \left[\frac{2q\varepsilon}{(V_x - V_a)} \frac{N_d N_a}{N_d + N_a} \right]^m \quad [85] \quad (3.1)$$

- where the charge Q is indeed a nonlinear function of applied voltage (V_a), V_x is the barrier potential voltage, N_a is the acceptor density of the *p-type*, N_d is the donor density of the *n*-type, q is electron charge, ε is the silicon permittivity, m is the coefficient grading (i.e. $m=1/2$) and A is the area of the junction and d_i is the thickness of the intrinsic region in the *pin* junction as shown in equation (3.3).

The capacitance of the junction diode depends on the voltage applied to it. In photo parametric mode, the mean applied voltage V_a across the photodiode junction is the *ac* pumping voltage $V(t)$. Substituting $V(t)$ for V_a in equation (3.1), the voltage variable capacitance C_j can be expressed by:

$$C_j = \frac{A}{2} \left[\frac{2q\varepsilon}{(V_x - V(t))} \frac{N_d N_a}{N_d + N_a} \right]^{1/2} \quad (3.2)$$

And in case of *pin* photodiode, the voltage variable capacitance C_j can be expressed by:

$$C_j = \frac{A}{2} \left[\frac{4\varepsilon^2}{d_i^2 + 2\frac{\varepsilon}{q}\frac{N_a + N_d}{N_a N_d}(V_x - V(t))} \right]^{1/2} \quad [85] \quad (3.3)$$

The pumping signal can be expressed as:

$$V(t) = V_p \cos(\omega_p t) \quad (3.4)$$

Where V_p is the peak value of the pump signal and ω_p is the pump angular frequency. Variation in the applied voltage $V(t)$ results in a corresponding variation in the depletion-

layer capacitance c(t), and this, as seen from figure 3.4(a), resulting in time-dependent capacitance C(t), which can be expressed by:

$$C(t) = \left(\frac{1}{V_x - V(t)}\right)^{1/2}\left(\left(\frac{A^2}{4}\right)2q\varepsilon\left(\frac{N_d N_a}{N_d + N_a}\right)\right)^{1/2} \tag{3.5}$$

For simplicity lets: $$G = \left(\left(\frac{A^2}{4}\right)2\,q\,\varepsilon\left(\frac{N_d\,N_a}{N_d + N_a}\right)\right)^{1/2} \tag{3.6}$$

The mean value of the junction capacitance (C_{mean}) can be calculated by integrated equation (5): $$\int_0^T C(t)\,dt = G\int_0^T \left(\frac{1}{V_x - V(t)}\right)^{1/2} dt \tag{3.7}$$

$$C_{mean} = \frac{2G}{T}\left[\frac{\left(\frac{1}{|Vx - V_p \cos(w_p t)|}\right)^{1/2}\left(\frac{|V_x - V_p \cos(w_p t)|}{V_x - V_p}\right)^{1/2} F\left(\frac{w_p t}{2}\middle|\frac{-2V_p}{V_x - V_p}\right)}{W_p}\right]_0^T \tag{3.8}$$

- Where is F(x|m): Elliptic F[x,m] : elliptic integral of the first kind.

Figure 3.4(b) depicts the mean value of the junction capacitance at various applied voltages across the PD. The mean value of the junction capacitance will be used to calculate the input and output inductive reactance impedance, as mentioned earlier, which is (X_L=X_{Cmean}).

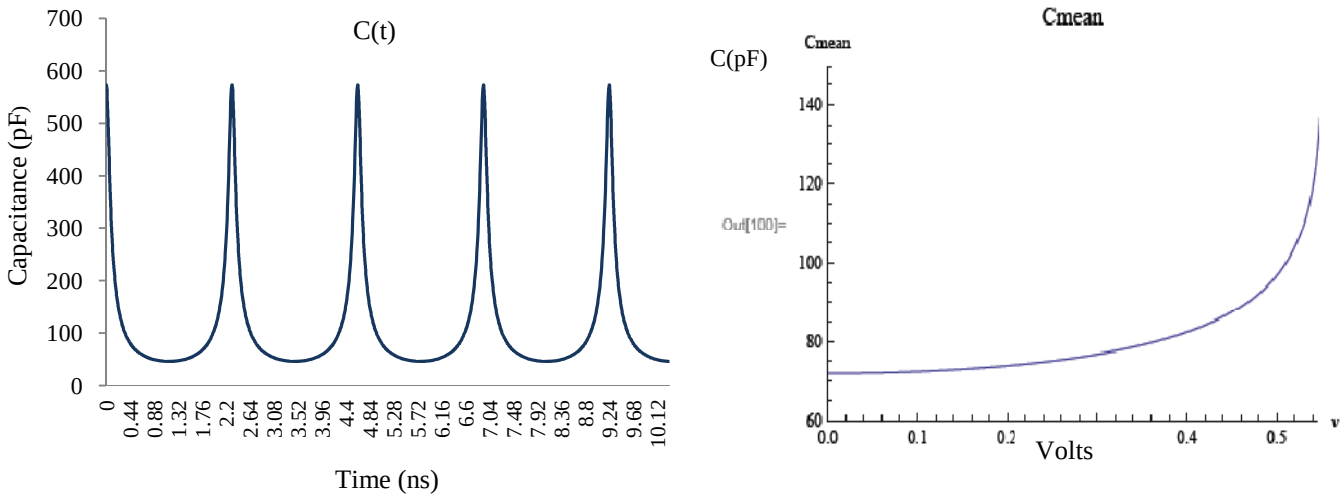

Figure 3.4(a) Resulting time-dependent capacitance; (b) Mean value of the junction capacitance

3.2 Further PPA Signal Analysis and Gain Theoretical Analysis

PPA signal analysis, in comparison with conventional PA, does not lend itself to the same analysis, as the power flow is from an optical input to an electrical output. The Manley-Rowe expressions shown in the previous chapter do not seem to be applicable in PPA analysis. This is because the PPA approach used allows the signal energy to be externally coupled by the incident radiation directly into the variable capacitance (i.e. varactor).

3.2.1 Development of the Theory of Operation

In this section, it will be assumed that the equivalent circuit for the PD can be represented as shown in figure 3.5, which consists of variable capacitance (depletion capacitance) connect in series with a fixed loss-resistance (Bulk resistance R_{bulk}); and the incident optical signal that represents a current source was shunted with the variable capacitance; where the bulk resistance is connected with them in series. Other stray capacitor and lead inductances were neglected, as their self-resonances are usually well outside the frequency range of interest.

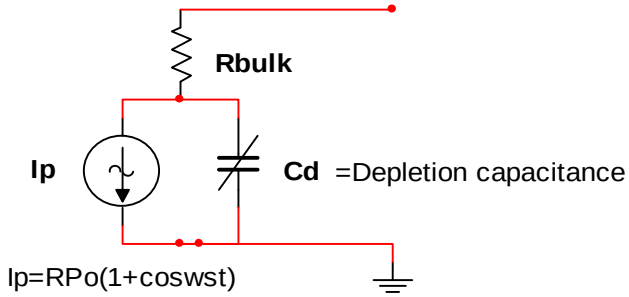

Figure 3.5 Equivalent circuit for varactor photodiode

It assumed that, the effect of applied frequency on the R_{bulk} would be very small (i.e skin effect and source effect concept), and as known the bulk resistance being voltage dependent particularly in *pn* junction; however bulk resistance was assumed as a fixed loss resistance at that applied frequency and applied *ac/dc* voltage.

It is also necessary to know the waveform of the pump voltage signal and to assume that its amplitude is very large; also it is necessary to drive the pump voltage from a sinusoidal voltage source of zero impedance as voltage pumping is, however, analytically more straightforward compared to current pumping analysis; the pump voltage can be represented as shown in equation (3.4). The time-dependent capacitance as shown in figure 3.4 was realized by voltage pumping, and varactor coefficient grading was assumed as for an abrupt junction with a coefficient of 0.5 to avoid complicated analysis. This parameter represents the gradient of the CV curve, which can lead to better conversion gain. Figure 3.6 illustrates an example of CV characteristics for different coefficient grading (m) where large value of coefficient is more favourable in PPA operation, as it shows the highest degree of nonlinearity, and the conversion gain follows ($A \propto dC/dV_a$).

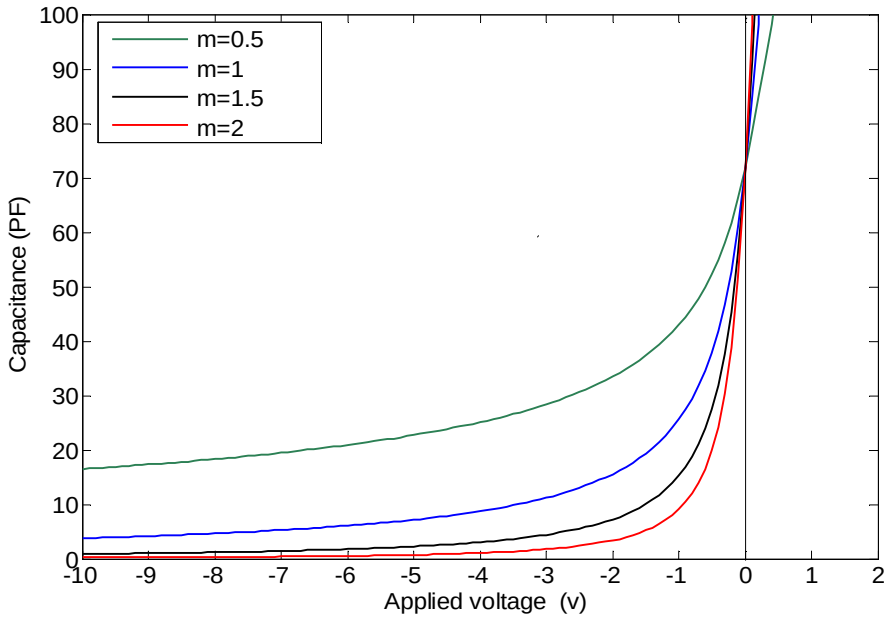

Figure 3.6 CV characteristics for different coefficient grading

The PPA theory analysis in this section can be considered as further analysis to the PPA analysis reported in [40, 82, 86] with a new definition to the gain theory analysis that capable to estimate the up-converter gain based on the effect of photodiode characteristics, the circuit configuration and the applied pump.

3.2.1.2 Definition of the Problem from First Principles

There is a basic difference which makes the PPA amplifier different from the classic parametric amplifier approach; this is due to the fact that the signal source is the current source rather than a voltage source with finite impedance, and therefore, a different approach is required. It is appropriate to consider that the PPA device operates in two modes simultaneously (i.e photo detection and parametric amplification).

The first assumption is that changes in voltage across the PD do not inhibit significantly (at least to first order effect), the relationship between input power & detected current; and high level pumping does not affect the photo detection process. The fundamental relation between input optical power and detected photo source current is:

$$I_p = P_s\left[\frac{\eta\,\lambda}{1240}\right] = RP_s \qquad [19] \qquad (3.9)$$

Where R is flux responsitivity in amps per watt, λ photon wavelength in nanometres, η quantum efficiency in electrons per photon, P_s radiant flux in watts (input optical signal) and P_o average value of optical power. The input detected photo current (I_p), when taking the form of modulated signal frequency (ωs) for 100% modulation of amplitude, can be represented as:

$$I_p = RP_0\left(1+\cos\omega_s t\right) \qquad (3.10)$$

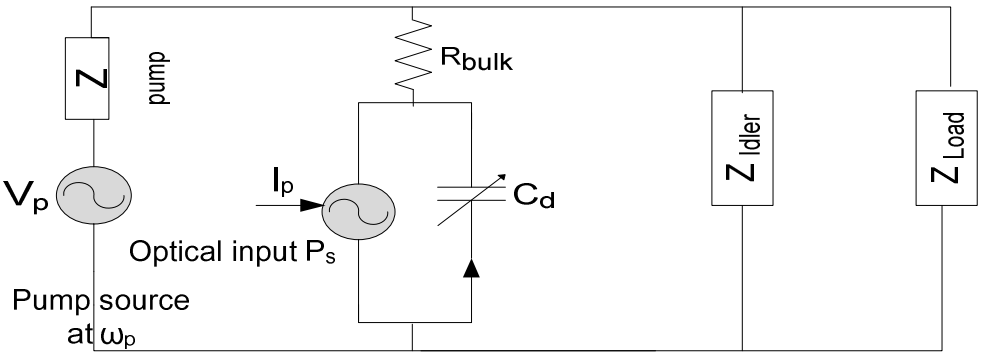

Figure 3.7 PPA equivalent circuit

The second assumption is that the dynamic capacitance of the PD is mainly controlled by the pump voltage, i.e the photo signal induced changes in the capacitance directly are small. The small signal equivalent circuit is illustrated in above figure 3.7.

As mentioned earlier, classic PA analysis does not apply to PPA analysis, due to the current source embedded with the PD, and the well-established theory (Manley and Rowe) in case of the photoparametric analysis cannot proceed further. The PPA analysis approach will transform the current source that represents the input optical signal to a voltage source, as illustrated in figure 3.8.

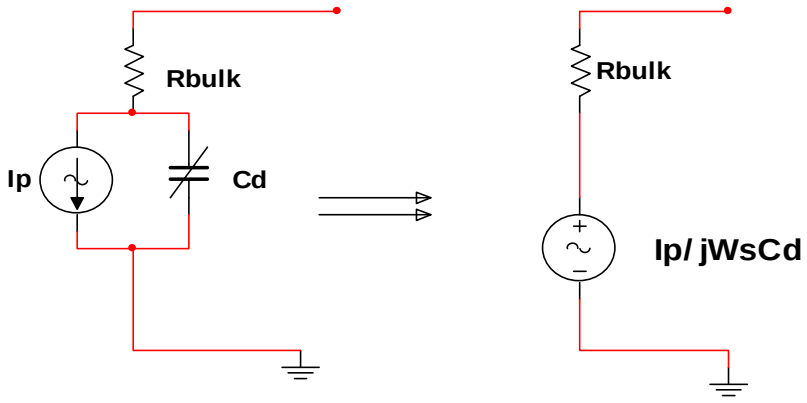

Figure 3.8 Current source to voltage source transformation

The general relationships developed by Manley and Rowe for the salient properties of four-frequency circuits can be applied and the pump modulates the capacitance of the varactor in such way that the signal power is amplified by the energy transfer from the pump. A filter network is then employed to collect the energy from the chosen sideband, as shown in figure 3.9.

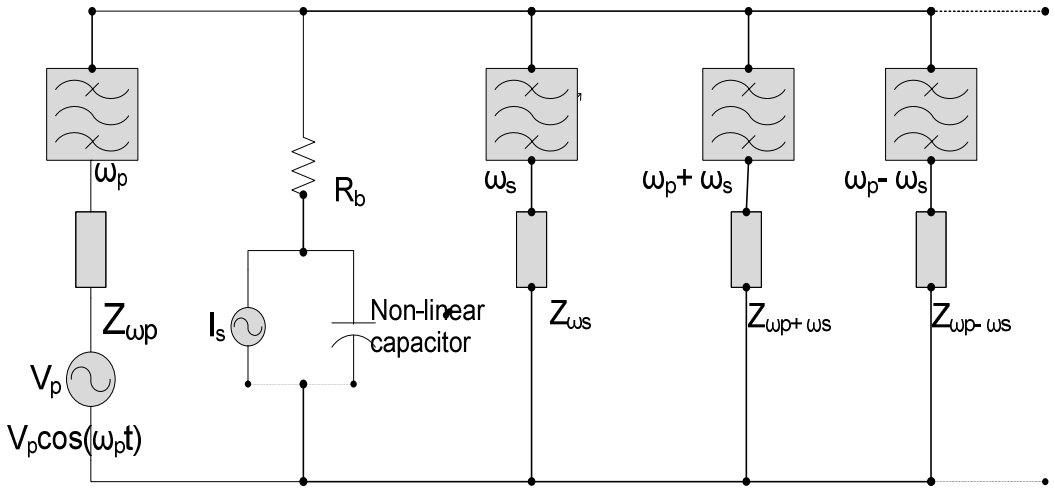

Figure 3.9 Idealized PPA configuration at equilibrium condition (zero bias mode)

3.2.2 PPA Up-conversion Gain Analysis

The modified equivalent circuit arrangement for PPA analysis is shown in figure 3.10. The *a.c* condition for the depletion capacitance C_d will first be examined at pump frequency (ω_p), as follows:

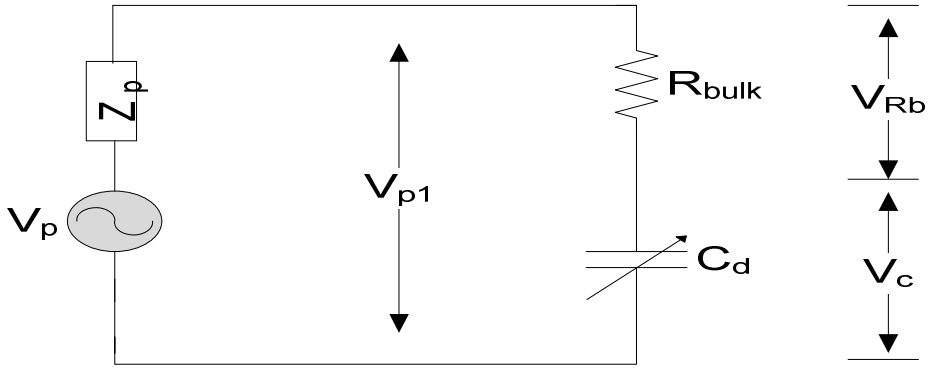

Figure 3.10 AC photo parametric equivalent circuit

The voltage over the PD is the same pump sinusoidal voltage source of zero impedance (V_p=V_{p1}) and is represented as:

$$V_{p_1} = V_{p1'} \cos \omega_p t \tag{3.11}$$

The time varying voltage across the dynamic capacitance (*Vc*) is equal to:

$$V_C = \frac{V_{p_1}}{1 + j\omega_p C_d R_b} \tag{3.12}$$

The overall voltage across the PD (i.e biased the junction) can be represented as:

$$V_{p1} = V_{Rb} + V_c \tag{3.13}$$

$$\left|V_{p1}\right| = V_{Rb} + \frac{V_{p_{1'}}}{1 + j\omega_p C_d R_b} \tag{3.14}$$

According to equation (3.12), the bulk resistance R_b can degrade the performance of the varactor parametric amplifier, particularly at high pump frequency (i.e. reactance impedance decrease at high pump frequency). Hence, a small R_b is preferable for parametric amplification, and leads to low electrical losses (i.e. only small amount of power can be dissipated); it also provides a fundamental limit as to the noise performance of the amplifier (i.e. minimum heat energy). The bulk resistance, as represented by the cutoff frequency, has generally been the dominant loss mechanism. A good varactor pumped weakly may be no better than a poor varactor pumped strongly, so the pumping level across the varactor is very important, and hence, a high capacitance variation is required for parametric efficiency.

The following analysis is conducted for PPA gain estimation. V_{p1} is the main applied voltage to drive the dynamic capacitance; it is assumed that the PD is an abrupt junction, and the depletion width for *pn* and *pin* junction is given respectively by [85]:

$$d_{pn} = \left(\frac{2\varepsilon\left(Vx - V_{p1}\right)}{q}\left(\frac{1}{N_a} + \frac{1}{N_d}\right)\right)^{1/2} \tag{3.15}$$

$$d_{pin} = \left(d_i^{\,2} + \frac{2\varepsilon\left(Vx - V_{p1}\right)}{q}\left(\frac{1}{N_a} + \frac{1}{N_d}\right)\right)^{1/2} \tag{3.16}$$

The depletion capacitance can be represented as:

$$C_d = \left(A\frac{\varepsilon}{d}\right) \tag{3.17}$$

Where *d* represents the sum of (x_n+x_p) for *pn* diode; x_n, x_p are the depletion layer widths in the n and p region for pn junction respectively. In the *pin* junction, d=x_n+x_p+x_i , and x_i represents the width of intrinsic layer.

For simplicity, a *pn* structure will be used for mathematical analysis in this section; the depletion capacitance for a *pn* junction can be represented as:

$$C_d = A\left(\frac{q\varepsilon}{2(V_x - V_{p1})}\frac{N_a N_d}{N_a + N_d}\right)^{1/2} \tag{3.18}$$

Let
$$\Delta = A\left(\frac{q\varepsilon}{2}\frac{N_a N_d}{N_a + N_d}\right)^{1/2} \tag{3.19}$$

$$C_d = \Delta.\frac{1}{(Vx - V_{p1})^{1/2}} \tag{3.20}$$

i.e
$$C_d{}^2 = \Delta^2.\frac{1}{(Vx - V_{p1})} \tag{3.21}$$

C_d is now described as function of V_{p1}, a fine-varying function. From equation (3.18),

$$(V_x - V_{p1}) = V_x + V_{Rb} + \frac{V_{p_1}}{1 + j\omega_p C_d R_b} \tag{3.22}$$

$$\left|V_x - V_{p1}\right| = \frac{\left[\left(V_x + V_{Rb} + V_{p_1}\right)^2 + \omega_p{}^2\, C_d{}^2 R_b{}^2 \left(V_x + V_{Rb}\right)^2\right]^{1/2}}{\left[1 + \omega^2{}_p C^2{}_d R^2{}_b\right]^{1/2}} \tag{3.23}$$

From equation (3.21)
$$\left(\frac{1}{C_d{}^2}\right) = \frac{(Vx - V_{p1})}{\Delta^2} \tag{3.24}$$

From equation (3.23), let
$$\frac{(Vx + V_{Rb})}{\Delta^2} = \frac{1}{D^2} \tag{3.25}$$

Substituting equation (3.18) for the overall applied voltage V_{p1} and taking the modulus of the complex quantity gives:

$$\frac{1}{C_d{}^2} = \frac{1}{D^2}\left[1 + \frac{\left(\frac{V_{p_1}}{Vx + V_{Rb}}\right)\left[2 + \left(\frac{V_{p1}}{V_x + V_{Rb}}\right)\right]}{1 + \omega_p{}^2 C_d{}^2 R_b{}^2}\right]^{1/2} \tag{3.26}$$

Where is V_{p1} represents the voltage across the PD and V_{p1}=V_c+V_{Rb}

$$\left(\frac{Vc\ +V_{Rb}}{Vx\ +V_{Rb}}\right)^2 << 2$$

This implies that the pump voltage across the junction is smaller than the barrier potential and the voltage across the bulk resistance. Therefore,

$$\frac{1}{C_d{}^2} \approx \frac{1}{D^2}\left[1+\frac{\left[2\left(\frac{V_c+V_{Rb}}{V_x+V_{Rb}}\right)\right]}{1+\omega_p{}^2 C_d{}^2 R_b{}^2}\right]^{1/2} \tag{3.27}$$

From equation (3.27), C_d^2 is involved on both sides. However, using a suitable approximation: Typically $\omega_p C_d R_b << 1$, and let $E = \frac{V_c + V_{Rb}}{V_x + V_{Rb}}$.

Also employing the theorem of: $(1+E)^{1/2} = 1 + \frac{1}{2}E$.

The diode capacitance in an approximation form is represented as:

$$\frac{1}{C_d{}^2} = \frac{1}{D^2}\left(1 + E\cos\omega_p t\right) \tag{3.28}$$

The small signal equivalent circuit is now examined. C_d is modulated by the pump voltage in complete fashion. Therefore, the previous analysis gives no allowance for idler and circuit signal loading. If a general load of magnitude $Z_L = R_L + jX_L$ is connected in the shunt across the PD, the magnitude of the load voltage can be presented as:

$$|V_L| = |V_a|\frac{(R_b + X_L)^{1/2}}{R_b + R_L} \tag{3.29}$$

Where V_a is the voltage appearing a cross the general load impedance and can be calculated based on the analysis of unloaded open circuit voltage shown in figure 3.11

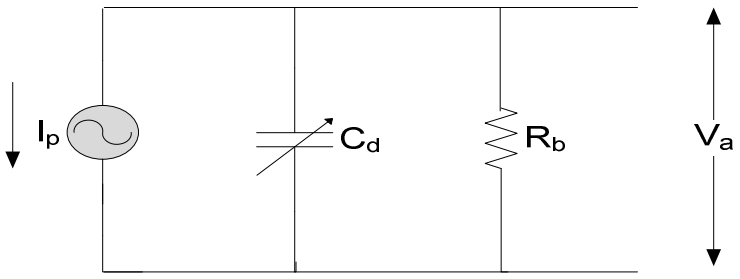

Figure 3.11 unloaded open circuit voltage (no pump)

$$V_a = I_p.Z \tag{3.30}$$

Where is $$Z = \frac{R_b}{1 + j\omega_s c(t) R_b}$$

In general, the pump circuit is matched to the baseband value of C_d and the unloaded value of V_a is given by:

$$V_a = -j\left[\frac{RP_o}{D\,\omega_s}\right]\left(\begin{array}{l}\alpha + \alpha\ cos\ \omega_s t + \beta\ cos\ \omega_p t + \frac{\beta}{2} cos\ (\omega_p - \omega_s)\ t + \\ \frac{\beta}{2} cos\ (\omega_p + \omega_s)\ t + ...\end{array}\right) \tag{3.31}$$

And $\alpha = 1 - \frac{E^2}{16} - \frac{15}{1024}E^4 + ...$ and $\beta = \frac{1}{2}E + \frac{3}{64}E^3 + ...$

Where is R is junction responsitivity, P_o is the average value of optical power, D is the term relating to diode model parameters to barrier potential and voltage across the bulk resistance, E is a parameter relating applied pump voltage to inbuilt barrier potential to the PD. For the value of E in this case, $\alpha \approx 1$ and $\beta = E/2$; β is more dependent on pump power and the terms involving α reflect only terms of ω_s by direct detection and other a dc term (i.e no pump state) and the others are dynamically modified by the pump.

Given that the output voltage at baseband frequency or pump frequency is dependent on the V_a and the load impedance, for comparison reasons, a purely resistive load is considered. The output (i.e pump) at an idler frequency ($\omega_p \pm \omega_s$) is given by:

$$|V_{Rl}| = -j\left(\frac{RP_o}{D\omega_s}\right)\left(\frac{\beta}{2}\right) = -j\left(\frac{I_s}{\omega_s C_d}\right)\left(\frac{\beta}{2}\right) \tag{3.32}$$

In order to consider the gain relative to the uncorrected output of no pumped system at idler frequency, the output (i.e no pump) is given by:

$$|V_{RL}| = -j\left(\frac{I_s}{\omega_i C_d}\right) \tag{3.33}$$

The condition for gain at the output in non degenerate mode is:

$$\left(\frac{I_s}{\omega_s C_d}\right)\frac{\beta}{2} \geq \left(\frac{I_s}{\omega_i C_d}\right) \tag{3.34}$$

i.e $$\omega_i \geq \left(\frac{2\omega_s}{\beta}\right) \tag{3.35}$$

The corresponding up conversion gain is given by the rate of equation (3.32) to equation (3.33)

$$A_v = \frac{\beta}{2}\left(\frac{\omega_i}{\omega_s}\right) \tag{3.36}$$

The PPA up conversion gain analysis predicts that the available gain is proportional to the ratio of first upper sideband to signal frequency. This is consistent with the Manley and Rowe analysis ($A_v=\omega_i/\omega_s$) and the second parameter β related to junction characteristics, the applied pump voltage and the applied pump frequency across the photodiode. However the new definition of β is different to what reported in [40, 82, 86] which given as:

$$\beta = \frac{E}{2} = \frac{V_{pump}}{Vx}.\frac{1}{2} \qquad [82, 86] \tag{3.37}$$

A new, more accurate elaborate definition of a β has derived which given as:

$$\beta = \frac{E}{2} = \frac{V_c + V_{Rb}}{Vx + V_{Rb}}.\frac{1}{2} \tag{3.38}$$

Where V_{p1} is given as: $$V_{p1} = V_{Rb} + Vc = V_{Rb} + \frac{V_{p_1}}{1 + j\omega_p C_d R_b} \tag{3.39}$$

The up conversion gain can be represented as:

$$A_v = \frac{1}{4}\frac{V_c + V_{Rb}}{V_x + V_{Rb}}\left(\frac{\omega_i}{\omega_s}\right) \tag{3.40}$$

The above gain expression is derived by normalising the magnitude of the up converted components to the corresponding baseband signal across an identical load. As mentioned before, bulk resistance degrades the performance of a varactor parametric amplifier particularly at high pump frequency. In addition, an increase in pump frequency leads to a proportional decrease in junction reactance impedance and an increase in β. In other words, β decreases proportionally to the increase in bulk resistance (i.e more power

dissipation occurs at large bulk resistor). It can be summarised that the above approach could predict amplifier performance according to gain equation (3.36). The concept of high gain being achieved if a high frequency is applied is no longer accurate without considering the junction characteristics and applied pump across the PD itself. This theory signal analysis will be referred to and compared with further work in chapter 4, which aims to reach a more realistic assessment, and performance optimisation can be achieved by using nonlinear circuit simulators, compared with the actual behaviour of the practical circuit with respect to gain conversion in chapter 5.

This section has presented gain analysis based on the PPA operating at equilibrium mode (no *dc* bias source). However, the analysis of the PPA operating in conductive mode (reverse bias) was derived, and it was found that the value of bias voltage (V_0) should be entered into the expression of β in equation (3.38), and was added to the denominator in equation (3.40) to become:

$$A_v = \frac{1}{4}\frac{V_c + V_{Rb}}{V_x + V_o + V_{Rb}}\left(\frac{\omega_i}{\omega_s}\right) \tag{3.41}$$

3.3 General Load Analysis

An equivalent circuit for general load matching analysis is shown in figure (3.12)

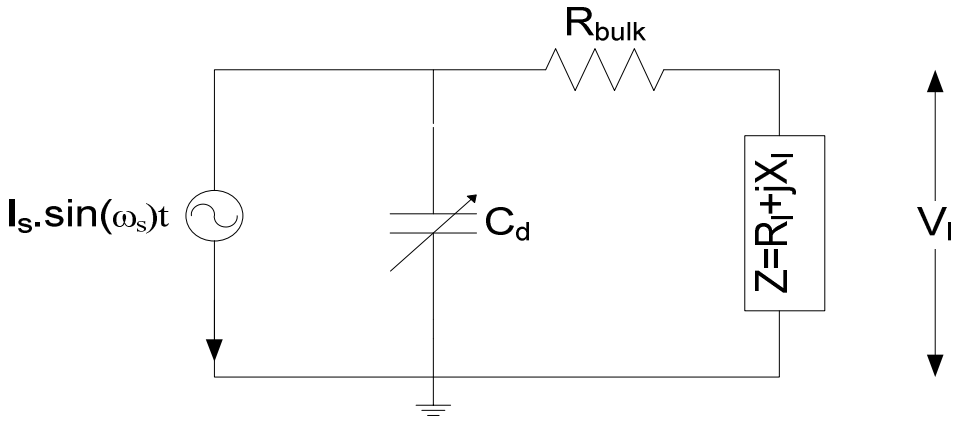

Figure 3.12 Equivalent circuit for load matching

Where I_s represent the photo current (I_p) at signal frequency. The load voltage can be represented as follows:

$$V_L = \frac{R_L + jX_L}{(R_b + R_L) + jX_L}.Vs \tag{3.42}$$

Where is V_s can be represented as:

$$V_s = I_s.\frac{1}{j\omega sCd + \left(\frac{1}{R_b + R_L}\right) + jX_L} = \frac{[(R_b + R_L) + jX_L]I_S}{1 + j\omega_s C_d (R_b + R_L) - \omega_s C_d X_L} \tag{3.43}$$

Hence

$$V_L = I_s.\frac{(R_L + jX_L)}{(1 - \omega_s C_d X_L) + j\omega_s C_d (R_b + R_L)} = I_s.\frac{(R_L + jX_L)((1 - \omega_s C_d X_L) - j\omega_s C_d (R_b + R_L))}{(1 - \omega_s C_d X_L)^2 + \omega_s{}^2 C_d{}^2 (R_b + R_L)^2} \tag{3.44}$$

The optimum situation for power transfer is for a matched load. The load is matched when imaginary parts are zero in the equation (3.44) for load voltage V_L:

$$jX_L(1 - \omega_s C_d X_L) - j\omega_s C_d (R_b + R_L) = 0 \tag{3.45}$$

In general $$X_L = \omega_s\left(C_d R_L (R_b + R_L) + C_d X_L{}^2\right) \tag{3.46}$$

$$\omega_s = \left[\frac{1}{C_d}\right]\frac{X_L}{R_L(R_b + R_L) + X_L{}^2} \tag{3.47}$$

From equation (3.46) $$X_L{}^2 - X_L\left(\frac{1}{\omega_s C_d}\right) + R_L(R_b + R_L) = 0 \tag{3.48}$$

$$X_L = \frac{\left(\frac{1}{\omega_s C_d}\right)^2 \pm \left(\left(\frac{1}{\omega_s C_d}\right)^2 - 4R_L(R_b + R_L)\right)^{1/2}}{2} \tag{3.49}$$

X_L providess two solutions. When the imaginary parts are zero, the V_L in equation (3.44) can be represented as:

$$V_L = I_s.\frac{R_L(1 - \omega_s C_d X_L) + \omega_s C_d X_L (R_b + R_L)}{(1 - \omega_s C_d X_L)^2 + \omega_s{}^2 C_d{}^2 X_L (R_b + R_L)^2} \tag{3.50}$$

Hence $$V_L = I_s.\frac{\omega_s C_d X_L R_b + R_L}{(1 - \omega_s C_d X_L)^2 + \omega_s{}^2 C_d{}^2 X_L (R_b + R_L)^2} \tag{3.51}$$

To maximise the output:

$$\left(\frac{dV_L}{dR_L}\right) = 0 = -I_s \cdot \frac{\left(2\omega_s{}^2 C_d{}^2 X_L{}^2 R_b + \omega_s{}^2 C_d{}^2 X_L 2R_L\right)}{\left((1-\omega_s C_d X_L)^2 + \omega_s{}^2 C_d{}^2 X_L (R_b + R_L)^2\right)^2} \tag{3.52}$$

Therefore $$2\omega_s{}^2 C_d{}^2 X_L{}^2 R_b + \omega_s{}^2 C_d{}^2 X_L 2R_L = 0 \tag{3.53}$$

At maximum output, the load resistance $R_L = -R_b$ shows that a negative resistance is necessary. The two value of X_L in equation (3.48) for which X_L=0 or $\left(\frac{1}{\omega_s C_d}\right)$ gives two solutions for the voltage (V_L):-

For a pure resistive load (i.e $X_L=0$)

$$V_L = I_s R_L = -I_s R_b \tag{3.54}$$

For tuned reactive (i.e $X_L=\left(\frac{1}{\omega_s C_d}\right)$)

$$V_L = \frac{I_S}{\omega_s{}^2 C_d{}^2 (R_b + R_L)} = \infty \tag{3.55}$$

The general load impedance is shown in figure 3.13, which shows that the maximum power transfer occurs when the pure load resistance is very small (i.e. close to zero ohms); a negative load resistance is required to achieve maximum power transfer. Moreover, the maximum power transfer condition is unstable when matched by a complex conjugate impedance. It can be seen that for stable power transfer, it is inevitable to use a low bulk resistance, as shown in the graph (*i.e* $R_L=R_b$). The load cannot be matched for maximum power transfer because this requires a negative real resistance. It also means an overall lossless system for infinite gain.

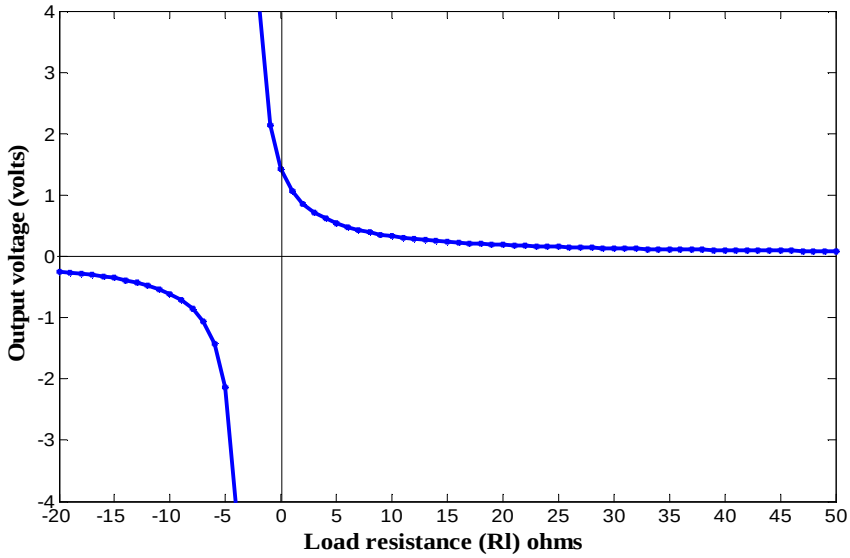

Figure 3.13 PPA output at general load impedance

3.4 PPA Up-conversion Consideration and Theoretical Performance Predication

The PPA gain in up conversion mode is directly dependent on four main parameters, as predicted in the theoretical analysis shown in the previous section (i.e equation 4.40). Firstly, the gain is dependent on the PPA external circuit configuration that can be identified as a PPA mode of operation (i.e zero bias mode or conductive mode); second, the gain is dependent on varying the pump frequency to baseband frequency, and is proportional to the ratio of upper sideband to signal frequency; third, the gain is dependent on the magnitude of the pump voltage across the PD; fourth, the gain is dependent on the PD characteristics in which the bulk resistance should be very small compared to the capacitive reactance impedance, which helps to provide more power signals to vary the dynamic capacitance, while low power dissipation can be lost due to the bulk resistor. In other words, if the bulk resistor is too large compared to capacitive reactance impedance, this can degrade the performance of the amplifier even if a large pump is applied.

The above four parameters are varied accordingly and were used for theoretical analysis evaluation. The PPA derived gain expression was used to predict the amplifier up conversion gain as shown in the following sections using MATLAB tool. Although this tool is not designed for nonlinear analysis, it can be used for the following scenarios to predict the estimated gain based on the derived expression.

In addition to the above considerations, the photo detection device used in the PPA mode of operation should exhibit good reponsitivity and can be optimised for maximum quantum efficiency, which commonly takes the form of a *pin* structure; also it is favourable to have small capacitive reactance impedance and very low bulk resistance; hence it will be easier to apply an external pump, and also much better for signal speed and frequency response. The most important requirement is the high nonlinearity of the *CV* characteristics.

3.4.1 Gain versus Various Bias Voltages

The parameters used in the theoretical evaluation were set as (R_b=6.5Ω, Pump power=15dBm, V_x=0.552volts, C_d=72pF, R_s=50Ω, ω_p=432.92MHz and ω_s=1MHz. These specific frequencies were used to show the viability of the theoretical approach and helped to compare this result with both simulation and practical results in the following chapters. In this section, the *dc* bias voltage was varied from zero to -30 Volts, as shown in figure 3.14. The maximum conversion gain was achieved at zero bias mode (i.e. 32.5dB gain). Then the gain is gradually reduced by increasing the reverse *dc* bias. The graph shows that the greatest steepness occurred at around zero bias voltage, due to junction behaviour in equilibrium mode (.i.e high nonlinearity). The gain follows the junction *CV* characteristics and this corresponds to verify the proposed mode of operation (i.e. equilibrium mode) where the junction behaves in a highly nonlinear way.

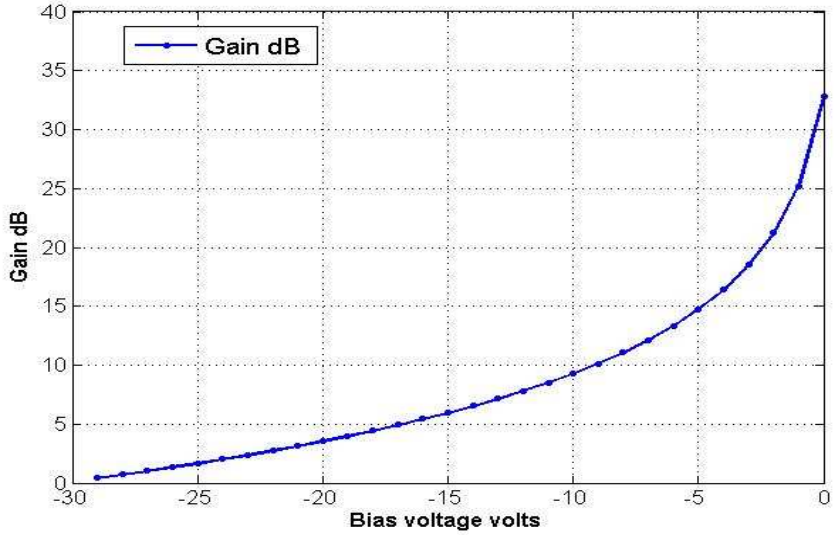

Figure 3.14 PPA gain at various reverse bias voltages

3.4.2 Gain versus Various Pump Frequency and Signal Frequency

The same parameters were used as section 3.4.1 for the same circuit configuration (i.e. zero bias mode). As mentioned before, the gain is dominated by the ratio of the Idler frequency over the RF optical frequency (ω_i / ω_s). The effect of this relation is plotted in figure (3.15), and these two frequencies were varied from 1 to 100 MHz and from 1 to 3000 MHz for optical signal and pump frequency respectively. Also, as shown in figure 3.16, the gain was varied with various pump signals at fixed 1MHz optical signals. Both graphs illustrate that the gain is directly related to the frequency ratio, and it is favourable to gain performance to have widely separated non-commensurate excitation frequencies. The gain, as shown in figure 3.14, increases in proportion to the increase in pump frequency; however in the theory gain analysis, the gain is a trade off between the ratio of (ω_i/ω_s) and the ratio of $\left(\frac{V_c + V_{Rb}}{V_x + V_{Rb}}\right)$ which was identified as the β factor, and therefore both ratios can used to optimise the performance of PPA. However it seems that the ratio of (ω_i/ω_s) leads to the possibility of better gain achievement. In other words, the change in

gain can be made with adjustment in these two terms by increasing one of the parameters in the numerator, or decreasing one of the parameters in the denominator.

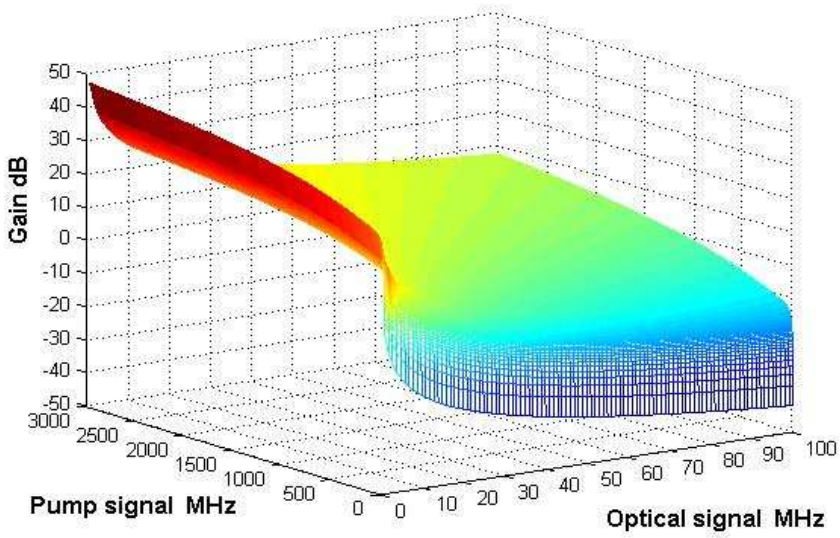

Figure 3.15 The effect of varying the pump and optical signal toward the gain

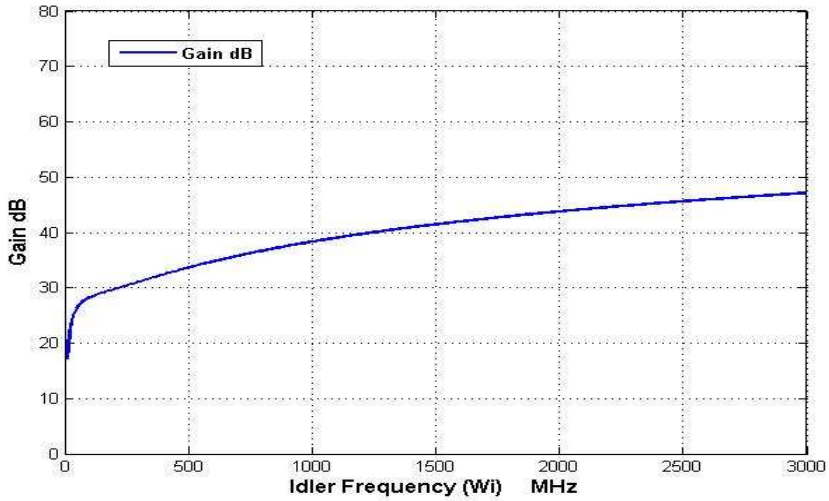

Figure 3.16 PPA gain at various pump signals for 1MHz optical signal

3.4.3 Gain versus Various Pump Power

The same parameters were used as in section 3.4.1 for the same circuit configuration (i.e. zero bias mode). In this section the input pump power was varied from -

30 dBm to 60 dBm, as shown in figure 3.17. As expected, the up-conversion gain increases with pump power level (i.e. V_c+V_{Rb}), the PPA gain is function of the applied power and increases linearly with the increase in the pump level (LO) and operates as an ordinary linear amplifier until the compression point. At very low pump power, the PPA behaves like a convention loss mixer (i.e. this was explained in next chapter).

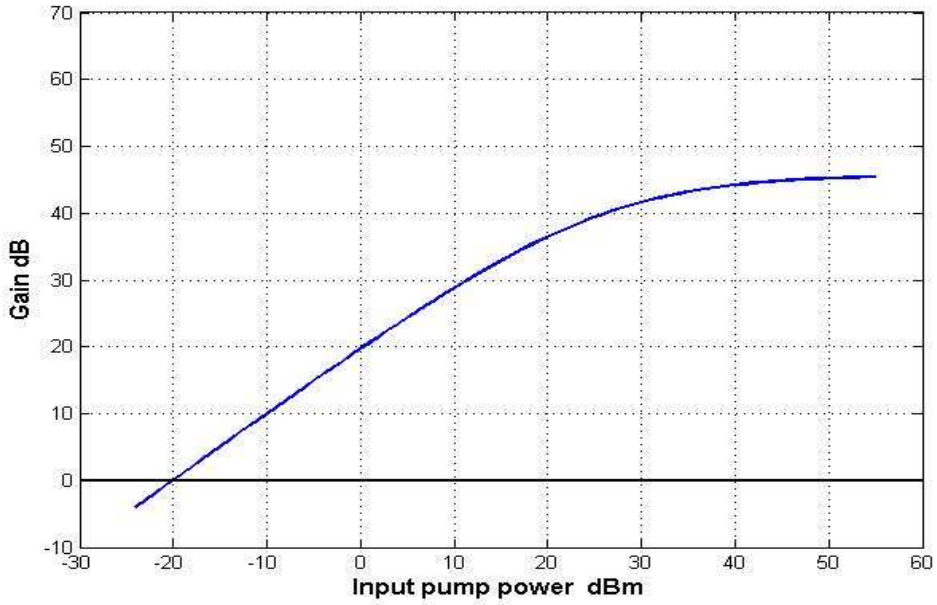

Figure 3.17 PPA gain at various input pump power (LO)

3.4.4 Gain versus Various Bulk Resistor

The same parameters were used as section 3.4.1 for the same circuit configuration (i.e. zero bias mode). In this section, the bulk resistor was varied from 0 to 50Ω as shown in figure 3.18. The idea of this scenario was to see the effect of the bulk resistor on overall gain. As mentioned before, large bulk resistance can increase the pump voltage across itself whereas at the same time, it can reduce the pump voltage across the variable capacitance, and therefore lead to a decrease in overall gain according to gain equation (3.40). Hence, a large value of the bulk resistor is not favourable for parametric

amplification, particularly at high frequency applications. The graph below illustrates that the maximum conversion gain can be achieved for very low bulk resistance.

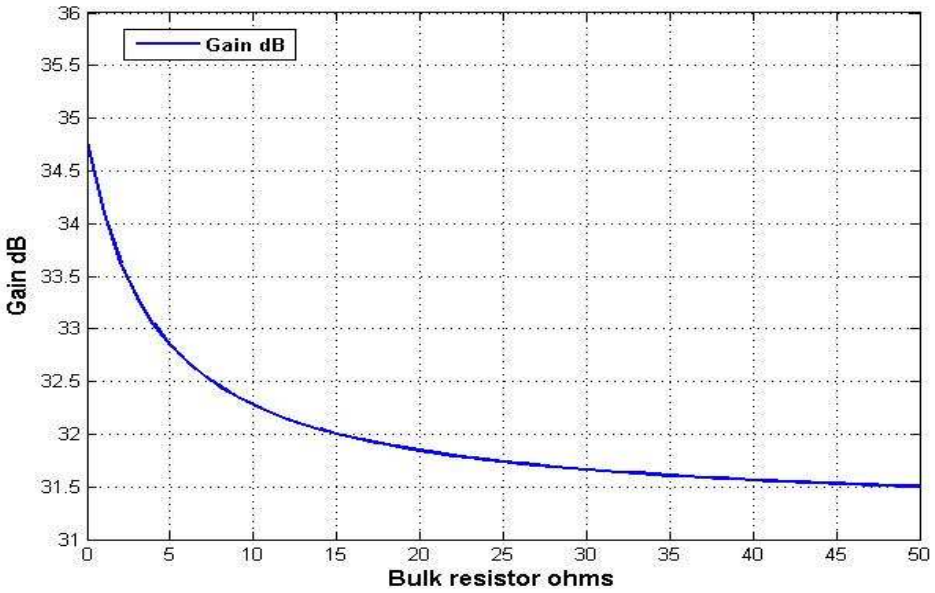

Figure 3.18 PPA gain at various bulk resistances

3.5 Summary

The benefit of employing the PPA at zero bias mode (i.e. no *dc* bias) is that the degree of nonlinearity of CV characteristic is higher, leading to potentially greater conversion gain, essential for optical communication as well as for wireless applications with tight power budgets. Input and output power admittance were considered and analysed, and should be proportional to the mean value of variable capacitance (C_{mean}) for optimum power transfer. Also, PPA general load analysis was presented, showing that optimum power transfer will require the load impedance to be low, and approximately equal to the bulk resistance or negative load impedance with ($R_L = -R_b$).

Further PPA theory gain analysis is presented with new derived gain expressions that are able to include all the parameters that affect the PPA performance, including the

external circuit configuration, junction characteristics and applied pump and source frequencies. The PPA theory analysis predicts that the gain is proportional to the ratio of the first harmonic to signal frequency. This is consistent with conventional PA analysis, in addition to presenting a new correction factor. The theoretical analysis can predict the up-conversion gain; however, such analysis can fall short of predicting other parameters that affect the amplifier operation, as the variable capacitance depends both on frequency and the voltage applied (i.e type of junction structure). Moreover, other effects such as the skin effect may affect amplifier efficiency. Therefore, a more realistic assessment, and also performance optimisation, can be achieved by employing powerful nonlinear simulation tools, followed by practical implementation as seen in the next chapters.

Chapter 4

4. Double Conversion Heterodyne Photoparametric Amplifier (DCHPPA) Modelling, Analysis and Simulations Results

The main objective of this chapter is to develop a versatile model for the DCHPPA circuit, which includes both an optoelectronics up-converter stage (PPA) and conventional down-converter stage (conventional mixer and filter) circuits. The aim in this chapter is to employ nonlinear simulator tools to examine the full circuit configuration and provide a good realistic assessment and better performance optimisation.

4.1. Introduction

A photoparametric amplifier (PPA) circuit would not be possible if nonlinearities did not exist. In electronic circuits, nonlinearities are responsible for phenomena that degrade system performance in many circuit designs such as small signal amplifiers [87]. However, it is often desirable for frequency conversion in such mixer and parametric amplifier circuits (due to harmonic generation). In practice, the passive components such as resistors and inductors and capacitors, can be observed to be nonlinear when operating at the extremes of their operation range by applying large voltages or currents, which can increase the temperature and result in resistance changes. Electronic circuits can be classified as time-invariant circuits (linear), which include only those frequencies available in the excitation waveforms, and do not generate new frequencies, and a time-variant circuit (nonlinear) that generates mixing products between the excitation frequencies and the frequency components of the time waveforms.

4.1.1. Nonlinear Circuit Analysis

A circuit consisting of semiconductor devices such as varactor diodes are often characteristic of a strongly nonlinear circuit which has very strong CV characteristics under bias voltage (ac/dc), and conventional quasilinear circuit analysis cannot be applied. Neither can Volterra series analysis or power-series analysis- be desirable for such a situation [87], as they are mainly desirable for weakly nonlinear circuit characterisation. There are other available approaches for nonlinear analysis using different techniques; these include Load Pull, Large-Signal Scattering Parameters, Quasistatic Assumption and Time domain, as well as frequency domain analysis.

The most dominant methods of nonlinear analysis are time domain (also called transient) analysis, and frequency domain analysis method or hybrid (mixed time and

frequency domain), which depends on how the linear and nonlinear elements are analysed. These methods are more desirable for nonlinear analysis, and depend on how the circuit can be classified (i.e. as a weakly or strongly nonlinear circuit). Time domain analysis can be seen as the most widespread [88] method for weak nonlinear circuit analysis, as it is based on the differential nonlinear equations that describe the circuit (Kirchhoff's equations), and can be performed by means of standard numerical integration methods. This method is more practical in terms of analyzing lumped element circuits, as well as any other circuits including two commensurate frequencies which can be seen as the same case for single tone analysis [89].

Time domain analysis generally uses numerical integration or, where possible, calculates the instantaneous value of the output (e.g. current) of an element from the instantaneous value of the input (e.g. voltage). In a high frequency circuit (e.g. microwave and millimetre wave) some components are difficult to model in the time domain and frequently have a time constant that differs by orders of magnitude. An analysis using a numerical integration technique is inefficient [77, 90], since the integration time step must be smaller than twice the smallest time constant, while the number of iterations is determined by the largest time constant [91]. However time domain analysis is not well suited when components are characterized in the frequency domain, for two main reasons; these are its inability to handle frequency domain quantities in a practical way (particular S parameters) and the difficulty of applying this method to circuits having multiple noncommensurate excitation frequencies (e.g. widely separated frequencies), and having large differences in amplitude such as PPA and mixer circuits, where the signal is said to be quasi-periodic. The reader is directed to [92] for a good review of the three most popular techniques of time domain analysis, which includes direct numerical integration, associated discrete circuit modelling and the shooting method.

The frequency domain method is widely used for analysing non linear circuits, and the most important technique is called harmonic balance (HB) analysis, which will be explained in next section. HB analysis is more applicable to strongly PPA nonlinear circuits (e.g. varactor diode) having two widely separated noncommensurate excitation frequencies with large differences in amplitude (quasi-periodic). These include a large pump signal (also called local oscillator LO) and small source signal (baseband signals). In this chapter, HB analysis will be used to optimise the DCHPPA system, which consists of multiple tones (3-tones) with various numbers of harmonics. The two other popular methods for frequency domain analysis are: power series and Volterra series, both of which are restricted to weakly nonlinear systems [90]. This is because of the algebraic complexity of determining the transfer functions of high order, as required with more strongly nonlinear circuits or with large signals. In other words, a very large number of harmonics must be included in the analysis[93].

Only two previous studies have been undertaken to model and simulate the PPA. The initial work was reported in [37, 94, 95], where the PPA circuit model was based on a *pn* junction diode, and simulated in transient analysis using a spice simulator package. The CV characteristics of the *pn* photodiode are modelled as a linear capacitor, without considering the bias dependent junction capacitance and the transport factor frequency dependency. This is applicable only for single small excitation frequencies with weak nonlinear elements. In such a case, Spice transient analysis runs purely in the time domain, while the junction frequency dependence was more difficult to model in the time domain. According to this research review and based on PPA configuration, transient analysis is computationally inefficient when it deals with multi excitation frequencies and strongly nonlinear components [92, 96]. Time domain analysis requires too much time to reach a steady state solution with excessive memory use, particularly when weak nonlinear

components exist in RF/MW circuits. Its limitations become clear when dealing with frequency conversion and mixer devices in which frequencies change over a wide spectrum. Moreover, at high frequencies, many linear components are best represented in the frequency domain. Simulating such linear models in the time domain by means of convolution can result in problems related to accuracy and stability [97], and, as mentioned earlier, the use of this method for analysing the PPA circuit is not efficient computationally. The severity of the problem becomes immediately evident when computing the response of a single tone excitation, due to the use of iterative methods to optimise the overall circuit, and the problem is even more acute when multiple excitations are used to study the PPA behaviour in a subcarrier multiplied scenario.

The second work for modelling and simulating the PPA was presented in [81, 98, 99]. The PPA circuit model was based on a *pn* junction photodiode model, and simulated using an HB technique provided by the Aplac simulator package. The *pn* photodiode circuit model was configured for a simply ideal current source, representing the optical modulated signal shunted to a *pn* junction diode. The equivalent circuit of the modelled PD was ideal in principle, and did not consider the PD responsitivity, or its frequency response with respect to detected optical signal. Moreover, the PPA circuit was configured by using a voltage source as the pump source (LO), with 1 ohm input impedance (source) and the PPA load impedance was configured as 50 ohms (resistor) connected in parallel to an output port with 50 ohms impedance that results in an overall load impedance of 25 ohms. In addition, the circuit configuration results in estimation of the value for the photocurrent which was set to a very high value, and did not correspond to the detected optical power signal. The PPA miss-matching impedance led to inaccurate results with respect to photoparametric amplifications, as both the input and output impedance must be matched

to 50 ohms, as for most RF systems. This is a minimum and simple requirement to validate the model with respect to simulation and practical results.

There are many simulation programs available. The most accurate commercial ones to handle high frequency effects are ADS by Agilent [100], and the AWR design environment [101] also known as MWO (*Microwave Office*). AWR was chosen to be used for modelling and simulating the whole system (DCHPPA). HB analysis will be the main core tool for performing frequency-domain simulation in this chapter.

4.2. Harmonic Balance in Perspective

HB was mathematically formulated in the late 60's [102], and was developed particularly in the mid -1980s as a frequency domain analysis technique for both linear and nonlinear circuits analysis at any frequency, but offering clear advantages at high frequency compared to transient analysis. Its attractiveness for microwave and millimetre wave application results from its speed and ability to simply represent the dispersive, distributed elements that are common at high frequencies. This technique has been shown to be an efficient approach for analysing and optimising steady-state, quasi-periodic, microwave and RF circuits [92, 93, 103, 104]. HB got its name because it is a method of balancing currents between the linear and nonlinear parts of the circuit, and it is applicable primarily to strongly nonlinear circuit such as the DCHPPA receiver which includes two strongly nonlinear circuits (i.e. PPA and mixer) operating under multitone excitation.

Many high frequency (HF) circuits are high-Q, implying that they exhibit transients that last over hundreds, and even thousands of carrier cycles. RF and MW designers are primarily interested in steady-state responses, and many HF circuits contain long time constants that require conventional transient methods to integrate over many periods of the lowest frequency. Transient analysis requires integration over a

considerable number of periods on the highest frequency sinusoid, and time is wasted in the process of simulating through the transients [105, 106]. Moreover, it can result in problems related to accuracy, causality or stability, particularly at HF, where all the distributed circuit elements are almost exclusively modelled, measured and analyzed in the frequency domain. HB simulators overcome these problems in a rather efficient manner, by resorting to frequency domain formulation of circuit equations (equations that arise from an application of Kirchoff's laws and the circuit elements constitutive relations). The frequency domain formulation can be obtained by substituting the unknown waveforms with their phasor equivalents, and then matching the phasor coefficients that correspond to distinct frequencies. There are many methods for formulating harmonic balance equations, such as conventional formulation, frequency time conversion and state variable formulation, which can be found in detail in [87, 107].

A number of algorithms have been proposed to obtain a solution to harmonic balance problems, and the solution can be obtained by several methods[82, 87, 108] such as, the optimization method which is a reasonable approach only for relatively simple problems. The relaxation method uses no derivative information (i.e *I/V*), and is relatively simple and fast, but it is not robust. The gradient method is an iterative technique, and can be used to solve either a system of equations (e.g using Newton-Raphson), or to minimize an objective function using a quasi-Newton or search method. The matrix methods for solving involve many technique (e.g. direct solvers, sparse solvers, keylov-subspace techniques, etc), which probably the main difference between the many implementation of the harmonic balance simulators. For instance, the MWO simulator utilises the Generalised Minimal Residual Method (GMRES) for harmonic balance analysis[87, 109, 110].

A common approach for nonlinear circuit analysis using HBT is to decompose the circuit into a linear and nonlinear sub network [103, 105, 111], as shown in Figure 4.1. The

figure illustrates the principle behind HB simulation, where the linear sub-circuit is analyzed in the frequency domain by conventional linear multi-port techniques, while the nonlinear sub-circuit is described in the time domain.

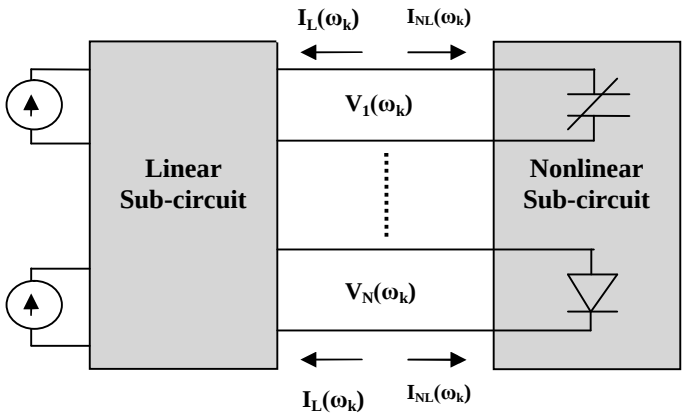

Figure 4.1 Circuit partitioned into linear and nonlinear sub-circuits.

The voltages at the interconnecting ports are considered as the unknowns, so the goal of HB analysis is to find the set of voltage phasors in such way that Kirchoff's laws are satisfied to desire accuracy. The HB analysis will find all the voltages as follows:

Find $$V_1(\omega_k), V_2(\omega_k), \ldots\ldots\ldots, V_N(\omega_k) \tag{4.1}$$

for all ω_k such that relation $\left|I_L(\omega_k) - I_{NL}(\omega_K)\right| < \varepsilon$ holds at each interconnecting port, where ω_k is the set of significant frequencies in the port voltage spectra, and ε specifies the desired accuracy. The voltages at connecting ports are expressed by Fourier series

expansions: $$V(t) = Re\left[\sum_{K_1=0}^{K_1}\sum_{K_2=0}^{K_2}\ldots\ldots\sum_{K_n=0}^{K_n} V_{K_1}, V_{k_2}, \ldots e^{j2\Pi(K_1 f_1 + \ldots\ldots K_n f_n)t}\right] \tag{4.2}$$

where n is the number of tones (sources), $f_{1\ldots n}$ are the fundamental frequencies of each source and $K_{1\ldots n}$ are the number of harmonic for each tone. The elegance of the HB approach in reference to the problems seen in time domain analysis, is because it uses a linear combination of sinusoids to build the solution, so it approximates naturally to the periodic and quasi-periodic signals found in steady state response. Moreover, HB

represents waveforms as coefficients of sinusoids, and converts the coefficient representation of the stimulus into a sampled data representation. This is the idea of converting from the frequency domain to time domain, which can be accomplished by the Inverse Fourier Transform; thus, the nonlinear devices are easily evaluated. Consequently, the results are then converted back into coefficient from using Forward Fourier Transform; (see the following flowchart diagram for more clarification regarding the HB method):

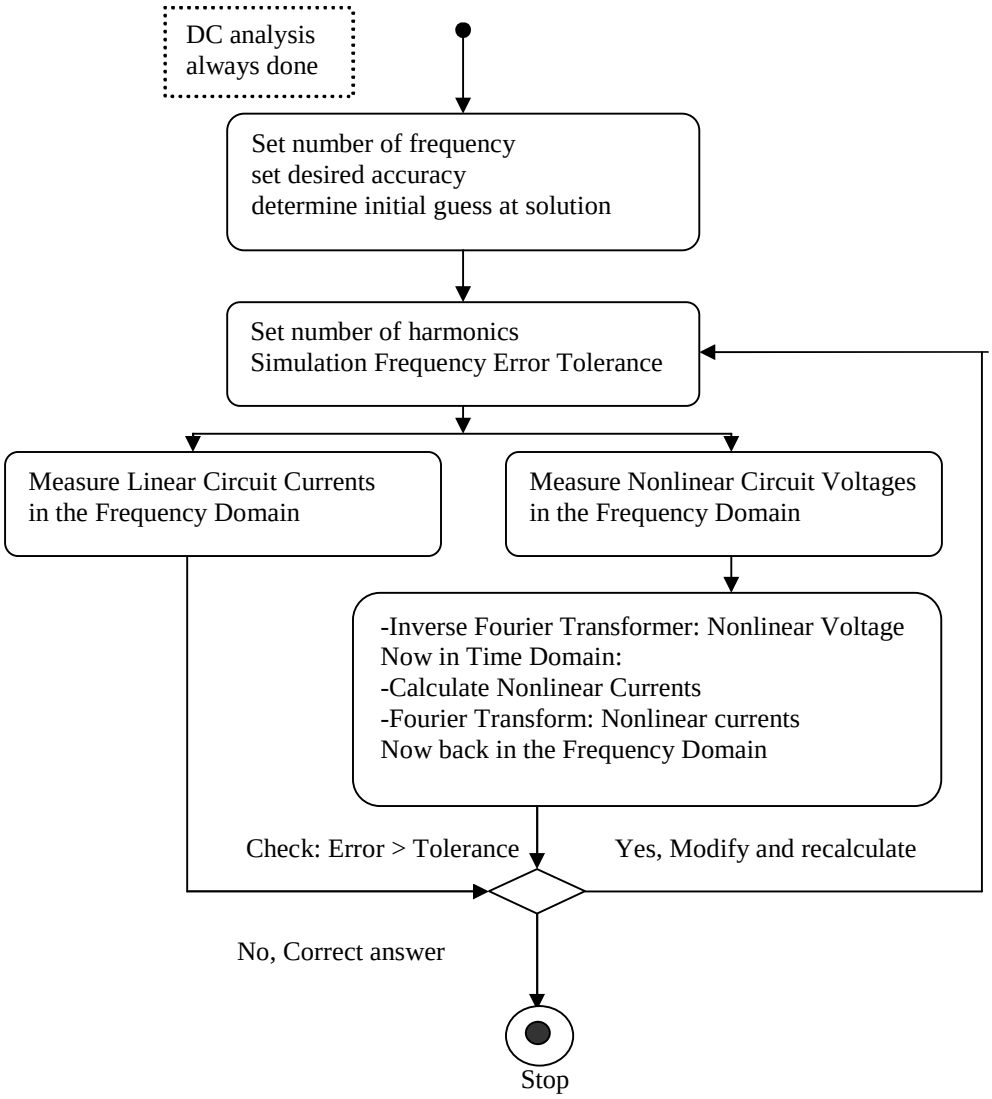

4.2.1. Advanced Multi-tone Harmonic Balance Analysis

Harmonic analysis is, at least as far as its everyday use is concerned. Its goal is to calculate the steady state spectra and waveforms for strongly nonlinear circuits under

periodic large-signal excitation. This technique can be generalized to cover the case of multitone excitation, where the input signals frequencies may be far apart. A clear example of this type of problem is the intermodulation calculation for the DCHPPA system for the two types of mixer (i.e. PPA and conventional down converter mixer). Frequency mixing in the PPA is quite similar to that of conventional mixers. In the PPA, there are two input signals, the LO signal (large signal) and RF input signals (small signal). The RF signal is presented by the input modulated optical baseband signal, generated within the device model (*pin* photodiode). The small modulated RF signal is multiplied by the LO signal in a nonlinear junction capacitance.

The object-oriented *MWO* simulator aims to perform noncommensurate multitone excitation analysis based on equivalent circuits composed of current sources proposed in [112, 113] which enables the full exploitation of the object orientation. All models are based on independent and voltage controlled current sources, as it is the only basic component needed to create more complicated models. The simulator has the facility to use two types of input file, a text file (script code) using net-list editor and the schematic script capture file which can automatically generate the net-list code from the circuit diagram. In addition, the tool provides its own program language, (Advanced Imagery Library AIL), which recognises all the normal standard functions as mathematical expressions written in a program-like manner, and can import other codes from various tools such as MATLAB, SPICE, etc.

4.2.1.1. Small-Signal Large-Signal Mixer Analysis

In the DCHPPA system, the PPA circuit (i.e. up-converter mixer) and the conventional double balanced mixer circuit (i.e. down converter mixer) can be analysed from the fast small-signal mixer analysis reported in [105, 109], where the RF signal is

much weaker than the LO signal. A small signal analysis method was employed in the MWO simulator that was preceded by a DC analysis using the Newton-Raphson method in order to find the operating point. The circuit is then linearised at this point and a sinusoidal phasor analysis is carried out. By using single-tone harmonic analysis, the operating point idea may be extended by employing a strong pump signal LO, and, as result, the nonlinear elements will have a periodic waveform as their operating point; in this case, the static and dynamic sources may be linearised and treated as time-dependent components. By using the Fourier Transform, the final solution was found by convolution, where the frequency-dependent components were replaced by a time-domain equivalent circuit, and the time-dependent components in the present case were replaced by their frequency-domain equivalent circuits.

In *MWO* harmonic analysis, the first step is to analysis the non-linear static sources; thus, all waveforms are represented in terms of Fourier series coefficients. For instance, periodic steady state voltage *u(t)* is expressed as

$$u(t) = U_{a,0} + \sum_{m=1}^{N} \left(U_{a,m} \cos m\omega_p t + U_{b,m} \sin m\omega_p t \right) \qquad (4.3)$$

where is $\omega_p = \frac{2\pi}{T}$, T represents the period of the pump signal, and N the number of harmonics in the pump LO signal. Coefficients $U_{a,m}$ and $U_{b,m}$ are real numbers: subscripts *a* and *b* refer to the cosine coefficients and sine coefficients respectively.

For a non-linear static component *i=i(u)*, the steady state current can be expressed as:

$$i(t) = I_{a,0} + \sum_{m=1}^{N} \left(I_{a,m} \cos m\omega_p t + I_{b,m} \sin m\omega_p t \right) \qquad (4.4)$$

Assuming that the periodic steady state voltage *u(t)* in (4.3) is known, then the coefficients of (4.4) are found by replacing *u(t)* in the non-linear characteristics *i=i(u)* and applying the FFT as follows:

- Firstly, from an initial guess $U_{a,m}^{0}$, $U_{b,m}^{0}$, the sample point values for *u(t)* are calculated using Inverse Fourier Transforms. The number of sample points is (at least) 2N.
- Secondly, values of *i(t)* are calculated at the sample points.
- Finally, coefficient $I_{a,m}^{0}$, $I_{b,m}^{0}$ are calculated using discrete Fourier transforms.

Each of the coefficients $I_{a,m}, I_{b,m}$ will become a nonlinear function of all the coefficients $U_{a,m}, U_{b,m}$, thus, each node of the circuit may be expanded into 2N+1 nodes having voltages $U_{a,m}, U_{b,m}$ after which currents $I_{a,m}, I_{b,m}$ are treated as normal non-linear static sources and then enabling a conventional DC analysis to be performed and all the convergence aiding technique provided in the simulator to be used. After convergence, the expanded nodes contain the spectral components of the node voltages.

The second step of HB analysis is the linearization of static and dynamic sources. After carrying out the single-tone harmonic analysis, the current waveform of the static source can be represented as:

$$i(t) = i(u(t)) \tag{4.5}$$

is known for the whole period of the pump LO signal. Linearisation of (4.5) equation yields a time-dependent conductance:

$$g(t) = \left[\frac{di}{du}\right] \tag{4.6}$$

Similarly, a dynamic source can be represented as:

$$q(t) = q(u(t)) \tag{4.7}$$

This creates a time-dependent capacitance which represented as:

$$c(t) = \frac{dq(t)}{du(t)} \tag{4.8}$$

The third step is small signal analysis; the RF signal (baseband) is turned on. The circuit is divided into non-linear (time-dependent) and linear (frequency-dependent) parts (figure

4.1). The frequency response of the frequency-dependent part can be calculated in a straightforward manner, where the time dependent part is computed by creating a frequency domain equivalent circuit with the aid of convolution [114, 115].

After LO signal analysis, the voltages and currents of the circuit are of the form (4.3) and (4.6). Applying (4.6) and (4.8), the frequency-domain representations for the conductance and capacitance become:

$$g(t) = G_0 + \sum_{n-1}^{2N} [G_{a,n} \cos n\omega_p t + G_{b,n} \cos n\omega_p t] \tag{4.9}$$

$$c(t) = C_0 + \sum_{n=1}^{2N} \left[C_{a.n} \cos n\omega_p t + C_{b.n} \cos n\omega_p t\right] \tag{4.10}$$

where ω_p is the LO angular frequency and *N* is the harmonics number used in large-signal LO analysis. Once both the conductance and capacitance are presented in a Fourier series expression, the final step is the analysis at RF angular frequency ω_s (baseband frequency), the small-signal current being obtained from convolutions;

$$I(\omega) = G(\omega) * U(\omega) = \int_{-\infty}^{\infty} G(\xi) U(\omega - \xi) d\xi \tag{4.11}$$

and

$$I(\omega) = C(\omega) * j\omega U(\omega) = \int_{-\infty}^{\infty} C(\xi)\, j(\omega - \xi) U(\omega - \xi) d\xi \tag{4.12}$$

where is *G(ω)* and *C(ω)* are the Fourier transforms of (4.9) and (4.10), respectively. The spectral components of *G(ω)* and *C(ω)*, as well as those of the small-signal voltages and currents are, shown in Figure 4.2[109].

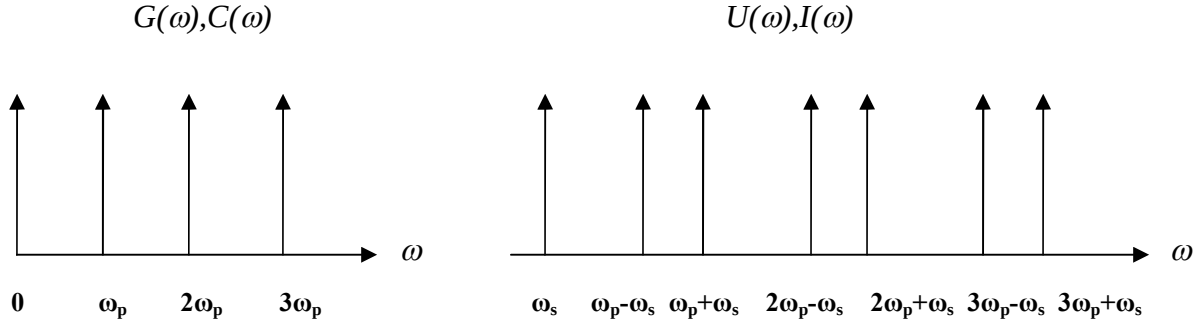

Figure 4.2 Frequency spectrum of large-signal G(ω),C(ω)and small-signal U(ω), I(ω).

The harmonic balance (HB) method is applicable primarily to strongly nonlinear circuit, such as conventional mixer and PPA circuits, Also it has been show to work well in the analysis of optoelectronics circuit [81, 116-118]. HBT can provide great benefits and can be employed to model a versatile DCHPPA receiver that includes both optoelectronic circuit (PPA) and conventional mixer circuit. In the PPA circuit, the HBT will be used to simultaneously model the optical field and the electric voltage, and the work will be extended to model the whole system using a very powerful commercial simulator with the advantage of using the multi-tone/multi-rate harmonic balance technique.

4.3. DCHPPA Circuit Development

4.3.1. PIN Photodiode Model Development

The core element to develop the PPA up-converter circuit model is the photodiode model. Hence, it is essential to have a precise model for the *pin* photodiode, in order to obtain accurate simulation results. *Pin/pn* photodiodes are quite similar in structure to *pin/pn* junction diodes except that their junctions are illuminated with external light, which forms a third “optical” terminal. An equivalent circuit of the photodiode is shown in Figure 4.3. In this model, the nonlinear capacitance of the photodiode is represented by a silicon varactor diode that has highly nonlinear characteristics, as it is one of the basic requirements for parametric amplification. The use of a silicon varactor diode is shown to work well in a conventional parametric amplifier, because the depletion layer capacitance is dependent on the applied voltage, as well as it exhibit a comparatively low level of noise when compared to those using other materials, and particular germanium. The overall series resistance (r_s) of the Photodiode represent the lead resistance plus the bulk resistance as shown below.

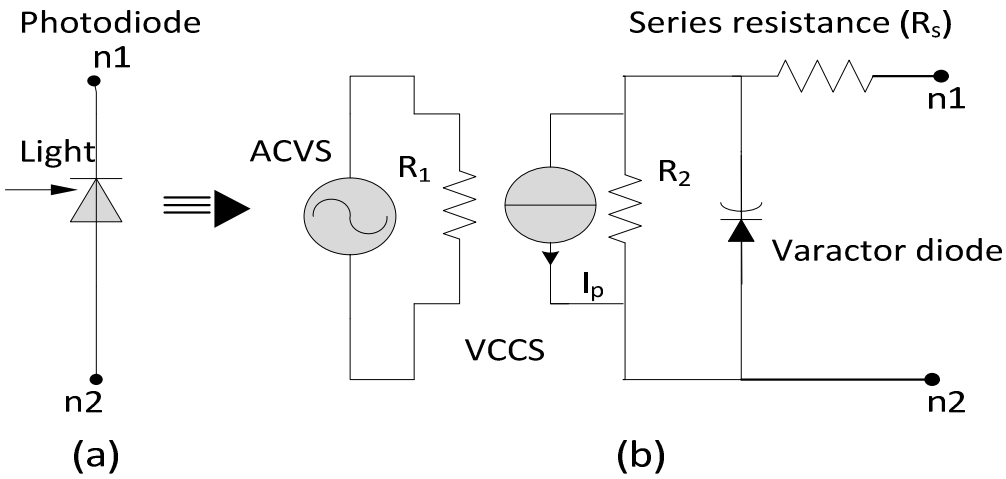

Figure 4.3 An equivalent circuit for photodiode.

Figure 4.3 shows the MWO schematic circuit diagram of the proposal model of the photodiode used in harmonic balance simulation. As can be seen, an AC voltage source (ACVS) is set to represent the incident optical power *Pi*, and allows for an independent specification of the tone number and the fundamental frequency of that tone. The voltage on ACVS is an analog for the optical power in watts incident on the photo detector. The optical signals are modelled as voltage quantities, expressed as a real number, as seen in figure 4.4. Alternatively, the optical signals can also be modelled as electrical power quantities, expressed as a real number in (dBm) using an input port with defined frequency, as it makes better use of the MWO features, particularly in some later simulation scenarios. A voltage-controlled current source (VCCS) with the varactor diode in parallel will represent the fully depleted *pin/pn* photodiode. The VCCS is used for modelling the photocurrent gain; gain M, known also as tranconductance ($M = \frac{\Delta I_{out}}{\Delta V_{out}}$), is set to represent the responsivity *R* of the photodiode (e.g *R*=0.62A/W). VCCS is used to implements the current source, with output photocurrent based on the following equation:

$$I_p = MV \frac{e^{-(jwt + A)}}{1 + j\frac{f}{F}} \qquad (4.13)$$

For an ideal current, the source the frequency *F* is set to zero, so the gain has no frequency dependence, where *A* is the phase offset, *t* is the time delay, *V* is AC voltage magnitude and *f* is the optical signal frequency. The ideal photon counter is impossible to realise in actual practice. A more realistic model of the photodetection process is based on the above formula. Where the ideal photon-to-photocarrier converter known as *photon counting* process [119] is replaced by one with a finite conversion efficiency, represented by equation 4.3 (i.e. equivalents to electrical low-pass filter), to account for the finite response time of a practical photodetector.

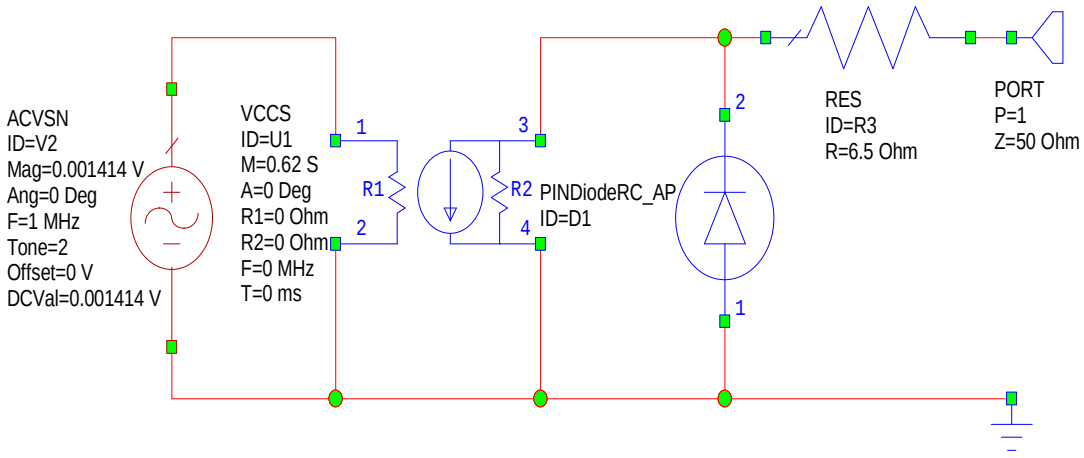

Figure 4.4 Photodiode schematic circuit diagram.

The photo-generated current *Ip* due to the incident optical signal is proportional to the radiant flux density [19]:

(4.14)

$$I_p = RPi$$

where *R* is the photodiode responsivity and is the output photocurrent produced per unit of average incident optical power (*Pi*) in A/W. Both the *R* and *Pi* can be expressed as follows:

$$R = \frac{q\eta\lambda}{hc} \tag{4.15}$$

$$Pi = \frac{hcN_{p_h}}{\lambda} \tag{4.16}$$

Where η is the quantum efficiency, *q* is the electron charge, h *is* the Planck's constant, *c* is the speed of the light, λ is the wavelength, and N_{ph} is the number of incident photons per second. As a result of illuminating the photodiode with an optical signal, the photodiode output current will increase by the amount of photocurrent (I_p) as shown in figure 4.5, thus:

$$I_{ph} = I_p + I_d \tag{4.17}$$

Where I_d is the current through the photodiode in the absence of incident light, known as the dark current.

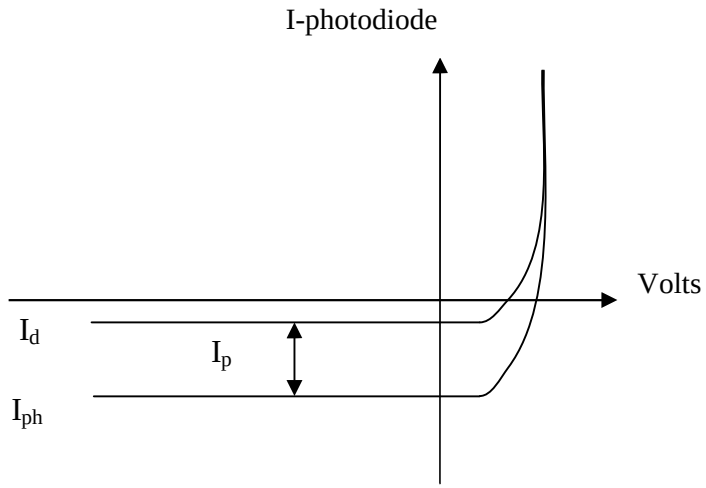

Figure 4.5 Photodiode IV curve with the effect of incident optical power.

As mentioned in the previous chapter, the parametric amplification is based mainly on the nonlinear behavior of the junction diode. There are numerous published works about modeling the *pn* and *pin* junction diode from various aspects; however, this approach is based on the *pin* junction diode model presented in [120, 121]. This model is able to model adequately such important effects as intrinsic layer charge storage, which is the dominate mechanism in governing such *pin* diode behavior as the impedance-frequency

characteristic, the current-dependent carrier lifetime, insertion loss and limiter action. In contrast, the *pin* diode model accurately describes a variety of *pin* diode geometries at high frequency and over a wide range of bias current, including zero bias.

The *pin* diode is characterized by a lightly-doped, so called intrinsic region, sandwiched between a heavily-doped p type and n type region. The *pin* diode full circuit simulator model describing the intrinsic region characteristics, and two *pn* junction elements used to model the *PI* and *IN* boundaries, are shown in figure 4.6 [105].

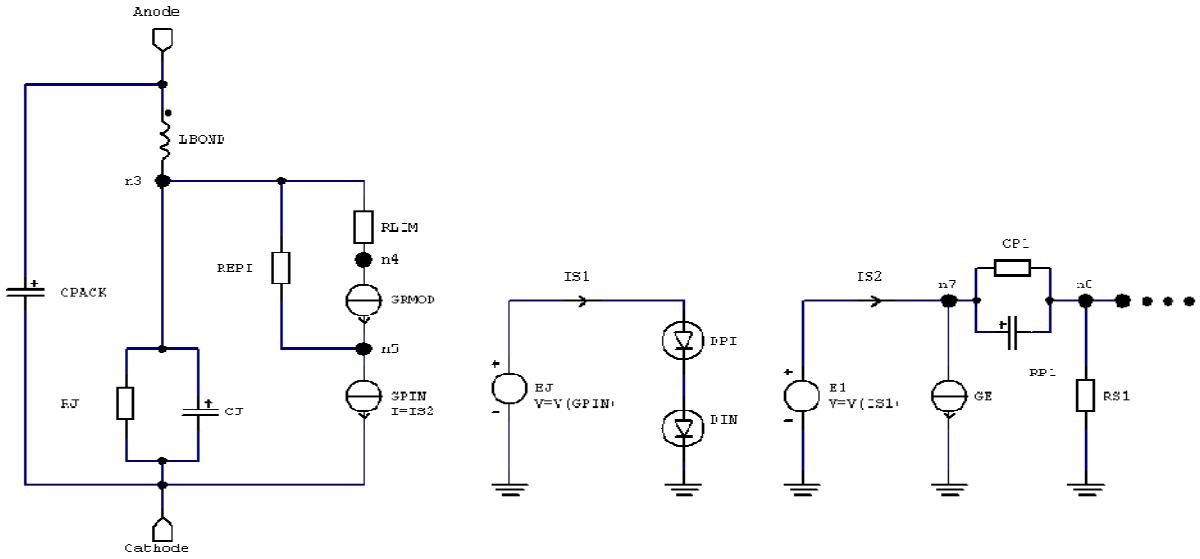

Figure 4.6 Equivalent circuits for PIN diode model: (a) PIN diode equivalent subcircuit, (b) PI and IN junction diode equivalent circuit, (c) two order equivalent circuit of the intrinsic region stored charge, and can be up to 8th order to improve simulation accuracy.

The *PI* and *IN* junctions are characterized by the default MWO nonlinear *PN* junction diodes and are connected in series, thus resulting in *I/V* characteristic for a *PIN* diode. In addition to the junction diodes, there are two more nonlinear elements in the above model, the controlled current source GRMOD and GE, the former describing the nonlinear series resistance, and the latter describing the current-dependent storage time. Their current equations can be found in [105, 121].

The two *PN* junction diodes can be combined into one, if their characteristics are the same. Otherwise the two diodes can be chosen to model the possibility of different reverse saturation currents in the two *PN* diodes, by such effects such as the difference in mesa diameters or surface passivation.

The *PIN* diode output current obeys the following equation [105]:

$$I_{pin} = I_{pi} = I_{in} \tag{4.18}$$

The sum of their voltages is the total voltage across the PIN diode

$$V_{pin} = V_{pi} + V_{in} \tag{4.19}$$

The junction currents are a function of the junction voltages:

$$I_{pi} = F_{pi}(V_{pi}) \quad \& \quad I_{in} = F_{in}(V_{in}) \tag{4.20}$$

These are the functions for the current based on equation (4.14, 4.18). However, the $F_{pi}(\ )$ and $F_{in}(\ )$ are not the same functions because the ideality factor (η) for the diodes N_{pi} and N_{in} are not equal, and can be expressed as follows:

$$N_{PI} = \frac{2N}{(1+B)} \quad \& \quad N_{IN} = \frac{NB}{(1+B)} \tag{4.21}$$

where *N* is the diode ideality factor and *B* is the mobility ratio. Finding an expression for current as a function of *PIN* diode voltage would require solving equations (4.20). It does not have a solution in closed form, as the equations are nonlinear. The MWO circuit simulator solves the currents equations numerically.

Each *PN* junction diode obeys its depletion current equation [105], and can be expressed as follows:

$$I_{d_{pi}} = I_{fr_{pi}} - I_{rv_{pi}} \tag{4.22}$$

$$I_{d_{in}} = I_{fr_{in}} - I_{rv_{in}} \tag{4.23}$$

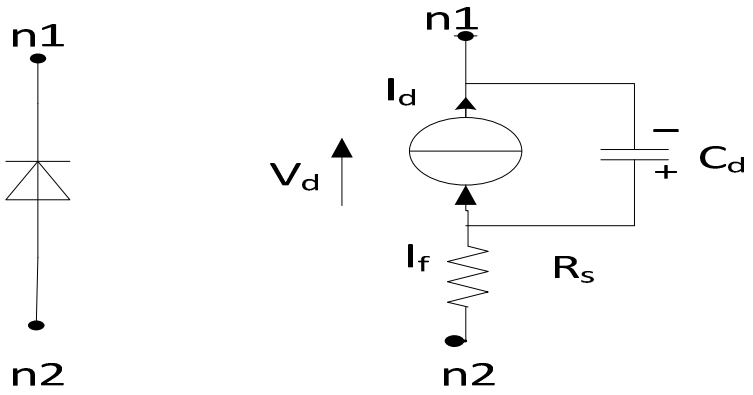

Figure 4.7 PN Diode model

The forward current I_{fr} for each *pn* junction is given by:

$$I_{fr} = a\left(\frac{I_n}{1+\left(\frac{I_n}{I_{KF}}\right)^{0.5}} + K_g I_{SR}\left(exp\ \frac{qV_d}{\eta_R KT} - 1\right)\right) \tag{4.24}$$

Table (4.1) will provide a brief description for each parameter,

Table 4.1 photodiode model parameters.

Parameters	Description
V_d	Voltage across the diode (voltage)
V_j	Silicon junction voltage (voltage)
C_d	Diffusion capacitance (farad)
C_j	Junction capacitance (farad)
C_{j0}	Zero-bias junction capacitance (farad)
C_{pt}	Total packaged capacitance (farad)
V_{BV}	High reverse breakdown voltage (voltage)
I_{KF}	High injection knee current (ampere)
I_{BV}	High reverse breakdown current (ampere)
I_{SR}	Recombination current constant (ampere)
I_{BVL}	Low reverse breakdown current (ampere)
I_s	Saturation current (ampere)
m	Grading coefficient
f_c	Grading coefficient for forward-bias depletion area capacitance formula
η	Emission coefficient of the diode
η_R	Recombination current emission coefficient
η_{BV}	High reverse breakdown ideality factor
η_{BVL}	Low reverse breakdown ideality factor
T	Absolute temperature of the diode (celsius)
a	Relative device area (meter)
q	Electron charge (coulombs)
k	Boltzmann's constant (joules/kelvin)
ρ	Intrinsic region resistivity
ε_r	Relative permittivity
ε_o	Electric permittivity

where I_n in equation (2.24) represents the ideal diode (Schockley) current, given by:

$$I_n = I_s\left(\exp\frac{qV_d}{\eta kT} - 1\right) \tag{4.25}$$

I_s is a proportional constant, called the current parameter (reverse saturation current). I_s can be determined from:

$$I_s = A^{**}T^2W_j\left(exp\,\frac{q\phi_b}{kT}\right) \tag{4.26}$$

Where is A^{**} is the modified Richardson constant (96 cm^{-2} K^{-2} for silicon); W_j is the junction area, and ϕ_b is the barrier height in volts, a constant usually approximately as 0.1 volts greater than the diffusion potential [87].

The expression, k_g , in equation 4.17 describes how the recombination current depends on the junction depletion layer width.

$$k_g = \left[\left(1 - \frac{V_d}{V_j}\right)^2 + 0.005\right]^{m/2} \tag{4.27}$$

The reverser current I_{rv} for each *pn* junction is given by:

$$I_{rv} = aI_{BV}\left(exp\left(\frac{-qV_d}{\eta_{BV}kT}\right) - 1\right)exp\left(\frac{-qV_{BV}}{\eta_{BV}kT}\right) + aI_{BVL}\left(exp\left(\frac{-qV_d}{\eta_{BVL}kT}\right) - 1\right)exp\left(\frac{-qV_{BV}}{\eta_{BVL}kT}\right) \tag{4.28}$$

The *PIN* diode used in this approach is the MWO improved model, with bias and frequency dependent on junction capacitance. The *PIN* junction capacitance frequency dependency is implemented according to:

$$C_j = C_{pt}\left(\frac{1 + \left(\frac{f}{f_r}\right)^2}{\frac{C_{pt}}{C_d} + \left(\frac{f}{f_r}\right)^2}\right) \tag{4.29}$$

Where C_{pt} is the total packaged capacitance and is given as parameter C_j for the *PIN* diode, and f_r is the dielectric relaxation frequency, given by:

$$f_r = \frac{1}{2\pi\rho\varepsilon_r\varepsilon_o} \tag{4.30}$$

The dynamic capacitance, C_d , is nonlinear, and follows the formula:

$$C_d = a\left(\tau\frac{\partial I_f}{\partial V_d} + C_j\right) \tag{4.31}$$

where the first term represents the diffusion capacitance, and C_j represents the junction capacitance, as shown in equation (4.32,4.33).

The AWR tools give the ability to implement the bias dependency in the junction capacitance according to the harmonic Spice formula (equation 4.22), or the AWR harmonic formula (equation 4.23). However, using the AWR formula represents the actual behaviour of the junction capacitance more accurately [105], particularly when a high forward voltage is applied, known as the valley voltage in the tunnel diode. In this approach, the commercial photodiode used in the research does not show the valley voltage changes in the *CV* characteristics, as shown in figure 4.11. Therefore, some of the parameters in the *PIN* diode equivalent circuit model shown in figure 4.6 have to be modified and calculated, and then reset again to match the practical measurements with respect to *CV/IV* characteristics. These parameters can be found in Appendix A1 and A2.

$$C_j = \begin{cases} \dfrac{C_{jo}}{\left(1 - \dfrac{V_d}{V_j}\right)^m} & ,when \quad V_d \le 0 \\ Cjo\left(1 + m\dfrac{V_d}{V_j}\right) & ,when \quad V_d \rangle 0 \end{cases} \tag{4.32}$$

$$C_j = \begin{cases} \dfrac{C_{j0}}{\left(1 - \dfrac{V_d}{V_j}\right)^m} & ,when \quad V_d \le f_c V_j \\ \dfrac{C_{j0}}{(1 - f_c)^m} \bullet \left[\dfrac{-m\left(1 - \dfrac{V_d}{V_j}\right)^2}{2(1 - f_c)^2} + 1 + \dfrac{m}{2} \right] & ,when \quad (2 - f_c)V_j > V_d > f_c V_j \\ \dfrac{C_{j0}}{(1 - f_c)^m} \bullet e^{\frac{m}{1 - f_c} \bullet \left(2 - f_c - \frac{V_d}{V_f}\right)} & ,when \quad V_d \ge (2 - f_c)V_j \end{cases} \quad (4.33)$$

Some of the important parameters to model the *PIN* photodiode are usually given in the manufacturer's data sheet, and some have been obtained from the supplier. However, if some parameters are unknown, they can be calculated or extracted using the AWR manual[105]. Table 4.2 presents some of the important parameters used to model the *PIN* photodiode, based on the Osram commercial photodiode *BPX61* (see Appendix A3 for BPX61 photodiode data sheet). The other parameters related to modeling the *pin* junction diode can be founded in Appendix A1 and A2.

Table 4.2 Some important parameters based on the Osram PIN photodiode.

Parameter	**Value**	**Parameter**	**Value**
Junction capacitance at zero bias	C_j=72 pF	High injection knee current	*Ikf*=5e-5 A
Forward grading coefficient	m=0.45	Respnsitivity	*R=0.62A/W*
Reverse grading coefficient	f_c=0.5	Speed of light	*C=3e8m/s*
Saturation current	I_s=3.5e-11 A	Plank constant	*H=6.63e-34J-s*
Ideality factor (emission coefficient)	N= 1.01	Electron charge	*q=1.6e-19C*
Series resistance	r_s=6.5 ohm	Wave lengthe	λ*=0.85μm*
Barrier potential voltage	V_x=0.552 v	Optical frequency = c/ λ	*3.529e14*

It is important to note that the incident optical power received which can help to determine the photocurrent value at this incident optical power is based on equation 4.14. The incident optical power for the photodiode was measured using an Ealing photometer device with sensitivity factor set to equal 1.776E-2 (cm^2/w) at an RF signal of 1MHz AM modulation signal with 850nm wavelength. The measured optical power P_i=1.414mW. Figure (4.8) shows the photocurrent used to model the optical signal at 1.414mw optical power.

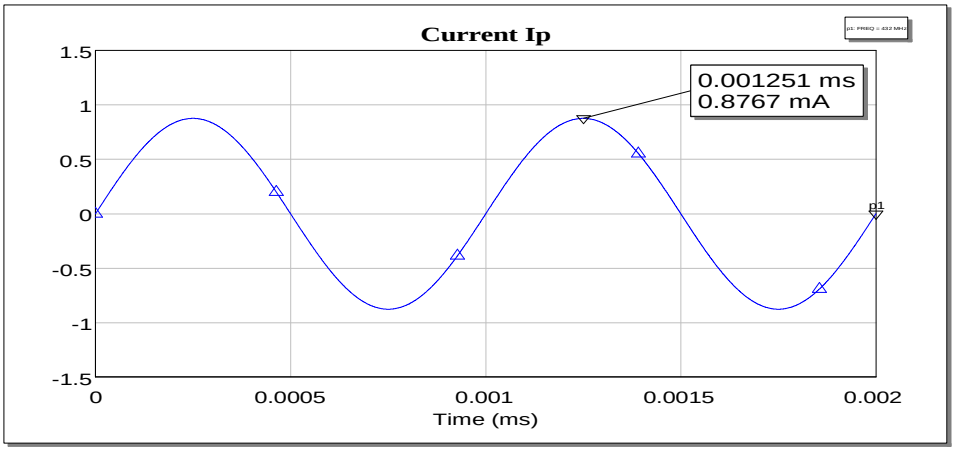

Figure 4.8 photocurrent of 1.414 mW incident optical power at 1MHz optical signal

The photo-generated current (I_p) due to the incident optical signal is proportional to the radiant flux density. Figure 4.9 shows the *IV* characteristic for different incident optical powers, and the photocurrent modelling the photodiode for 1 MHz optical signal at 1.414mW power is equal to I_p=0.877 mA according to equation 4.14.

To validate the model, the *PIN* photodiode was simulated for *DC* analysis at different incident optical powers; the simulation was run seven times for 0 to 5mW, including the 1.414mW optical power received at 1MHz modulated frequency. The simulation results for the *IV* characteristics for the photodiode model are shown in the

figure below. It shows an excellent agreement between the calculations and the simulation result for different optical intensities.

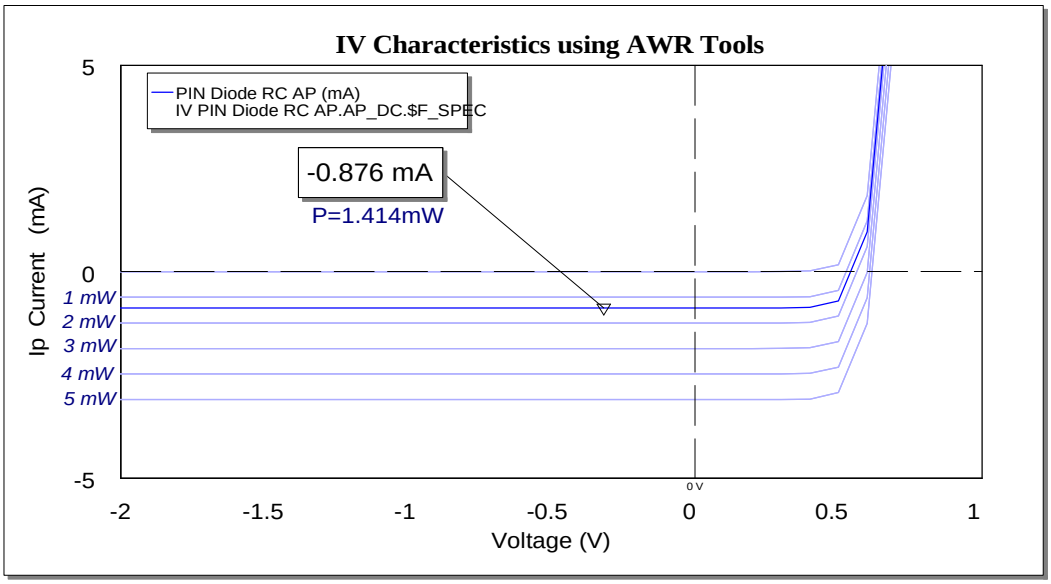

Figure 4.9 IV characteristics at different incident optical power

To verify the nonlinear characteristic of the *PIN* photodiode model, both the simulation and measurement of *IV* characteristics are plotted in figure 4.10; the *IV* photodiode was measured with a simple circuit using a normal current meter. (See Appendix A1 for more details about *IV* simulation setup and source code).

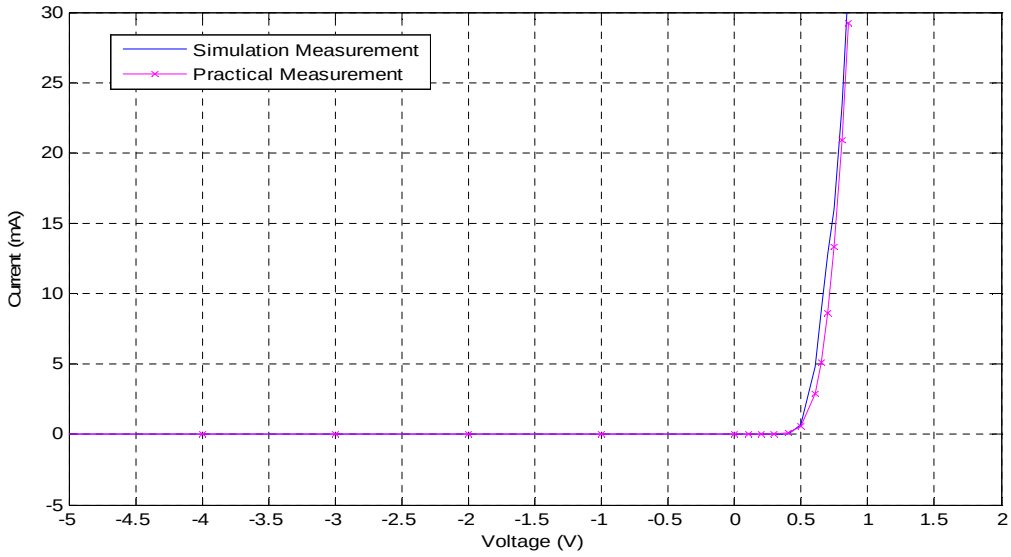

Figure 4.10 Simulation and measurement IV characteristics of the pin photodiode.

Both the measurement and simulation results of the IV characteristics show a very good correspondence, which has verified the validity of the photodiode model with an average of 3% difference between the simulation and measurement results. However *CV* characteristics can be seen as more important parameters to verify the model. This is because the PPA is dependent on the capacitance voltage characteristics of the junction capacitance, as the amplifier conversion gain follows the gradient of the *CV* curve. Higher gain can be achieved if the junction operates at a high steep *CV* curve (zero bias). To verify the photodiode model, junction capacitance has to be nonlinear. Figure 4.11 shows both the simulated and measurement results of the photodiode *CV* characteristics at 1 MHz signal frequency. The measured results were performed by using a capacitance meter (Boonton model BD72) with ±2% accuracy.

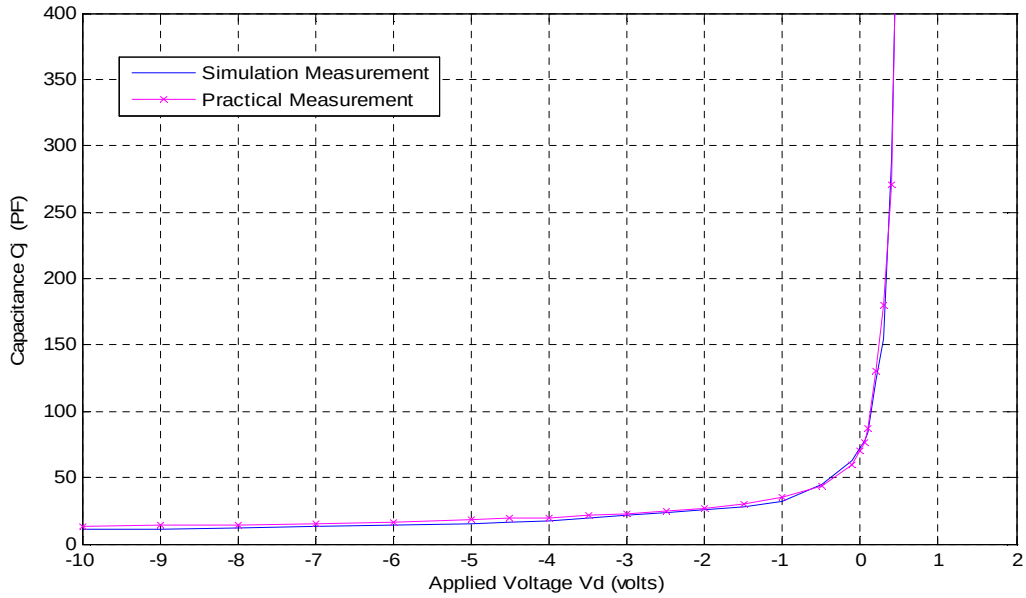

Figure 4.11 Simulated and measured CV characteristics of the PIN photodiode.

The simulation result was based on a circuit diagram showed in Appendix A2 (see Appendix A2 for more details about *CV* simulation setup and source code). As seen from the above graph, the *CV* characteristics of the simulated result showed very close agreement with the measured results. However, there is almost an average of 3%

difference between the simulation and measurement results, depending on the applied voltage. The result shows an excellent correspondence that verifies the validity of the photodiode model.

In addition, to validating the *pin* photodiode, an attempt had been made to model the *pn* harmonic *Spice* junction diode and *pn AWR* harmonic junction diode, based on the bias dependency formula in equation 4.32. Figure 4.12 shows the *CV* characteristics for three different *pn/pin* photodiode models. The plot shows positive agreement with respect to the *CV* curves, and the simulation results in the next section will provide a good indication that the principle of parametric amplification are based mainly on the nonlinear characteristic of the junction diode, and are not based on the *pin* or *pn* structure which has not been found to be the case, as reported in many published papers.

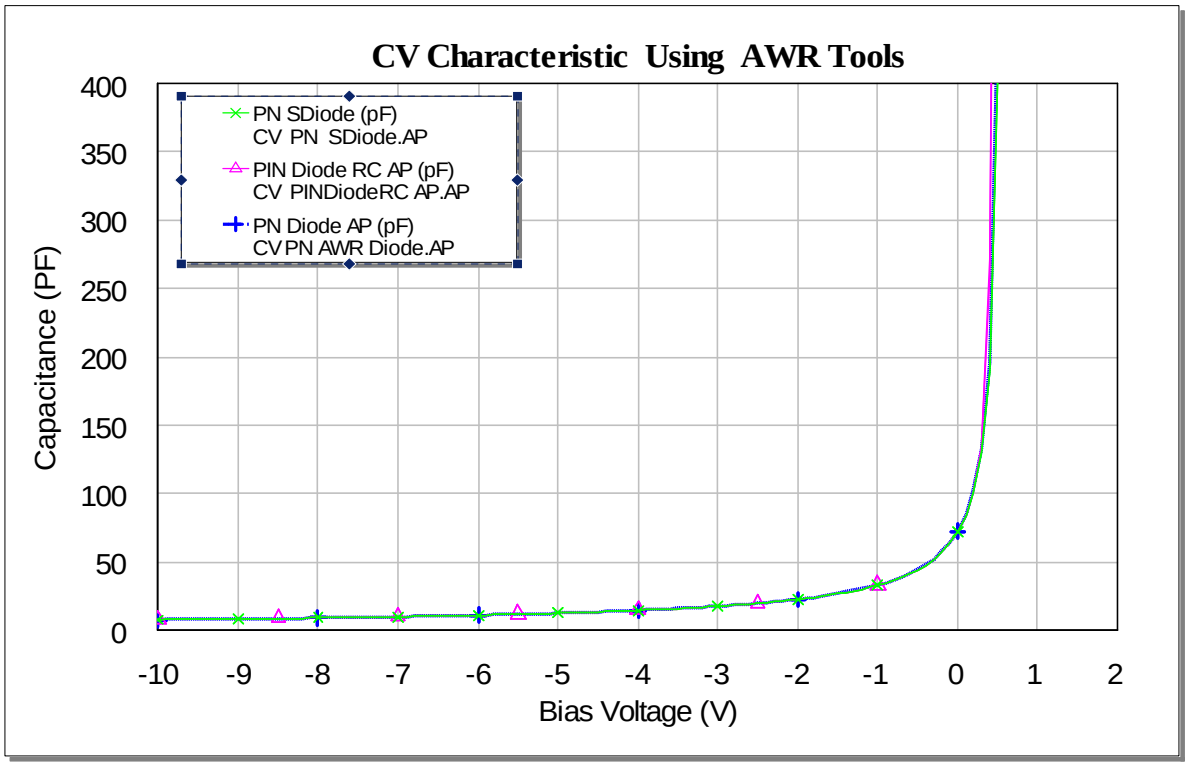

Figure 4.12 Simulated CV characteristics for different junction photodiode.

4.3.2. Double Balanced Mixer Model Development.

The most commonly used mixer for RF/MW frequencies is the double balanced mixers (DBM) of the ring or star configuration. The ring mixer is more amenable to a low frequency application, in which transformers can be used, but it is also practical in high frequency applications [122]. The advantages of a double-balanced mixer over a single balanced mixer are the increased linearity and improved suppression of spurious products; in other words, all even order products of the LO and the RF are suppressed and there is inherent isolation between all ports. The disadvantages are that they require a higher level LO drive, and require at least two transformers (i.e baluns).

The theoretical analysis of the single and double balanced mixer is well established and considered mature[107, 122, 123]. The aim in this section is to model a ring DBM, which can be used as a conventional down-converter mixer to recover the original baseband signal. The designed model is based on a UHF commercial ring mixer configuration (ZAD-1H+) supplied by Mini-circuits, which was used in practical implementation. Figure 4.13 shows the schematic circuit of the ring mixer (ring modulator) model. The circuit consists of two transformers that provide isolation for all ports, and four identical Schottky diodes. Schottky diodes are very fast switching devices, and are ideal for a diode resistive mixer, as they have virtually no minority carrier effects, and provide the best possible conversion loss and noise figure.

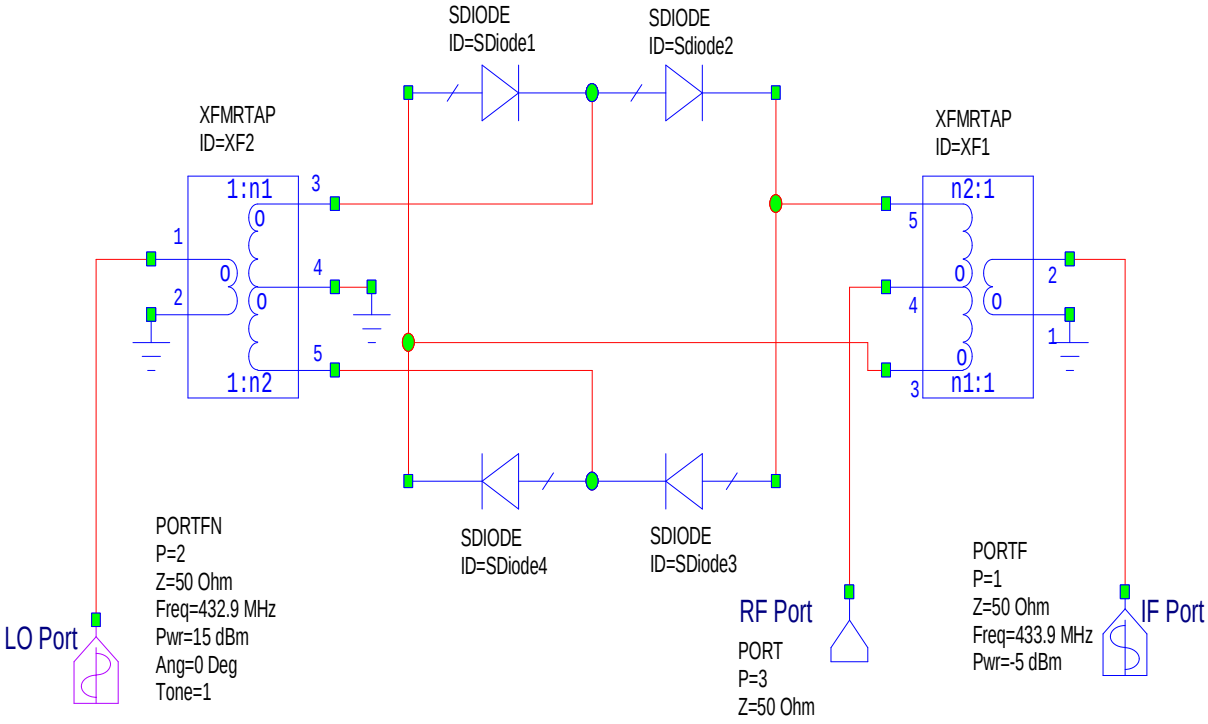

Figure 4.13 schematic diagram of double balanced mixer.

It can be seen from the above schematic diagram that the mixer was configured for 15dBm pumping power (LO port) at 432.92 MHz frequency and -5dBm (IF port) signal power at 433.92MHz. The output frequency of the down-converter mixer (RF port) was the difference between the LO and IF frequency and other spurious products. The *IV/CV* characteristic of the Schottky diode obeying equations 4.25 and harmonic Spice equation 4.32 respectively. Table 4.3 provides some important parameters of the junction diodes that have been used to model the DBM.

Table 4.3 ideal schottky diode parameters model based on AWR tools.

Parameter	**Value**
Junction capacitance at zero bias	C_j=0.13 pF
Forward grading coefficient	m=0.5
Reverse grading coefficient	f_c=0.5
Saturation current	I_s=2.2e-8 A
Ideality factor (emission coefficient)	N= 1.0
Series resistance	r_s=16 ohm
Barrier potential voltage	V_x=0.5 v
High injection knee current	Ikf=0 A

Figure 4.14 shows the conversion loss of the DB mixer model at different LO power levels; for instance, at 15dBm pump power, the conversion loss is about 4.8dB. Figure 4.15 shows the DBM output spectrum of the down conversion mixer. It can be seen that there are no spectral components, and all the even order products of the LO and the RF are suppressed.

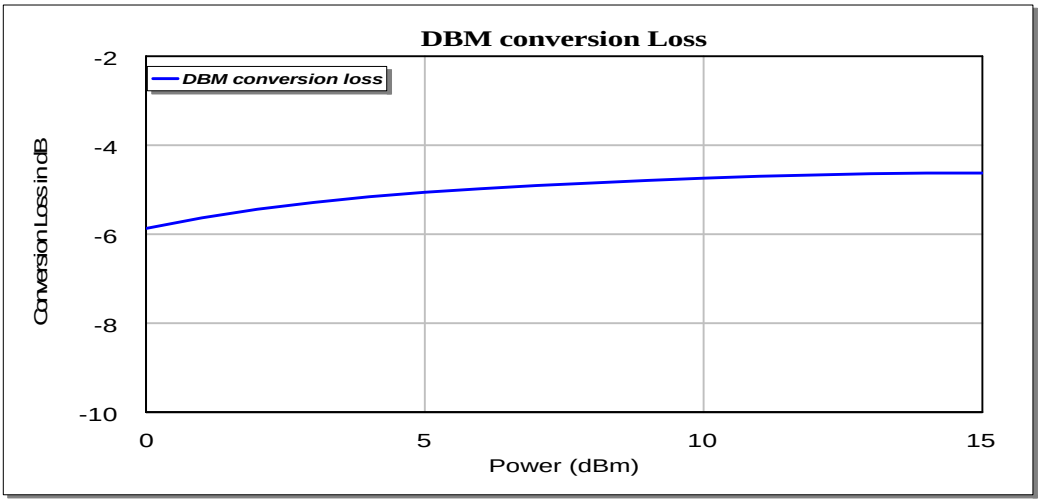

Figure 4.14 Conversion loss of DBM.

However, due to the lack of some technical information from the mixer supplier, such as diode parameters, the mixer model exhibits a 4.8dB conversion loss compared to 6dB for the commercial mixer. In contrast, the model shows a very good result with respect to the down conversion DBM technique and conversion loss, as seen in the graphs below (figure 4.15).

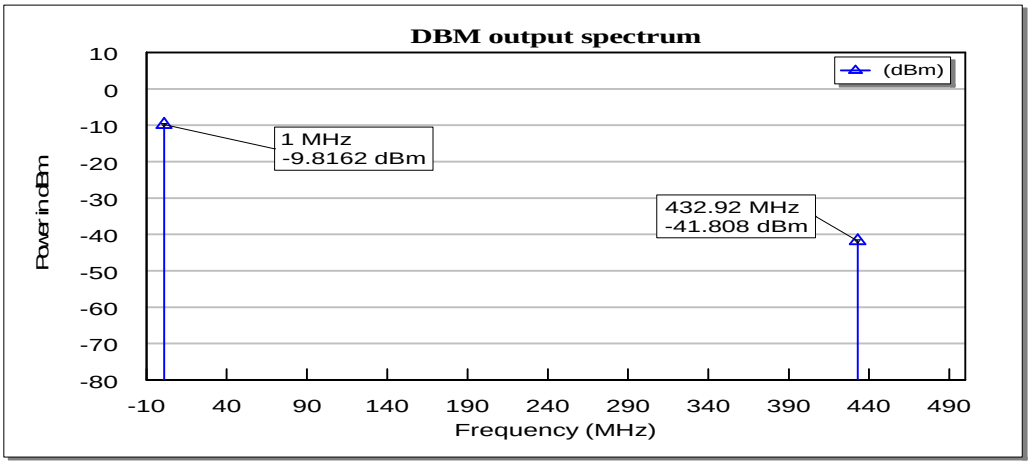

Figure 4.15 IF output spectrum for down converter DBM.

4.4. Simulation Realisation.

Prior to any practical implementation, it is necessary to model and simulate the DCHPPA to optimise the performance of the system. The simulation provides a pictorial view of the interaction of the optoelectronic mixing occurring between the optical signal and the pump signal in up-converter amplifier. It may also predict some other merits that can hardly be recognised in the practical measurement such the effect of grading coefficient and bulk resistor. Moreover, it can also predict the effect of other parameters that may not been considered in the theoretical analysis, as it provides the flexibility to determine the most important parameters that affect the parametric amplification technique. A novel HB simulation technique has been developed here to simulate the operation of the DCHPPA system, which consists of an up-converter parametric amplifier circuit and the down converter mixer circuit. The research aims to use a nonlinear circuit

simulator that examines the circuit's configuration and provides a good, realistic assessment and better performance optimisation.

The simulation was conducted on a Windows XP machine with an Intel core 2 processor of 1.86GHz speed and 2GB of RAM. The HB analysis is based on the AWR HB simulation environment version 8.0 (Microwave Office, USA), used to optimise the performance of the designed model. Multitone HB analysis was used to analyse the DCHPPA receiver; a large signal (LO pump frequency) being set to tone 1, as it is the largest input power signal and the small signal (optical frequency RF) was set to tone 2. The number of harmonics in each tone was set to 2, as the simulation analysis is interested only in the first order of an InterModulation product (beat frequency IM) to obtain the conversion gain. There are a number of important parameters that need to be set to obtain an accurate result when using HB simulation; Nodal algorithm was used for HB analysis, a sparse matrix solver was used for AC/DC analysis, and a trapezoid integration method was used for transient analysis. Moreover, the iteration was set to 25 for the number of attempts to solve the circuit, which guaranteed that no convergency difficulties were found. Moreover, the harmonic order was set to a max of 9, considered as the desired level of Fourier series truncation, and the HB simulator was able to compute its solution waveforms to an adequate degree of accuracy.

4.5. PPA Circuit and Simulation Results

It was important to verify that the circuit model was operating as intended. Performing both HB and AC analysis will enable evaluation of the PPA up-converter in both the time and frequency domains, as well as check the mixing tones (sources) mechanism and observe their parametric amplification output products.

The PPA schematic circuit in the non-degenerate mode was configured as shown in figure 4.16. The circuit was configured to operate in zero bias modes (equilibrium mode). The small input signal was configured for a 1.414mW optical signal, modulated at 1 MHz. The large pump signal had a frequency of 433.92MHz, with a pump power of 15dBm. 50 ohms impedance was used for both source and load ports, as is common for most RF system. The simulation experiments were conducted in the UHF frequency range. These frequencies were determined principally by the convenience of using commercially-available components as well as showing the viability of the theoretical approach, and comparing the simulation results with practical results (see Appendix A4 for more details about up-converter simulation setup and source code).

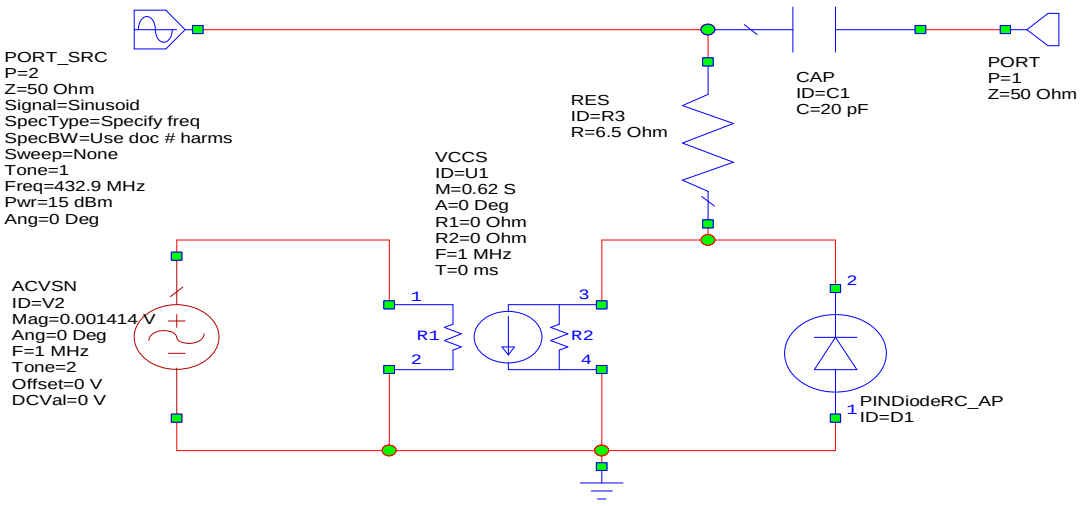

Figure 4.16 schematic circuit for PPA

Figure 4.17 shows the PPA output waveforms in the time domain. The resultant waveforms show the transient curve of pump frequency 432.92 MHz signal with amplitude modulation. There are side tones, with 1 MHz offset around the 432.92 MHz signal. The time domain graph verifies the mixing signals operation, and the waveform shape is a result of a small sinusoid signal, with a smaller amplitude added to another signal of higher frequency and larger amplitude. The resultant waveform varies with time according to the

variation of the lower frequency sinusoidal. Figure 4.18 shows the waveform signal over the nonlinear capacitance. It can be seen that the voltage across the junction capacitance is smaller than that across the *PIN* photodiodes. This is because the voltage across the photodiode represents the sum of the voltages across the series resistance and the junction capacitance (i.e. voltage divider concept).

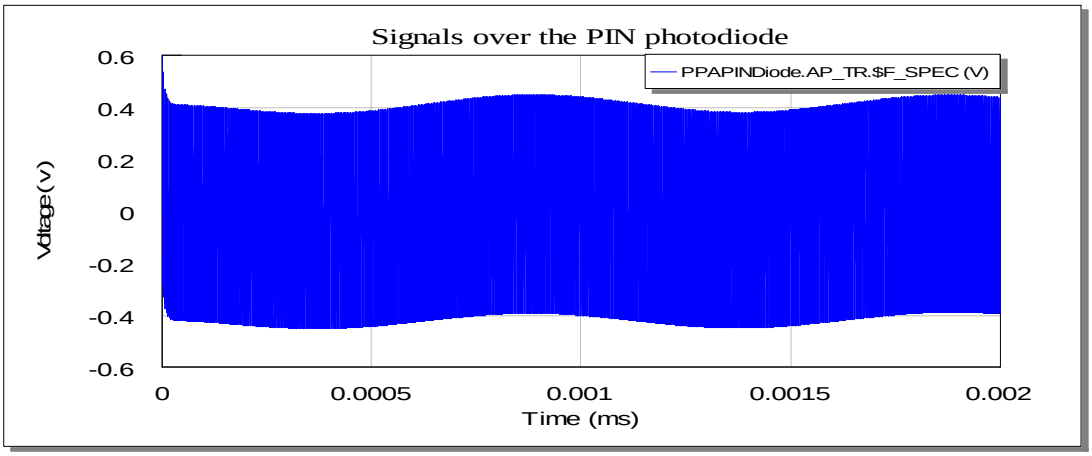

Figure 4.17 PPA simulated output voltages across the up converter load

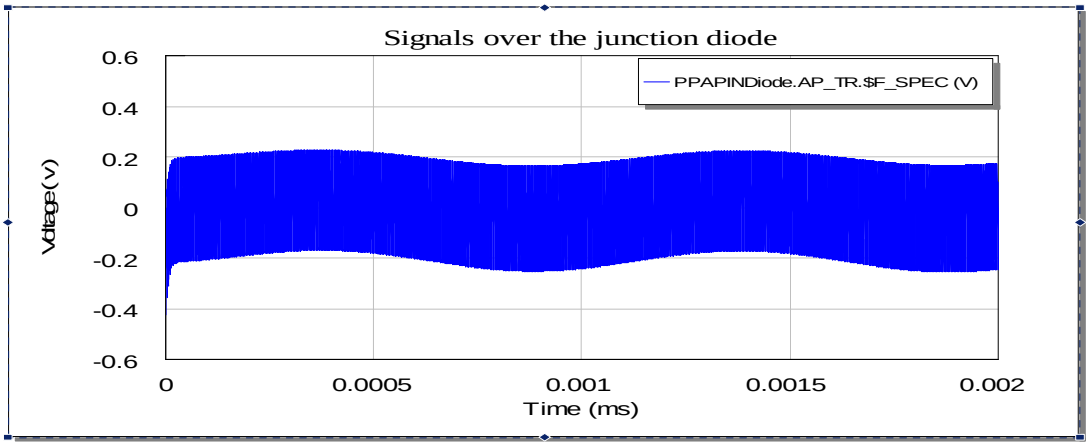

Figure 4.18 Simulated voltage over the nonlinear junction capacitance.

Figure 4.19 shows the simulated frequency spectrum of the PPA up-converter. It can be seen that the baseband signal 1MHz (RF) with -64.2dBm power was pumped by 15dBm electrical power (LO) at a frequency of 432.92MHz. Multitone HB Simulation results show that the optoelectronic mixing at the junction are the result of both upper and lower side band intermediate frequencies (IF) and their harmonics. A 23.81dB of up-

converter gain at 433.92MHz (IF) was predicted. The spectrum graph was limited to plotting only the first harmonic intermediate modulation (up/down converter), the pump frequency and the optical modulated frequency. Various tests were performed to validate the PPA model, such as operating in DD/IM mode, where the sole input is the RF signal without the pumping signal. Another mode is where is the sole input is the pump signal, without a photo detection current.

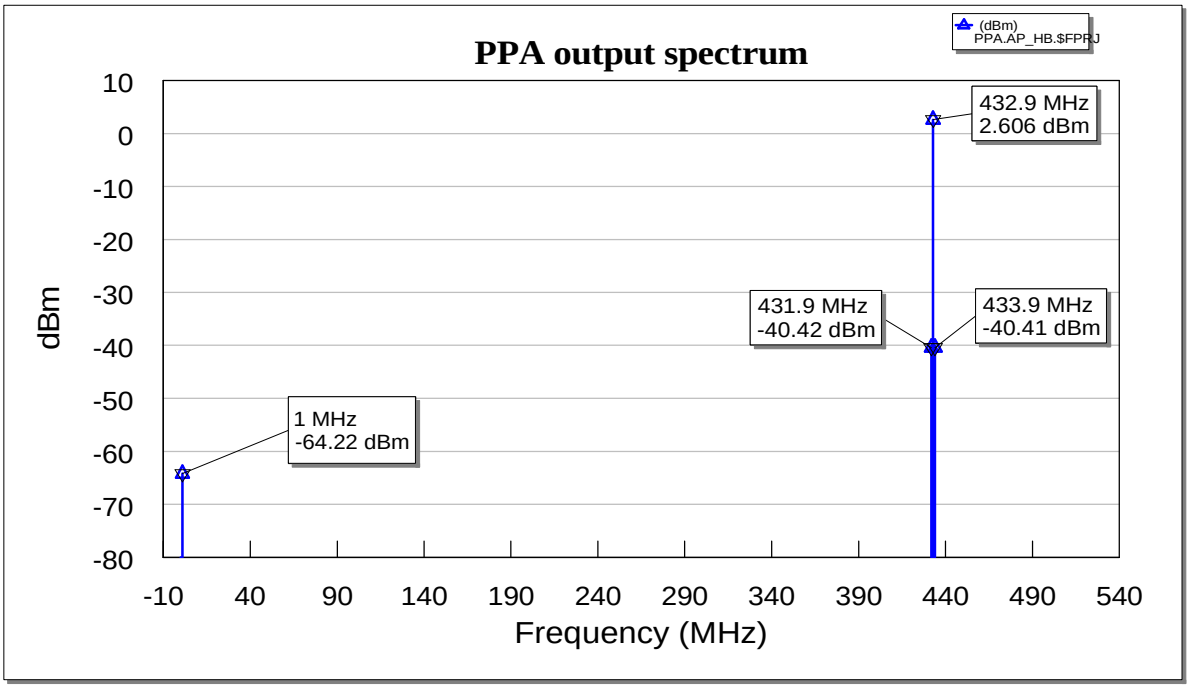

Figure 4.19 Simulated frequency spectrum of PPA up converter.

Figure 4.20 shows the frequency spectrum for three different photodiode models, based on *pn/pin* structures where the same junction parameters were used and their CV characteristics were shown in figure 4.12. The results indicate that the parametric amplification is based mainly on the *CV* characteristic of the photodiodes, and is not on the structure of PD as a *pn* or *pin* type. However, the latter can be seen as much better for frequency response and photo-detection efficiency.

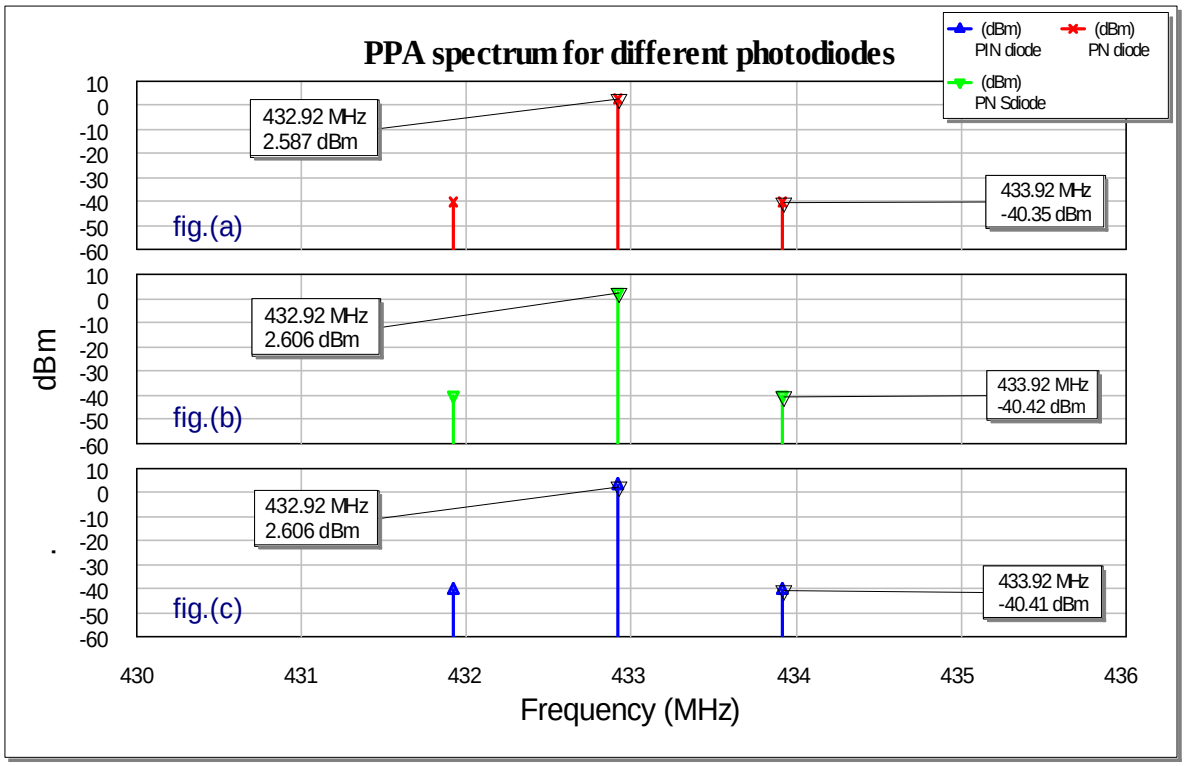

Figure 4.20 simulated frequency spectrum of PPA up converter for different pn/pin photodiode (a) pn photodiode, (b) pn spice photodiode, and (c) pin photodiode.

A number of different simulation scenarios were performed which were more helpful in validating the theoretical analysis in the previous chapter, as well as predicting other parameters that can affect PPA performance with respect to conversion gain. The same PPA schematic circuit entities were used in the flowing scenario unless stated otherwise. (See Appendix A3 for more details about the simulation setup).

4.5.1. PPA Gain versus Various Bias Voltages.

The schematic entries of the PPA model shown in figure 4.16 were used in addition to a bias-T circuit to supply the bias voltage from a DC source voltage. The DC bias voltage was varied from 0 to -15 volts, with 16 simulation points. Figure 4.21 shows that the gain gradually reduced when the reverse bias voltages were increased. The simulation results show that the maximum conversion gain can be achieved at zero bias voltage

(equilibrium mode), where 0 dB gain was predicted at -24 volts, and a reverse bias voltage as illustrated in figure 4.22. According to both figures, it can be seen that the gain drops from 23.8dB to 18.23dB with respect to the reverse bias voltage of 0 volts and -1 volts respectively; the gain then starts to decrease gradually based on how steep the CV curve was. This is in excellent correspondence to verify the proposed zero bias mode approach (equilibrium mode), where the junction behaves in a highly nonlinear way, as predicted in the previous chapter. (See Appendix A5 for simulation setup and source code).

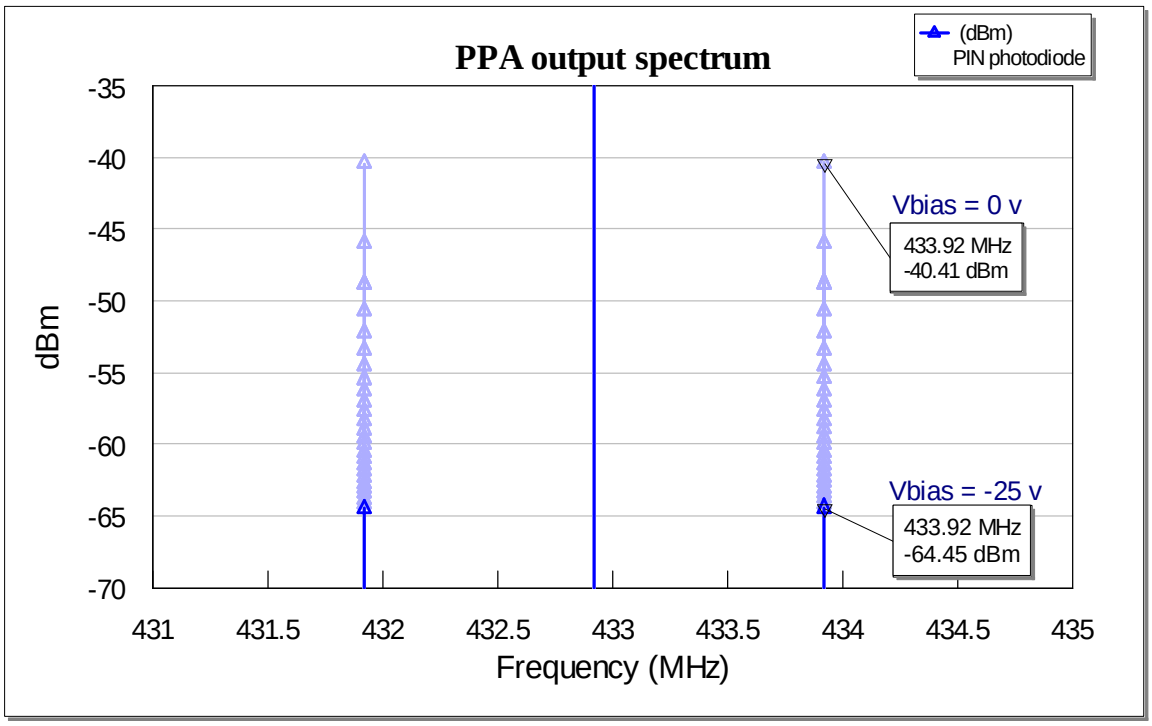

Figure 4.21 Simulated frequency spectrum of PPA up converter for various bias voltages.

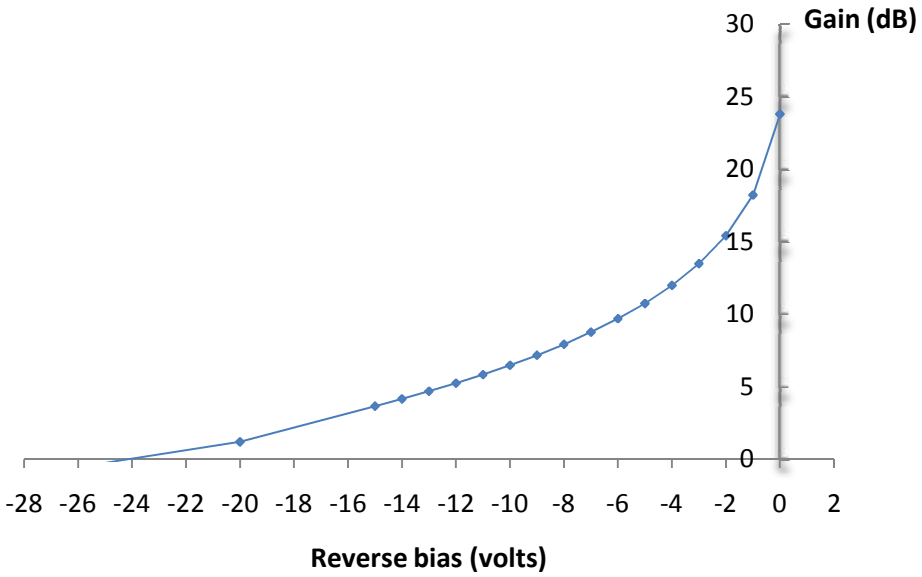

Figure 4.22 Up converter gain for various reverse bias voltages.

4.5.2. PPA Gain versus Various Pump Power.

In this scenario**,** the same schematic entries of the PPA model shown in figure 4.16 were used. The simulation was performed by varying the pump power from -10dBm to 27dBm with 37 simulation points, as shown in the simulated frequency spectrum below in figure 4.23. The PPA up converter gain variation with respect to pump power level is shown in figure 4.24. The gain increases linearly with LO pump power, and the PPA operates as an ordinary linear amplifier. At the low LO pump, with the amplifier conversion gain observed at around -8dBm power, the gain initially increases reaching a maximum value and then decreases after the compression point. The 1 dB gain compression occurs at around 25dBm pump power, where 30.85dB gain was achieved; the amplifier at this stage behaves as a nonlinear amplifier.

Increasing the pump after compression points results in no increase in gain and at some points, starts to decrease, this is because the LO voltage over the photodiode has overcome the barrier potential voltage of the PD and causes an undesirable forward current

to flow through the PD. However, it has been shown that the compression point occurs at a higher pump level when the photodiode operates at a high DC reverse bias voltage, as shown in figure 4.25. This is because the variation of LO voltage over the photodiode will be greater, and therefore this greater LO pump will not cause any an undesirable forward current to flow through the PD. In contrast, at the same power level in both scenarios (i.e. Zero bias mode, -1v bias mode), a better gain was predicted at zero bias mode.

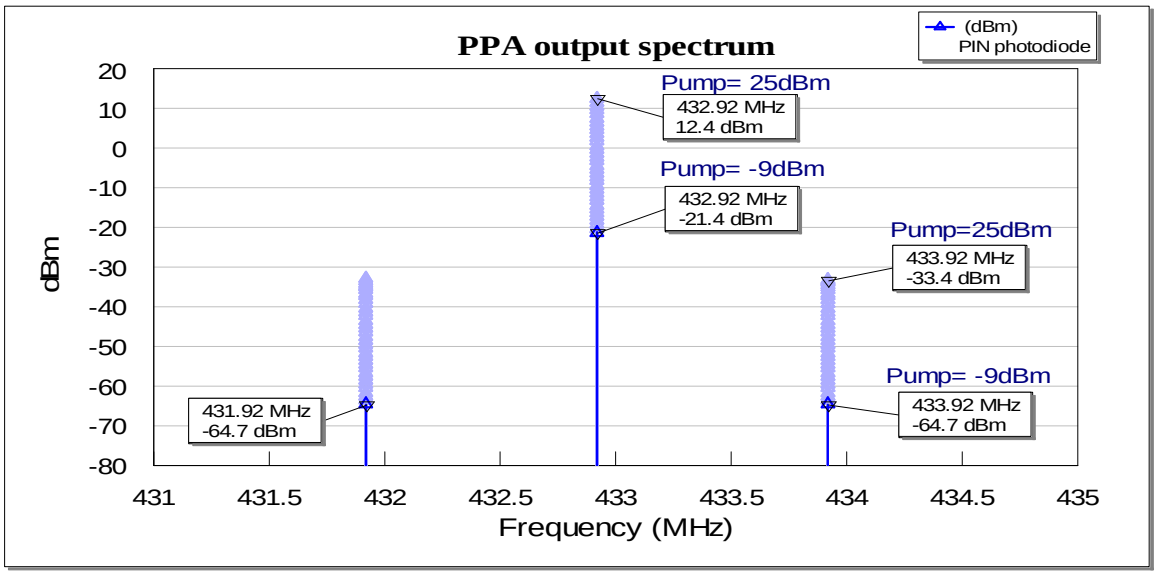

Figure 4.23 Simulated frequency spectrum of PPA up converter for various pump power.

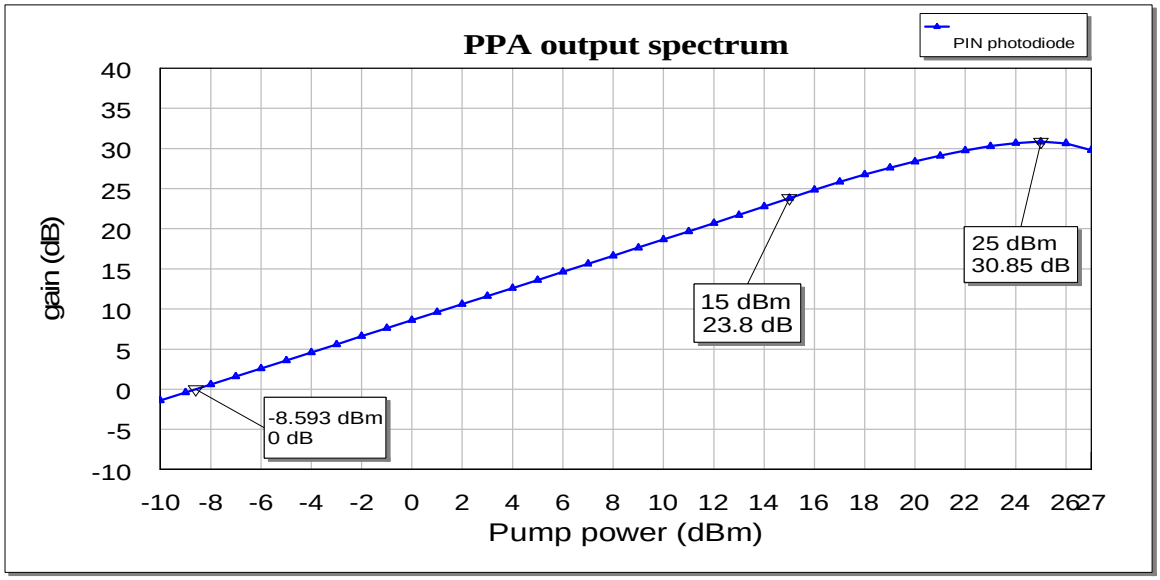

Figure 4.24 PPA up converter for various pump power.

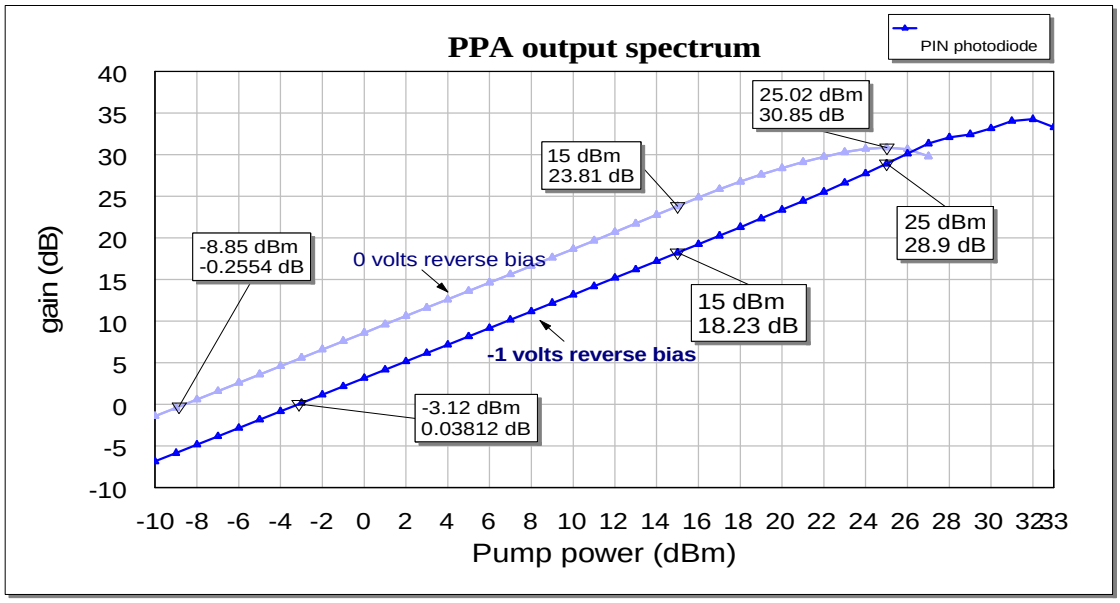

Figure 4.25 PPA up converter gain for 0 and -1volts bias at various pump power.

According to the above graphs, the simulation results show that the gain is directly related to the pump power. As the LO pump increases, so the PD current will increase too, resulting in extra shot noise which can affects the noise figure of the PPA. HB analyses show that the gain is a function of the pump power, as predicted in the aforementioned theory analysis. The signal at idler frequency has been boosted due to energy transfer from the pump signal to the first harmonic frequency, known as power flow in a conventional parametric amplifier. In addition, the gain increases with pump power below the compression point, and the compression point occurs at high pump power when PPA operates under DC reverse bias compared to the PPA in equilibrium mode.

4.5.3. PPA Gain versus Various Optical Frequencies and Optical Intensity.

The PPA signal theory analysis in the previous chapter has shown that the up-conversion gain was dominated by the ratio of the upper side band frequency over the optical frequency (f_i/f_s). It is necessary to simulate the PPA for various optical signals. To

do this, the PPA schematic entries shown in figure 4.16 were used; the HB simulation was performed by varying the DD modulated optical frequency from 1MHz to 20 MHz with a 1MHz interval. Figure 4.25 shows that a number of different modulated optical signals (RF) were received by the photodiode, for 1.414mW incident optical power.

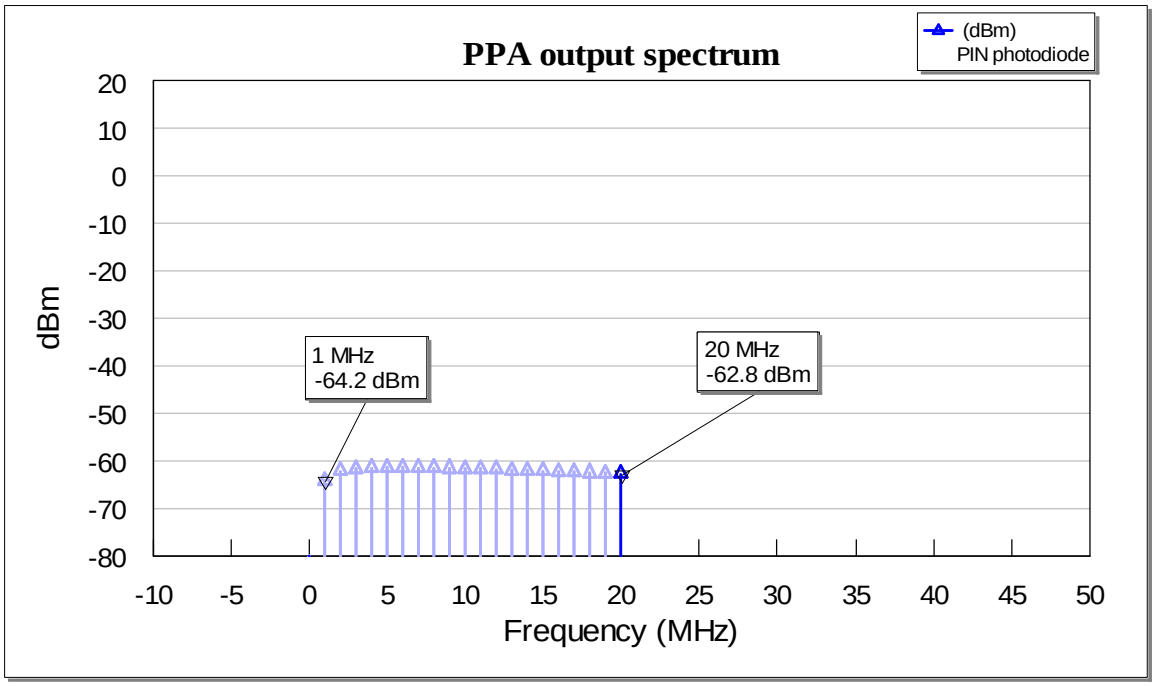

Figure 4.26 simulated frequency spectrum for various modulated optical signals.

These received signals are based on the photocurrent gain equation 4.13, where the gain has frequency-dependence which represents a non-ideal LED transmitter with respect to photodiode frequency response, and the output RF received signals was measured with a flatness of ±2dB in this frequency range. This can verify the frequency response of the modelled input optical frequency with the practical measurement of the photodiode frequency response, as shown in the next chapter.

Figure 4.27 shows the PPA up-converter output spectrum for various RF input signals. It can be seen that the highest gain was achieved by the RF signal frequency at 1MHz, with a gain of 23.8dB. The gain starts to decrease gradually by increasing the RF signals, as illustrated. It has been shown that no gain will occur if the PPA detects a higher

RF signal frequency than 19 MHz. The PPA conversion gain starts reducing for 20MHz RF signals, with 0.68dB gain loss. The gain will decrease according to the increase in RF signals, as predicted in the theoretical analysis, where the gain is proportional to the ratio of (ω_i/ω_s).

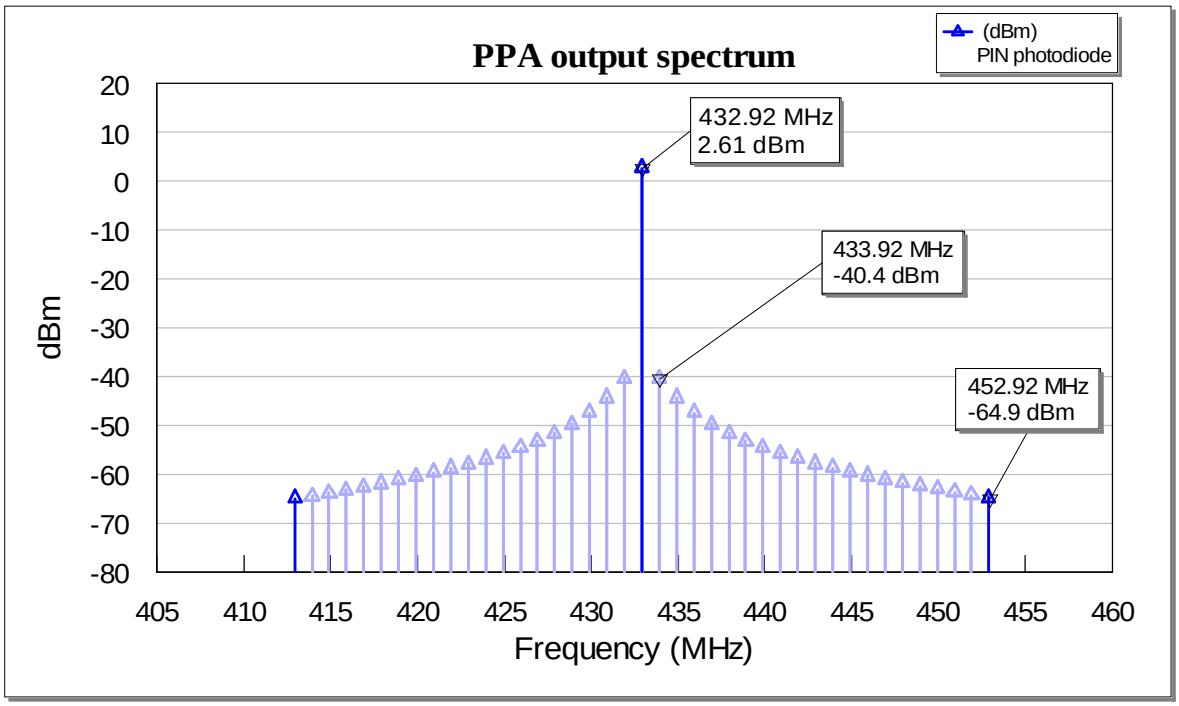

Figure 4.27 Simulated PPA up converter spectrum for various RF signals

The simulation was repeated for various pump powers at 432.92MHz, with various optical RF signals, as shown in figure 4.28; it can be seen from the graph that the predicted gains for various RF signals 1MHz, 5MHz, 10MHz, 15MHz, 20MHz were proportional to the pump signal. For instance, at the 5MHz optical signal, the conversion gain started to occur when almost 2.7dBm pump power was applied; however the PPA works as a conventional mixer with conversion loss at low pump power (i.e pump < 2.7 dBm). In contrast, the gain is inversely proportional to the RF signals, as predicted in the signal theory analysis.

In addition to the above analysis, the HB simulation investigated the effect of the RF signal power on the PPA conversion. The simulation was repeated by varying the detected RF signal for 1mW to 9mW optical power, with a 2 mW interval. Figure 4.29 shows the output spectrum for the PPA. It is clear that the gain is proportional to the detected RF power signal.

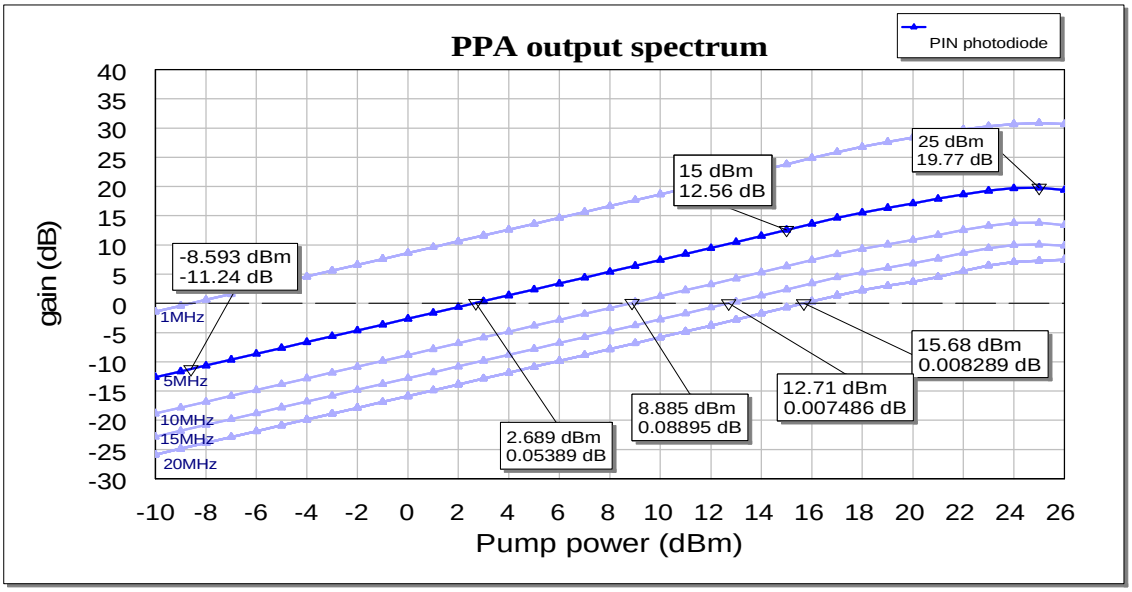

Figure 4.28 Simulated PPA conversion gain at various RF signals.

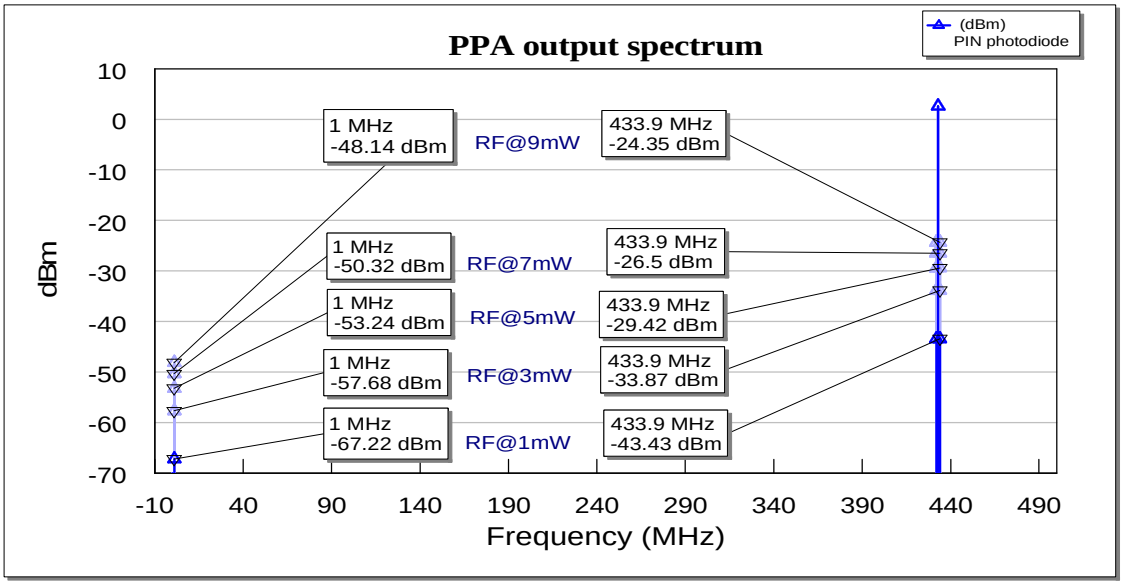

Figure 4.29 Simulated PPA up converter spectrum for various RF power level.

4.5.4. PPA Gain versus Various Pumping Frequency.

In continuing to analyse the effect of the pump frequency to the RF optical frequency as mentioned in previous section, the PPA circuit was simulated by varying the pump frequency from 100MHz to 1000 MHz, with 10 simulation loops to obtain the up-converter gain at idler frequencies. The simulation was repeated for three different scenarios: firstly, the experiment was run with 15dBm pump power at 1MHz detected RF signal; secondly, the pump power was set to 5dBm for 1MHz detected RF signals; thirdly, the pump power was set to 15dBm with a 10MHz detected RF signal. Figure 4.30 shows the spectrum analysis for the PPA converter at various pump frequencies. The gain at fixed input pump power (i.e. 15dBm) was not always found to be proportional to the ratio of pump frequency to RF frequency, as reported in [37, 82, 99]. However, on the signal theory analysis, the up-converter gain is a trade off between the ratio of pump frequency and the RF frequency, in addition to the amount of pump power applied to the junction capacitance at pump frequency. Indeed, the PPA operates as a voltage divider; the pump voltage to the PD is divided between the bulk resistance and the capacitive reactive impedance, obeying the voltage divided concept.

In contrast, applying a high frequency pump will reduce the capacitive reactance impedance, which results in decreasing the varying voltages over the reactance impedance (i.e. increase the voltage over the bulk resistance), as shown in time domain analysis in figure 4.31. It can be seen from the graph that three pump frequencies were used for simulation, being: 241MHz, 432.92MHz and 900MHz. The output signal applied to the junction capacitance varied with different pump frequency. Parametric amplification was based mainly on the variable nonlinear capacitance. Therefore low capacitance variation, even at high frequency pump, will not always lead to optimum conversion gain, as shown

in figure 4.30. To achieve high gain at high pump frequency, a large pump power is required.

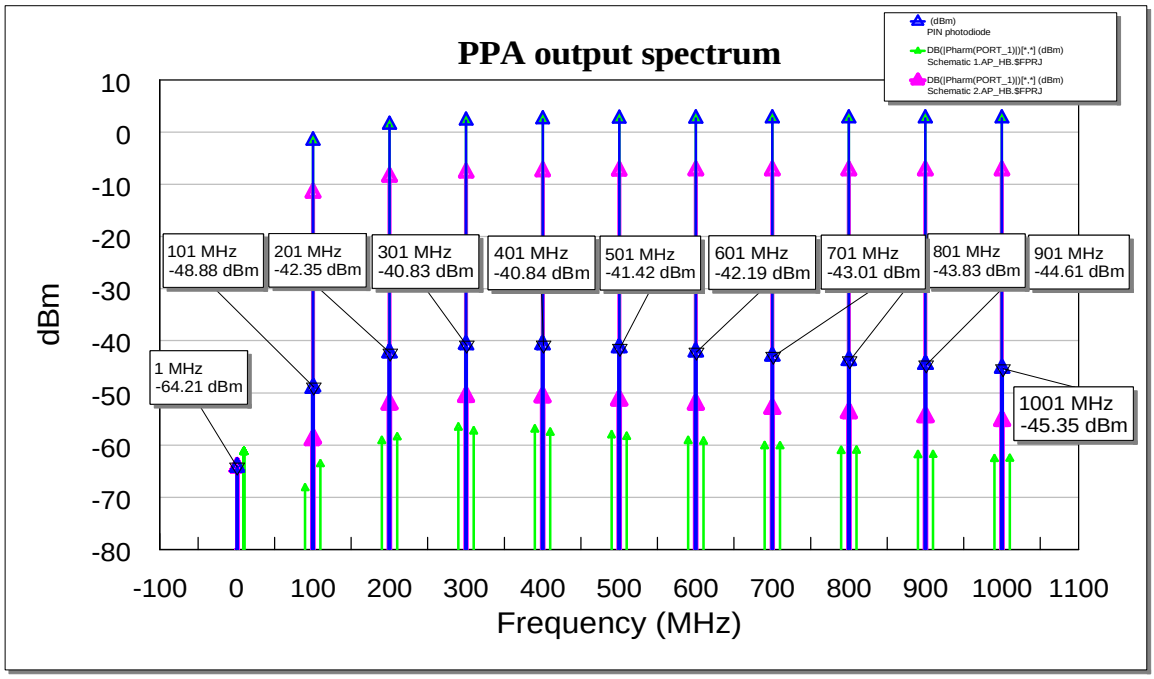

Figure 4.30 Simulated PPA converter spectra for various pump frequencies. Scenario 1(blue colour), scenario 2 (red colour) scenario 3 (green colour)

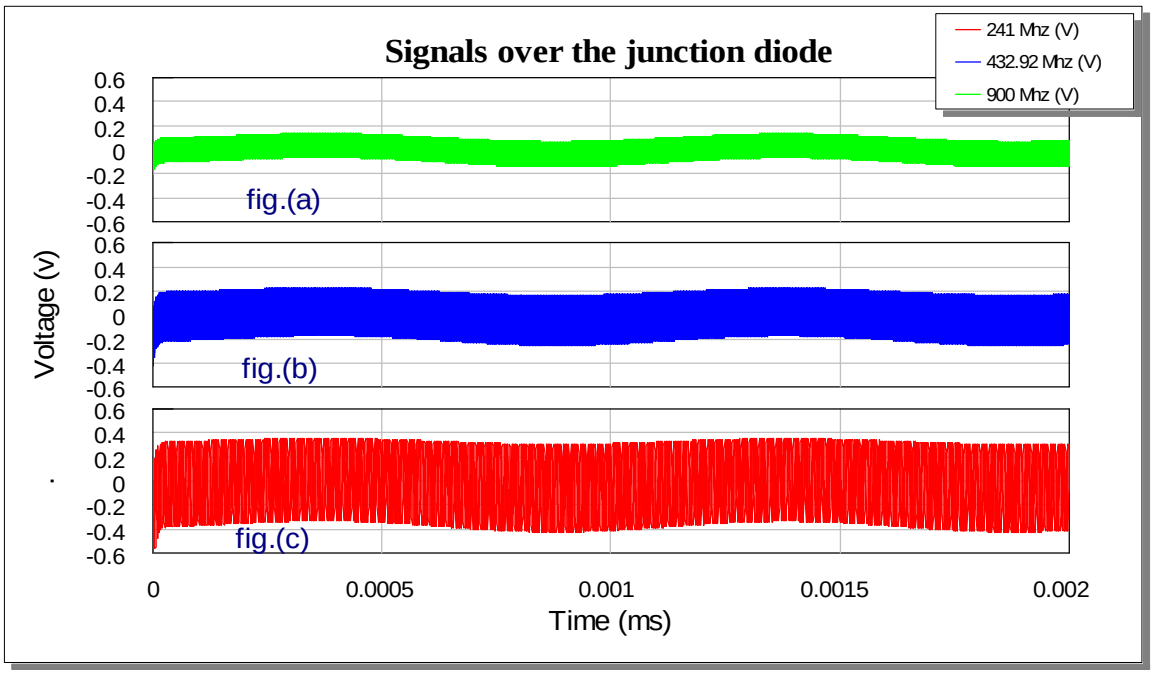

Figure 4.31 Output voltage applied to the junction capacitance at various pump frequencies.

In addition, the PD bulk resistance (r_s), is also known as one of the key elements in the PPA noise figure, and can also have a direct effect on conversion gain; hence, the lower r_s is the better for conversion gain, as shown in figure 4.32. The PPA was simulated by varying the value of series resistance from (1,6.5,20,100,200,300) ohms, with six simulation loops, at 15dBm pump power. The graph depicts that, if the PD has a bulk resistor over 300 ohms; the PPA starts working as a conventional mixer with conversion loss. According to the above analysis, the simulation analysis was found to be in good agreement with the analytical gain expression given in the previous chapter.

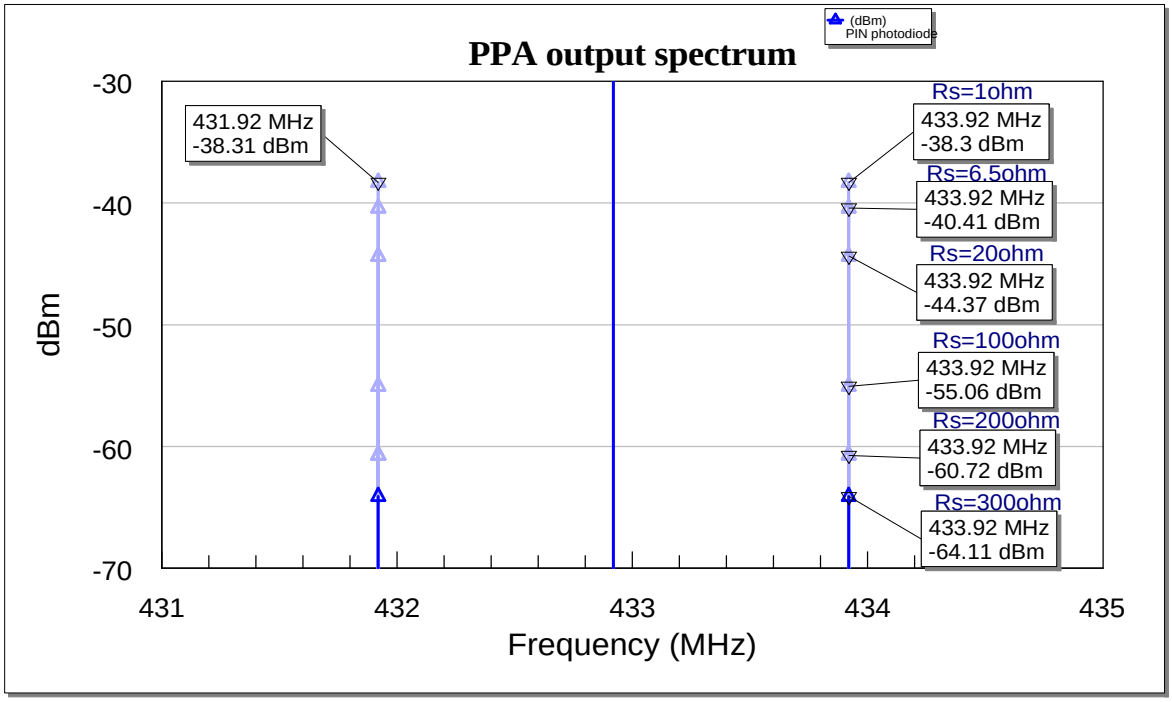

Figure 4.32 Simulated frequency spectrum of PPA up converter for various series resistance.

4.5.5. PPA Gain versus Various Grading Coefficients

A variable capacitance junction may be referred to as abrupt, hyper abrupt, or super hyper abrupt. These refer to the change in junction capacitance by changing the applied voltage. These junctions offer a relatively large change in capacitance which is more

desirable for parametric amplification, and can also be seen as a disadvantage for PD application with respect to photo detection efficiency and frequency response. For instant, a relatively large change in C_j can enhance harmonic levels [124, 125]. Varying the applied voltage of abrupt junctions over the rated limits, can change capacitance by a 4:1 ratio (i.e *m=0 to 0.5*), hyper abrupt by 10:1 (*m=0.5to 1.0*), and super hyper abrupt by 20:1 (*m=1 to 2.0*) where *m* represents the grading coefficient. For instance, a diffused junction with linear technology *(m*<0.33) is not desirable for parametric amplification.

A super hyper abrupt photodiode, known as a retrograded junction, is more favourable for a PPA due to the large steepness in the CV curve. PD with super hyper abrupt junction gives a highly steep CV curve, particularly at zero bias voltage. HB simulation was used to investigate the effect of the grading coefficient (*m*) on the PPA conversion gain. The simulations were run by varying the value of *m* from (*m*=0.1 to 2.0), with 20 simulation points, as shown in figure 4.33; high gain can be achieved when *m*=2.0. Figure 4.34 predicted the gain slope at various *m* values. The gain increases linearly with *m* as expected, and corresponds to junction *CV* curve behaviour. When the CV curve gets steeper and steeper, further gain can be achieved. As mentioned in signal theory analysis, the value of *m* was assumed to be a default value in the CV equation, which is equal to (*m=0.5*). The HB simulation tools predicted the effect of the grading coefficient to the conversion gain, as it can give up to 40%, compared to the theoretical analysis, as shown in figure 4.33. By applying curve-fitting techniques, as shown in Appendix A6, the curve fitting function for various *m* can be presented in the form of:

$$f(m) = a + bm + cm^2 + dm^3 + fm^4 \qquad (4.24)$$

where *f(m)* represents the gain correction factor, and constant a= 3.9E-04, b = 2.1E+00,c =2.5E-01 and d =-1.6 . According to the above analysis, the PPA corresponding conversion gain can be predicted in the form of:

$$\text{Gain (A)} \approx \text{Gain}_{(theory\ analysis)} \cdot f(m)$$

The analysis predicts that the up-converter gain is directly dependent on the pump frequency (ω_i/ω_s), consistent with Manley and Rowe analysis, and is also dependent on the input pump power across the nonlinear capacitance, and is highly related to the photodiode characteristic such as bulk resistor, reactance impedance at pump frequency and the type of abrupt junction with respect to the grading coefficient value.

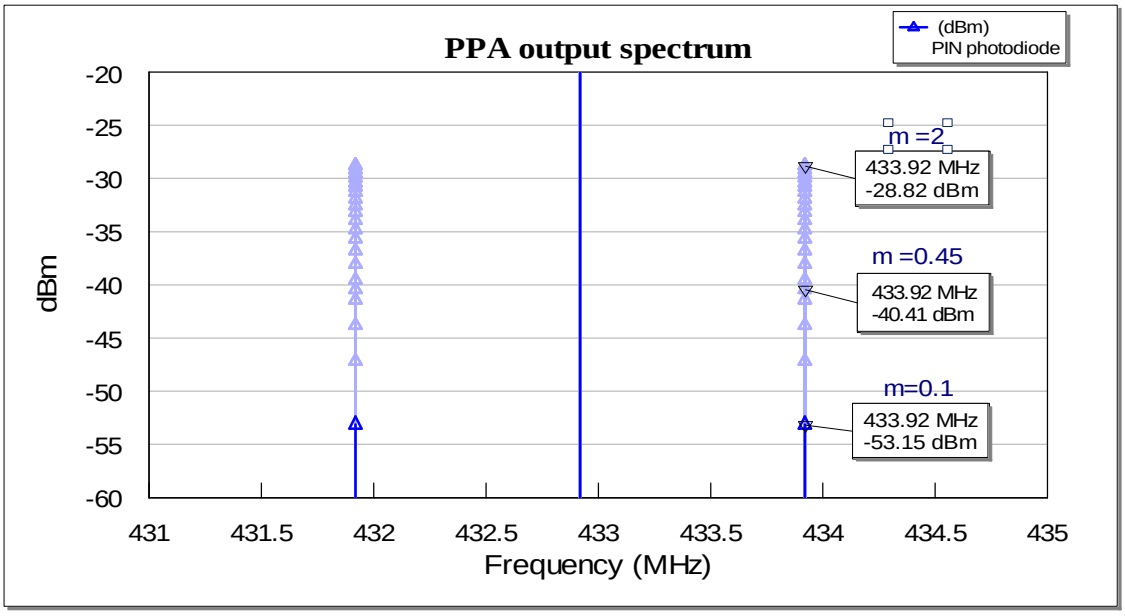

Figure 4.33 Simulated spectrum of PPA up converter for various grading coefficient (m).

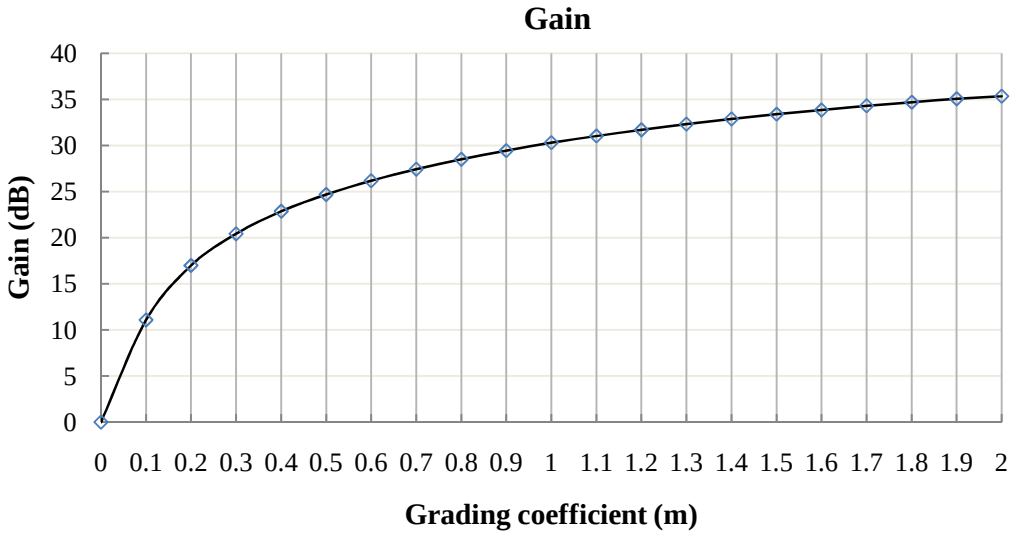

Figure 4.34 PPA up converter gain for various grading coefficient (m)

4.6. DCHPPA Circuit and Simulation Results

The schematic circuit diagram of the DCHPPA is shown in figure 4.35. The optical receiver consists of a double heterodyne conversion system, representing the pre and post-front optical receiver. The pre-front optical circuit (stage one) consists of a PPA circuit, which translates the received signal spectrum from the optical carrier frequency to an upper IF, at which detection, amplification and optoelectronic mixing can be done with single PD. The post-front optical circuit (stage two) consists of signal processing (IF filters) and a down-conversion mixed (DBM) circuit, which passes only the desired IF frequency and performs down-conversion mixing to recover the original baseband. A full description of the design of DCHPPA and system analysis will be covered in the next chapter. The DCHPPA receiver model consists of a PPA circuit, DBM circuit, 5^{th} order LC low pass Butterworth filter circuit (LPF) that has a maximally flat amplitude response, as shown in figure 4.37 [123, 126] .Two functional block, bandpass filters (BPF) provided by the AWR simulators were employed for the design of the bandpass SAW filter, which was implemented in a practical circuit as seen in the next chapter, are not within the research scope. Also used was a two-way functional block splitter with 3dB insertion loss. (See Appendix A7 for more details about the simulation setup and source code).

As mentioned in the previous section, the optical modulated signal was received at 1MHz, with -64.22 dBm signal power, the PPA up-converter circuit exhibited 23.84dB gain at a frequency of 433.92 MHz for 15dBm pump power, the DCHPPA technique overall subsequently exhibited a 15.92dB baseband signal gain over the modulated optical signal, as shown in figure 4.36(a) (e.g. also exhibited 22.93 dB gain at 25dBm pump power). The graph in figure 4.36(b) showed the output waveform of baseband signal at 1MHz frequency. The recovered signal had a peak voltage of 0.001205 volts, which corresponds to -48.3dBm signal power.

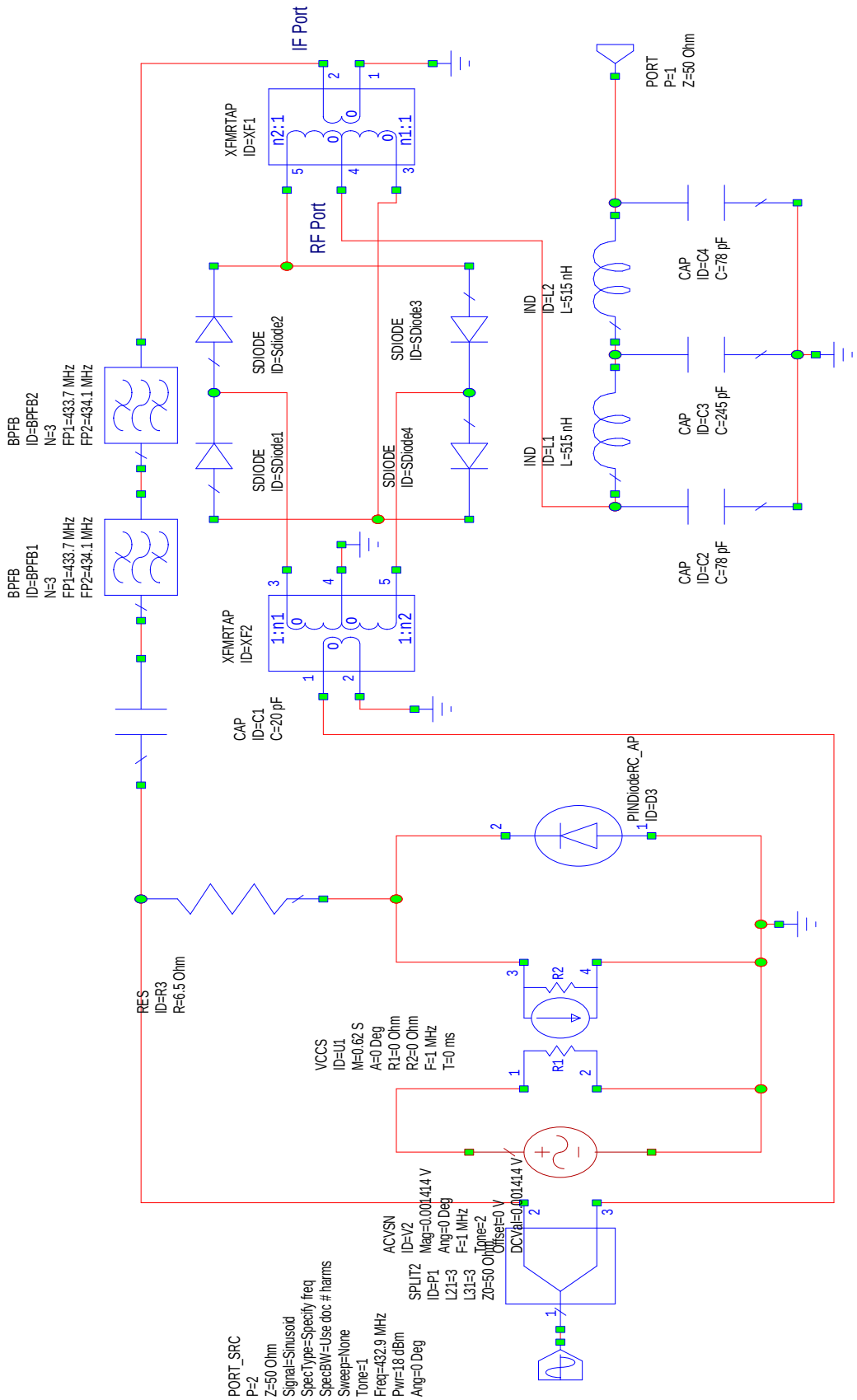

Figure 4.35 Schematic circuit diagram of DCHPPA

Most simulation tools become affected by time-variant reactance. The problem is with the different phase in the time-variant reactance impedance, as it keeps changing all the time.

It is clear that DCHPPA stage one has introduced a 23.84db gain over the RF signal, whereas stage two has a 7.92dB gain loss, which is due to the filter insertion loss and DBM conversion loss. The modelled DCHPPA circuit arrangement presented in this section shows the viability of the approach. Moreover, a full description of the optimised DCHPPA configuration circuit (i.e. stage two) will be presented in the next chapter, which aims to reduce the insertion loss and add extra conversion gain. (See Appendix A8 for advance DCHPPA system setup).

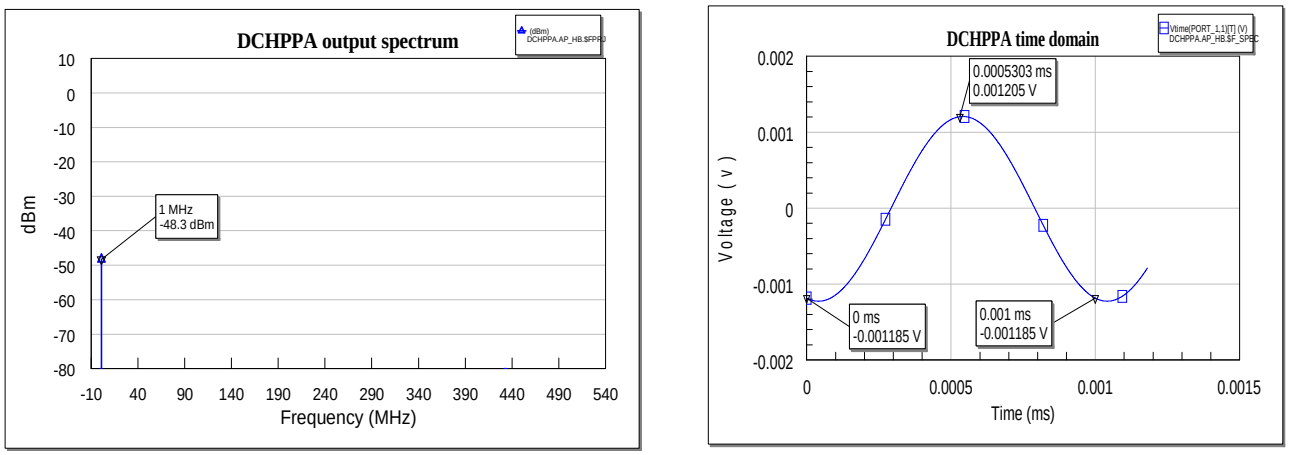

Figure 4.36 Recovered baseband signal at (a) output frequency spectrum, (b) time domian

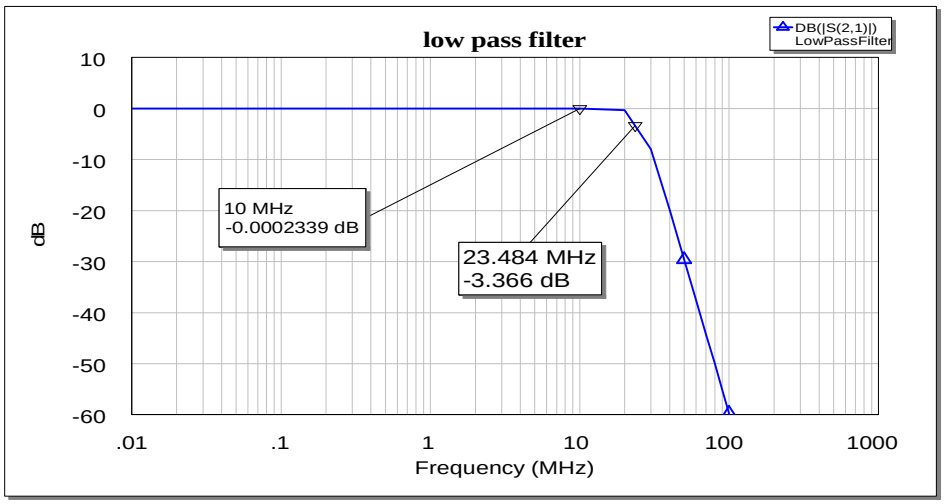

Figure 4.37 Simualted frequency response of LPF

4.7. Summary

A novel DCHPPA circuit design model has been described. The two stages of system modelling and simulation for the design of optical front-end receiver were presented. These included the first stage as the up-conversion circuit (PPA), and the second stage as the down conversion circuit (mixer). An accurate *pin* photodiode equivalent circuit model was employed to model the PPA circuit. The PPA configuration was successfully simulated that represents actual nonlinear dynamic junction capacitance behaviour. The PPA has a baseband detection, gain and frequency conversion all together in the first stage, so the DCHPPA system gain and noise figure at the baseband component are predominantly given by the PPA. An actual DBM equivalent circuit model was implemented in the second stage, which may have gain and baseband recovery at low cost. An object-oriented tool with multitone harmonic balance features was used to verify and optimise the performance of the designed system model (i.e. particularly at PPA circuit configuration) as it demonstrates the behavioural models' ability to accurately predict the effect of PD parameters and the PPA circuit configuration of the photo parametric amplification. The simulation experiments provided a good realistic assessment and better performance optimisation with respect to gain conversion. Multitone HB analysis was used to model the complete front end optical wireless DCHPPA circuit, which demonstrated the viability of the approach conventionally with respect to the baseband recovery signal. The simulation experiments were conducted in the VHF, UHF and MW frequency range. However, UHF frequencies were determined principally by the convenience of using commercially-available components, as well as it can show the viability of the theoretical approach and compare the simulation results with the practical results. The simulation analysis was found to be in good agreement with the PPA analytical gain expression. The results show that the gain is directly related to the level of pump power over the variable

capacitance, and also proportional to the ratio of idler frequency to RF signal frequency as predicted in the aforementioned theory. Also, if there is a limit to the LO pump power; the gain may be recovered by appropriate adjustment of the pump frequency, based on the gain analytical formula. For optimum conversion gain, the PD in the PPA stage should operate at equilibrium mode, and exhibit high nonlinearity (e.g. super hyper abrupt) with low bulk resistance; where there is a minimum noise figure and low insertion loss is desirable in the down-conversion stage. DCHPPA have properties that make them potentially attractive for use in future optical wireless communication systems.

Chapter 5

5. DHCPPA Experimental Implementation and Practical Results

In this chapter, the experimental arrangement and the result of the front-end optical wireless receiver are shown. This includes the optoelectronics up-converter stage-1 (PPA), IF signal processing stage-2 and down-converter stage-3 circuits. Also described is the new hardware design of the DCHPPA, capable of high gain, high selectivity and low noise operation. Experiment configuration for the non-degenerate mode is discussed, which leads to optimum high gain at the first idler frequency, as well as additional gain at a baseband recovery signal. The practical receiver has been built and tested in VHF and UHF as a sequel to the simulation configuration, and its parameters were set to demonstrate the simulated model presented in the previous chapter, which helps to compare with simulation results and verify both the simulation and theoretical analysis.

5.1 Introduction

In designing a free space optical wireless receiver, the first consideration is the selection of a receiver technique that can convert the received optical signal into an electrical signal. In most cases, amplification is required to bring the electrical signal up to a useful level, while at the same time keeping the noise level down. However, selectivity can be as important as sensitivity when considering a super heterodyne technique in both electrical and optical domains; the receiver must have sufficient bandwidth to recover the entire signal. Moreover, too much bandwidth increases the noise and adds other non-desired signals, and thereby deteriorates the SNR.

There are two different techniques used in free space optical wireless communication; coherent and incoherent optical communications. The focus here is on incoherent optical communications, which can utilize as a homodyne or heterodyne detection technique; the homodyne uses optical/electrical LO to produce a stable local signal that has the same frequency as the incoming RF signal. However in photo homodyne detection, the receiver operates by mixing a locally generated optical field with the received field, prior to photo detection. This added local field aims to improve the detection of the weaker received field in the presence of the interval receiver thermal noise; the use of homodyne detection is often called (spatial) coherent detection[48].

Conventional heterodyne detection employs converting the RF to an intermediate frequency or IF (also called beat frequency), which may be either higher or lower than RF frequencies, early heterodyne receivers always down-converted to a lower IF frequency. The reason for this is purely practical [127], the super heterodyne front-end receiver works by frequency converting as heterodyne with additional mixer stages that work to convert the IF to a standard RF/MW frequency with an appreciable amplitude, minimising noise,

particularly at the detection stage. The optical heterodyne receiver has a SNR advantage over direct photo detection because the use of strong LO signal serves to make all the receiver noise sources, other than photo detector shot noise, comparatively small [128].

5.2 Optical Wireless DCHPPA System

The idea behind the double conversion approach (up-converter, down-converter) is to recover the baseband components at the source frequency (ω_s); it is clearly desirable in many applications to recover the signal at baseband, as originally transmitted from the other end. In this approach the photodiode is pumped, and its output current mixed with a local oscillator source (LO), resulting in an output signal at the IF. The first selected upper sideband IF harmonic (ω_i) with its desirable gain will mix again with the same local source (LO) to recover the baseband signal as showed in figure 1.7. As a result, high gain and ultra low noise can be achieved in the up-converter PPA first stage, where high selectivity and additional gain can be performed in the IF signal processing (stage two), and the down converter (stage three) is used to recover the baseband signal within the relatively low noise region.

There are many advantages to be gained by using this technique in such a receiver, for example: 1) by de-multiplexing the IF signals to baseband signal frequencies, it is easier to recover each sub-carrier and therefore its information content; 2) down-conversion means that lower frequencies are used subsequently, and, in general this means a lower cost in comparison to the use of high frequencies components subsequently; 3) filtering out noise and unwanted signals at IF stage frequencies is more helpful than trying to do so at baseband (BB) recovery stage; 4) even with the additional low loss components in IF stages can have less effect and more benefit compared to as found in a conventional super heterodyne receiver with respect to receiver noise figure (Friss Formula), the overall

NF is primarily established by the NF of its first PPA amplifying stage; 5) a double conversion approach can perform as a highly selective optical receiver for an SCM system; 6) the heterodyne technique has been shown to work very well in many conventional radio receivers, and it demonstrates superior sensitivity and selectivity.

5.3 DCHPPA Stage One: PPA Experimental Work and Results

The PPA up-converter circuit design is a crucial element to be considered in front-end receiver design, as it is the key element to achieving better SNR for the whole receiver. Therefore high gain and ultra low noise is more desirable with respect to receiver sensitivity, particularly at the first stage. The performance requirements of the PPA up converter can be divided into three principle functions: photo detection, amplification and frequency conversion, whereas the received optical signal can be converted into a high electrical signal, combined with an increase in amplitude to certain levels required for effective utilization of these signals.

5.3.1 Choosing the Photodetector

The photo-parametric mode of operation involves optical detection, optoelectronic mixing and frequency conversion, as well as signal amplification within a single junction photodiode; therefore the choice of junction type of photodiode is very crucial, and as mentioned in previous chapters the *pin* junction has several advantages over the *pn* junction. However, in the PPA approach, concern is mainly with the nonlinearity utilization of the junction which is beneficial for parametric amplification, as the photodiode should exhibit a very good optical conversion, high sensitivity at operating wavelength, large detection area, large electrical response, short response time and minimum noise (high stability and reliability). The most requirements for parametric

operation are to have high nonlinearity in the CV curve and the capacitance variation depends strongly on the applied voltage *Cj=f(Va).*

Several commercial *pn/pin* photodiode characteristics were studied, and their CV curves were practical measured using a Boonton 72B capacitance meter (USA) with a 1MHz test signal and 2% accuracy. The photodiodes were an OSD-5T by Centronic, a PBX61 by Osram, a BPX65RT by Centronic, an OPF430 by Optek, a BPV22F by Vishay and a BPV10NF by Centronic. Their CV curves were plotted respectively, as shown in Figure 5.1.

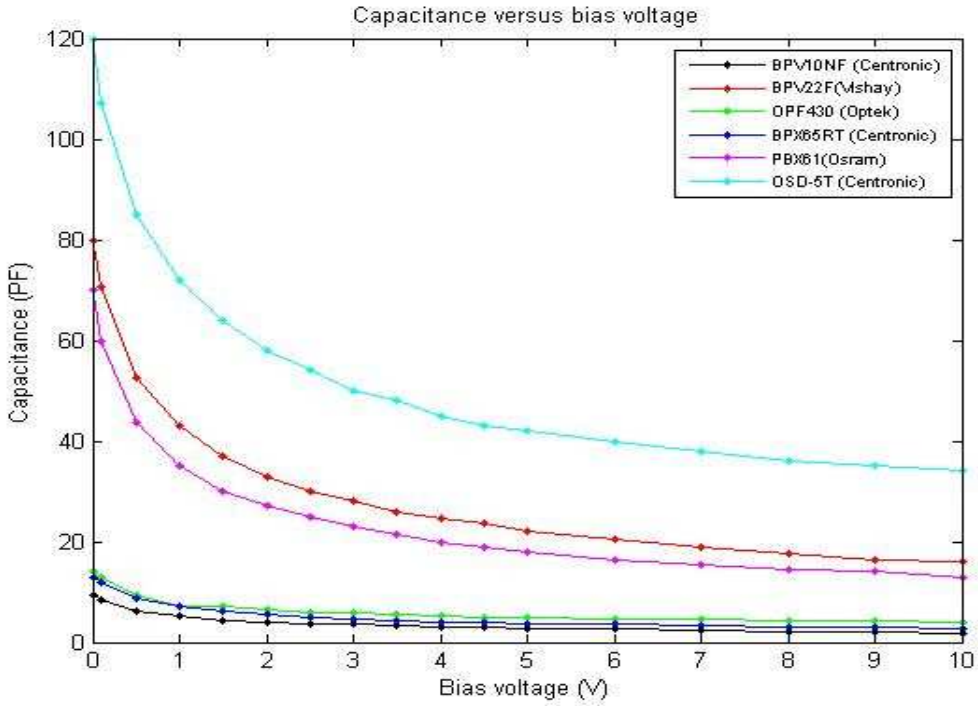

Figure 5.1 Practical measured CV characteristics for several pn/pin photodiodes

For optimum parametric amplification, as mentioned in section 4.5.5, the junction should offer a relatively large change in capacitance with change in applied voltage (e.g. dC/dV_a) and is not as reported in [82, 129, 130] where high attention is paid to what is called high tunabilty, which is the ratio of C_{max}/C_{min} ,which has to be as high as possible (more than ten), where as this has not been found to be the case. The above figure depicts only the CV curves at reverse bias mode (conductive mode), where only three photodiodes

were selected that have a large step curve around the zero bias voltage, which corresponds to large reverse grading coefficient *(m)*. The photodiodes were an OSD-5T by Centronic, a BPV22F by Vishay and a PBX61 by Osram. The three selected photodiodes were then studied at both photoconductive and photovoltaic modes, and their CV and IV characteristics were measured and plotted, as shown in figure 5.2.

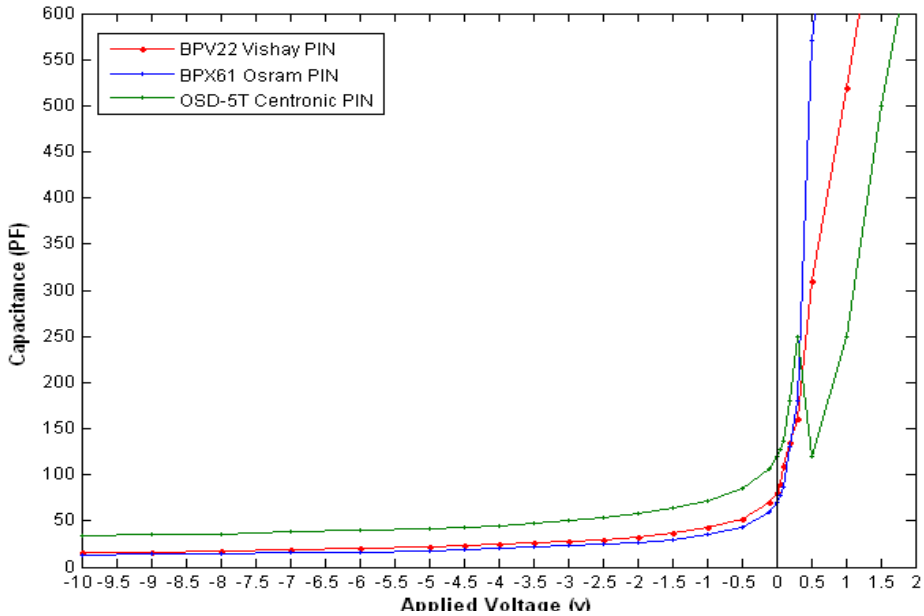

(a)

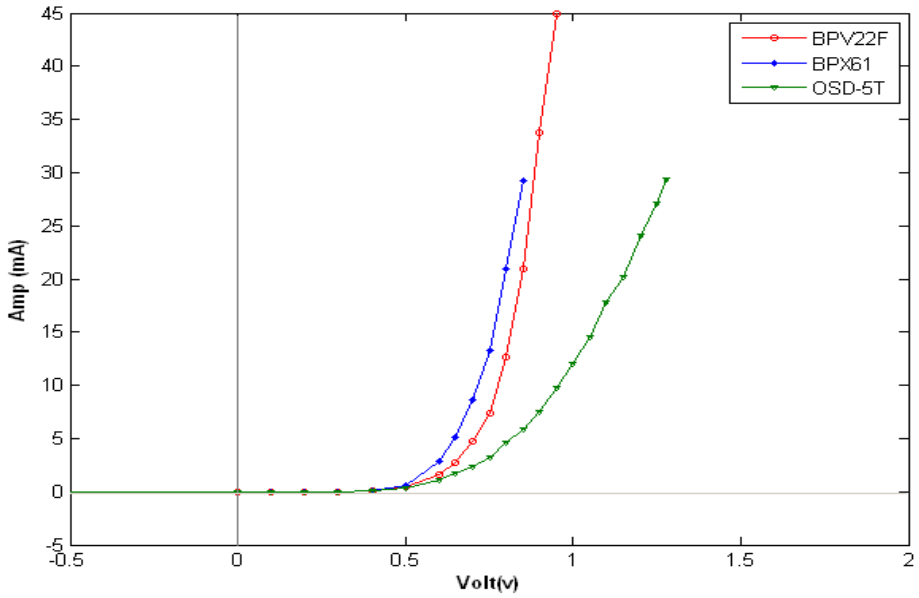

(b)

Figure 5.2 PD practical measured of (a) CV characteristics; (b) IV characteristics

The IV curve can be used to predict the parasitic series resistance (r_s) of the photodiode and the smaller value of r_s is the more desirable for parametric operation, as it can provide large voltage variation over the variable capacitance (i.e. voltage divider concept), and also it is the principle noise limitation in the PPA. The graph below illustrates the CV curve for the photovoltaic mode, which corresponds to forward grading coefficient (f_c) and the large steep curve is more desirable.

Based on the findings discussed above, the OSRAM BPX61 *pin* photodiode was selected for practical demonstrations. Although a *pin* photodiode is more desirable for photo detection and frequency response, it can also provide a wider CV curve compared to a *pn* junction. This may, at first, not seem appropriate, as the CV characteristic of a *pin* diode can be less dependent on bias. Nevertheless, in reality this has not been found the case. BPX61 photodiode parameters can be founded in *Table 4.2* in the preceding chapter.

5.3.2 PPA Experimental Work and Circuit Configuration

The PPA up-converter circuit configuration is shown in figure 5.3, and was configured in tests for an optical wireless link operating at 850 nm. The circuit is simultaneously a photo detector and up converter PPA with two resonators, the input resonator (L_1) being tuned to pump frequency that guarantee weak shunting of the signal by the internal resistance of the pump generator, and the output resonator (L_2) tuned to the idler frequency at ($\omega_p + \omega_s$). The PD was followed by resonant L2, and connected to a 50 Ω impedance spectrum analyser. The PPA up converter arrangement essentially consists of a photodiode, conjugately matched at the pump frequency as well as the desired idler frequency. In order to receive the maximum output power at the first upper sideband signal, it is very important to match the photodiode with both input and output circuit; hence the value of L_1 and L_2 were obtained according to the applied frequency as

mentioned in chapter 3. Previous works [129, 131-137] used a circulator circuit or stub tuner circuits to pump the PD and extract the up/down IF frequency. However, even with a well designed circulator, it is possible to obtain a residual pump power at the output port and most of the present-day circulators provide almost about 20dB isolation, and this may also affect the bandwidth limitation. In addition it is desirable to have fairly low reactance to keep circuit losses to a minimum.

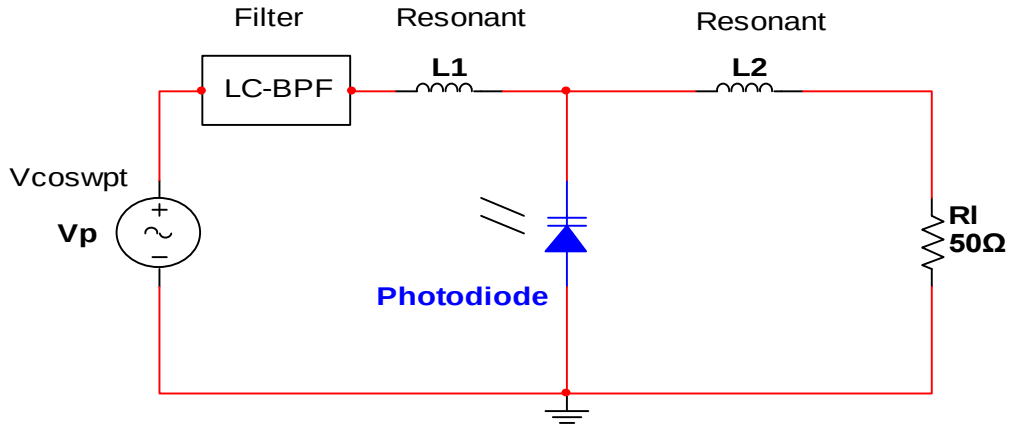

Figure 5.3 PPA up-converter equivalent circuit

In PPA circuit design, a different approach was used without the need for a circulator; the passive LC-BPF band pass filter provided a convenient method of applying a high pump to the photodiode junction, whilst at the same time providing isolation, reducing local oscillator sideband noise and blocking dc from passing through to the variable junction. Moreover, a high return loss figure is more desirable in such filter. It is essential that the photo-parametric diode should exhibit very good optical conversion efficiency in addition to pronounced nonlinearity in the *CV* curve. Although the available commercial BPX61 junction capacitance is based on an abrupt junction with grading coefficient, $m = 0.45$, and parasitic series resistance, measured at $r_s = 6.5\ \Omega$ which makes of very suitable as a photodetector with good frequency response. But super hyper abrupt ($m = 1$ *to* 2) junctions are more desirable for parametric operation, as they give a much greater *dC/dVa* characteristic.

In terms of fabrication of the circuits, breadboard and veroboard are too capacitive at high frequencies; hence, a FR-4 laminate PCBs with constant impedance microstrip techniques were employed, i.e. short rounded tracks rather than long tracks. TX-line MWO tools were used for the analysis and synthesis of transmission line structures according to the applied frequency. Surface mount components provide better high frequency performance than through-hole components, due to having shorter leads and hence lower parasitic reactance. All the designed PCBs were fitted into a Die-cast box, which naturally shielded for RF and EMI.

For practical reasons, the PPA circuits are implemented on two PCB circuits; a photodiode detector PCB circuit, which contains the *pin* photodiode, and two resonators L1 and L2; filter circuit which based on LC-BPF circuit [see Appendix B1]. The pump source, LO, is fed to the LC-BPF circuit directly from a function generator (Rohde & Schwarz SML03, 9KHz-3.3GHZ, GERMANY), followed by the input resonant that connects to the junction cathode, where the junction anode is grounded. The PPA circuit is quite similar to a simple DD/IM approach, as the photodiode output signal can be measured directly from the cathode via a 50Ω coaxial cable.

In non-degenerate photo-parametric mode, the receiver is operated at equilibrium mode (i.e. zero bias) by pumping the photodiode through the input tuned circuit connected to the cathode, and the measurement of the mixing output signals can only be done through the cathode via the output tuned circuit connected to the 50 ohm spectrum analyzer. There are many advantages to be gained by pumping the junction at equilibrium mode in such a receiver: for example: 1) the junction capacitance is highly nonlinear at zero *dc* bias mode, as shown in figure (5.1a), and the ratio of dc/dv_a can be as much high as possible, which is more desirable for parametric amplification; 2) also, there is smaller shot noise due to low dark current under equilibrium condition; 3) there is no reverse bias leakage current; 4)

better thermal noise due to no bias resistor; 5) better power consumption. In the other hand, too much pump power can cause forward current to flow through the PD and increase noise. The aim of this approach is to achieve high gain in an upconverter stage, and then a double conversion superheterodyne recovery technique can be used to recover the baseband components at the source frequency (ω_s).

5.3.2.1 LED Drive Circuit

The optical wireless links transmit information by employing an optoelectronic light modulator, typically a light emitting diode (LED); the emitter driver design was based on high current gain Darlington pair transistor amplifiers, as shown in figure 5.4 (see Appendix B2 for LED drive circuit). The designed drive circuit must cause the light output from the LED source to follow accurately an input voltage waveform (signal generator) in both amplitude and phase. The LED used was from Vishay Semiconductors, type TSHG6400, which had a peak wavelength of 850nm with 18MHz modulation bandwidth and typical radiant power of 50mW, classified as class 3B in terms of safety.

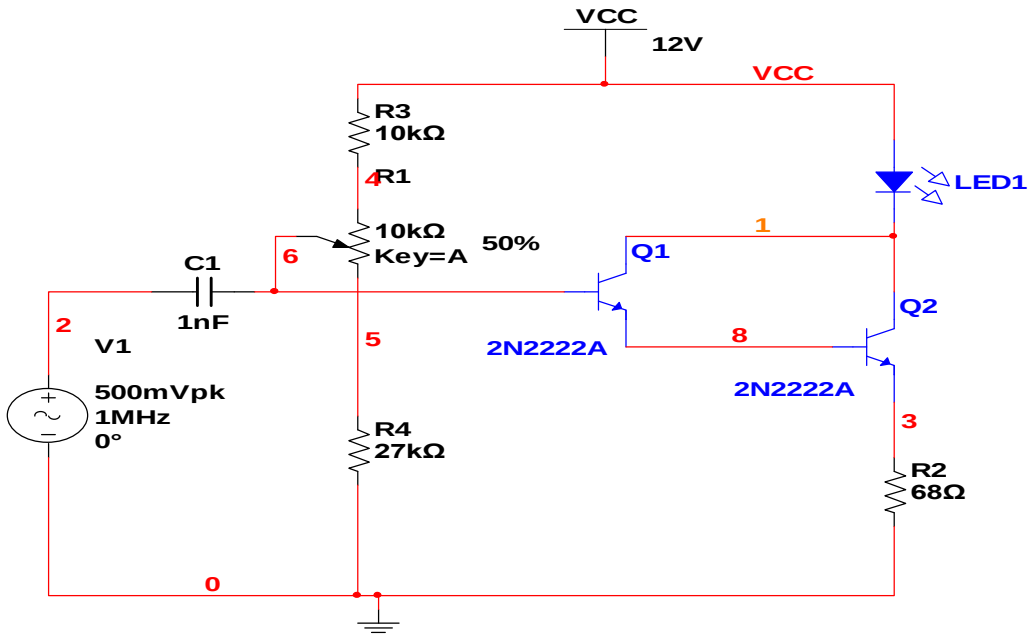

Figure 5.4 Darlington pair current gain amplifier (LED drive circuit).

In the practical implementation, two *npn* transistors were used to implement the Darlington amplifier with other through-hole components, as shown in the graph. Designing a high current gain amplifier requires a high wattage resistor (i.e. R2) and high power transistor (i.e. Q2) or a heat sink is needed for Q2 to pass a large current.

5.3.3 DCHPPA Stage 1: PPA Practical Results

For practical reasons, and to show the viability of the approach conveniently, experiments were conducted in the VHF and UHF frequency range. This particular frequency was determined principally by the convenience of using commercially-available components. The PD detector circuit was placed on an x-y-z micro-positioner so that it could easily be aligned with the transmitter IR beam. The distance between the LED and the PD was set to approximately 30 mm, in order to collect maximum intensity illumination (see Appendix B3 for DCHPPA experiments setup). Also, two signal generators, a power amplifier, spectrum analyzer, and a twin output power supply were used in this practical arrangement for biasing the LED and biasing the PD (in non equilibrium mode experiments). The signal generator supplying the input voltage waveform to the LED was a Marconi Instrument 2019 (80KHz-1024KHz, UK), set to generate signals at 1MHz-5MHz, with an amplitude of 0.5V. A Rohde & Schwarz SML03 (9KHz-3.3GHZ, GERMANY) signal generator was used as the LO with the Amplifier Research model 50W1000AM4 (USA), capable of providing an RF level up to 39dBm. The spectrum analyzer was an Advantest R3131 (9KHz-3GHz, TAIWAN). The oscilloscope used was a Tektronix TDS 3032C (300MHz, USA). The network analyzer used was an Agilent technologies E5071B (300KHz-8.5GHz, USA).

The photo-detector circuit was carefully aligned geometrically to produce the highest photocurrent. The optical signal was modulated at 1 MHz, as shown in figure

5.5(a), with a measured optical power of 1.414mW that corresponds to the -64.39dBm measured at the spectrum analyzer. A pump frequency of 241 MHz and 432.92 MHz was used. Previously published work [138] demonstrated the PPA up converter in the VHF frequency range (241MHz). However, the frequency operation for this demonstration was increased and set to the UHF frequency range (432.92MHz). This provided a widely separated frequency to a 1 MHz optical source frequency, compared to VHF, and helped to verified the effect of the (ω_i/ω_s) term in the gain equation, and utilize the effect of high pump and high frequency on the behaviour of the variable capacitive impedance at parametric operation. In addition, a VHF frequency was used as well in some experiments to help to show the viability of the theoretical analysis and compare practical results for both UHF and VHF. The PPA practical measurement was conducted through an on-off operation. Firstly, the optical modulated signal was measured as DD/IM without any pumping, as shown in figure 5.5a.

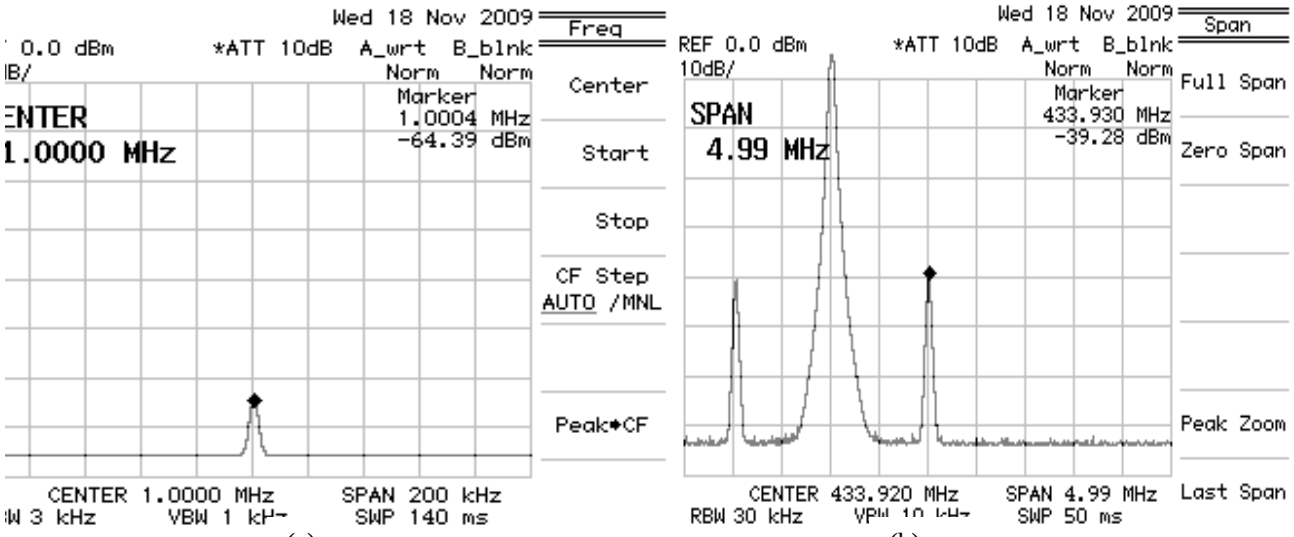

Figure 5.5 Frequency spectrum of (a) 1 MHz modulated optical signal-direct detection response; and (b) up-down converter signals pumped by 432.92 MHz, pump power 22 dBm (25.11db gain for the up-converter signal).

A -64.39dBm source signal was detected at 1MHz frequency. Secondly, the PPA pumped at 432.92MHz with 22dBm pump power. Indeed, the actual pump was 26 dBm pump power from the signal generator, as there was a 4-dB insertion loss due to LC-BPF; the maximum RF input power of the Mini-circuit LC-BPF model SXBP-425+ was 0.5W (i.e +27dBm). The pump power was restricted to +26 dBm to avoid any damage to the BPF. The frequency spectrum of the up converted signals is shown in figure 5.5b. The graph illustrate that the optoelectronics mixing occurs due to the photo parametric operation. The mixing frequency occurs between the three frequency components of the signal, idler and pump waves in such a nonlinear element, and the energy flows from strong pump wave to weak signal and idler waves. This flow of power introduces a negative conductance into the signal circuit. Two sideband first IF harmonics were generated obeying ($\omega_{IF}=\omega_P\pm\omega_S$); an upper sideband IF harmonic of 433.92MHz, and a lower down sideband harmonic IF of 431.92MHz.

Experimentally, the proposed PPA mode of operation (equilibrium mode) worked well, and may be summarised as follows: A 25.11 dB of up converter gain at upper beat frequency was achieved, compared to a 29.72dB up converter gain in simulation results. In addition, by employing the input/output tune circuit to the PPA circuit configuration, the up-converter gain improved by almost 3dB compared with a PPA circuit, without considering the input/output admittance power. Moreover, the frequency spectrum in figure 5.5b showed that the gain in the up converter signal was a little higher (i.e. almost 1dB) than that for the down converter signal, as predicted in the aforementioned gain equation in chapter 3.

It was essential to measure the waveform across the *pin* photodiode at the pumping operation, for two reasons; first, it can help to predict the level of the pump voltages across the junction and therefore avoids excessive level of pump voltage which can overcome the

barrier potential voltage of the junction (0.554V) and cause undesirable forward current to flow through the photodiode. Second, it also helped to predict the value of r_s of the photodiode (measured value of $r_s \approx 6\ \Omega$). Figure 5.6 shows the level of pump voltage over the junction.

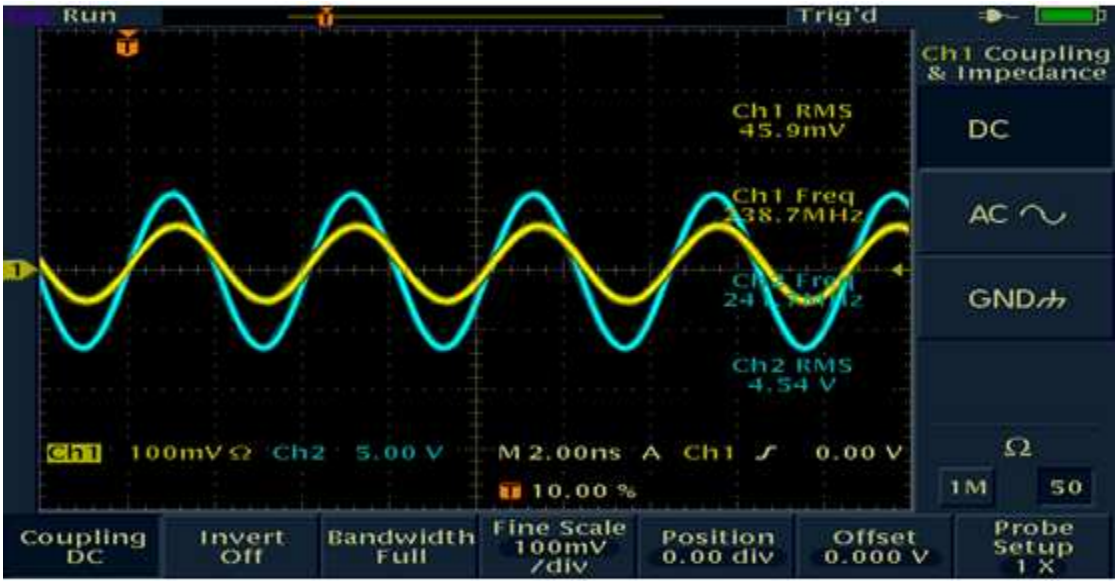

(a) 5dBm

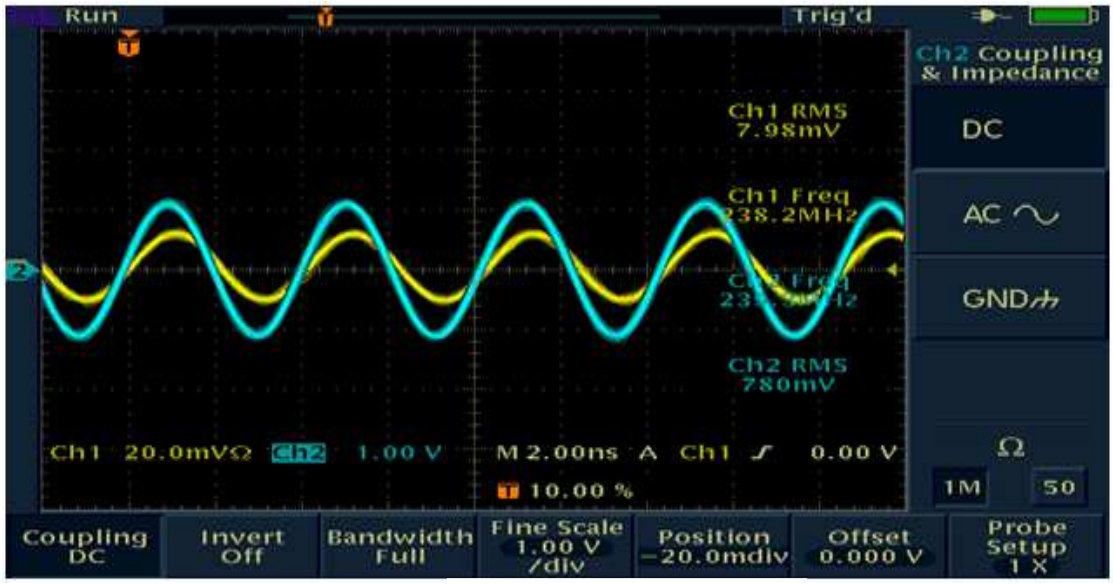

(b) 20dBm

Figure 5.6 Pumping voltage level across the PD

The signal for *ch1* was measured via a high impedance probe device with attenuation of *X10* across the photodiode and *ch2* signal was measured direct from the

pump source. The experiment was run with two different pumping power signals 5 and 20 dBm at 241MHz pump frequency a VHF frequency was used in this experiment due to limited frequency range of the oscilloscope 300MHz. The measured voltage across the PD was almost ($V_d \approx 0.1V_p$). A number of different experiments are discussed in the next section, as shown in the preceding chapter, to provide more help in understanding the effect of other experimental parameters and circuit configurations on the PPA up-conversion gain. The same experimental configuration will be used in the next sections unless a different circuit configuration is being considered.

5.3.3.1. PA Gain versus Various Bias Voltages

In this experimental configuration, the PPA up-converter circuit configuration shown in figure 5.3 was used, and an additional external mini-circuit bias-T (ZFBT-4R2GW+ 0.1-4200MHZ) was installed, as shown in the experimental arrangement layout showed in Appendix A5. The bias T with 50Ω matching impedance was used to guarantee an optimum SNR by providing a convenient method of biasing the photodiode and ensuring that the output mixing frequencies (i.e. *RF*, *IF* and *LO*) flow completely to the load (spectrum analyzer) and that other *DC* signals will be rejected from flowing to the load. The reverse bias voltage varied from 0 to -5 volts with 0.5 volt intervals, as shown in figure 5.7 (see result table in Appendix B4).

Experimentally, the maximum conversion gain was achieved at equilibrium mode (i.e. zero bias). In both VHF,UHF operating frequencies, the gain dropped from 25.1dB to 19.9dB (i.e. 5.2dB drop gain) with respect to the biasing voltage of 0 volt and -1 volts respectively; compared to a 5.57dB drop in simulation results as shown in Figure 4.21 and figure 4.22. The gain then started to decrease gradually following the CV characteristics. This represents an excellence corresponding to verifying the proposed PPA mode of

operation. The practical results showed very good agreement with the simulation results as reported in chapter 6.

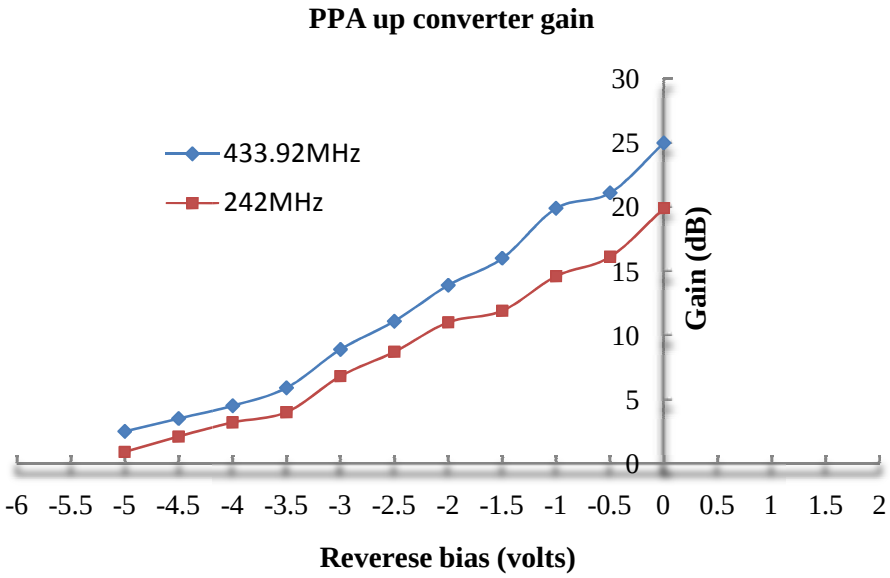

Figure 5.7 PPA up-converter gain for different bias voltages at UHF and VHF frequencies

5.3.3.2 PPA Load Impedance Analysis

A convenient way to measure the output current on the PD is to convert it to a voltage with a load resistor (i.e. spectrum analyser or oscilloscope) and in some cases; a pre amplifier is required to boost the weak signal to a standards level, with the penalty of additional noise with respect to receiver sensitivity. The PPA has been shown to overcome such issues and provide high sensitivity as compared to a PD followed by pre-amp [43, 139, 140], or avalanche photodiodes [137].

However, the PD has a capacitance proportional to its area, which also determines the time response ($\tau = RC$). In the PPA operation, the junction capacitance will be forced to increase proportionally to the level of pump power, as mentioned in chapter 3, which is recognized as the mean value of capacitance (C_{mean}). As a result, the PPA mode of operation provides a low time response which can be seen as a disadvantage of the PPA with respect to a low frequency signal. Although high gain can be achieved due to

pumping the junction, this can affect the gain bandwidth product (GBP) of the PPA. In practise, the fastest photodiode has very small capacitance, even if it has a very large detection area such as a *pin* structure, and, in most cases, it operates under high reverse bias and low load resistor which helps to improve the time response of the PD to fast signals, but this can also reduce the sensitivity for very weak light signals, due to driving a leakage current (dark current) occurring from the biasing voltage source. Large dark current has noise associated with it, which may limits the sensitivity of the receiver; however the main limit to the sensitivity is (I_pR_L), so if the R_L is small then the output voltage is small.

Therefore, some practical experiments were performed to measure the PPA load impedance, based on the circuit configuration. As shown in figure 5.8, the designed circuit represents an impedance matching transformer with loss (>20dB) according to the value of the resistors used.

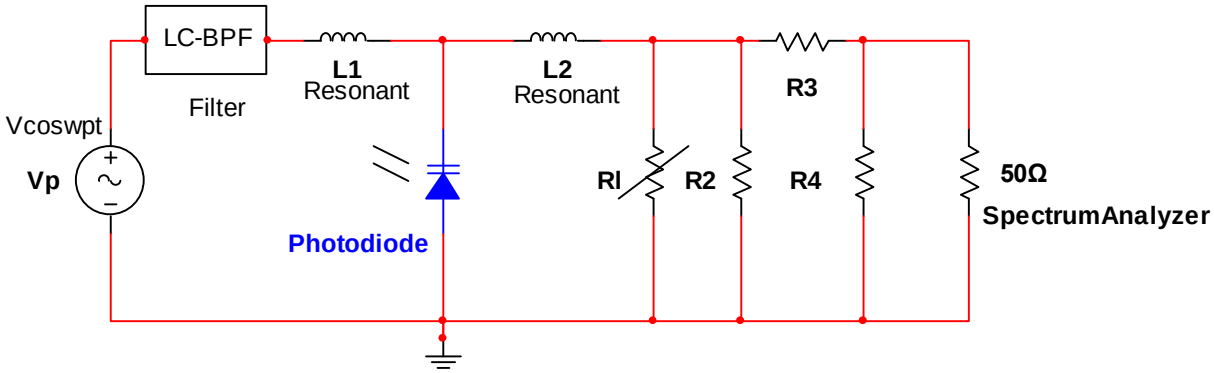

Figure 5.8 PPA up-converter gain with impedance transformer circuit

The impedance matching circuit aims to maximize the power transfer to the load, whilst minimizing the reflection from the load; the PPA load impedance was measured by varying the load impedance according to $R_L=R_1//R_2\ (R_3+R_4)$. The PPA up-converter gain experiments were performed at both VHF and UHF frequencies with two levels of pump power and different circuit configurations, as shown in figure 5.9. The graph illustrates that

the maximum power transfer occurs at low load impedance, and the up-converter gain at low load exhibits an increase of an average of 3dB, compared to 50 ohms load impedance conditions.

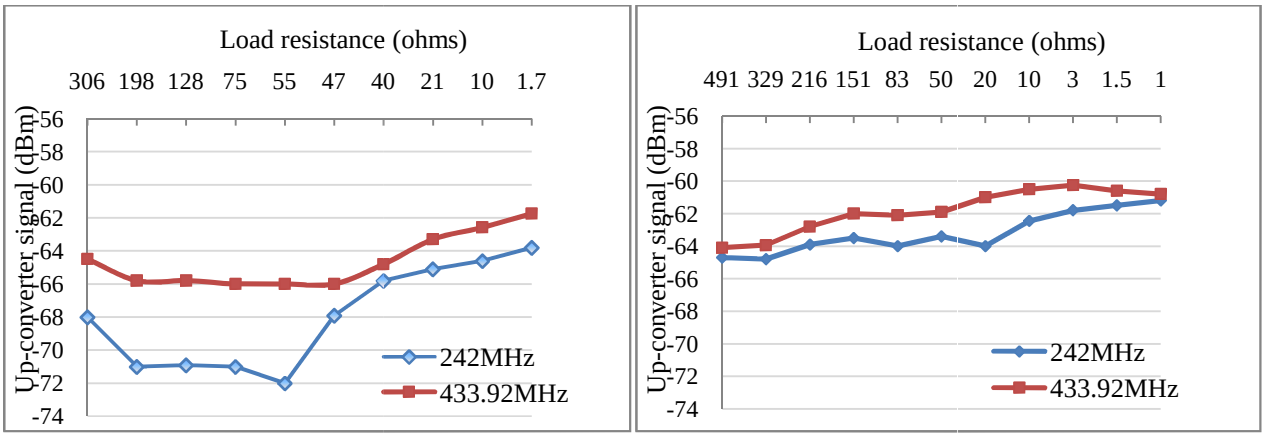

(a) 15 dBm pump power without tune circuit ***(b) 15 dBm pump power with tune circuit***

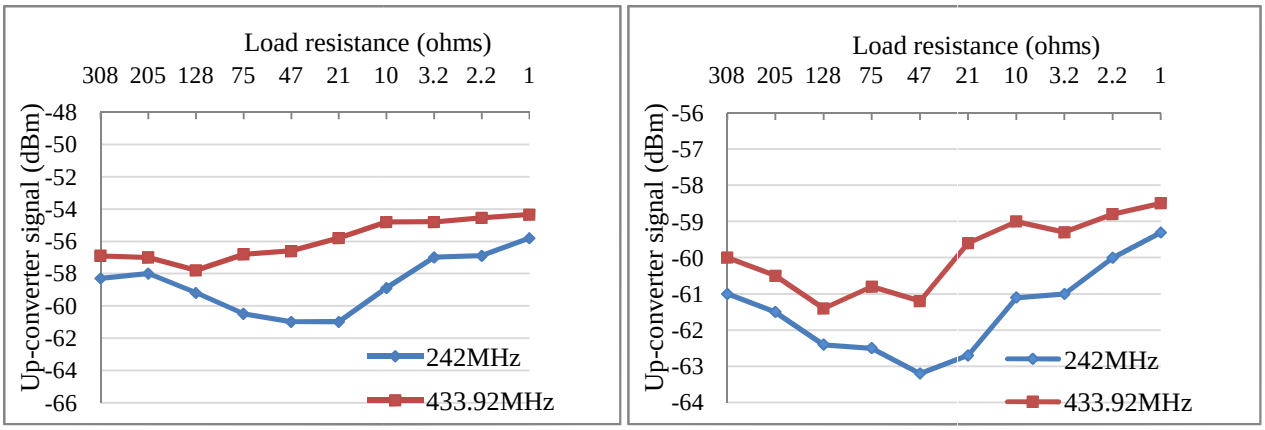

(c) 20dBm pump power with tune circuit ***(d) 20dBm pump power without tune circuit***

Figure 5.9 Measured PPA load impedance

The practical results verified the predicted analytical analysis in chapter 3, showing that the PPA performs much better at low impedance, which can provide high GBP. However, as most RF/ MW systems adopt a 50 Ω impedance, the state of the art for the available commercial impedance transformer provides almost 3dB insertion loss at UHF frequency. It is a trade off between gain and bandwidth; and for practical reasons and the

availability of the standard 50Ω commercial components, and to avoid additional noise due to the impedance matching circuit (as the signal would not have to travel to both load ports), it would be more convenient to measure the performance of PPA results on a standard 50Ω basis.

Alternatively, the PPA up-converter gain may perform well with a sustaining circuit (i.e. negative resistance), however some important considerations regarding the noise performance of parametric operation are: the inherent noise of the sustain circuit and stability problem due to excess gain or excess negative resistance. In addition, in terms of the practical implementation of the load impedance matching circuit, different in-house RF transformers were designed and tested, and two commercial Mini-circuit RF transformers TCM8-1+ and TX16-R3T+, with tunes ratios of 8 and 16, respectively, were implemented and used (the circuit can be found in appendix B5). It was found that the PPA was very susceptible to any shunted reactance impedance, and this can reduce the performance of the PPA with respect to conversion gain. It can be argued that, to adapt the circuit for complete power absorption of the pump power at the PD cathode, corresponds to setting the load impedance equal to bulk resistance, which is the optimum load condition for the signal.

5.3.3.3 PPA Gain versus Various Pump Power

In this experimental configuration, the PPA circuit configuration, shown in figure 5.3, was used, and the practical results were performed by varying the pump power from -4dBm to 27dBm with a 1dBm interval, as shown in figure 5.10. The experiments were conducted at both UHF and VHF frequencies and the beat signals at 433.92 and 242 MHz were measured by a spectrum analyser. The gain increases linearly with the pump power, and the PPA operates as ordinary linear amplifier; the observed gain starts at a pump

power of -2dBm and 0dBm for UHF and VHF frequency respectively. The graph shows that due to the large pump, the 1dB gain compression for UHF and VHF frequencies occurs at around 25dBm (with 26.6dB gain achieved) and 20dBm (with 20.3dB gain) respectively; the PPA then starts to operate as a nonlinear amplifier. Increasing the pump after a compression point will lead to large voltage variation over the PD, and will excess its barrier voltage and cause an undesirable forward current to flow through the junction. Also of note is that due to this undesirable large forward current, the detected signal (i.e. RF source signal) measurement was affected, and no longer provides the accurate reading that corresponds to the photo current generated due to the incident optical power.

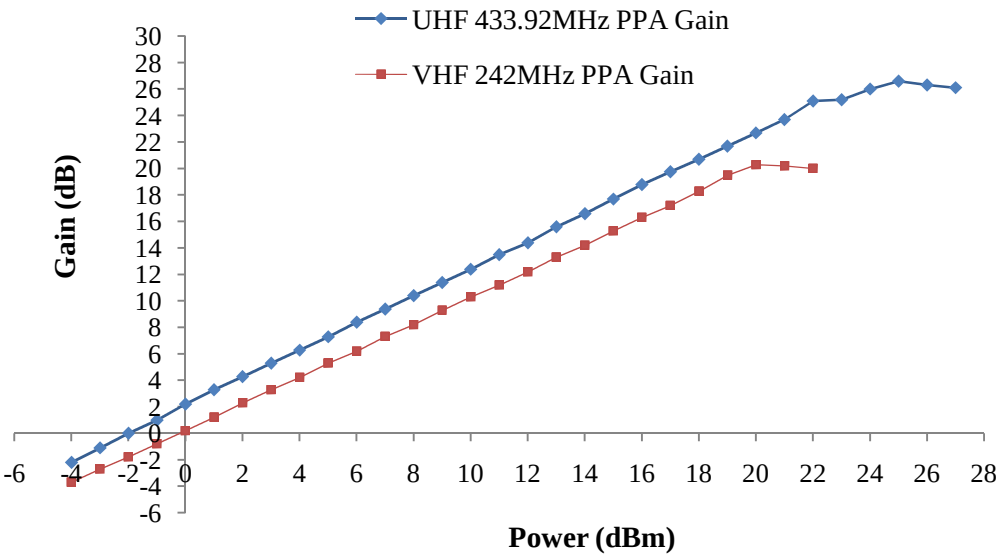

Figure 5.10 PPA Up-converter gain for different pump power signal

It may be concluded that the gain is directly related to pump power, and also related to the IF frequency, as predicted in theoretical analysis. However, the practical result proves that the 1 dB compression occurs at high frequency (UHF), compared to low frequency (VHF). This means that the capacitive reactance impedance of the junction keeps changing according to the applied pump frequency, and this results in a reduction of the applied pump power over the junction (i.e. voltage divider concept), as shown in figure

4.30 in the simulation results. In other words, the pump voltage over the reactance impedance at UHF is not the same as in VHF. This is because the reactance impedance has a different value at each applied frequency, even if the same pump level is applied from the function generator; therefore the gain is related to the pump voltage over the reactance impedance, and also related to its value at applied frequency. In contrast, to achieve high gain at high pump frequency, large power is needed, as most of the power is dissipated in r_s; based on the above finding, this can verify the new gain theory analysis as reported in chapter 3. Optoelectronics mixing in PPA appears very promising as a means of linear amplification and frequency conversion of incoherent optical signals (see Appendix B6 for data result table).

In this section, the work continues to analyse the effect of the ratio of the pump frequency to the RF source frequency, as shown above, with 241MHz and 432.93 MHz pump frequencies. The PPA equivalent circuit was configured as shown in figure 5.11; the PD was pumped directly via the function generator (i.e. that has internal r_s of 50 ohms), without the use of any series pass tuned circuits or BPF circuit. Measurement at other frequencies was not possible due to the lack of any other commercial BPF that operates at different cut off frequencies as supplied by Mini-circuit, and which provided the same circuit configuration with the same insertion loss, as well as the same degree of isolation. Also, in practical terms, it was very challenging to design an LC passive filter for these frequencies [141], particularly with a high degree of isolation and low insertion loss; therefore, the simple PPA circuit was used only to show the viability of the approach at different pump frequencies.

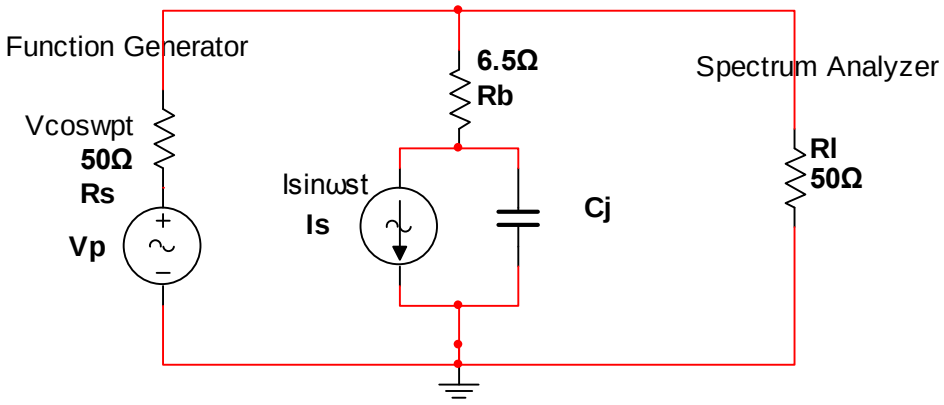

Figure 5.11 PPA Up-converter equivalent circuit for different pump frequency

Experimentally, the PD was pumped with 19dBm at various pump frequencies as shown in figure 5.12. The graph show that the gain is not always proportional to pump frequency without considering the pump voltage over the reactance impedance as mentioned before. This may be explained by this example at 19dBm pump power, which corresponds to V_{pump}=2.814 volts (equals to 1.99V_{RMS}), with the voltage V_D across the photodiode at 241MHz and 432MHz pump frequencies being equal to V_D=0.182V_{pump} and V_D=0.142V_{pump} respectively; the voltage across the variable capacitance V_C at 241MHz and 432MHz pump frequency are V_C=0.448V_D and V_C=0.311V_D respectively. In contrast, the voltage across the variable capacitance is proportional to the reactance impedance value. At high frequency, pumping low voltage variation occurs over the capacitance. The optimum PPA up converter gain can be achieved by giving due consideration to the level of the pump power, as well as the relationship between the beat frequencies over the source frequency. It also is important to have a very low bulk resistance. At high bulk resistance, most of the applied pump power across the PD is dissipated in the series resistance (r_s). However, applying the same voltage variation over the variable capacitance at any pump frequency as a result of high gain corresponds to the highest pump frequency used. It can be argue that the practical result, as shown in figure 5.10, can give a good indication of the

conversion gain at various frequencies. However, at high frequency, the result can be less accurate, due to not considering the micro-strap technique.

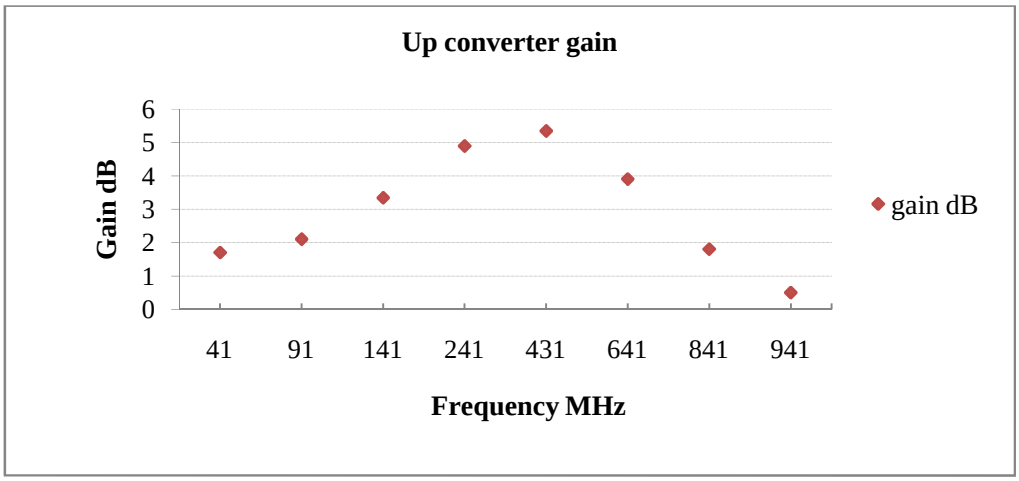

Figure 5.12 PPA Up-converter equivalent circuit for different pump frequency

5.3.3.4 PPA Gain versus Various Optical Frequencies

As mentioned before, the PPA signal theory analysis in the previous chapter showed that the up-conversion gain was dominated by the ratio of the upper sideband frequency over the optical frequency (f_i/f_s) if the same voltage is applied to the reactance at any pump frequency. It is helpful to analyse the PPA operation at various input optical signals. The PPA frequency response was measured by the same circuit configuration used in figure 5.3. Initially, the f_{IF} was fixed at 433.92MHz, while the optical modulation frequency, f_s, and the pump frequency, f_p,were swept according to (f_p= 433.92-f_s).

The experiments were performed by varying the DD modulated optical frequency from 1MHz to 5 MHz with a 1MHz interval, as shown in figure 5.13, while the PPA set as inactive where no pump was applied. The graph shows the frequency response of the detected RF signals, measured with a flatness of almost ±2dB in this frequency range, as compared to ±3dB in the simulation results. This can verify the frequency response of the modelled input optical frequency of the photodiode frequency response shown in chapter 4.

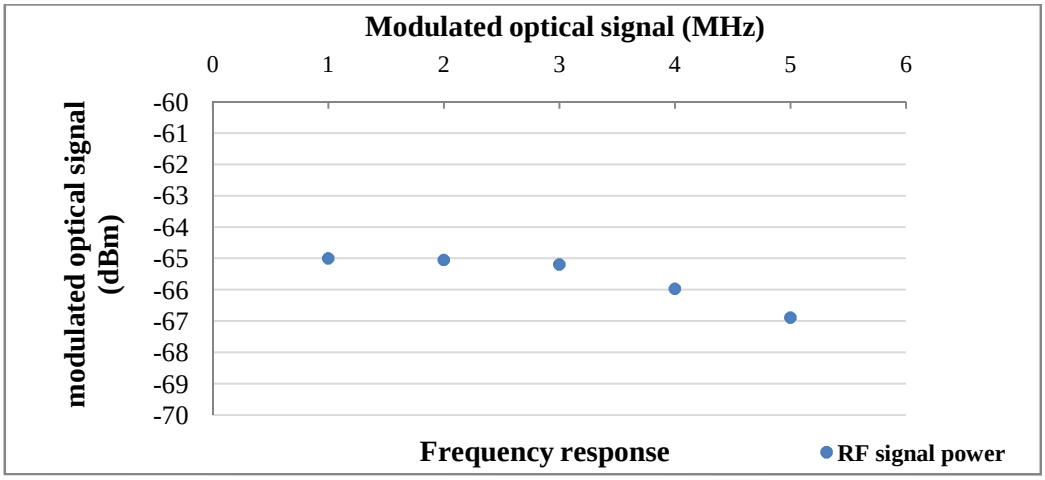

Figure 5.13 Frequency response at various optical signals

The PPA was then set to the active condition and practical results were obtained by sweeping the optical signal from 1MHz to 5Mhz at 1Mhz intervals, while the IF signal was fixed and the pump signal had to be decreased according to (f_p= 433.92-f_s). The PPA up-converter summary of results is plotted in table 5.1.

Table 5.1 PPA frequency response at various optical signals

Optical signal (R_F) MHz	**R_F (dBm)**	**Pump signal (F_P)MHz**	**Intermediate signal (F_{IF}) MHz**	**Up-converter gain (dB)**
1.0	-65.00	432.92	433.92	25.36
2.0	-65.05	431.92	433.92	21.07
3.0	-65.19	430.92	433.92	17.05
4.0	-65.97	429.92	433.92	14.58
5.0	-66.89	428.92	433.92	12.83

It can be seen that the highest gain, 25.3dB, was achieved when the RF signal frequency measured 1MHz. The gain then started to decrease according to an increase in RF signals, as predicted in the theoretical analysis, where the gain is proportional to the ratio of (ω_i/ω_s).

5.4 DCHPPA Circuit Configuration and Practical Result.

5.4.1 DCHPPA Stage 2: IF Signal Processing Circuit Configuration

The idea of the DCHPPA design, based on the super heterodyne principle, exists in conventional RF/MW radio receiver, which is still the most popular technique since it was invented in 1918. In the superheterodyne, dual, down-conversion mixing technique is used as shown in figure 5.14.

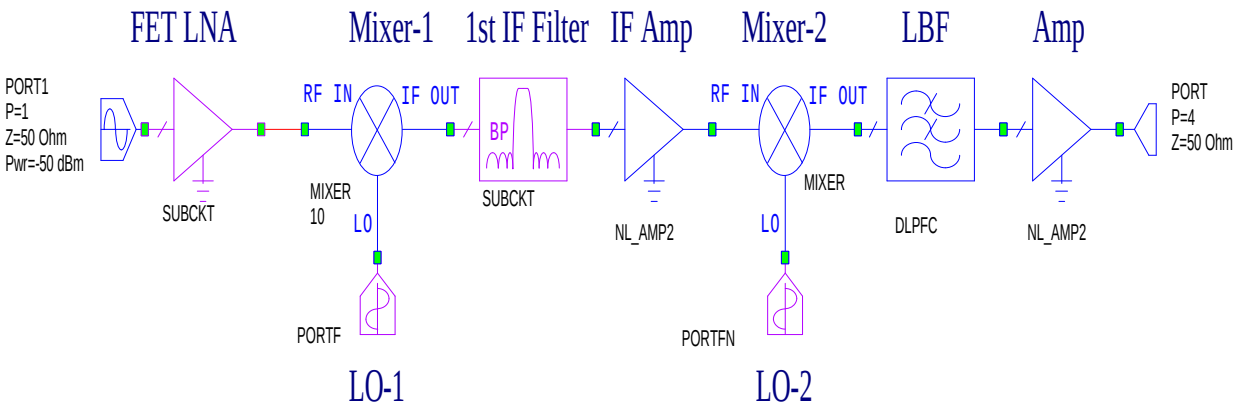

Figure 5.14 System diagram for super heterodyne double down conversion

Also the heterodyne approach has been seen as a very attractive technique for an optical SCM system, particularly in terms of a long haul application; it can also be more applicable for a free space application, as seen in this chapter. In the SCM optical receiver, as shown in figure 5.15 [75], the optical signal can be detected by the PD and then amplified by a low noise amplifier LNA, which results in amplification of all the received signal (i.e desired and non-desired signals), including the PD noise occurring due to the optoelectronic signal converter. These output signals will feed to the mixer for down or up-conversion and then the pre selector BPF will be employed to reject the images. The IF

will feed again into the second up/down mixer, which aims to recover the original baseband signals to achieve better gain and better receiver sensitivity. In general, the multiple conversion technique has been shown to work well in many RF/MW receivers, but it is more complicated compared to a simple photo-detection circuit.

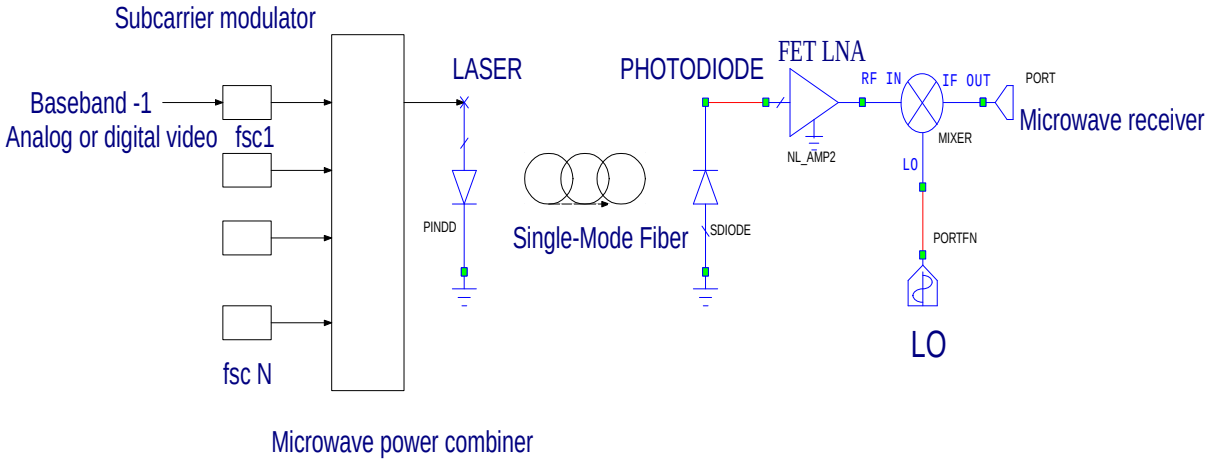

Figure 5.15 System diagram for a microwave-multiplexing light wave system

The DCHPPA acts in a parallel manner to a conventional double superheterodyne detector system, but without the noise penalty that normally occurs. Photoparametric amplification is used at the first stage instead of a resistive/transistor-based mixer or preamplifier front end circuit. In this section, the practical demonstration of the DCHPPA will be presented. Figure 5.16 shows the circuit configuration of the DCHPPA receiver. Each stage requires careful consideration of the choice of components. The whole circuit was divided into three stages, each stage with its sub-circuits; the PPA circuit stage 1, which includes passive LC band pass filter circuit and the photo detector circuit as explained in previous section; IF Signal processing stage two, which includes the pre selector cascading band pass filters followed by an IF amplifier circuit, followed by a

second IF cascading bandpass filters; down converter mixer stage 3, which includes a passive LC bandpass filter circuit and DBM circuit, followed by a low pass filter.

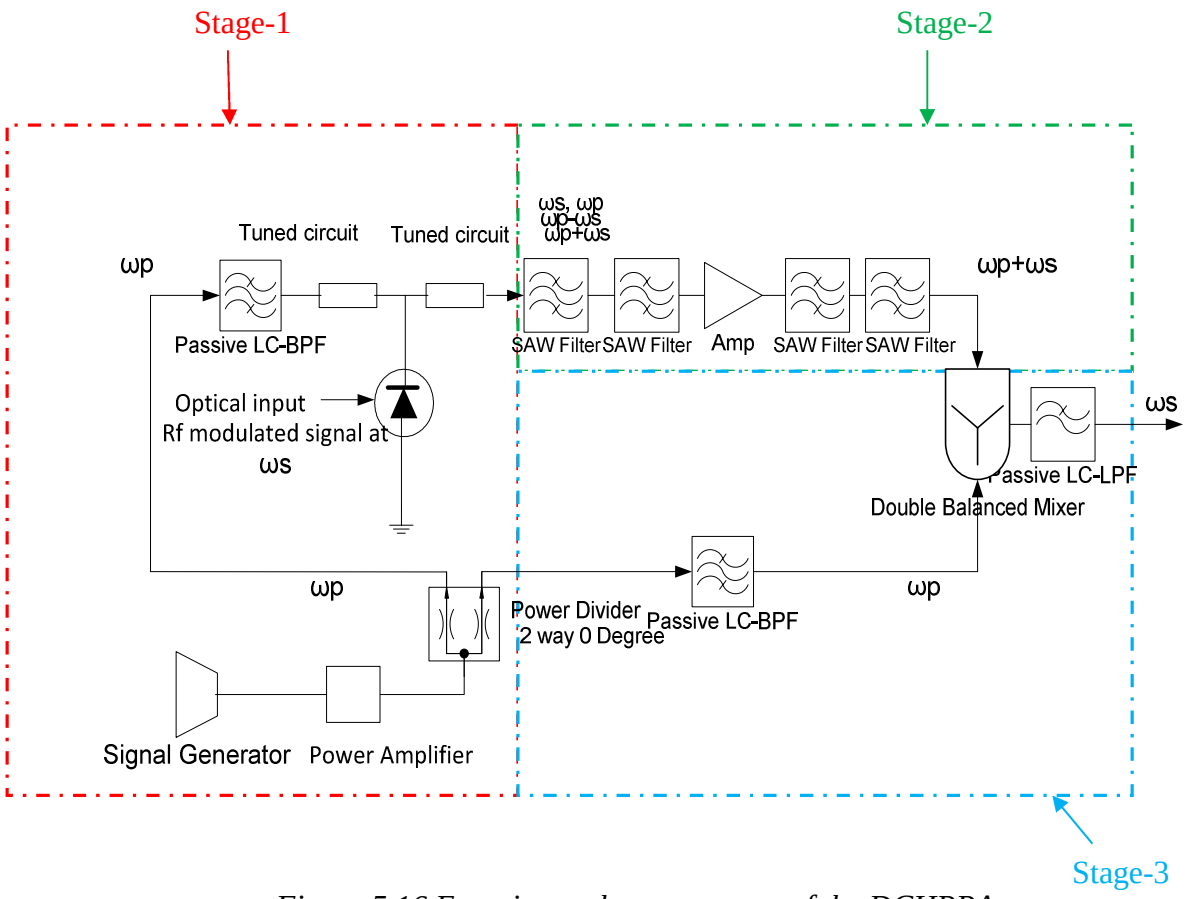

Figure 5.16 Experimental arrangement of the DCHPPA

As illustrated in the graph, the same pump source (LO) was used for the up-converter and down-converter via a 2-way, 0 degree power splitter (i.e. no phase shift) device. The LO was injected via high quality band pass filters that provide a convenient method of applying the pump to the PD (i.e. mixer one) as well as the DBM circuit (i.e. mixer two), whilst at the same time providing isolation, reducing LO sideband noise and blocking *dc* components from passing through. The up-converter mixer works to convert an RF signal (1MHz) to the first upper sideband signal IF (RF+LO; 433.92MHz), where 432.92MHz was used as the LO pump frequency. The down-converter mixer works to

recover the desired baseband channel (1MHz) from the IF signal (433.92MHz). A picture of the final setup can be seen below in figure 5.17.

As mentioned before, the signal processing stage two required a considerable amount of attention; in particular with respect to selectivity and sensitivity, the most important in this stage is selectivity; however, sensitivity is also desirable. In contrast, there are four frequencies in the PPA output spectrum (*ωp,ωs,ωp±ωs)* with their harmonics (i.e third and fifth order; $\omega_{IF}=m\omega_s \pm n\omega_{LO}$) at various level of powers. As shown in figure 5.5(b). At 22dBm pump power, the LO signal level (i.e. 432.92MHz) was measured over the PD to about 10dBm using a spectrum analyzer.

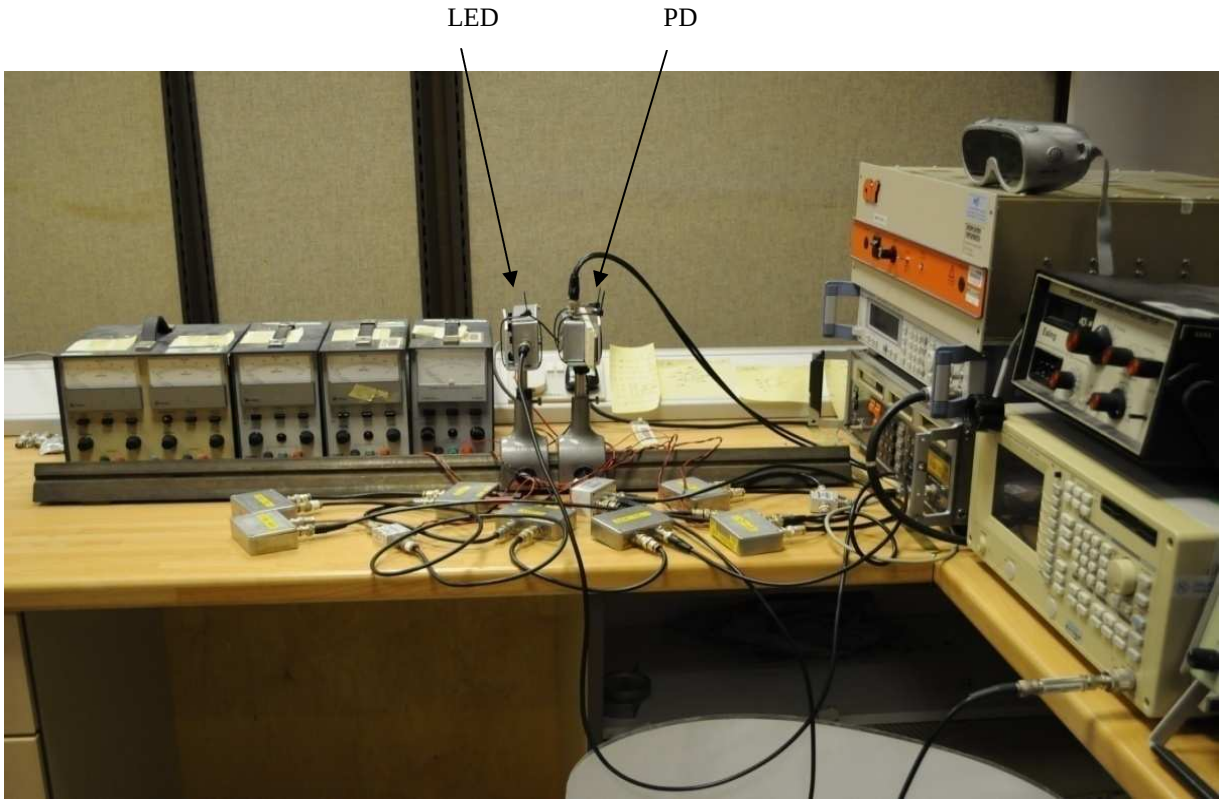

Figure 5.17 Final DCHHPA system set-up

At high pump, the LO signal over the PD can lead to serious drawbacks if its PD output is connected to the following stages without drastic consideration. For example, it can saturate the DB mixer (mixer two) due to a high level of input power, as well as forcing the

SAW BPF to an unstable condition or damage. Therefore minimizing the LO level of power at the PPA output is one of the key considerations; a limiter circuit was used to reduce this effect; however, due to both frequencies (i.e. 432.92MHz and 433.92MHZ) being close to each other (e.g. almost commensurate frequencies), the desired IF harmonic was affected as it is weaker than the LO.

In addition, the preselector IF SAW filter should have two primary functions, one being to accept a high input power, such as LC passive filters and ceramic filters. Secondly, it must provide high selectivity with low insertion loss, such as a Crystal filter [142]. A high-Q commercial Crystal filter was used in a previous published paper [143] at the VHF frequency range. The filter was from Filtronics INC (FN-3809) with a 240MHz centre frequency and 100 KHz pass bandwidth. The input power level was up to 5dBm, and it exhibited a good frequency response as shown in figure 5.18a. Although it showed high selectivity, it can be unstable at high pump power and economically, it is very expensive (i.e. 250$) (see Appendix B7 for schematic circuit). Most of the present-day crystal filters start being unstable when the input power exceeds zero dBm, and may result in poor performance, as reported in [81] .

Ambitiously, a Surface Acoustic Wave (SAW) filter may overcome the previous issues with respect to selectivity, rejection, low loss, input power and cost (i.e. less than 2$), employing such components offering substantial yet affordable benefits in the access network. Also it was shown to work well in both analogue and digital transceivers (i.e. AMPS, GSM) with a very good performance for frequency/phase noise, and it exhibited long term stability [144, 145]. Several SAW filters were implemented and tested for better selectivity performance. Two narrow band commercial SAW BPF filters with 120KHz pass bandwidth (Epcos-B3760, +10dBm input power) were cascaded in series, and two inductors were connected in series between the filters to build a virtual 50Ω point in

between the filters to compensate for the capacitive part of the filter impedance (see Appendix B8). The designed ultra narrow band pre IF filter aims to provide greater steepness to the filter edge and high selectivity, while maintaining low insertion loss, as shown in figure 5.18b. Moreover, it provides high stability, cost effectiveness and a better frequency response performance compared to the Crystal Filter, as illustrated in figure 5.18a.

The pre IF SAW filters were used and performed as a good preselected to pass only the desired IF signals, remove the noise outside its bandwidth, and also eliminate other odd- and even mixing products from breaking through. Moreover, these provided high isolation for unwanted frequencies, such as RF and LO, which could cause additional distortion products, and which are reduced in severity. High selectivity and low insertion loss are more desirable at this stage.

The IF amplifier in stage two is responsible for providing additional gain to the receiver to render incon sequential any noise introduced in the subsequent stages, as well as providing isolation by rejecting the reflect power form subsequent stage to pass back to the pre IF SAW filter. A mini-circuit variable LNA (ZFL-500LN) was used with 24db gain and 2.9dB noise figure. This amplifier can be used as what is known as an Automatic Gain Controller amplifier (AGC) at IF stages, which consists of a variable-gain amplifier and automatic gain controller mechanism that keeps the output swinging constantly over a wide range of input swings, and which seems to be more desirable for diffuse and quasi-diffuse optical links, particularly for mobile wireless receivers where the incident detected power signal may vary, due to mobility. In general, any appreciable amplitude with very low noise figure is desirable at this stage; two mount surface mini-circuit IF amplifiers (TAMP-72LN+) with very low noise figure (i.e 1dB) were connected in series, matched to 50 Ω

and successfully implemented and tested; each amplifier has almost about a 20dB gain; the cascaded IF amplifiers resulted in 40 dB gain overall (see appendix B9).

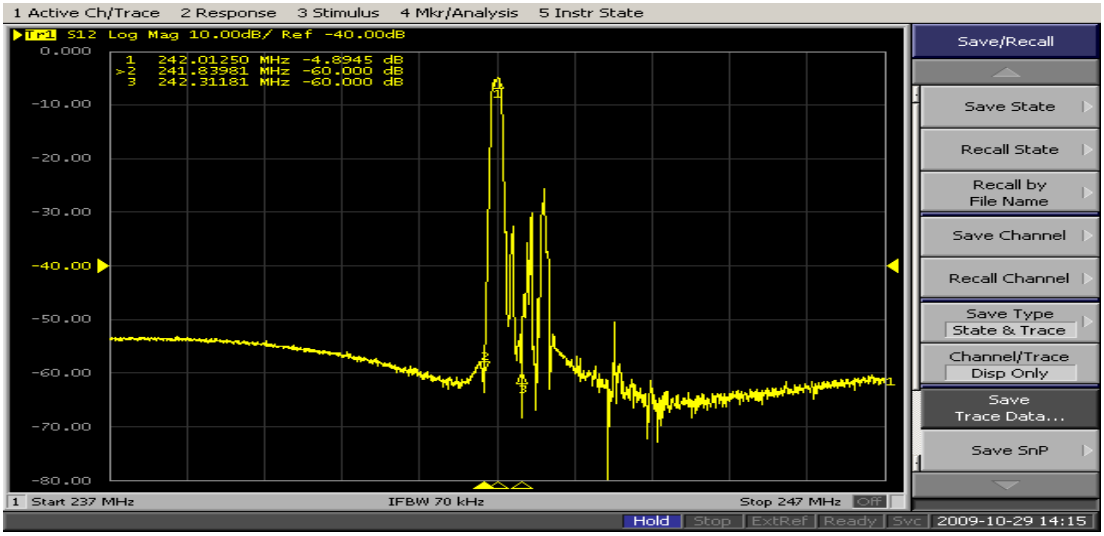

a) crystal filter (4.9dB insertion loss);

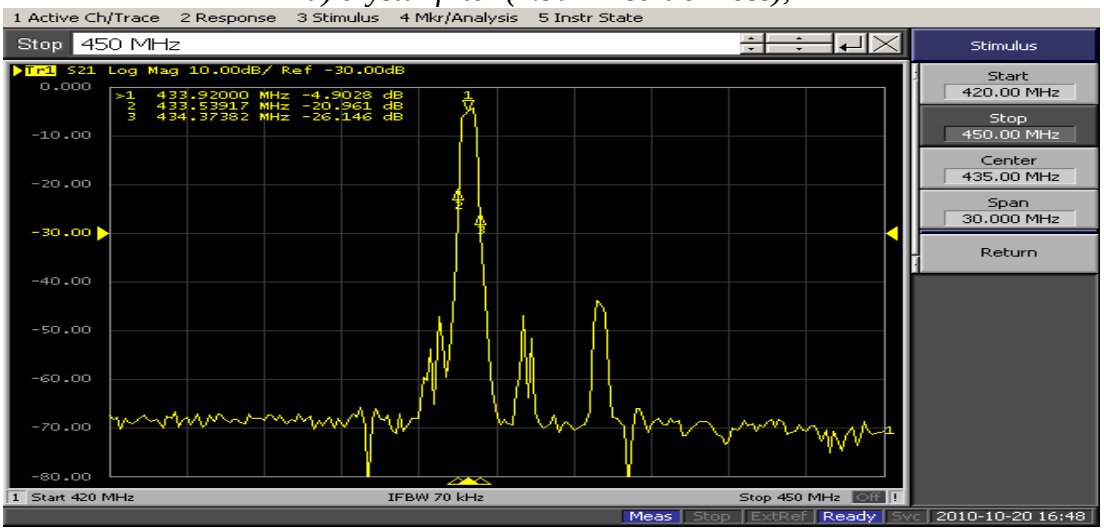

b) pre IF cascading SAW-760 filter (4.9dB insertion loss);

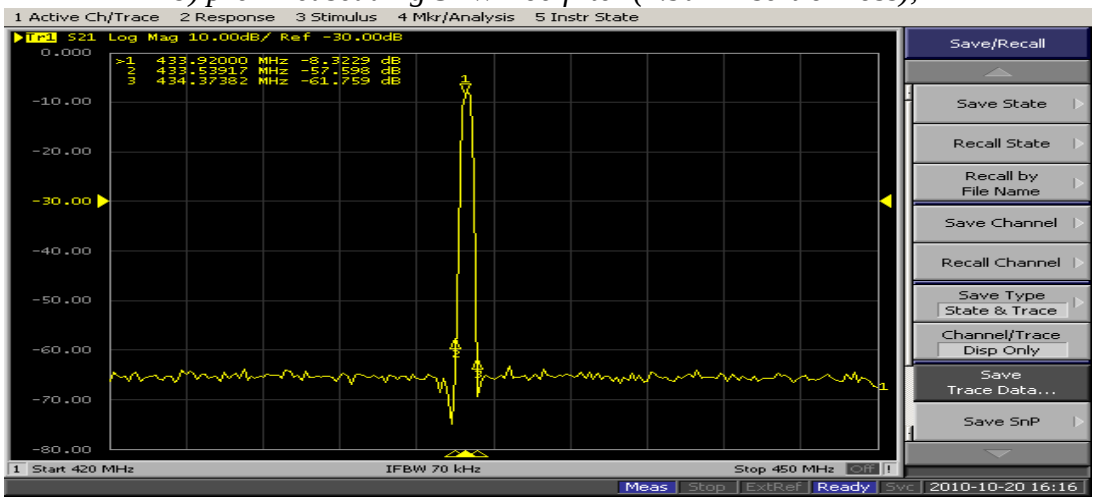

c) Post IF cascading SAW-790 filter (8.3 dB insertion loss).

Figure 5.18 Frequency responses of IF BPFs

In the third step in stage two, the LO signal is still the main cause of the distortion products, even if it has been minimized in the previous stage; therefore a cascading of two ultra narrowband SAW filters (Epcos-B3790, +5dBm input power) in series were designed and connected in series and matched to 50Ω impedance to be used as a post IF filter (see Appendix B10). The high ultra narrowband post IF filter aims to provide greater steepness at the filter edge and high selectivity, as shown in figure 5.18c; and pass only the desired IF signal whilst suppressing all other LO, harmonics and noise signals, as seen in the next practical results section.

5.4.2 DCHPPA Stage 3: Down Converter Circuit Configuration

Once the baseband signal translates to a higher frequency (IF) and passes through the multi-stages of IF signal processing, the up converter signal can be down converted to the desired frequency by conventional means, as shown in figure 5.16. The output of the IF stage is fed to the passive DBM (Mini-circuit ZAD-1H+), the LO for which originates from the same source pump used at the first stage via a high-Q passive BPF filter, which provides a convenient method of applying the pump, forming a *dc* blocking filter, rejecting other LO sideband frequencies, and any other noise generated through the two way power splitter (Mini-circuits ZFS-2-1W+, 3.3dB insertion loss at applied frequency). The use of the passive mixer has a stable output at an even higher LO pump, without the need for an additional *dc* source. However, it has approximately a 6dB conversion loss, which might decrease the total system gain; but this conversion loss was already considered and compensated for in the IF stage two (i.e. IF amplifier). The output of the down-converter DBM mixer is channelled through a passive LPF (less than 0.1dB insertion loss), which passes only the desired baseband signal and eliminates other mixer products. At this stage, the baseband modulation can be recovered at low cost (i.e. no variable attenuator or phase shifter or additional dc source). Another possibility is to use an active DB mixer with

conversion gain (see Appendix B11). However, a voltage variable attenuator circuit is needed to adjust and bring down the pump level to the required LO active mixer level, as well as an additional dc source supply being needed. It can be argued that resistors and active devices are the main source of noise. Therefore, the design has considered both the noise level and power consumption for wireless devices.

5.4.3 DCHPPA Stage 2: IF Signal Processing Practical Results

The bock diagram for the DCHPPA, second stage, is shown in figure 5.19. All the designed PCB circuits were tested and their performances were measured at each stage. Experimentally the PPA up-converter stage showed a 25.11dB of up-converter gain at a frequency of 433.92MHz, as shown in figure 5.5(b).

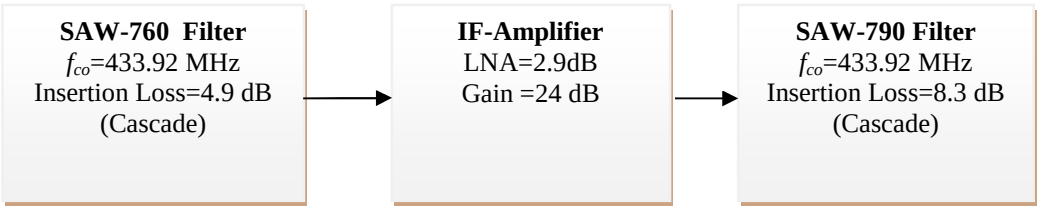

Figure 5.19 Block diagram for DCHPPA stage2: IF signal processing stage

The pre IF SAW filter (cascade-760) showed superb rejection and isolation for the unwanted RF and LO signals, as shown in figure 5.20(b); the graph showed 48dB signal isolation in the pump frequency [i.e. +12dBm-(-36.14dBm)]. This can be seen as promise result compared to 20dB isolation for a well-designed circulator. Also it can provide a convenient way to extract the IF desired signal with only ≈ 3 dB insertion loss.

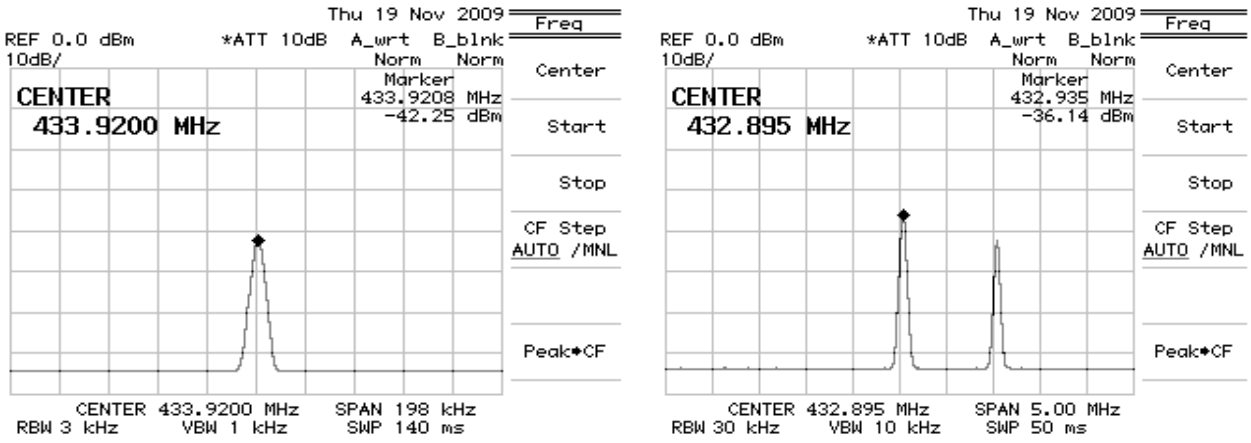

(a) (b)

Figure 5.20 Frequency spectrum of up-converter signal after pre IF SAW BPF showing (a) 2.97dB insertion loss in 433.92MHz; and (b) 48dB insertion loss in the pump signal 432.92).

As described in the previous section, the IF desired signal then fed to an IF amplifier (i.e. 24dB gain) for additional gain, and then fed to an ultra narrow post-IF SAW (790) filter. The results show that the IF signal processing stage provides an additional gain to the original PPA up-converter signal with 15.31dB gain (i.e. 40.25dB gain in total), as shown in figure 5.21(a). The graph show that the LO pump power was isolated, with almost 83dB signal isolation to the LO [i.e. 12dBm-(-71.03dBm)], measured over the PD at pump frequency operation as shown in figure 5.21(b).

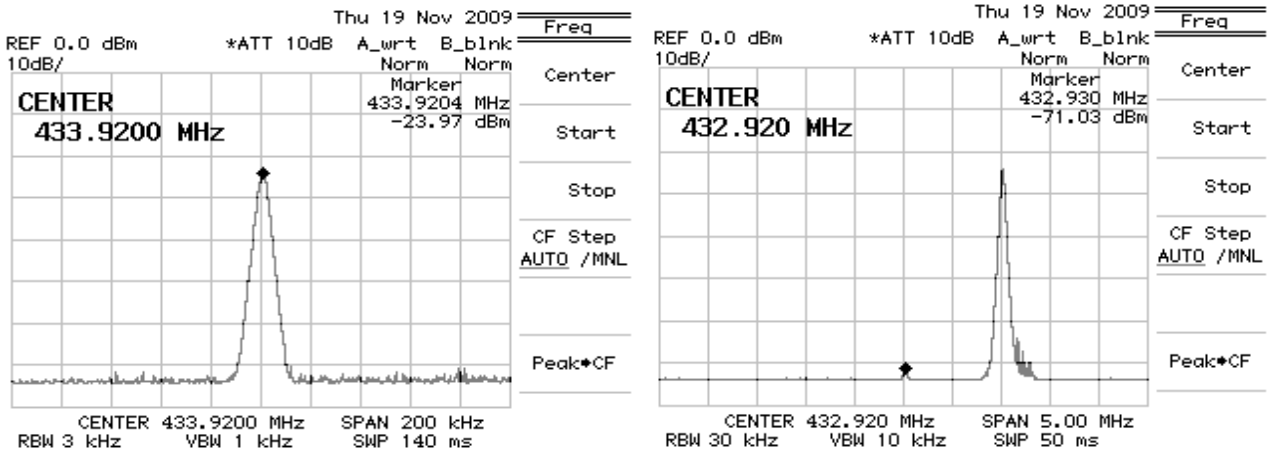

(a) (b)

Figure 5.21 Frequency spectrum of up-converter signal after post IF SAW BPF (790) showing (a) 15.31dB gain over original up converter signal; and (b) another 34dB insertion loss in the pump signal 432.92).

5.4.4 DCHHPA Stage 3: Baseband Recovery Results

Experimentally, the DCHPPA technique overall subsequently exhibited a 34.9 dB baseband signal gain over the modulated optical signal, as shown in figure 5.22. This result was obtained by employing a passive DB mixer with about 6 dB conversion loss. However, an active mixer can be used instead of passive mixer, as reported in our previous work [143]; the receiver would exhibited almost 44.9 dB baseband signal gain over the optical signal.

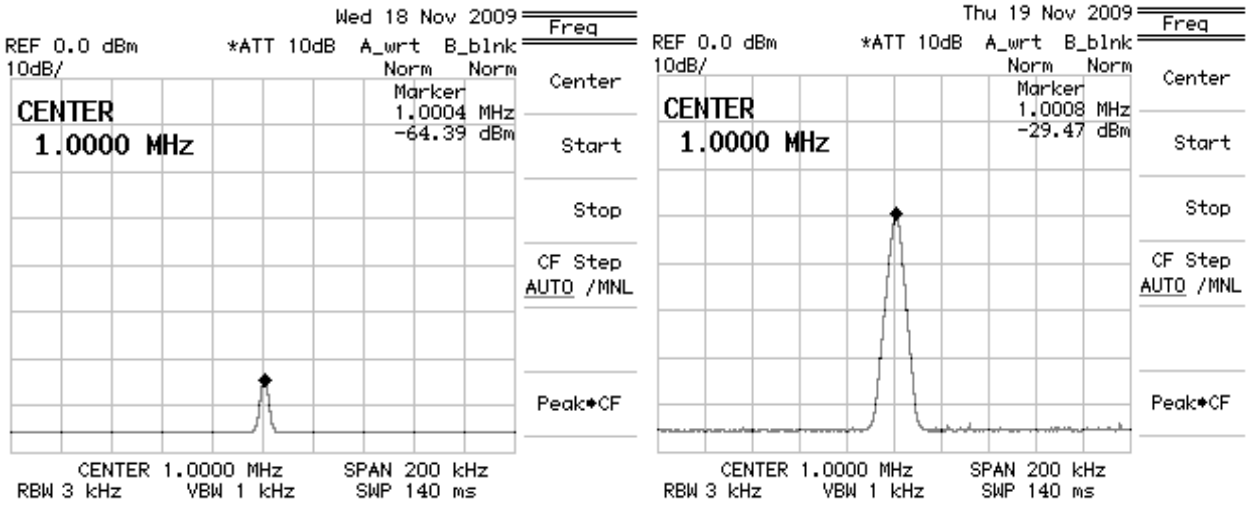

(a) (b)

Figure 5.22 Frequency spectrum of (a) 1 MHz modulated optical signal-direct detection response; and (b) 1 MHz recovered baseband signal using DCHPPA showing 34.92dB gain over the modulated optical signal.

In another practical scenario, the experiment was performed by varying the DD modulated optical signal from 1 MHz to 5MHz as performed in section 5.3.3.4. The DCHPPA system recovered the baseband signals as shown in table 5.2, the gain decreased according to the increase of RF signals; therefore, the increase in DCHPPA gain is proportional to the increase in PPA gain. It can be surmised that, without achieving desirable gain at PPA stage one, it is worthless to have gain at the baseband signal recovery. In other words, the highest gain at the PPA stage one is more desirable with respect to receiver sensitivity (i.e. SNR).

Previous work [16, 129] in non-degenerate up-converter mode reported a similar approach to recovering the baseband signals, with the result of 7.41dB and 12.5 dB gain respectively; results were achieved with a different design and techniques. Another possibility is to use the parametric amplifier as down-converter mixer, due to its ultra low noise figure compared to that of a conventional mixer, but extra care needs to be taken due to the complex input matching circuit required.

Table 5.2 DCHPPA frequency response at various optical signals

Optical signal (R_F) MHz	**Pump signal (F_P)MHz**	**Recovered baseband signal (F_b) dBm**	**DCHPPA gain (dB)**
1.0	432.92	-29.47	34.92
2.0	431.92	-33.39	31.0
3.0	430.92	-36.86	27.53
4.0	429.92	-40.44	23.95
5.0	428.92	-44.08	20.31

5.5 Gain Chain DCHPPA System.

The current proliferation of optical wireless devices result in large diversity of designs and most of the future devices need better sensitivity, and have a requirement to be aware of energy scale-down. Significant attention was paid to increasing the sensitivity and reducing energy consumption, such that, the PPA works in equilibrium mode (i.e. no bias source), employed passive components, low power components and low loss components in designing the OW receiver.

All the receiver components can have a direct affect on is the noise figure (NF), according to Friis formula for NF calculation. An important consequence of this formula is that the overall NF of the RF/MW receiver is primarily established by the NF of its first

amplifying stage (i.e. PPA stage). Subsequent stages have diminishing effect on SNR and do not have a drastic affect, but everything must be done in maximizing the gain and dynamic range. The overall receiver NF can be expressed as:

$$F_{receiver} = F_{PPA} + \frac{F_{rest} - 1}{G_{PPA}} \tag{5.1}$$

where F_{rest} is the overall noise factor of the subsequent stages and G_{PPA} is the PPA gain; the overall NF of the receiver ($F_{receiver}$) is dominated by the noise figure of the PPA if the gain is sufficiently high.

According to the above, the schematic circuit diagram of an optical gain chain DCHPPA system is shown in figure 5.23. The diagram below shows typical components used to build the receiver, as mentioned in the previous section, in addition to a new stage added to the IF signal processing stage, which includes the IF amplifier and other SAW BPF. The main advantage is in the superior sensitivity that designers almost take for granted; additional gain in the IF stage makes the desired IF signal levels high enough for noise sources at the IF signal processing stage so as to have a negligible effect on the SNR.

As mentioned earlier, all the receiver components were built in individual PCBs and were connected by 50Ω coaxial cables. In the gain chain DCHPPA circuit configuration, two Mini-circuit IF LNA amplifiers (TAMP-72LN+ operates at 5 volts) were built in a cascade, with each amplifier having a 20dB gain and a very low noise figure (i.e. 1 dB). This type of amplifier can improve a system spur-free dynamic range, which is often the critical driver in many receiver applications. Moreover, it helps subsequent stages (i.e. stages two and three) to enable greater sensitivity for receiver applications.

Experimentally, the gain chain DCHPPA technique overall subsequently exhibited a 56.25 dB baseband signal gain over the modulated optical signal, as shown in figure 5.24.

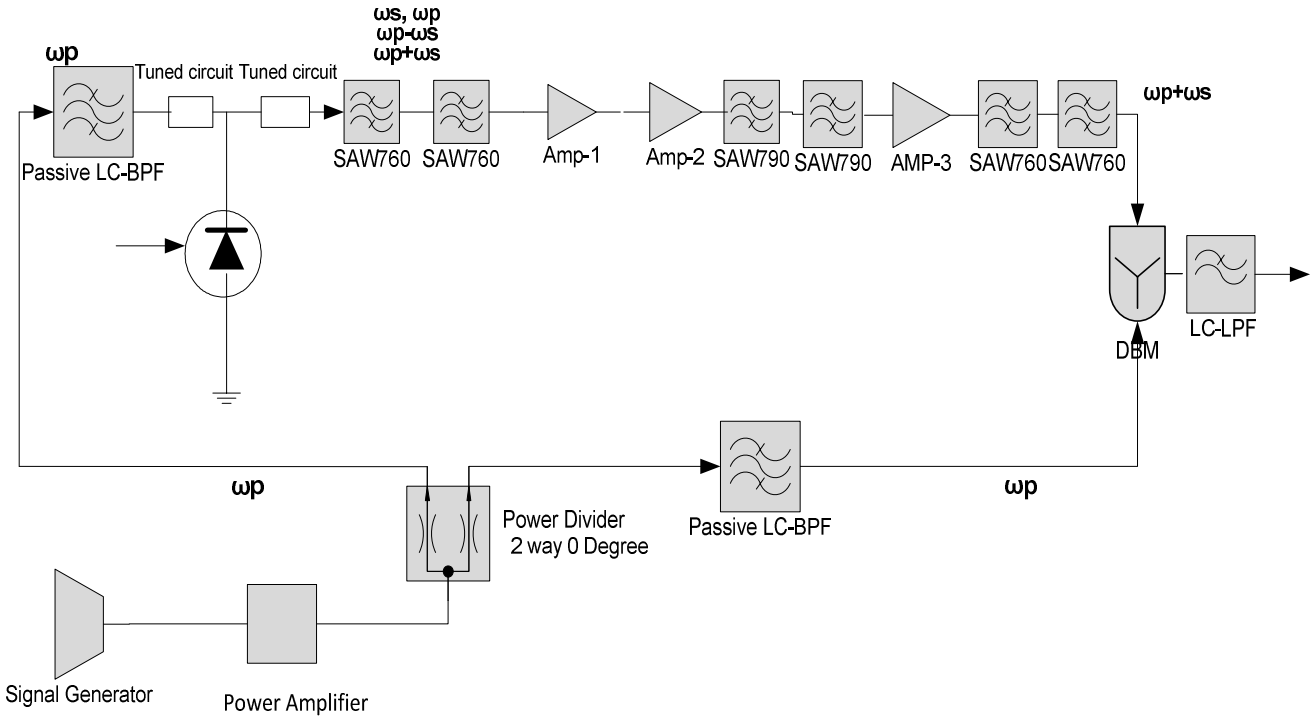

Figure 5.23 Gain chain DCHPPA circuit diagram

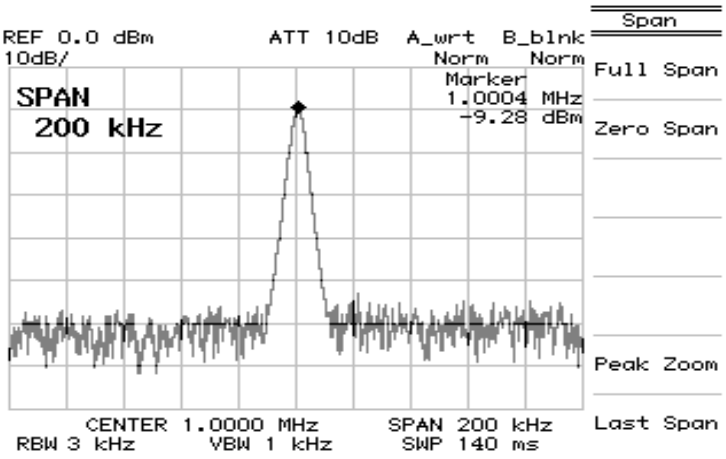

Figure 5.24 Frequency spectrum of 1 MHz recovered baseband signal using chain gain DCHPPA showing 56.25dB gain over the modulated optical signal.

The technique can be seen as a promising approach to achieve high gain at low cost, compared to other optical amplifiers designed for free space or a long-haul environment, such as EDFAs and PSA amplifiers. Although the practical implementation for the whole receiver as individual PCBs circuits performed well and exhibited desirable baseband signal gain over the modulated optical signal, implementing the whole receiver

on only one PCB circuit, as shown in (Appendix B12), can provide better performance with respect to noise and conversion gain; this because all the components are implemented in one BCP with short transmission lines (e.g. as coaxial cable at high frequency has high signal attenuation and long signal delay), this can also increase the compactness and reduction of parasitic effects, and makes the system easy to isolate using a die-cast box. Effort was made to consider all the PCB technical requirements, particularly at high frequency; however the performance regressed, as compared to employing individual BCP circuits. Both passive and active surface mount components were employed, which can cause a ground loop problem. Moreover, cascade amplifiers may oscillate when mounted together, or due to not being physically separated, which can cause coupling feedback that might also need extra care to decouple the *dc* power supply lines that feed the two stages.

5.6 Summary

To summarise, a novel approach to the design of an optical wireless receiver has been presented, based on the superheterodyne principle but using photoparametric amplification at the first stage instead of a resistive/transistor based mixer. The designed OW receiver acts in a parallel manner to a conventional double super heterodyne detector system, but without the noise penalty normally incurred. DCHPPAs have properties that make them potentially attractive for use in future optical wireless communication systems. In particular, they can provide a very high gain with high selectivity, combined with very low noise operation. The experimental work described in this chapter includes the design and implementation of wide band test-bed which showed that, the gain frequency variation was in accordance with theory and simulation. The tests on the up-converter, though, in a preliminary stage (i.e. PPA) have indicated promise, and can be implemented satisfactorily

using a PD in equilibrium mode, leading to potentially greater conversion gain at lower penalty (i.e. in power and noise); the PPA is better at quite a low load impedance, which can provide a better GBP; as has also been shown, the gain is related to the pump power over the reactance impedance, the value of reactance impedance at applied frequency, and the idler frequency over the source frequency. In addition, the junction should exhibit high nonlinearity, with very low parasitic resistance.

The tests on the second stage (i.e. IF signal processing) indicated a promise, and can be implemented satisfactorily using SAW filters and very low noise amplifiers that lead to potentially high selectivity and sensitivity, with additional gain at an early stage also leading to a cost-effective solution. Tests on the third stage (recovery baseband) indicate good results, and are implemented by using passive and low loss components (i.e. DB mixer); alternatively, an active mixer can provide better overall conversion gain but an additional attenuation circuit and power source is needed to accomplished the work. The DCHPPA technique overall subsequently exhibited a 34.9 dB baseband signal gain over the modulated optical signal. In addition, it seems that employing a chain gain DCHPPA technique to be preferred, as is subsequently exhibited by a 56.3 dB baseband signal gain over the modulated optical signal, which can maximize the SNR at signal frequency; this technique can bring up the signal gain to certain levels required for effective utilization. Optoelectronics mixing in DCHPPA appears very promising as means of linear amplification and frequency conversion of optical signal that offers the prospect of significant benefits to OW and FSO, as well as offering improved performance in fibre access networks (i.e. wireless and long haul applications). The next chapter is concerned with performance analysis as well as analysing the noise performance of the amplifier, as high gain is meaningless without a full appreciation of the SNR aspects.

Chapter 6

6. Performance Analysis and Noise Analysis

An analysis of the up-conversion PPA is given with respect to three approaches, theoretical simulation and experiment results. Noise analysis and discussion of both the DD/IM photodetection technique and the incoherent heterodyne (PPA) technique included the DCHPPA stages are also presented; both, signal to noise ratio and noise figure analysis have been experimentally presented.

6.1 Performance Analysis of Theoretical, Simulation and Practical Results

The research in this section continues to identify and quantify important variables and parameters that optimise the performance of a front-end optical wireless receiver. The DCHPPA was successfully demonstrated and measured in the previous chapter; the core element in this receiver being the up-converter PPA first stage. The receiver performance usually depends on the photo-detector device itself (i.e. photodiode) and the design technique (i.e. external photodetector circuit). The main challenge of designing a high sensitivity receiver is how to deal with the conflict requirement of gain and bandwidth and the noise performance, which, in most cases interacts aversely with the previous two requirements. This section continues to examine the effect of the external circuit on the performances of the amplifier with respect to conversion power gain, bandwidth and noise. These will include the effect of load impedance, the *dc* biasing source and the applied pump power. It is worth comparing the theoretical, simulation and practical results which helps to validate the theoretical and simulation models presented in chapter 3 and 4 with the experimental setup result in chapter 5.

6.1.1 Load Impedance Effect

A convenient way to measure the PD output current is to convert it to a voltage within a load resistor. The up-converter PPA was simulated by varying the value of load resistance at 15dBm pump power, as shown in figure (6.1). A 23.81 dB up-converter gain was predicted at 50Ω load impedance. The gain increases in proportion to the decrease in load impedance. For example, when the load impedance is equal to the series resistance (R_l=R_b), the gain improves by 6.2dB, compared to the 50 Ω load. Moreover, the gain improves by 8.6dB when (R_l=-R_b).

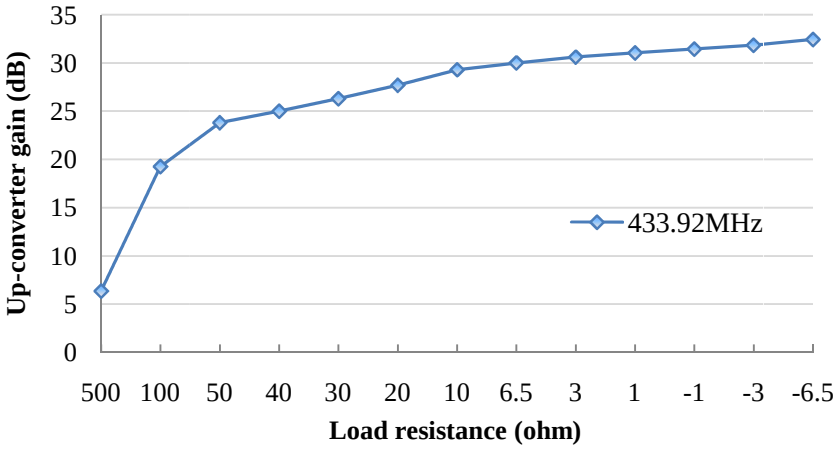

(a)

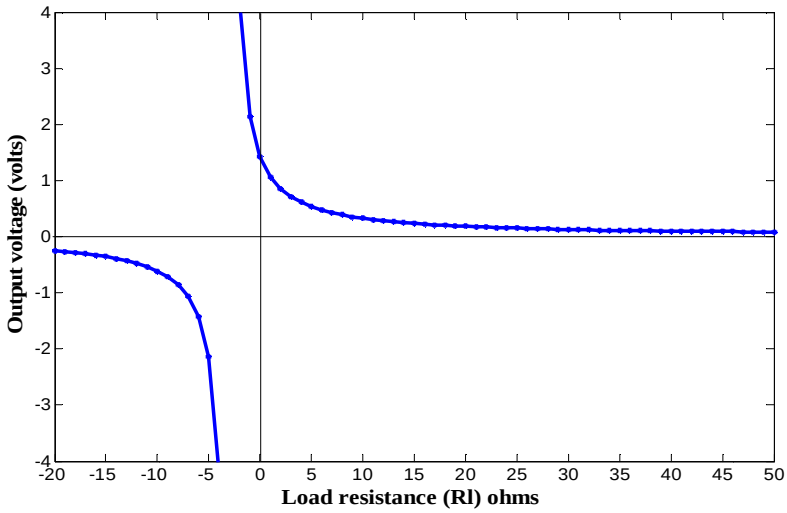

(b)

Figure 6.1 PPA load impedance (a) Simulation result; (b) Theoretical result

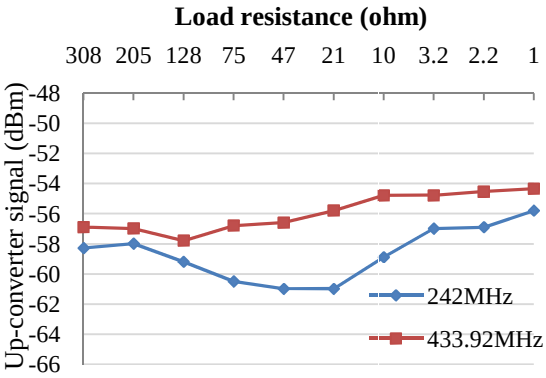

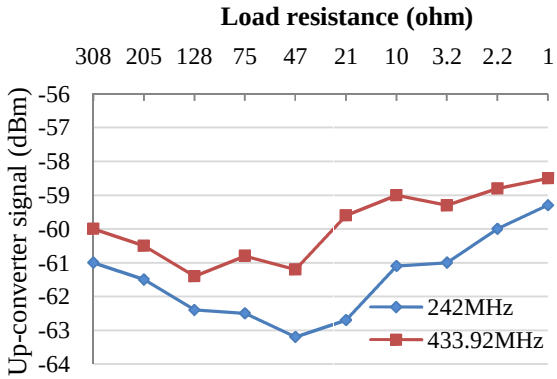

(a) 20dBm pump power with tuned circuit *(b) 20dBm pump power without tuned circuit*

Figure 6.2 Measured PPA Load impedance

The simulation result verified the theoretical result, as shown in figure 6.1b, the optimal power transfer occurred at very low load impedance, particularly when ($R_l = -R_b$), and hence, the PPA can be considered as a low impedance amplifier. Practical experiments were also performed (as mentioned in the previous chapter); the measurement results are shown in figure 6.2. The graph illustrates that the maximum power transfer occurs at low load impedance (i.e. 1Ω) and the up-converter gain at low load exhibits an increase of an average of 3dB, compared to 50 ohms load impedance. The practical results verified both the predicted simulation results and the analytical analysis, as shown in figure 6.1 and 6.2; the three results presented the same pattern with very good agreement. It is clear that the PPA performs much better at low impedance, and hence can provide high GBP. The high GBP may increase the amplifier thermal noise, due to operating at low load resistance. It is a trade-off between GBP and receiver noise; this conflict helps the designer to choose the load impedance value, based on receiver application requirements. Clearly, for optimum load conditions and complete pump power absorption across the junction, the load impedance must be set as equal to bulk resistance.

The research has shown that a PPA may be able to provide unexpected gains at low load impedance, in comparison to standard optical wireless receivers, and also perform well at zero bias for the photodiode. Tuning the pump circuits to suppress feedthrough improves the performance of the PPA even more, such that a broader bandwidth operation is possible using this with low load impedance, and also noticeable improvements in up-conversion gain are seen.

6.1.2 Biasing Circuit Effect

The research has shown that a PPA under zero bias modes leading to potentially greater conversion gain. The benefit of this mode is that the degree of nonlinearity of the

CV characteristics is high. The PPA performance was evaluated by varying the dc bias source, as shown in figure 6.3 at 15dBm pump power. A 32.5, 23.8 and 17.1 dB up-converter gain were predicted in theoretical, simulation and practical results respectively. The gain then gradually reduced by increase the reverse *dc* bias voltage. The greatest steepness occurred between the zero bias and -1volt due to the high degree of nonlinearity. The gain curve starts to follow the junction characteristics according to the degree of steepness of the CV curve until it reaches the zero gain point, in which the PPA starts to act as a loss mixer. The graph shows that the theoretical and simulation models are highly linear compared to the practical results. However, the three approaches presented the same pattern. This represents a very good agreement between the three approaches, which helps to predict the performance of PPA under any *dc* bias conditions.

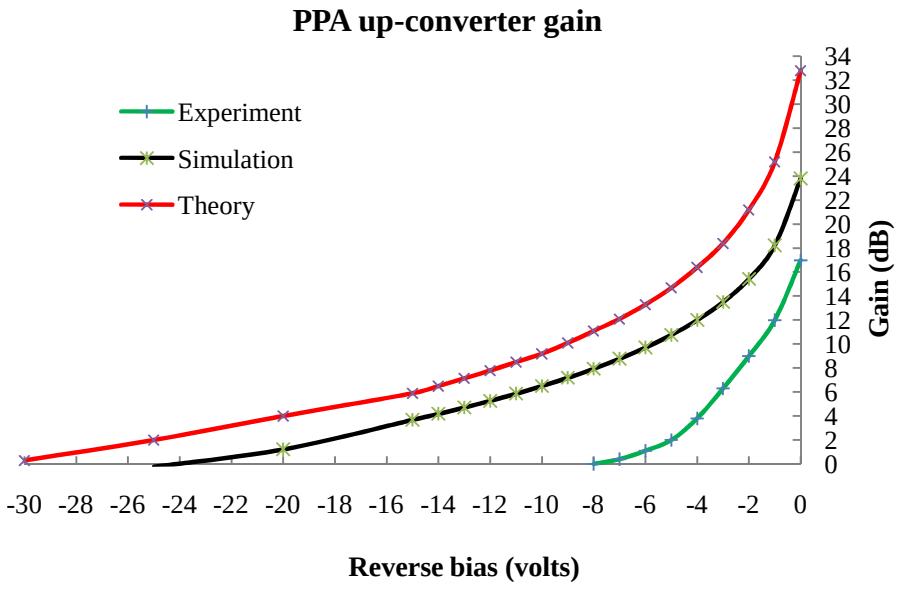

Figure 6.3 Gain related to various reverse bias voltages

The main advantage of operating in equilibrium mode is the highest gain which is essential for a wireless application with a tight power budget. Furthermore, this mode provides low noise performance, caused by bias current (i.e. leakage current noise) and bias resistance (i.e. Thermal noise). However, there is one main restriction in this mode,

which is to avoid forward biasing the photodiode, which may incur noise and other penalties (i.e. increase the forward current and hence increase the dark current). The main drawback of this mode is the low frequency response and low speed, compared to photodiodes under high reverse bias.

6.1.3 Pump Power Effect

Gain roll off is an inherent phenomenon in this type of parametric amplifier (ω_i/ω_s), the PPA up-converter gain is also related to the level of the applied power across the nonlinear junction, as predicted in the gain formula, where low bulk resistance and low reactance impedance is desirable. The gain may be optimised through the appropriate adjustment of the ratio of pump voltage across the junction to the voltage across the reactance impedance and series resistance. It is clear that small series resistance compared to reactance impedance can provide better gain conversion. Figure 6.4 illustrates the relationship between gain and applied power; the three approaches show that gain increases linearly with the applied power, which verifies the concept of the linear amplifier, where the amplifier output signal is strongly based on the input signal multiplied by the gain. Low pump makes the amplifier behave like a loose mixer and very large pump can lead to 1dB gain compression (i.e. explained in previous analysis), whereas the amplifier starts to behave as a nonlinear amplifier. The three approaches follow the same trends, presenting a very good agreement and close results. The high gain or the high gain bandwidth products (GBP) is meaningless without a full appreciation of the noise aspect.

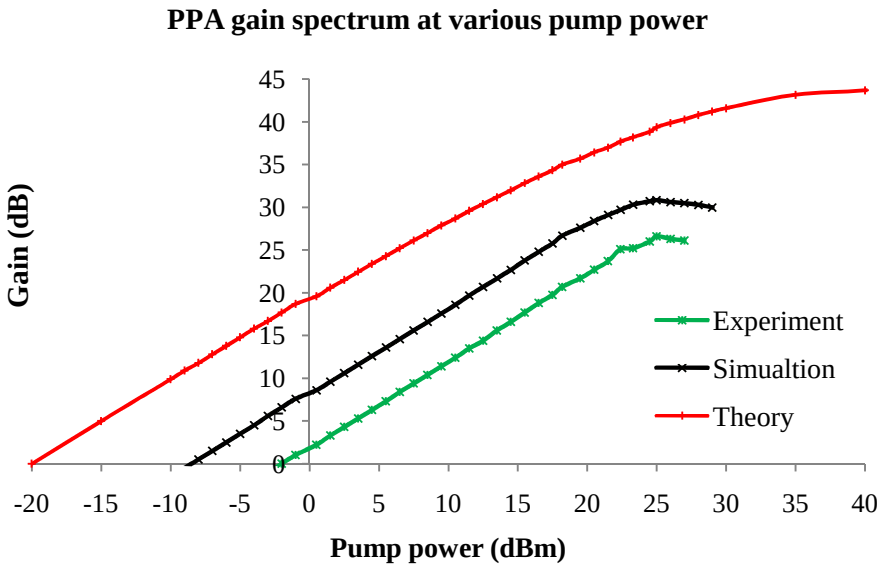

Figure 6.4 Gain related to various pump power

6.2 Noise Analysis

The term noise describes the unwanted components of an electrical signal that tend to disturb the transmission and processing of the signal; in other words, it refers to any signal present in the receiver other than the desired signal. It may broadly classify noise according to its source, as either external or internal to the system. External induced noise and internally generated noise and both sources lead to degradation of the signal quality, and put a lower limit on the sensitivity of any system. External noise includes those disturbances that appear in the system as a result of an action outside the system (i.e. noise from 60 Hz power lines and static caused by electrical storm). Internal noise includes all noise that is generated within the system itself. All resistors and semiconductor components have an internal source of noise, and produce a discernible noise. However, the photo-detector semiconductor has an additional source of noise due to the incident optical power and optical background noise. Noise in the optical detector can also be described as being either additive (i.e. when there is no optical signal present) or signal dependent (i.e. when optical signal present) and the amount of a signal dependent noise is also frequently proportional to the signal power (i.e. the noise is effectively multiplied by

the signal power). An understanding the origins of noise helps to characterise the performance of wireless IR photodetector receiver, as the amount of noise present in a photodetector system is the primary factor that defines its sensitivity.

6.2.1 Photodetection Noise Sources

The optical signal at the end of an optical link (i.e. fibre or free space) is often highly attenuated, and so any optical detector noise should be as small as possible, to prevent any degradation of the signal quality and put a lower limit on the receiver sensitivity. Noise in the photo-detection process arises from radiation entering the detector and from internally generated noise. There are many types of noise source in photo detection, as shown in figure 6.5.

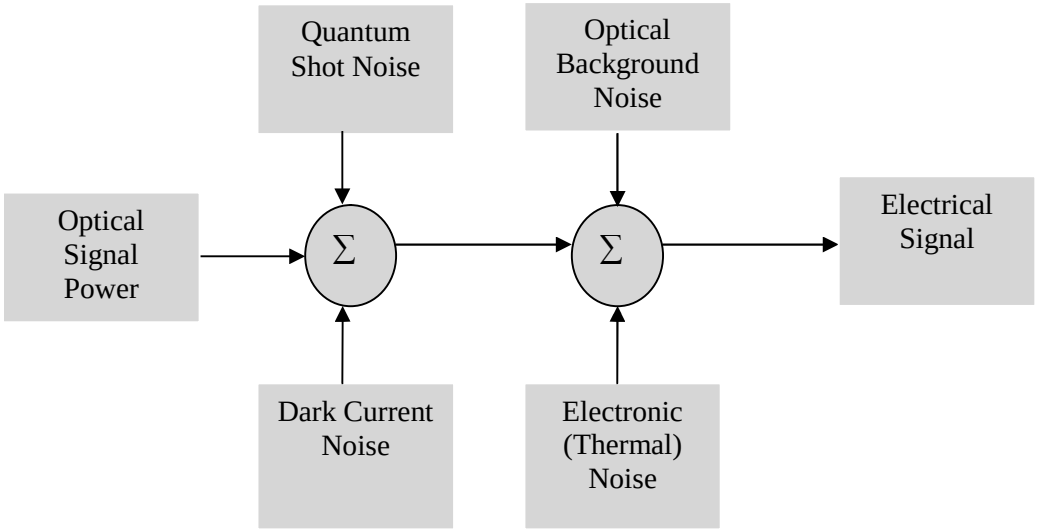

Figure 6.5 Noise source in photo-detector system

The major noise sources which can significantly affect the system sensitivity are shot noise, dark noise and thermal noise, as other noise sources are considerably negligible compare to these. A review analysis of noise sources, especially in semiconductor photodetectors, can be found in [119, 146].

Noise, being a random process, cannot be described as en explicit function of time, as there is no way to determine exactly what value of noise process will have at any future time; and the most widely used characteristic is the root-mean-square (RMS) value [119]. Noise can also be characterised in the frequency domain; this technique is in fact preferred for noise analysis and the most important frequency domain characteristic of noise process is its Power Spectral-Density (PSD). PSD is defined as the Fourier transform of the time-domain autocorrelation function and the impact of this relationship is that the PSD corresponds to the time-averaged noise power that present in a 1Hz bandwidth amount the measurement frequency. The following section will examine the type of noise sources commonly found in photodetector, and how can be represented in the optoelectronic communication system.

6.2.1.1 Shot Noise

Noise in the photodiode is primarily due to shot noise, which is related to dark current and photo current and any other currents flowing through the junction, such as bias current. The random nature of the generation of carriers in the junction yields also a random current fluctuation that make up the shot noise, which result of the random arrival rate of photons from the source of radiant energy under measurement and ambient background illumination (i.e. shot noise is far smaller for optical fibre than for OW). The effect of this process can be represented as a noise source, and can be expressed either as a voltage source or a current source. The mean-square value of the shot current for *pin* photodiode is given by:

$$\langle i_{sh}^2 \rangle = 2q(I_p+I_d)B \qquad (A^2) \tag{6.1}$$

where q is the electron charge, I_p is the photo-generated current, I_d is the dark current, and B is the noise measurement bandwidth.

6.2.1.2 Thermal Noise

Thermal noise, also known as Johnson noise, is a result of thermally induced random fluctuations in the charge carriers in a resistance. These carriers are in random motion in all resistance at a temperature higher than zero. The shunt resistance and the bulk resistance and the load resistance in a photo detector has Johnson noise associated with it. The mean-square value of the thermal current for *pin* photodiode is given by:

$$\langle i_{th}^2 \rangle = 4kTB/R \quad (A^2) \tag{6.2}$$

where k is Boltzmann's constant, T temperature, in degrees Kelvin (i.e. 290K, IEEE standard) and R resistance in ohms. The total noise current generated in a photodetector is given by:

$$\langle i_n^2 \rangle = B\,(2q(I_p+I_d) + 4kT/R) \quad (A^2) \tag{6.3}$$

There are also other noise sources known as *Excess Noise,* that exceeds shot noise at very low frequency, in which noise power varies inversely with the frequency (*1/f*) also known as modulation noise or flicker noise, and thought caused by the imperfection in the junction materials, and it is insignificant at high frequency.

6.2.2 Photodetection Noise Analysis

In any communication receiver, it is useful to consider the limits of the performance of a system set by the SNR. In order to investigate the performance for the optical receiver in DD/IM detection, the most important parameter in the analysis of a communication system is the signal to noise ratio in the receiver (SNR). The SNR for DD/IM detection is defined as:

$$(S/N) = (\text{Signal Power}/\ \text{Total Noise Power}) \tag{6.4}$$

In contrast, the dominated noise in the DD/IM is due to the thermal noise (at very low ambient light) and the shot noise (at very high ambient light). In referring to the commercial used photodiode and its parameters as shown in chapter 4 and 5, the photodiode photocurrent was calculated at 1.414mW power signal, and equals *Ip*=0.87mA (i.e. Responsitivity *R*=0.62). The calculated photo-detector shot noise at 9MHz bandwidth is (i_{sh}=5*10^{-8} *Amp*). The thermal noise current for the photodetector at 9MHz bandwidth with 290^{o}K degree and 50 ohms load is (i_{th}= 5.4*10^{-8} *Amp*), Also, the mean square dark current (i.e. due to the bulk and leakage current) at 2 *nA* dark current as defined in: ($<i_{db}^{2}>$ = *2q(Id)B* (A^2), the calculated noise value is (i_{db}=*7.58**10^{-11}Amp). Thus for this photodetector at high optical power (p=1.414mW), the RMS thermal noise is similar to the RMS shot noise, whereas the dark noise current is negligible compared to shot and thermal noise, as any current less than 10^{-8}Amp, introduces negligible noise [69].

However at low power incident light (i.e. 0.14mW), the RMS thermal noise is about 3.4 times greater than the RMS shot noise current. It is clear that the contribution of thermal noise may be reduced by increasing the value of the load resistor, although this reduction may be limited by bandwidth considerations. The signal to noise ratio for direct detection SNR is given by:

$$SNR = \left[\frac{i_s^{\,2}}{i_{th}^{\,2} + i_{sh}^{\,2}} \right] \qquad (6.5)$$

For example, the SNR at 9MHz bandwidth with an incident optical power of 1.414*mW* is equal to 81.5dB, where the SNR for low optical power such as 0.141*mW* decreased to 63.49dB. Clearly, the SNR decreases proportional to optical power decrease. Furthermore, the SNR value also decreases proportional to the bandwidth increase. In contrast, when the optical power signal is relatively high, then shot noise power dominates; the SNR is

referred to as being a quantum noise limited or shot noise limited. However, when optical power is low, the thermal noise dominates, and the SNR is called thermal noise limited.

In addition to SNR performances, a particular receiver can also be characterised by its noise figure (NF) and the noise factor (F) [147], where ($NF=10logF$). NF is a measure of how much noise is added by the photodetector or the preamplifier or following the main amplifier. The NF is a versatile method to determine the quality of such an amplifier, and how much degradation of the SNR is contributed by the photodetector, and it is a key element in measuring receiver sensitivity (i.e. $S_{reciver}=F*K*T*B$). Therefore, it is helpful to determine the noise factor (F) of the photodiode theoretically, as it is quite unacceptable to measure this experimentally, due to it operating at different domains; (optical as input and electrical as output). The SNR at the input of the photodiode (SNR_{in}) in the dark condition is given by :

$$SNR_{in} = \left[\frac{i_s^{\,2}}{i_{th}^{\,2}} \right] \tag{6.6}$$

Where the SNR at the output of the photodiode (SNR_{out}) is given by equation 6.5. The noise factor (F) and the Noise figure (NF) are given by:

$$F = SNR_{in} / SNR_{out} = \left[\frac{\frac{4KTB}{R} + 2qI_p B}{\frac{4KTB}{R}} \right] \tag{6.7}$$

$$NF= 10\ log\ ((SNR_{in} / SNR_{out})= SNR_{in,dB} - SNR_{out,dB} \tag{6.8}$$

At, $1.414mW$ incident optical power, the calculated noise factor (F) of the photodiode is 1.87, which equivalents to 2.7dB noise factor (NF). These values may vary according to the photodetecor temperature, incident optical power, bandwidth and load impedance. The above analysis provides a brief idea of the noise sources associated with the photodetector

itself; however, the noise associated with optical sources such as the quantum shot noise of optical sources is difficult to control at the receiver end, and will result in the degradation of optical sensitivity, which may expressed as an optical power penalty [148].

6.2.3 Photoparametric Up-converter Noise Analysis

The noise in photodetection system is mainly dominated by the thermal noise and shot noise. Coherent detection (i.e. heterodyne and homodyne) has been shown in [49] contains very sensitive techniques, and provide excellent rejection of adjacent channels. However, incoherent-heterodyne PPA technique also exhibited low noise performance, due to mixing and amplification incurred inside the variable reactance impedance. The author in [149] made a comprehensive analysis of the effect of variable capacitance (i.e. reactance impedance) amplifications in the case of bulk resistance being the only parasitic element. The calculation for both idler frequencies (up/down frequencies) showed that the noise figure for the amplifier is basically determined by the dynamic quality factor of the diode (Q). The larger Q is, the lower the noise figure which can be obtained, and it is impossible to build a low-noise amplifier if capacitance variation is small (i.e. abrupt junction). Moreover, the author in [32] showed that the variable capacitance amplifier can have less than a 1dB noise figure in cooled conditions. In PPA operation, particularly the up-converter approach, the noise were theoretically analysed in detail in [69, 71, 137, 150] and was shown to have better SNR compared to the photodiode, followed by preamplifier, and it was also shown that it had better SNR at a few hundred MHz bandwidth, compared to a photomultiplier (APD).

6.2.3.1 PPA Noise Analysis

SNR is quite a common performance criterion in communication systems measurements. The analysis of the photoparametric amplifier in terms of SNR must be

undertaken in two circumstances: Firstly, without any pump applied, the system acts as normal DD/IM technique. Secondly a more interesting mode is the photoparametric technique. In the latter case, the up-converter mode of operation leads to an increase in the mean value of the junction capacitance (C_{mean}) which may act adversely with the system bandwidth. The DCHPPA system may also limit the receiver bandwidth, due to the High-Q BPF in the IF signal processing stage (i.e. second stage, $BW= fc/Q$). At the beginning, it is essential to measure the frequency response of the PD with no pump applied; this can help to estimate the PPA frequency response according to the applied voltage across the junction. As a consequence, a more accurate and realistic SNR measurement can be obtained for the PPA with and without pump conditions.

The frequency response of the photo-detector is measured practically. It is configured for the same detecting optical signal modulated at 1MHz and measured using a 50Ω spectrum analyser. The frequency response measurement was undertaken only in the case of the photodetector system, in the absence of any pump circuit as shown in figure 6.6, which show a 9MHz bandwidth. However, at PPA with pump, the applied pump will bias the junction, resulting in an increase in the C_{mean} value, and hence leading to less bandwidth compared to the no pump condition.

Experimentally, the work performed in the previous chapter uses only a single carrier modulated signal (ω_s) without baseband modulation. In this case, the carrier to noise ratio (CNR) will be used as a measure of predetection signal quality of the RF signal at the front-end system, whereas the SNR is usually a measure of post-detection signal quality after demodulation and it is a useful metric to quantify a baseband signal (i.e. video or audio channel) quality. It is quite common in telecommunication that the CNR is often the SNR of the modulated signal if the above distinction is not necessary, the term SNR is often used instead of CNR.

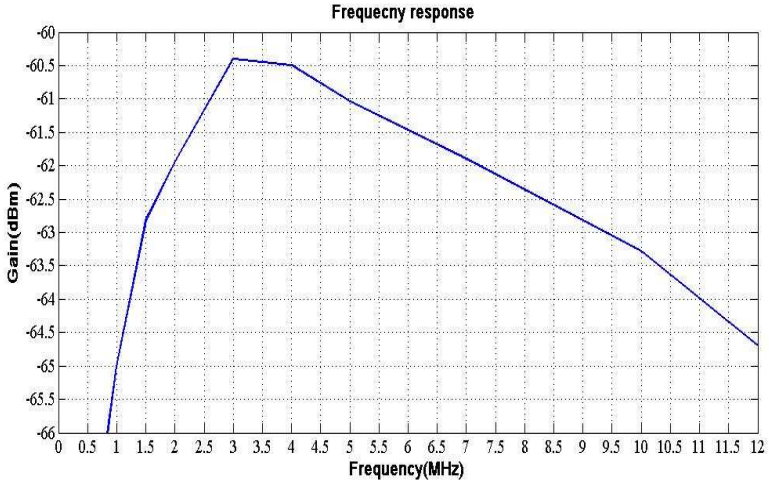

Figure 6.6 Frequency response of photodetector system

In practical terms, both the signal power and the noise power of the photodetector were measured in the absence of a pump, using a 50 ohms spectrum analyser. Firstly, when measuring the CNR with the spectrum analyser, it is important to ensure that, the analyser displays the external noise floor, not its own internal noise floor, as shown in figure 6.7(a). To verify the spectrum analyser measurement, the noise floor must be dropped at least 10dB when the RF input is disconnected. The optical signal and its PSD were measured as shown in figure 6.7(b,c) respectively.

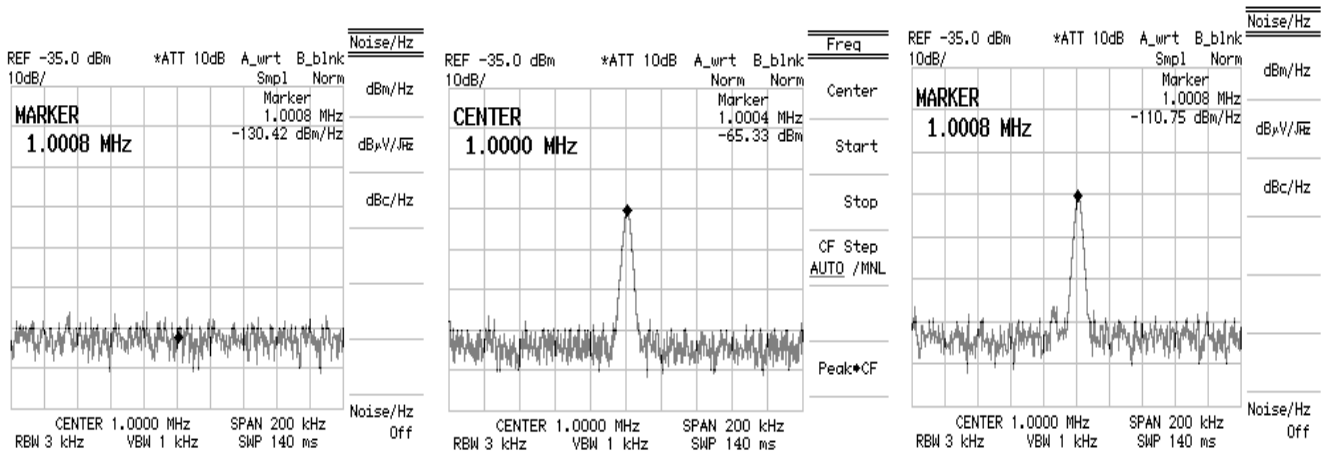

(a) (b) (c)

Figure 6.7 Frequency spectrum of (a) spectrum analyser internal noise floor (b) DD/IM optical power signal; and (c) Noise power spectral density at the receiver.

Figure 6.7(a) shows that the analyser has Excess Noise Ratio (ENR) of > 44 dB, compare to ideal floor noise density power that a thermal noise source has at the reference temperature of 290K (i.e. P=KTB, -174dBm/Hz). Figure 6.7(c) shows that the measured noise due to optoelectronics operation increases by almost 20dB. This increase was a consequence of a thermal shot, and current noise, in addition to the background optical noise. To calculate the power that the source will have in a BW, the PSD is added to the dB (BW). As the noise is a random signal, its power is distributed over it is usable bandwidth BW, and hence the noise power is proportional to the system BW.

For example, the CNR for photodetection can be calculated as follows: A -110.75dBm/Hz amplified noise module with 1Hz, BW will have a minimum of:

The available noise power (N) at BW $= PSD+10\ log(BW\text{-}Hz)$ (6.9)

$= -110.75+10\ log\ (1Hz)= -110.72dBm.$

Hence, CNR_{dB} at (1Hz-BW)$= 10\ log\ (S/N) = S_{dBm} - N_{dBm}$ (6.10)

$= -65.06-(-110.75)= 45.42dB.$

The CNR for DD/IM optical PD receiver at 1Hz bandwidth is equal to 45.42dB; the CNR value below 40dB will generally result in an unacceptable QoS because of the objectionable amount of noise in the baseband, and good engineering practice targets end-of-line analogue video signal use between 45dB and 55dB [119]. The CNR at 9MHz bandwidth was calculated based on the above formula, and its result is shown in table 6.1. The CNR at 9MHz is equal to -24.12dB, this very small SNR may be acceptable, due to the very low input optical power (-65.33dBm).

Secondly, the CNR was measured for photoparametric technique at various conversion gains, as listed in table 6.1; the noise power spectral density (PSD) and the signal power at 20dB up-converter gain are shown in figure 6.8.

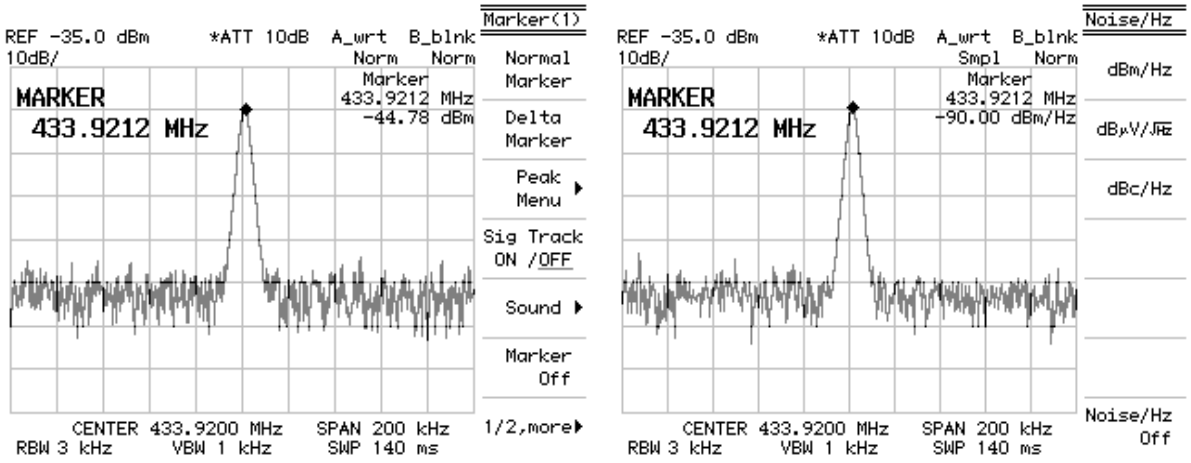

(a) (b)

Figure 6.8 Frequency spectrum at 20dB gain of (a) Up-converter power signal; and (b) Up-converter noise power spectral density.

Table 6.1 CNR measurements at various configurations

Circuit Configuration	**CNR(dB) at 1Hz-BW**	**CNR(dB) at 9MHz-BW**	**CNR(dB) at 7MHz-BW**
Photodiode DD/IM	45.42	-24.12	
PPA Up-converter gain with 5 db	45.28	-24.26	
PPA Up-converter gain with 10 db	44.9	-24.67	
PPA Up-converter gain with 15 db	44.8	-24.73	
PPA Up-converter gain with 20 db	45.22	-24.32	-23.23

The above table shows that at 1Hz bandwidth, the CNR of the photodetector compares slightly better to the photoparametric amplifier; the PPA technique at the same bandwidth increases the noise at almost 0.22dB, compared to DD/IM. For instance, if the photodetector has a noise figure of 2.7dB, then the up-converter PPA noise figure will be 2.92dB. Previous works [38, 68, 129, 151] investigate the performance of PPA with respect to the noise figure; they show that in the noise figure of PPA is (3.4, 3.0, 1.1, and 1.1dB) respectively, the latter indicated that the PPA noise figure can have a low value at high gain.

As mentioned before, the PPA operation under high pump will reduce the bandwidth according to the value of the C_{mean}. For example, at 20dB up-converter gain, as shown in the above table, the applied pump will reduce the photodetector bandwidth from 9MHz to 7MHz, if the reduction in bandwidth (9 MHz to 7 MHz = 1.29 times, or 1.11 dB) is more than the noise figure. For instance, if the NF of the PPA at 7 MHz is 0.89 dB, equivalent to a ratio of 1.26 times, then the improvement in CNR compared to DD/IM is [1.11 dB – 0.89dB = 0.22 dB], about 1.05 times as a numerical ratio. Obviously, the available noise power at the receiver is a summation of the PSD plus the receiver bandwidth, as shown in equation (6.9). Therefore, the photodiode has a larger bandwidth than the PPA system, so the CNR at the photodiode is smaller than the SNR at the output. The PPA can slightly improve the CNR compared with the photodetector, but with the bandwidth expenses. It is necessary not to apply a high pump across the photodiode and avoid driving the junction to a high forward current (i.e. increase the dark current) as shown in the *IV* junction characteristics in chapter 4, or drive the junction to the compression point, which results in high NF, and hence degrades the improvement in SNR.

The operation of parametric amplification should lead to a low noise figure when a highly nonlinear junction is employed. However, the implemented PD junction in this research exhibited very low nonlinearity (i.e. abrupt junction, *m=0.45*), and hence showed very low improvement with respect to the noise figure, as well as showing low conversion gain at the low pump. Furthermore, there are an additional noise caused from the receiver implementation it self as it was built in many individuals boards connecting via coaxial cables and BNC connecters leads to increase the number of series parasitic resistances.

In practice, it is very complicated to measure an accurate SNR without building a complete real time system with real baseband modulation (i.e. modulation and

demodulation circuits), as the SNR is a metric to quantify the baseband signal after demodulation; and then compared to photodiode, followed by LNA or photomultiplier, this measurement can provide a more accurate result with respect to SNR; however, the CNR and SNR are often used interchangeably, and are more or less in line with each other. The experimental result verified the computed result showed in [38], as the PPA can provide an amplified output with a noise factor (F) nearly equal to that of the un-amplified output of the same photodiode. The authors in [71, 131, 137] show that the PPA performs much better than the photomultiplier amplifier at low bandwidth modulation.

6.2.4 DCHPPA Noise Analysis

The advantage of the PPA approach is the power gain associated with it at the front stage, and the main attraction compared to other optical wireless approaches is the optimum overall noise figure, as the total noise figure of the receiver is a consequence of the Friss Formula, with the assumption that all the stages have the same modulation bandwidth.

$$F_r = F_1 + \frac{F_2 - 1}{G_1} + \frac{F_3 - 1}{G_1 G_2} + \ldots\ldots\ldots .$$

The above formula shows the overall noise factor of the receiver. It is clear that G_1 should be set to as high a value as possible, to minimise the effect of F_2 at the second stage (i.e. pre-amplifier), and this makes the first stage crucial; this is also the case with respect to *G2* and *G3*. The whole DCHPPA system can slightly increase the NF of the front-end system over the up-converter PPA first stage, as mentioned in the previous chapter. Practically speaking, it would be inadequate to compare the PPA carrier to the noise ratio with the whole DCHPPA system, due to different bandwidth at each sub-circuit; the DCHPPA has small bandwidth, due to the high-Q bandpass SAW filter (i.e. 120KHz) compared to the PPA first stage. To obtain a low noise figure in the DCHPPA system, it is desirable to have

low loss IF devices with very high gain and low NF at as early a stage as possible, so as to minimise the effect of the later stage. It is clear that the up-converter PPA first stage is the main core for improving SNR, and makes the first stage crucial. In contrast, the PPA can provide a better quality of reception, and generally higher communication accuracy and reliability than low SNR ratios, but with the expense of bandwidth.

For example, in case1: for DD/IM technique, the *pin* PD have F_1=1.87 (NF=2.7dB) and unity gain as no amplification inside the junction itself. Case2: for PPA technique, the PPA as stage one has F_1=1.96 (NF=2.92dB) with G1=20dB gain. Both the techniques were followed by LNA with F2=3.16 (NF=5dB) and G2=20dB gain. By using the Friss formula, the total receiver noise figure in case one is NF_{r1}=5.54 with a 20dB gain, whereas the total receiver noise figure in case two is NF_{r2}=2.97 with a 40dB gain. The photoparametric technique exhibited a smaller noise figure compared to PD, followed by the pre-amplifier, which clearly shows that the high gain at stage one will provide better total noise figure for the whole receiver. It may be concluded that PPA can provide better noise performance compared to the photodetector, followed by the preamplifier, hence, the better the noise figure is, the less the degradation for the receiver SNR.

The same analysis may be applied to the DCHPPA implemented receiver. It is clear that high gain with low insertion loss at early stages is more favourable with respect to receiver noise performance, and as mentioned in previous chapter, the choice of receiver components such as IF filters and IF Amplifiers were highly selected with respect to low loss and noise figures, even with cost and power efficiency (i.e. passive devices or low power devices). The research has computed the total noise figure for both receivers configurations, DCHPPA and Gain Chain DCHPPA, as reported in section 5.4 and 5.5 respectively; the first configuration has a 3.04dB noise figure with almost 24.7dB gain, whereas the second configuration (gain chain DCHPPA) has a 3.0dB noise figure with

almost 62dB gain NF. This result verified that high gain and low insertion loss at an early stags will outperform, and the last stage will have a very low effect, and results in a low increase in the total noise figure, and hence a very small degradation on the SNR. Any high loss device at a later stage may have an insignificant effect on the overall performance of the receiver with respect to SNR. Implementing the whole receiver in a single board (MMIC chip) can help to reduce the parasitic effect (series resistances), and hence provide better SNR.

6.3 Summary

Performance analysis was conducted on theoretical, simulation and practical approaches; this presented a very good agreement, and a close result. This showed that the photoparametric amplifier may be able to offer unexpected gains and bandwidth improvement at low load impedance in comparison to a standard optical wireless receiver, but sensitivity is limited by thermal noise. Noticeable improvements in up-conversion gain are seen at zero bias modes. The three analyses follow the same trend, presenting a close result, and the practical result verified the mathematical and simulation models presented in preceding chapters.

Shot noise and thermal noise are predominate noise sources in both the Photodetector (DD/IM) and the PPA. A reduction of shot noise is possible by using a low power transmitted signal or a very narrow optical filter, or operating at very low ambient background light. A reduction of thermal noise is possible by increasing the load resistance which acts adversely with the bandwidth and the gain. Furthermore, a reduction of reverse bias current to very low steady state *dc* level will reduce unwanted broadband noise (i.e. equilibrium mode has only very small leakage current). A high pump can increase noise due to driving the photodiode to photo-voltaic mode and increasing the dark current, or due

to reach the compression point. A high nonlinear photodiode can perform much better with respect to noise performance. Larger responsitivity (R) may reduce the quantum noise and improve the optical detecting efficiency. A measurement of the signal and noise was carried out with parametric amplification, and without amplification. From the measurement of NF in both cases, NF was determined at NF=2.92dB, with a power gain of 20dB. Consequently, the PPA was shown to have added a very small noise over photodetection, due to the parametric effect (i.e. Δ_{NF}=0.22dB), but with the advantages of offering power gain and low noise by mixing products in a single junction. Overall PPA noise performance is shown to be potentially better than the photodetection receiver, followed by the preamplifier, and provides better receiver sensitivity, but with a bandwidth penalty. Furthermore, as mentioned in chapter 2, the PPA was shown to outperform APD, resulting in a lower noise figure at a few hundred MHz bandwidths.

Chapter 7

7. Conclusions and Future Work

In this chapter, the conclusions of the work undertaken in this thesis, as well as future research work, will be detailed.

7.1 Conclusions

A novel approach to the design and optimisation of high sensitivity front-end optical receivers has been presented and discussed. It is based on the superheterodyne principle, but using the photoparametric amplification technique at the first stage, instead of a resistive/transistor-based mixer. The up-converter optoelectronic mixing approach offers low noise photo-detection, amplification and frequency conversion, with the aim of recovering the baseband electrical signal at high gain with overall noise performance. Over the preceding chapters, the research has shown that a DCHPPA system can be implemented satisfactorily based on a commercial *pin* photodiode, which was also encouraged to work simultaneously as a parametric amplifier. Because of this, the DCHPPA acts in a parallel manner to a conventional double superheterodyne heterodyne detector system, but without the noise penalty normally incurred in the first stage that commonly exists in a conventional front-end system.

In chapter 1, an overview of optical wireless communication systems was presented, and the challenges and the key motivations for designing high sensitivity front-end optical receivers were presented. The concept of a photo-parametric amplification technique using up-converter optoelectronic mixing was discussed. Chapter 2 reviewed the literature, presenting an overview of the optical detection techniques, followed by a review of the conventional parametric amplifier and their nonlinear device theory. This was followed by a comprehensive review of the prior work of the development of the PPA theory of operation, signal analysis and practical work. The main background was found to be more helpful in devising a new ideal for designing, investigating and optimising the front-end optical receiver, based on photoparametric techniques. The rest of this chapter provides a summary of the conclusion and the main contributions of this research which

were discussed in chapter 3 to 6.This includes the theoretical, simulation, practical set-up and results of the front-end system.

The research in chapter 3 has shown that a PPA may have optimum performance under a zero reverse bias mode; the benefit of using no bias is that the degree of nonlinearity of CV characteristic is higher, leading to potentially greater conversion gain, low noise and better cost and power effectiveness, essential for optical communication as well as for wireless applications with tight power (i.e. mobile terminal). Input and output power admittance were theoretically analysed, and it was found that for optimum power transfer; the input/output admittance should be proportional to the mean value of variable capacitance (C_{mean}). PPA general load analysis was theoretically presented, showing that optimum power transfer will require load impedance to be low, and approximately equal to the value of bulk resistance (R_b); however, low negative load impedance ($R_L = -R_b$) can be considered, but with the penalty of stability. PPA theory gain was developed and newly derived gain expressions were presented. The formula is able to consider most of the parameters that affect PPA performance, including external circuit configuration, junction characteristics and the ratio of applied pump frequency to the optical source frequency.

A novel DCHPPA circuit design model has been described and analysed in chapter 4. The simulation required the use of advanced nonlinear simulation tools; known as *Microwave Office* with Harmonic Balance Technique (HBT) features, to model accurately the whole front-end system. This due to the strong nonlinearities of the circuit, plus the use of a very small signal source frequency, which is much weaker than the pump frequency, known as noncommensurate multitone excitation analysis. A new, more accurate *pin* photodiode was modelled as a core element of the PPA circuit model and successfully simulated. The model represents actual nonlinear dynamic junction capacitance behaviour with respect to *CV* and *IV* characteristics; furthermore, photodiode responsitivity and finite

frequency conversion efficiency (i.e. photon counting process) were also considered and validated with the practical photodetector. The whole DCHPPA systems, including the IF signal processing stage and DB mixer stage, were modelled and simulated, and the baseband signal was successfully recovered at the predicted gain. The simulation experiments conducted in the VHF, UHF and MW frequency range provided a realistic assessment and better understanding of performance optimisation with respect to power gain conversion. The simulation analysis was found to be in positive agreement with the analytical analysis presented in chapter 3, and demonstrated the behavioural model's ability to accurately predict the effect of PD parameters and the PPA circuit configuration of the photo parametric amplification. Furthermore, for optimum conversion gain, the PD in the PPA circuit should operate at an equilibrium mode and exhibit a strong nonlinearity junction (e.g. super hyper abrupt junction) with very low bulk resistance and very low load impedance, where low insertion loss components at down-conversion stage are desirable.

In chapter 5, a new design of the DCHPPA system was presented, and a wide band test-bed was successfully implemented. The system hardware was divided into three main stages, each stage mounted in separate PCBs; the first stage represents the up-converter PPA circuit, the second stage represents the IF signal processing circuits, and the third stage represents the conventional down converter circuits. The experiments result in the up-converter, though at a preliminary stage, have indicated promise, and can be implemented satisfactorily using a *pin* photodiode at equilibrium mode, leading to potentially greater conversion gain at lower penalty of power and noise. A proof of principle experiments at VHF and UHF has demonstrated a measure up-converter gain of in excess of 20dB and 26dB respectively; with the potential of higher figures by employing a strong nonlinear junction, as predicted in the simulation result, where the gain can increase up to 40% more. It was found that PPA can provide unexpected gains at low load

impedance in comparison to standard optical wireless receivers. Tuning the pump circuits to suppress feedthrough improves the performance of the PPA even more, such that a broader bandwidth operation is possible using this with low load impedance, and noticeable improvements in up-conversion gain are also seen, which provide a better GBP. The power gain was found to be related to the pump power over the variable reactance impedance and also related to the ratio of idler frequency over the source frequency. Low bulk resistance helps the variable capacitance to absorb most of the applied power across the junction, and hence improve conversion gain. The PPA experimental results were very convincing, since the gain frequency variation was in accordance with theoretical calculation and simulation result.

The tests on the second stage (i.e. IF signal processing) indicated a promise, and was implemented satisfactorily using low cost SAW filters and low noise IF amplifiers (i.e. strengthen IF signal). The designated stage leads to potentially high selectivity and sensitivity with better rejection of other unwanted signals outside the bandwidth, as well as being able to minimise the other signals' interference and distortions; it also provide good isolation among the cascaded stages (prevent feedback signal from breaking through). Tests on the third stage (recovery baseband signal) indicate good results, and are implemented by using passive and low loss components (i.e. DB mixer and LPF). The DCHPPA technique overall subsequently exhibited a 34.9dB baseband signal gain at UHF over the modulated optical signal. Employing a chain gain DCHPPA technique would be preferred, as is subsequently exhibited by a 56.3 dB baseband signal gain over the modulated optical signal; this technique can bring up the signal gain to certain levels required for effective utilization and hence increase sensitivity.

In chapter 6, performance analysis was conducted on theoretical, simulation and practical approaches. It was found that the three analyses follow the same trend, showing a

very good agreement, and presented close results; the practical result verified the mathematical calculation, and the simulation results presented in preceding chapters. In terms of noise analysis perspective, practical measurement of the signal and noise of the PPA was carried out with parametric amplification, and without amplification. It was found that there is only a little extra noise occurrence, due to the process of photoparametric operation, and the predominant sources of noise in PPA are the thermal noise and the shot noise as found in any photodetecotr receiver. 2.7dB noise figure was computed for the photodetector for no pump being applied; however, at 20dB power gain, the PPA showed a 2.92dB noise figure. Consequently, the PPA added only a very small noise over the DD/IM technique, and with almost of (i.e. Δ_{NF}=0.22dB), this figure considerably has insignificant effect in accordance with the advantages of offering power gain and frequency conversion in a single junction. It was found that the PPA is a crucial element with respect to sensitivity (i.e. noise performance) as a whole DCHPPA system, since the high gain and low noise figure at the first stage can help to minimise the noise effect of the later stages. The DCHPPA may not easily improve the SNR compare to photodetector, but it can lower the total receiver noise figure.

Overall, optoelectronic mixing in the DCHPPA appears to be very promising as a means of linear amplification and frequency conversion in detecting (incoherent-heterodyne) optical signals that offers the prospect of significant benefits to OW and FSO, as well as offering improved performance in fibre access networks (i.e. wireless and long haul applications). PPA noise performance is shown to be potentially better than the photodetection receiver, followed by the preamplifier, and provides better receiver sensitivity, low cost and power effectiveness, but with bandwidth limitation. The aim of this research has been achieved, and the DCHPPA can ambitiously replace the SCM/WDM receiver in Millimetre-wave radio-over-fibre and wireless optical systems. Clearly, as with

any research, there is still further work that needs to be done, as detailed in the next section.

7.2 Future Work

Further research work can be explored and suggested as a result of employing this technique to improve the performance of the front-end optical receiver system. One of the greatest challenges in this technique is the bandwidth limitation, particularly at the IF signal processing stage, where a high-Q bandpass filter was necessary to eliminate other signals from breaking through such as pump frequency, lower IF frequency and other harmonics frequencies. Further investigation needs to be conducted to enhance the bandwidth at this stage, as it has been shown that the PPA at the first stage can provide high gain bandwidth products (GBP). Further work may also be done to design and develop high-Q bandpass filter at Millimetre-wave frequency, as the state of the art of commercial SAW filter offers only a few GHz centre frequencies.

There is some other work also that needs to be done to make this system a commercial reality, though this work has shown that the basic premise of the double conversion heterodyne photoparametric amplifier is viable. Further experimental investigation is required to develop the DCHPPA using Microwave Monolithic Integration Circuits (MMICs), or integrating the whole system in a single PCP; this can increase compactness and reduce parasitic effects. More practical implementation is required to investigate the use of low source impedance of the pump source, as it is very hard to obtain high pump power at 50Ω source resistance; it may be suggested that the whole system should adopt low input/output resistance, but this may adversely affect the noise performance.

Experimental comparisons between a numbers of optical detection techniques could be carried out in order to verify the differences, advantages, and disadvantages of a number of real optical systems. The most important challenge for further work, and the only way to confirm and demonstrate the ultimate feasibility of the DCHPPA in practical situations, is to deploy the DCHPPA in practical fibre or optical wireless systems, including modulation and demodulation circuits, and to evaluate the complete link performances with respect to bandwidth and SNR. However, until that time, it is the conclusion of this work that photoparametric amplification appears to be the most suitable solution for a low cost, low noise, narrowband front-end optical wireless receiver.

Bibliography

[1] M. J. McCullagh and D. R. Wisely, "155 Mbit/s optical wireless link using a bootstrapped silicon APD receiver," *Electronics Letters,* vol. 30, pp. 430-432, 1994.

[2] J. Elmirghani, "Optical Wireless Systems and Networks," *Communications Magazine, IEEE,* vol. 36, pp. 70-71, 1998.

[3] M. Hoa Le, Z. Ghassemlooy, D. O'Brien, and G. Faulkner, "Indoor Gigabit optical wireless communications: Challenges and possibilities," in *Transparent Optical Networks (ICTON), 2010 12th International Conference on*, pp. 1-6, 2010.

[4] K. D. Langer and J. Grubor, "Recent Developments in Optical Wireless Communications using Infrared and Visible Light," in *Transparent Optical Networks, 2007. ICTON '07. 9th International Conference on*, pp. 146-151, 2007.

[5] D. J. T. Heatley, D. R. Wisely, I. Neild, and P. Cochrane, "Optical wireless: the story so far," *Communications Magazine, IEEE,* vol. 36, pp. 72-74, 79-82, 1998.

[6] A. Street, P. Stavrinou, D. O'brien, and D. Edwards, "Indoor optical wireless systems–a review," *Optical and Quantum Electronics,* vol. 29, pp. 349-378, 1997.

[7] A. Boucouvalas, "Free space optical communications," *IEE Proc, Optoelectronic.,* vol. 143, 1996.

[8] R. J. Green, H. Joshi, M. D. Higgins, and M. S. Leeson, "Recent developments in indoor optical wireless [Optical wireless communications]," *Communications, IET,* vol. 2, pp. 3-10, 2008.

[9] A. Al-Ghamdi and J. Elmirghani, "Multiple spot diffusing geometries for indoor optical wireless communication systems," *International Journal of Communication Systems,* vol. 16, pp. 909-922, 2003.

[10] F. R. Gfeller and U. Bapst, "Wireless in-house data communication via diffuse infrared radiation," *Proceedings of the IEEE,* vol. 67, pp. 1474-1486, 1979.

[11] C. D. Knutson, J. M. Brown, and IrDA, *IrDA Principles and Protocols* vol. 1: MCL Press, 2004.

[12] R. Ramirez-Iniguez and R. Green, "Indoor optical wireless communications," in *Optical wireless communications (Ref. No 1999/128)*, IEE Colloguium 1999, pp. 14/1-14/7, 1999.

[13] D. O'Brien, "Indoor optical wireless communications: recent developments and future challenges," in *Proceeding of SPIE,* San Diego, CA, USA, p. 74640B, 2009.

[14] P. Smulders, "60 GHz radio: prospects and future directions," in *Proceedings Symposium IEEE Benelux Chapter on Communications and Vehicular Technology*, Eindhoven, 2003.

[15] S. Qazi, "Challenges In Outdoor and Indoor Optical Wireless Communications," presented at the International conference on wireless networks ICWN, Las vegas, USA, 2006.

[16] M. S. Leeson, R. J. Green, and M. D. Higgins, "Photoparametric amplifier frequency converters," in *Transparent Optical Networks, 2008. ICTON 2008. 10th Anniversary International Conference on*, pp. 197-200, 2008.

[17] " American National Standard for the Save Use of Laser ANS/Z136.1," ed. New York: ANS, 1996.

[18] A. C. Boucouvalas, "Indoor ambient light noise and its effect on wireless optical links," *Optoelectronics, IEE Proceedings,* vol. 143, pp. 334-338, 1996.

[19] J. R. Barry, *Wireless infrared communications,* vol. 280: Springer, 1994.

[20] J. M. Kahn and J. R. Barry, "Wireless infrared communications," *Proceedings of the IEEE,* vol. 85, pp. 265-298, 1997.
[21] J. B. Shlomi Arnon, George Karagiannidis, Robert Schober, Murat Uysal, *Advanced Optical Wireless Communication Systems*: Cambridge, 2012.
[22] R. Qahwaji, R. Green, and E. Hines, *Applied Signal and Image Processing: Multidisciplinary Advancements*: IGI Global, 2011.
[23] J. G. Proakis, "Wiley encyclopedia of telecommunications," ed: Hoboken, New Jersey : Wiley, 2003.
[24] A. Mahdy and J. S. Deogun, "Wireless optical communications: a survey," in *Wireless Communications and Networking Conference, WCNC. 2004 IEEE*, vol. 4, pp. 2399-2404, 2004.
[25] J. M. H. Elmirghani, H. H. Chan, and R. A. Cryan, "Sensitivity evaluation of optical wireless PPM systems utilising PIN-BJT receivers," *Optoelectronics, IEE Proceedings,* vol. 143, pp. 355-359, 1996.
[26] R. Y. Chen, H. Tsung-Shuen, and H. Chih-Yuan, "A CMOS infrared wireless optical receiver front-end with a variable-gain fully-differential transimpedance amplifier," *Consumer Electronics, IEEE Transactions on,* vol. 51, pp. 424-429, 2005.
[27] D. O'Connell and A. Morrison, "CMOS transimpedance amplifier for use with multiple APD geometries," presented at the Proc. Irish Signals and Systems Conference, Belfast, 2004.
[28] R. J. Green and M. G. McNeill, "Bootstrap transimpedance amplifier: a new configuration," *Circuits, Devices and Systems, IEE Proceedings G,* vol. 136, pp. 57-61, 1989.
[29] M. J. N. Sibley, *Optical communications*: Palgrave Macmillan, 1990.
[30] J. R. Barry, J. M. Kahn, W. J. Krause, E. A. Lee, and D. G. Messerschmitt, "Simulation of multipath impulse response for indoor wireless optical channels," *Selected Areas in Communications, IEEE Journal on,* vol. 11, pp. 367-379, 1993.
[31] fSONA-Communications-Corporation, "WAVELENGTH SELECTION FOR OPTICAL WIRELESS COMMUNICATIONS SYSTEMS," ed, February 2001.
[32] D. P. Howson and R. B. Smith, *Parametric amplifiers*: McGraw-Hill, 1970.
[33] J. Decroly, L. Laurent, J. Lienard, G. Marechal, and J. Vorobeitchik, *Parametric amplifiers*: Macmillan, 1973.
[34] R. J. Green, "Optical communications: past, present and future," *Electronics & Communication Engineering Journal,* vol. 1, pp. 105-114, 1989.
[35] K. DAVID, "Analysis of Four~ Frequency Nonlinear Reactance Circuits," *IRE Transaction on Microwave Theory and Techniques*, pp. 274-283, 1960.
[36] A. Khanifar, M. Milovanovic, and R. J. Green, "Degenerate mode of operation in photoparametric amplifying devices," in *Microwave Conference, 25th European,* pp. 870-874, 1995.
[37] A. Khanifar and R. J. Green, "Photoparametric amplifiers for subcarrier-multiplexed communication systems," *Optoelectronics, IEE Proceedings,* vol. 146, pp. 223-230, 1999.
[38] P. Penfield, Jr. and D. E. Sawyer, "Photoparametric amplifier," *Proceedings of the IEEE,* vol. 53, pp. 340-347, 1965.
[39] D. J. Roulston, "Low-noise photoparametric up-converter," *Solid-State Circuits, IEEE Journal of,* vol. 3, pp. 431-440, 1968.
[40] A. Khanifar and R. J. Green, "Photo-parametric amplifier/converter in subcarrier multiplexed lightwave communication systems," in *Microwave Symposium Digest, 1992., IEEE MTT-S International*, vol. 2, pp. 761-764, 1992.

[41] J. Hansryd, P. A. Andrekson, M. Westlund, L. Jie, and P. O. Hedekvist, "Fiber-based optical parametric amplifiers and their applications," *Selected Topics in Quantum Electronics, IEEE Journal of*, vol. 8, pp. 506-520, 2002.
[42] I. N. Ross, P. Matousek, and J. L. Collier, "Optical parametric chirped pulse amplification," in *Lasers and Electro-Optics (CLEO 2000)*, pp. 249, *2000*.
[43] S. Saito and Y. Fujii, "On the noise performance of a photoparametric amplifier," *Proceedings of the IEEE*, vol. 52, pp. 978-979, 1964.
[44] S. M. Idrus and R. Green, "Photoparametric up-converter for millimeter-wave fibre-radio system," presented at the Int. IrDA/IEE/IEEE Seminar, Warwick, sept. 2003.
[45] H. Izadpanah, T. ElBatt, V. Kukshya, F. Dolezal, and B. K. Ryu, "High-availability free space optical and RF hybrid wireless networks," *Wireless Communications, IEEE*, vol. 10, pp. 45-53, 2003.
[46] T. Okoshi, "Recent advances in coherent optical fiber communication systems," *Lightwave Technology, Journal of*, vol. 5, pp. 44-52, 1987.
[47] D. A. Kleinman and G. D. Boyd, "Infrared Detection by Optical Mixing," *Journal of Applied Physics*, vol. 40, pp. 546-566, 1969.
[48] R. M. Gagliardi and S. Karp, "Optical communications," *New York, Wiley-Interscience*, vol. 1, pp. *445*, 1976.
[49] J. M. Senior and M. Y. Jamro, *Optical fiber communications: principles and practice*: Prentice Hall, 2009.
[50] R. Otte, L. P. De Jong, and A. H. M. Van Roermund, *Low-power wireless infrared communications*: Springer, 1999.
[51] Q. V. Davis and W. K. Kulczyk, "Optical and electronic mixing in an avalanche photodiode," *Electronics Letters*, vol. 6, pp. 25-26, 1970.
[52] A. Seeds and B. Lenoir, "Avalanche diode harmonic optoelectronic mixer,", pp. 353-357, 1986.
[53] E. Jones and J. Honda, "A low-noise up-converter parametric amplifier," in *WESCON/59 Conference Record*, pp. 99-107, 1959.
[54] D. Chakraborty, "Intermodulation in parametric amplifiers," *Proceedings of the IEEE*, vol. 57, pp. 1297-1298, 1969.
[55] E. Sard, B. Peyton, and S. Okwit, "A Positive Resistance Up-Converter for Ultra-Low-Noise Amplification," *Microwave Theory and Techniques, IEEE Transactions on*, vol. 14, pp. 608-618, 1966.
[56] J. T. DeJager, "Maximum Bandwidth Performance of Non- degenerate Parametric Amplifier with Single-Tuned Idler Circuit," *Microwave Theory and Techniques, IEEE Transactions on*, vol. 12, pp. 459-467, 1964.
[57] G. L. Matthaei, "A Study of the Optimum Design of Wide-Band Parametric Amplifiers and Up-Converters," *Microwave Theory and Techniques, IRE Transactions on*, vol. 9, pp. 23-38, 1961.
[58] P. Bura, R. Camisa, W. Y. Pan, S. Yuan, and A. Block, "Design Considerations for an Integrated 1.8-GHz Parametric Amplifier," *Solid-State Circuits, IEEE Journal of*, vol. 3, pp. 86-90, 1968.
[59] P. García-Fernández, R. Banerjee, and R. Loudon, "Nonclassical properties of nondegenerate parametric oscillators and amplifiers using two-mode operators," *Optics Communications*, vol. 100, pp. 381-388, 1993.
[60] R. Weglein and F. Keywell, "A low-noise X-band parametric amplifier using a silicon mesa diode," *Microwave Theory and Techniques, IRE Transactions on*, vol. 9, pp. 39-43, 1961.

[61] J. M. Manley and H. E. Rowe, "Some General Properties of Nonlinear Elements-Part I. General Energy Relations," *Proceedings of the IRE,* vol. 44, pp. 904-913, 1956.
[62] H. E. Rowe, "Some General Properties of Nonlinear Elements. II. Small Signal Theory," *Proceedings of the IRE,* vol. 46, pp. 850-860, 1958.
[63] D. K. Adams, "Analysis of Four-Frequency Nonlinear Reactance Circuits," *Microwave Theory and Techniques, IRE Transactions on,* vol. 8, pp. 274-283, 1960.
[64] M. K. Giles and W. E. Freitag, "Photoparametric Amplifying Upconverter," ed: DEPARTMENT OF THE NAVY WASHINGTON DC, 1976.
[65] Y. FUJII, T. KIMURA, K. KUROKAWA, S. SAITO, and Y. Uno, "Detection and amplification of the microwave signal in laser light by a parametric diode," 1962.
[66] D. E. Sawyer, "A nondegenerate photoparametric amplifier," *Proceedings of the IEEE,* vol. 51, pp. 1238-1238, 1963.
[67] K. Garbrecht and W. Heinlein, "Noise performance of photo diodes in parametric amplifiers," *Proceedings of the IEEE,* vol. 52, pp. 192-193, 1964.
[68] M. I. Grace and D. E. Sawyer, "UHF photoparametric amplifier," *Electron Devices, IEEE Transactions on,* vol. 13, pp. 901-903, 1966.
[69] D. J. Roulston, "Low-noise performance of photo diode envelope detectors in the megacycle range," *Proceedings of the IEEE,* vol. 52, pp. 1067-1067, 1964.
[70] J. C. Tandon and D. J. Roulston, "Comparison of avalanche photodiode and photo parametric upconverter signal-to-noise ratio " *Solide-State Elctronics,* vol. 16, pp. 1503-1505, 1973.
[71] J. Tandon and D. Roulston, "Effect of base parameters on signal-to-noise ratio in silicon P+-NN+ photoparametric upconverter diodes," *Solid-state electronics,* vol. 16, pp. 1181-1184, 1973.
[72] D. J. Roulston, "Very low noise photodetector system using p-i-n diode and baseband parametric upconvertor," *Electronics Letters,* vol. 16, pp. 595-596, 1980.
[73] C. L. Mears and T. E. Batchman, "Low Noise Amplifiers For optical Heterodyne Receivers," in *Southeastcon '81. Conference Proceedings*, pp. 401-405, 1981.
[74] V. I. Korneichuk, "A method of improving the sensitivity of fibre optic communication receivers using parametric pre-amplifiers," *Izvestiya VUz.Radio Elektronika,* vol. 26, pp. 83-85, 1983.
[75] R. Olshansky, "Microwave subcarrier multiplexing: new approach to wideband lightwave systems," *Circuits and Devices Magazine, IEEE,* vol. 4, pp. 8-14, 1988.
[76] R. J. Green, "MICROWAVE AMPLICFICATION WITHIN ILLUMINATED P-N DIODE STRUCTURE," in *Microwave Opto-Electronics, IEE Colloquium on,* p. 4/1, 1994.
[77] A. Khanifar, R. J. Green, A. Khosrowbeygi, N. T. Ali, and M. Milovanovic, "The analysis of photoparametric amplifying devices and characteristics," in *Microwave Symposium Digest, 1995., IEEE MTT-S International,* vol.3, pp. 1503-1506, 1995.
[78] R. Green and A. Khanifar, "Diode Structure For Photoparametric Amplifier," presented at the Banglore Golden Jubilee Conference, 1996.
[79] R. Green and A. Khanifar, "Photoparametric Amplifier Configurations," presented at the International Conference on Fibre Optics and photonics, India, 1996.
[80] S. M. Idrus and R. J. Green, "Photoparametric amplifier for optical wireless communication system," in *High Frequency Postgraduate Student Colloquium, 2001. 6th IEEE*, pp. 168-173, 2001.

[81] S. M. Idrus and R. J. Green, "Performance analysis of the photoparametric up-converter using harmonic balance techniques," in *High Frequency Postgraduate Student Colloquium*, pp. 23-28, 2004.
[82] S. M. Idrus, "Theoretical and practical performance of a pphotoparametric optical wireless receiver," 2004.
[83] S. M. Idrus, R. J. Green, and S. M. Supa'at, "Nonlinear analysis for performance characterization of a photoparametric amplifier," in *Applied Electromagnetics, 2005. APACE 2005. Asia-Pacific Conference on*, p. 5, 2005.
[84] A. Uhlir, "Similarity considerations for varactor multipliers," *The microwave journal*, pp. 55-59, 1962.
[85] B. G. Streetman and S. K. Banerjee, *Solid state electronic devices* vol. 10: Prentice Hall, 2005.
[86] R.J.Green, "Optoparametric Amplifiers -Theory and Operation, Project Repoprt for GEC," Bradford, 1990.
[87] S. A. Maas, *Nonlinear microwave and RF circuits*: Artech House Publishers, 2003.
[88] C. E. Christoffersen, "Global modeling of nonlinear microwave circuits," Citeseer, 2000.
[89] W. R. Curtice, "Nonlinear analysis of GaAs MESFET amplifiers, mixers, and distributed amplifiers using the harmonic balance technique," *Microwave Theory and Techniques, IEEE Transactions on*, vol. 35, pp. 441-447, 1987.
[90] G. W. Rhyne, M. B. Steer, and B. D. Bates, "Frequency-domain nonlinear circuit analysis using generalized power series," *Microwave Theory and Techniques, IEEE Transactions on*, vol. 36, pp. 379-387, 1988.
[91] L. O. Chua, "Computer-aided analysis of electronic circuits," *Prentice-Hall Series in Electrical and Computer Engineering, Englewood Cliffs: Prentice-Hall*, vol. 1, 1975.
[92] R. J. Gilmore and M. B. Steer, "Nonlinear circuit analysis using the method of harmonic balance—A review of the art. Part I. Introductory concepts," *International Journal of Microwave and Millimeter Wave Computer Aided Engineering*, vol. 1, pp. 22-37, 1991.
[93] R. J. Gilmore and M. B. Steer, "Nonlinear circuit analysis using the method of harmonic balance—a review of the art. II. Advanced concepts," *International Journal of Microwave and Millimeter Wave Computer Aided Engineering*, vol. 1, pp. 159-180, 1991.
[94] V. Anand, D. G. Haigh, A. Khanifar, C. A. Losada, J. K. Pollard, D. R. Webster, and A. E. Parker, "Use of SPICE in communications research," in *SPICE: Surviving Problems in Circuit Evaluation, IEE Colloquium on*, pp. 11/1-11/9, 1993.
[95] A. Khanifar, V. Anand, and A. E. Parker, "Photoparametric amplifier/converter in hightwave communication systems," in *Microwave Conference, 23rd European*, pp. 314-316, 1993.
[96] F. Giannini, G. Leuzzi, and Knovel, *Nonlinear microwave circuit design*: Wiley Online Library, 2004.
[97] M. Heimlich, "The advantages of multi-rate harmonic balance (MRHB)," ed, http://web.awrcorp.com/content/Downloads/AWR-MRHB-White-Paper.pdf.
[98] S. M. Idrus, R. J. Greenland, and S. M. Supa'at, "Nonlinear analysis for performance characterization of a photoparametric amplifier," in *Applied Electromagnetics, 2005. APACE 2005. Asia-Pacific Conference on*, p. 5, 2005.
[99] S.M.Idrus and R.J.Green, "Photo parametric up-converter for millimetre-wave fibre-radio system," presented at the International IrDA/IEE/IEEE Seminar, Warwick, 2003.

[100] "Agilent EEsof EDA http://eesof.tm.agilent.com."
[101] "AWR Corp. http://web.awrcorp.com/."
[102] E. M. Baily, "Steady state harmonic analysis of nonlinear networks," Stanfors University 1968.
[103] M. Nakhla and J. Vlach, "A piecewise harmonic balance technique for determination of periodic response of nonlinear systems," *Circuits and Systems, IEEE Transactions on*, vol. 23, pp. 85-91, 1976.
[104] K. S. Kundert, G. B. Sorkin, and A. Sangiovanni-Vincentelli, "Applying harmonic balance to almost-periodic circuits," *Microwave Theory and Techniques, IEEE Transactions on*, vol. 36, pp. 366-378, 1988.
[105] "AWR corporation 'awr ver.8.0 reference manual' ", ed, 2008.
[106] (2004). *Agilent Technologies 'Guide to harmonic Balance Simulation in ADS'* Available: http://www.ece.uci.edu/eceware/ads_docs/pdf/adshbapp.pdf
[107] G. D. Vendelin, A. M. Pavio, U. L. Rohde, and MyiLibrary, "Microwave circuit design using linear and nonlinear techniques," 1990.
[108] S. A. Maas, Ed., *Nonlinear microwave Circuits*. Artch House, 1993.
[109] G. A. S. Machado, "Low-power HF microelectronics: a unified approach," 1996.
[110] Y. Saad and M. H. Schultz, "GMRES: A generalized minimal residual algorithm for solving nonsymmetric linear systems," *SIAM J. Sci. Stat. Comput.*, vol. 7, pp. 856-869, 1986.
[111] V. Rizzoli, C. Cecchetti, A. Lipparini, and F. Mastri, "General-purpose harmonic balance analysis of nonlinear microwave circuits under multitone excitation," *Microwave Theory and Techniques, IEEE Transactions on*, vol. 36, pp. 1650-1660, 1988.
[112] M. V. P.Heikkila, and T. Veijola, "Harmonic Balance of Non-Linear Circuit with Multitone Excitation," in *Proceedings of the 10th European Conf. on Circuit theory and Design*, Copenhagen, pp. 802-811, 1991.
[113] P.Heikkila, "Object-oriented Approach to Numerical Circuit Analysis," PhD, Helsinki University of Technology, 1992.
[114] H. Jokinen, M. Valtnen, and T. Veijola, "Fast analysis of nonideal Switched-Capacitor circuits using Convolution," in *Proceeding of the European Conference on Circuits Theory and Design*, Davos, pp. 941-946, 1993.
[115] H. Jokinen and M. Valtonen, "Small-signal harmonic analysis of non-linear circuits," *International journal of circuit theory and applications*, vol. 23, pp. 325-343, 1995.
[116] H. Harun, S. M. Idrus, A. B. Mohammad, and N. Mohamed, "HBT Optoelectronic Mixer Design for Radio over Fiber System," in *High Capacity Optical Networks and Enabling Technologies, 2008. HONET 2008. International Symposium on*, pp. 107-110, 2008.
[117] C. Liu, Y. Betser, A. Seeds, D. Ritter, and A. Madjar, "Optoelectronic mixing in three-terminal InP/InGaAs heterojunction bipolar transistors,", vol. 1, pp. 359-362, 1997.
[118] L. Westbrook, "Harmonic balance simulation of laser fields under multitone SCM modulation," *Electronics Letters*, vol. 28, pp. 2245-2247, 1992.
[119] S. B. Alexander, *Optical communication receiver design*: SPIE-International Society for Optical Engineering, 1997.
[120] R. H. Caverly, N. V. Drozdovski, L. M. Drozdovskaia, and M. J. Quinn, "SPICE modeling of microwave and RF control diodes," in *Circuits and Systems, 2000. Proceedings of the 43rd IEEE Midwest Symposium on*, vol.1, pp. 28-31, 2000.

[121] N. Drozdovski, L. Drozdovskaia, R. Caverly, and M. Quinn, "Modeling the zero and forward bias operation of PIN diodes for high-frequency applications," *Solid-state electronics*, vol. 46, pp. 2001-2008, 2002.
[122] S. A. Maas, "Microwave mixers," *Norwood, MA, Artech House, Inc.*, vol. 1, p 368 , 1986.
[123] A. u. Program. *RF & Microwave Electronic Design Course*. Available: https://awrcorp.com/download, 2009
[124] H. Jiang and P. Yu, "Equivalent circuit analysis of harmonic distortions in photodiode," *Photonics Technology Letters, IEEE*, vol. 10, pp. 1608-1610, 1998.
[125] R. R. Hayes and D. L. Persechini, "Nonlinearity of pin photodetectors," *Photonics Technology Letters, IEEE*, vol. 5, pp. 70-72, 1993.
[126] A. I. Zverev, *Handbook of filter synthesis*: Wiley, 1967.
[127] J. J. Carr, *Microwave and wireless communications technology*: Butterworth-Heinemann, 1997.
[128] W. B. Jones, *Introduction to optical fiber communication systems*, 1987.
[129] A. Khanifar and R. Green, "Photoparametric amplifiers for subcarrier-multiplexed communication systems,", pp. 223-230, 1999.
[130] S. A. Malyshev and A. L. Chizh, "pin Photodiodes for Frequency Mixing in Radio-Over-Fiber Systems," *Lightwave Technology, Journal of*, vol. 25, pp. 3236-3243, 2007.
[131] D. Roulston, "Very low noise photodetector system using pin diode and baseband parametric upconvertor," *Electronics Letters*, vol. 16, pp. 595-596, 1980.
[132] S. Idrus and R. Green, "Photoparametric amplifier for optical wireless communication system,", pp. 168-173, 2001.
[133] A. Khanifar, R. Green, A. Khosrowbeygi, N. Ali, and M. Milovanovic, "The analysis of photoparametric amplifying devices and characteristics,", vol. 3, pp. 1503-1506, 1995.
[134] A. Khanifar, V. Anand, and A. Parker, "Photoparametric amplifier/converter in hightwave communication systems,", pp. 314-316, 1993.
[135] A. Khanifar, M. Milovanovic, and R. Green, "Degenerate mode of operation in photoparametric amplifying devices," pp. 870-874, 1995.
[136] A. Khanifar and R. Green, "Photo-parametric amplifier/converter in subcarrier multiplexed lightwave communication systems," vol. 2, pp. 761-764, 1992.
[137] D. Roulston, "Low-noise photoparametric up-converter," *Solid-State Circuits, IEEE Journal of*, vol. 3, pp. 431-440, 1968.
[138] R. J. Green, H. A. Alhagagi, and E. L. Hines, "Double conversion heterodyne photoparametric amplifier," in *Transparent Optical Networks (ICTON), 12th International Conference on*, 2010.
[139] P. Penfield Jr and D. Sawyer, "Photoparametric amplifier," *Proceedings of the IEEE*, vol. 53, pp. 340-347, 1965.
[140] L. Anderson and B. McMurtry, "High-speed photodetectors," *Proceedings of the IEEE*, vol. 54, pp. 1335-1349, 1966.
[141] R. S. M. S. G. K. R. Laker, "Design of Analog Filters: Passive, Active RC and Switched Capacitor," ed: Englewood Cliffs, NJ: Prentice-Hall, 1990.
[142] R. G. Kinsman, "A history of crystal filters," pp. 563-570, 1998.
[143] R. J. Green, H. A. Alhagagi, and E. L. Hines, "Double conversion heterodyne photoparametric amplifier," in *Transparent Optical Networks (ICTON), 2010 12th International Conference on*, pp. 1-4, 2010.
[144] C. Campbell, *Surface acoustic wave devices for mobile and wireless communications* vol. 1: Academic Pr, 1998.

[145] C. C. W. Ruppel and T. A. Fjeldly, *Advances in surface acoustic wave technology, systems and applications* vol. 1: World Scientific Pub Co Inc, 2000.
[146] N. B. Lukyanchikova, *Noise research in semiconductor physics*. Amsterdam: Gordon and Breach Science publishers, 1996.
[147] R. Ramirez-Iniguez, S. M. Idrus, and Z. Sun, *Optical wireless communications: IR for wireless connectivity*: Auerbach Publications, 2008.
[148] K. Ogawa, "Considerations for Optical Receiver Design," *Selected Areas in Communications, IEEE Journal on,* vol. 1, pp. 524-532, 1983.
[149] M. Uenohara, "Noise Consideration of the Variable Capacitance Parametric Amplifier," *Proceedings of the IRE,* vol. 48, pp. 169-179, 1960.
[150] D. J. Roulston, "Performances des detecteurs photoparametricues a resistance positive," *Onde Electrique,* vol. 45, pp. 122-130, 1965.
[151] R. Green, C. Sweet, and S. Idrus, "Optical wireless links with enhanced linearity and selectivity [Invited]," *Journal of Optical Networking,* vol. 4, pp. 671-684, 2005.

Appendix A

Appendix A1: IV Simulation Set-up.

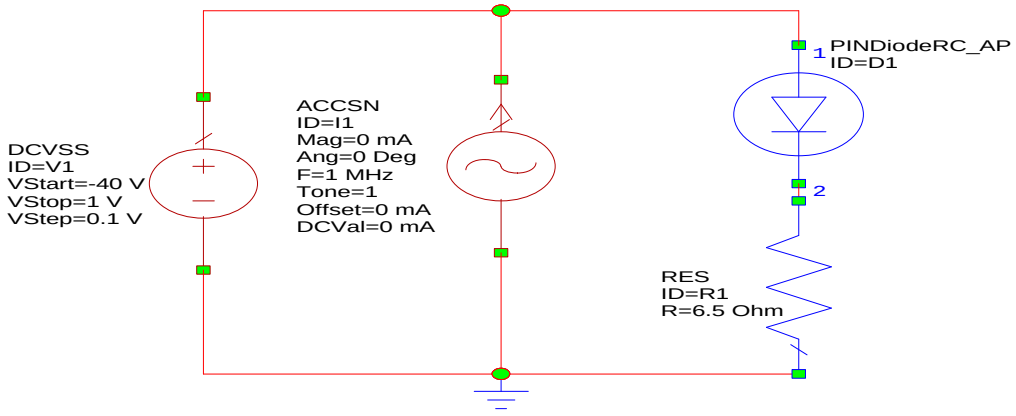

Schematic Circuit Diagram for IV Simulation Measurement.

```
  DIM
   CUR   MA
   ANG   DEG
   FREQ  MHZ
   VOL   V
   CAP   PF
   IND   NH
   RES   OH
   TIME  MS
   LNG   MM
   TEMP  C
CKT
ACCSN 2 0 ID="I1" Mag=0 Ang=0 F=432 Tone=1 NHarm=0 &
    NSamp=2 Offset=0 DCVal=0
DCVSS 2 0 ID="V1" VStart=-40 VStop=1 VStep=0.1
PINDiodeRC_AP 2 3 ID="D1" SCRIPT={""} B=3 BV=30 CJ=72 &
    CPACK=0 FC=0.5 IBV=1e-007 IF=100 &
    IKF=0.06 IKNEE=2 IS=3.5e-008 LBOND=0 M=0.45 MODEL_LEVEL=2   &
    N=1.01 REPI=0 RF=0.65 RHO=100000 RLIM=0.6 RP=1e+015 &
    RS=0 TAU=2e-008 VJ=0.552 W=0.006 WD=1e-007&
    TEMP=28
RES 0 3 ID="R1" R=6.5
DEF0P "IV PIN Diode RC AP"
----------------------------------------------------------------
$Visual System Simulator
$Version 8.04r build 4268 Rev1 (60469)
$Aplac netlist file
$Schematic Name: IV PIN Diode RC AP

Prepare
+ ADDDCPATH TAUDC=1e+008
```

```
+ ERR=0.001 ABS_ERR=1e-012 U=1 RMIN=1e-005 RMAX=1e+011 GMRES_M=100
ZEROPIVOT=1e-020
+ FNOM=0 TEMP=298.15 TNOM=298.15
VERSIONOPTION="tran0sourceonlyintrandc"
VECTOR AWR_SWP_VAR_1 -40 + 1
VAR AWR_SWP_INDX 0

$*************** SUBCIRCUITS *****************
DefModel awr_subckt_1 2 2 1 PARAM 7 Mag Ang Offset DCVal ACMag ACAng
TRAN_F  GLOBAL_PARAM 1 AWR_SWP_INDX
Curr J_TR 1 2 SIN=[0,Mag,TRAN_F,0,0,Ang*180/PI] OFFSET=Offset
DC=DCVal NO_SS
Curr J_HB 1 2 TONE=[1] (Mag'Ang*180/PI-90) AC=(ACMag'ACAng*180/PI)
OFFSET=Offset NO_TRAN
EndModel
$*************** END SUBCIRCUITS *****************

awr_subckt_1 ACCSN!I1 1 0 Mag=0 Ang=0 Offset=0 DCVal=0 ACMag=0
ACAng=0 TRAN_F=432000000
Volt DCVSS!V1 1 0 DC=AWR_SWP_VAR_1[AWR_SWP_INDX]
PINDiodeRC D1 1 2 TEMP=301.15 WD=3e-006 B=3 BV=30 CJ=7.2e-011 CPACK=0
EPS=1.17e-005 FC=0.5 IBV=1e-010 IF=0.1
+ IKF=6e-005 IKNEE=0.002 IS=3.5e-011 LBOND=0 M=0.45 MODEL_LEVEL=2
N=1.01 REPI=0 RF=0.65 RHO=100000
+ RLIM=0.6 RP=1e+015 RS=0 TAU=5.7e-008 VJ=0.552 W=3e-006
Res RES!R1 0 2 6.5 TEMP=290

AWRSaveResults
+ VOLTAGES 2 1 2
+ CURRENTS 6 ACCSN!I1,1 ACCSN!I1,2 D1,1 DCVSS!V1,1 DCVSS!V1,2
RES!R1,1
+ DCOPS
Sweep "AWR_INTERNAL_SWEEP" DC
+ LOOP 411 VAR AWR_SWP_INDX LIN 0 410
EndSweep
$Netlist End
```

Appendix A2: CV Simulation Set-up.

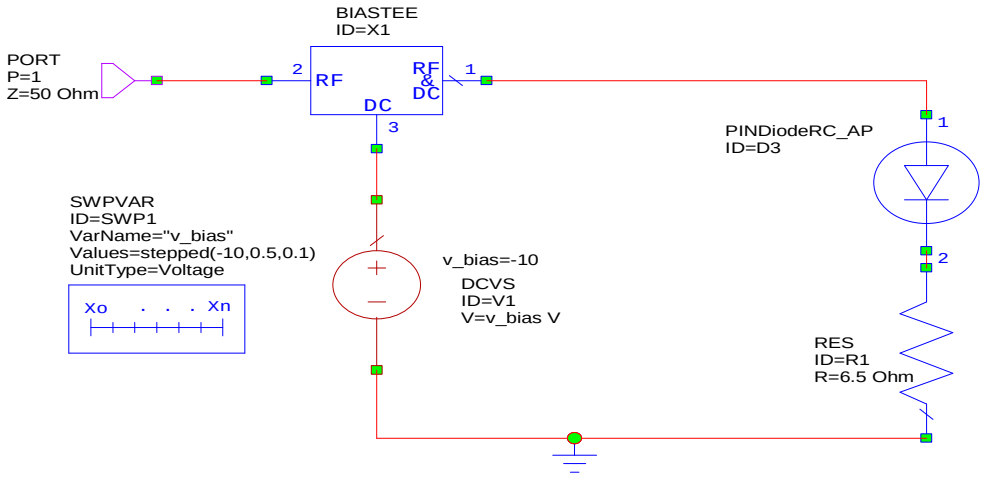

Schematic Circuit Diagram for CV Simulation Measurement.

```
     DIM
    VOL    V
    CAP    PF
    CUR    MA
    IND    NH
    RES    OH
    TIME   MS
    LNG    MM
    TEMP   C
VAR
   v_bias=-10
CKT
BIASTEE 3 1 2 ID="X1"
DCVS 2 0 ID="V1" V={ v_bias }
PINDiodeRC_AP 3 0 ID="D3" SCRIPT={""} B=3 BV=30 CJ=72 &
    CPACK=0 FC=0.5 IBV=1e-007 IF=100 &
    IKF=0.06 IKNEE=2 IS=3.5e-008 LBOND=0 M=0.45 MODEL_LEVEL=2  &
    N=1.01 REPI=0 RF=0.65 RHO=100000 RLIM=0.6 RP=1e+015 &
    RS=0 TAU=2e-008 VJ=0.552 W=0.006 WD=1e-007&
    TEMP=28
SWPVAR ID="SWP1" VarName={"v_bias"} Values=stepped(-10,0.5,0.1) &
    UnitType=13
PORT 1 P=1 Z=50
DEF0P "CV  PINDiodeRC AP"$Visual System Simulator
$Version 8.04r build 4268 Rev1 (60469)
```

$Aplac netlist file

```
$Schematic Name: CV PINDiodeRC AP
```

```
Prepare
+ NOISE
+ ADDDCPATH TAUDC=1e+008
```

```
+ ERR=0.001 ABS_ERR=1e-012 U=1 RMIN=1e-005 RMAX=1e+011 GMRES_M=100
ZEROPIVOT=1e-020
+ FNOM=0 TEMP=298.15 TNOM=298.15
VERSIONOPTION="tran0sourceonlyintrandc;maxadm=1e6"
VECTOR AWR_SWP_VAR_1 1000000000 + 2000000000
VECTOR AWR_SWP_VAR_2 -10 0
VECTOR AWR_SWP_VAR_4 -10 0
VAR AWR_SWP_INDX 0
$*************** SUBCIRCUITS ****************
$*************** END SUBCIRCUITS ****************
Cap CAP!X1 1 2 1e-005
Ind IND!X1_U1 3 1 0.001
Volt DCVS!V1 3 0 DC=AWR_SWP_VAR_4[AWR_SWP_INDX]
PINDiodeRC D3 1 0 TEMP=301.15 WD=1e-006 B=3 BV=30 CJ=7.2e-011 CPACK=0
EPS=1.17e-005 FC=1 IBV=1e-010 IF=0.1
+ IKF=6e-005 IKNEE=0.002 IS=3.5e-011 LBOND=0 M=0.45 MODEL_LEVEL=2
N=1.01 REPI=0 RF=0.65 RHO=100000
+ RLIM=0.6 RP=1e+015 RS=0.1 TAU=5.7e-008 VJ=0.552 W=1e-006
 Port PORT!PORT_1 2 0 PORT=1 Z=(50, 0)
AWRSaveResults
Sweep "AWR_INTERNAL_SWEEP" DC
+ LOOP 212 VAR AWR_SWP_INDX LIN 0 211
  Analyze AC FREQ=AWR_SWP_VAR_1[AWR_SWP_INDX]
EndSweep
$Netlist End
```

Appendix A3: OSRAM BPX61 Data Sheet

Silizium-PIN-Fotodiode
Silicon PIN Photodiode
Lead (Pb) Free Product - RoHS Compliant

BPX 61

Wesentliche Merkmale
- Speziell geeignet für Anwendungen im Bereich von 400 nm bis 1100 nm
- Kurze Schaltzeit (typ. 20 ns)
- Hermetisch dichte Metallbauform (ähnlich TO-5)

Features
- Especially suitable for applications from 400 nm to 1100 nm
- Short switching time (typ. 20 ns)
- Hermetically sealed metal package (similar to TO-5)

Anwendungen
- Lichtschranken für Gleich- und Wechsellichtbetrieb
- IR-Fernsteuerungen
- Industrieelektronik
- „Messen/Steuern/Regeln"

Application
- Photointerrupters
- IR-remote controls
- Industrial electronics
- For control and drive circuits

Typ Type	Bestellnummer Ordering Code
BPX 61	Q62702P0025

Grenzwerte
Maximum Ratings

Bezeichnung Parameter	Symbol Symbol	Wert Value	Einheit Unit
Betriebs- und Lagertemperatur Operating and storage temperature range	T_{op}; T_{stg}	– 40 … + 125	°C
Sperrspannung Reverse voltage	V_R	32	V
Verlustleistung, T_A = 25 °C Total power dissipation	P_{tot}	250	mW

Kennwerte (T_A = 25 °C, Normlicht A, T = 2856 K)
Characteristics (T_A = 25 °C, standard light A, T = 2856 K)

Bezeichnung Parameter	Symbol Symbol	Wert Value	Einheit Unit
Fotoempfindlichkeit, V_R = 5 V Spectral sensitivity	S	70 (≥ 50)	nA/lx
Wellenlänge der max. Fotoempfindlichkeit Wavelength of max. sensitivity	$\lambda_{S\,max}$	850	nm
Spektraler Bereich der Fotoempfindlichkeit S = 10% von S_{max} Spectral range of sensitivity S = 10% of S_{max}	λ	400 … 1100	nm
Bestrahlungsempfindliche Fläche Radiant sensitive area	A	7.00	mm^2
Abmessung der bestrahlungsempfindlichen Fläche Dimensions of radiant sensitive area	$L \times B$ $L \times W$	2.65 × 2.65	mm × mm
Halbwinkel Half angle	φ	±55	Grad deg.
Dunkelstrom, V_R = 10 V Dark current	I_R	2 (≤30)	nA
Spektrale Fotoempfindlichkeit, λ = 850 nm Spectral sensitivity	S_λ	0.62	A/W
Quantenausbeute, λ = 850 nm Quantum yield	η	0.90	Electrons Photon
Leerlaufspannung, E_v = 1000 lx Open-circuit voltage	V_O	375 (≥ 320)	mV
Kurzschlussstrom, E_v = 1000 lx Short-circuit current	I_{SC}	70	µA

Kennwerte (T_A = 25 °C, Normlicht A, T = 2856 K)
Characteristics (T_A = 25 °C, standard light A, T = 2856 K) (cont'd)

Bezeichnung Parameter	Symbol Symbol	Wert Value	Einheit Unit
Anstiegs- und Abfallzeit des Fotostroms Rise and fall time of the photocurrent R_L = 50 Ω; V_R = 5 V; λ = 850 nm; I_p = 800 µA	t_r, t_f	20	ns
Durchlassspannung, I_F = 100 mA, E = 0 Forward voltage	V_F	1.3	V
Kapazität, V_R = 0 V, f = 1 MHz, E = 0 Capacitance	C_0	72	pF
Temperaturkoeffizient von V_O Temperature coefficient of V_O	TC_V	– 2.6	mV/K
Temperaturkoeffizient von I_{SC} Temperature coefficient of I_{SC}	TC_I	0.18	%/K
Rauschäquivalente Strahlungsleistung Noise equivalent power V_R = 10 V, λ = 850 nm	NEP	4.1×10^{-14}	$\frac{W}{\sqrt{Hz}}$
Nachweisgrenze, V_R = 10 V, λ = 850 nm Detection limit	D*	6.6×10^{12}	$\frac{cm \times \sqrt{Hz}}{W}$

Relative Spectral Sensitivity
$S_{rel} = f(\lambda)$

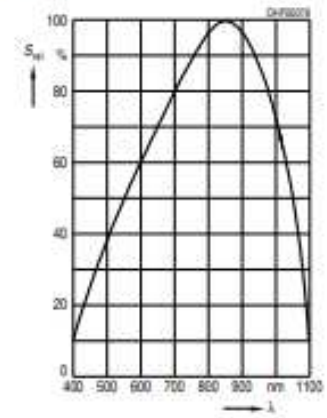

Photocurrent $I_P = f(E_v)$, V_R = 5 V
Open-Circuit Voltage $V_O = f(E_v)$

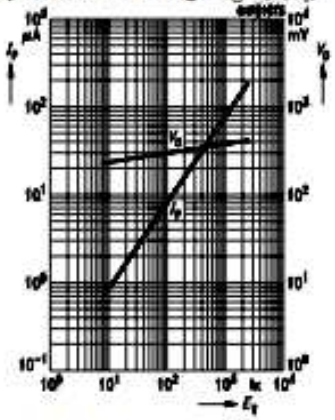

Total Power Dissipation
$P_{tot} = f(T_A)$

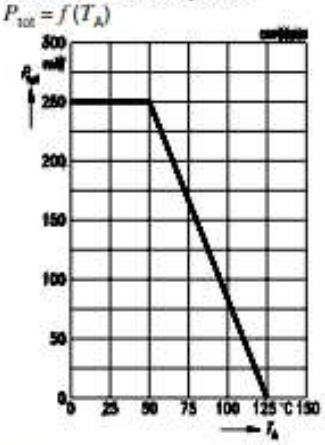

Dark Current
$I_R = f(V_R)$, $E = 0$

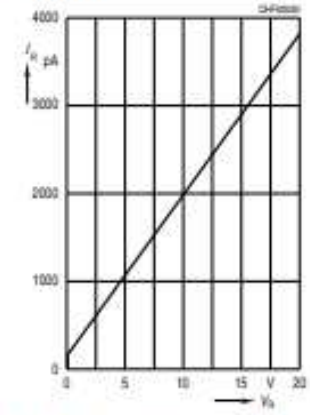

Capacitance
$C = f(V_R)$, f = 1 MHz, $E = 0$

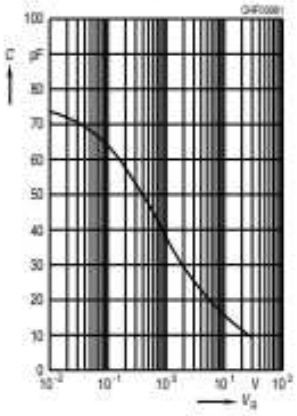

Dark Current
$I_R = f(T_A)$, V_R = 5 V, $E = 0$

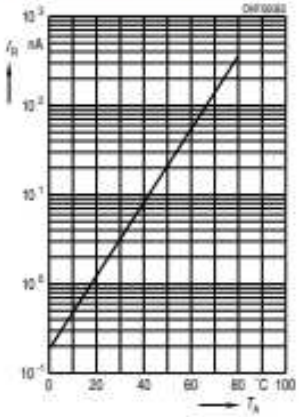

Directional Characteristics
$S_{rel} = f(\varphi)$

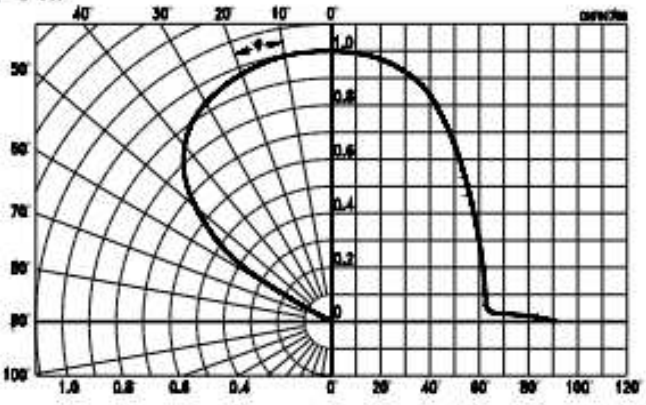

Maßzeichnung
Package Outlines

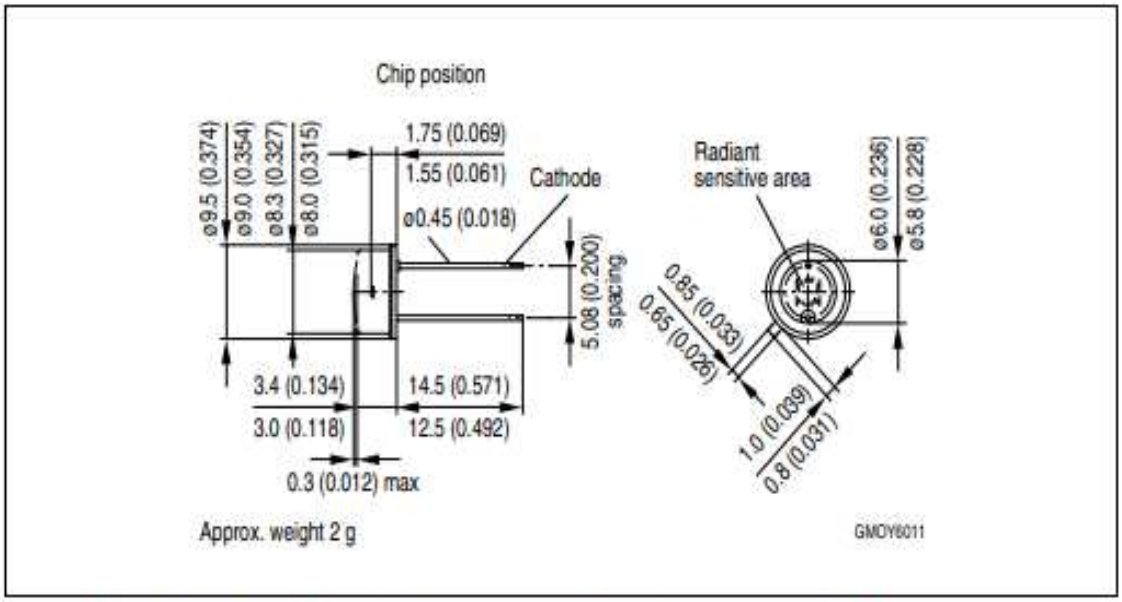

Maße werden wie folgt angegeben: mm (inch) / Dimensions are specified as follows: mm (inch).

Lötbedingungen
Soldering Conditions
Wellenlöten (TTW) (nach CECC 00802)
TTW Soldering (acc. to CECC 00802)

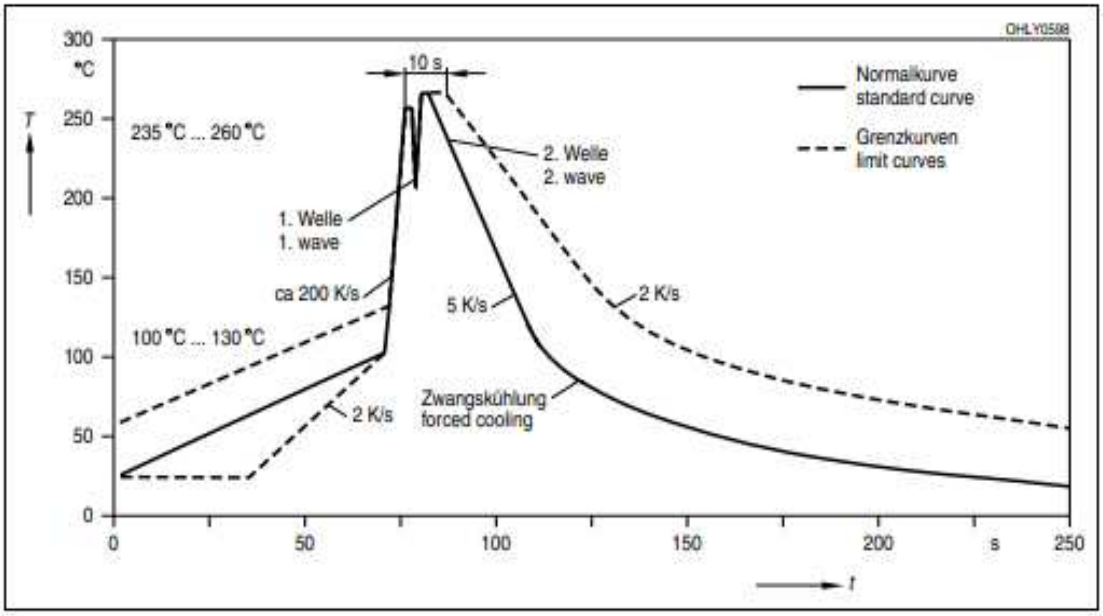

Published by
OSRAM Opto Semiconductors GmbH
Wernerwerkstrasse 2, D-93049 Regensburg
www.osram-os.com

The information describes the type of component and shall not be considered as assured characteristics.
Terms of delivery and rights to change design reserved. Due to technical requirements components may contain dangerous substances. For information on the types in question please contact our Sales Organization.

Packing

Please use the recycling operators known to you. We can also help you – get in touch with your nearest sales office. By agreement we will take packing material back, if it is sorted. You must bear the costs of transport. For packing material that is returned to us unsorted or which we are not obliged to accept, we shall have to invoice you for any costs incurred.

Components used in life-support devices or systems must be expressly authorized for such purpose! Critical components [1] , may only be used in life-support devices or systems [2] with the express written approval of OSRAM OS.

[1] A critical component is a component usedin a life-support device or system whose failure can reasonably be expected to cause the failure of that life-support device or system, or to affect its safety or effectiveness of that device or system.

[2] Life support devices or systems are intended (a) to be implanted in the human body, or (b) to support and/or maintain and sustain human life. If they fail, it is reasonable to assume that the health of the user may be endangered.

Appendix A4: PPA Up-converter Simulation Set-up.

```
DIM
    RES  OH
    CAP  PF
    COND  /OH
    ANG  DEG
    FREQ  MHZ
    TIME  MS
    VOL  V
    CUR  UA
    IND  NH
    LNG  MM
    TEMP  C
CKT
RES 3 1 ID="R3" R=6.5
CAP 1 2 ID="C1" C=20
VCCS 4 0 3 0 ID="U1" M=0.62 A=0 R1=0 R2=0 F=1 T=0
ACVSN 4 0 ID="V2" Mag=0.001414 Ang=0 F=1 Tone=2 NHarm=0 &
    NSamp=1 Offset=0 DCVal=0.001414
PINDiodeRC_AP 0 3 ID="D3" SCRIPT={""} B=3 BV=30 CJ=72 &
    CPACK=0 FC=0.5 IBV=0.0001 IF=0.1 IKF=6e-005 IKNEE=2000 &
    IS=3.5e-005 LBOND=0 M=0.45 MODEL_LEVEL=2 N=1.01 &
    REPI=0 RF=0.65 RHO=100000 RLIM=0.6 RP=1e+015 &
    RS=0 TAU=2e-008 VJ=0.552 W=0.006 WD=1e-007 TEMP=28
PORT 2 P=1 Z=50
PORT_SRC 1 P=2 Z=50 Signal=0 SpecType=1 SpecBW=0 Sweep=0 &
    Tone=1 Hint=0 NSamp=1 Freq=432.92 Pwr=15 Ang=0
DEF0P "PPAPINDiode"
```

```
$Visual System Simulator
$Version 8.04r build 4268 Rev1 (60469)
$Aplac netlist file
$Schematic Name: PPAPINDiode
#load     "C:\\Program     Files\\AWR\\AWR2008\\models\\ele_defs.dll"
type=awrmodel
Prepare
+ ADDDCPATH TAUDC=1e+008
+  ERR=0.001  ABS_ERR=1e-012  U=1  RMIN=1e-005  RMAX=1e+011  GMRES_M=100
ZEROPIVOT=1e-020
+              FNOM=0              TEMP=298.15              TNOM=298.15
VERSIONOPTION="tran0sourceonlyintrandc"

$*************** SUBCIRCUITS *****************
DefModel awr_subckt_1 2 1 2 PARAM 7 Mag Ang Offset DCVal ACMag ACAng
TRAN_F  GLOBAL_PARAM 1 AWR_SWP_INDX
Gyrator G1 1 2 3 0
Curr   J_TR   3   0   SIN=[0,Mag,TRAN_F,0,0,Ang*180/PI]   OFFSET=Offset
DC=DCVal NO_SS
Curr J_HB 3 0 TONE=[0,1] (Mag'Ang*180/PI-90) AC=(ACMag'ACAng*180/PI)
OFFSET=Offset NO_TRAN
EndModel
DefModel awr_subckt_2 1 1 PARAM 1 Z  GLOBAL_PARAM 1 AWR_SWP_INDX
Res R1 1 0 1 Z=Z NOISELESS
EndModel
DefModel awr_subckt_3 1 1 PARAM 4 Z TRAN_F PWR_INDX ANG_INDX
Gyrator G1 1 0 2 0
VECTOR Pwr0 0.502973
VECTOR Ang0 0
```

```
Curr                    J_TR                    2                    0
SIN=[0,Sqrt(Z)*Pwr0[PWR_INDX],TRAN_F,0,0,Ang0[ANG_INDX]*57.2958]
Res Y 2 0 1 Y=Z NOISELESS
EndModel
$*************** END SUBCIRCUITS *****************
Res RES!R3 6 2 6.5 TEMP=290
Cap CAP!C1 3 5 2e-011
LinearModel VCCS!U1 4 1 0 6 0
+ PARAM 6 T=0 M=0.62 A=0 R1=0 R2=0 F=1000000
awr_subckt_1 ACVSN!V2 1 0 Mag=0.001414 Ang=0 Offset=0 DCVal=0.001414
ACMag=0.001414 ACAng=0 TRAN_F=1000000
Cap CAP!X1 2 3 1e-005
Ind IND!X1_U1 4 2 0.001
Volt DCVS!V1 4 0 DC=0
PINDiodeRC D3 0 6 TEMP=301.15 WD=1e-007 B=3 BV=30 CJ=7.2e-011 CPACK=0
FC=0.5 IBV=1e-010 IF=1e-007 IKF=6e-011
+ IKNEE=0.002 IS=3.5e-011 LBOND=0 M=0.45 MODEL_LEVEL=2 N=1.01 REPI=0
RF=0.65 RHO=100000 RLIM=0.6
+ RP=1e+015 RS=0 TAU=2e-011 VJ=0.552 W=6e-006
awr_subckt_2 PORT!PORT_1 5 Z=(50, 0)
awr_subckt_3 PORT1_F!PORT_2 2 Z=(50, 0) TRAN_F=432920000 PWR_INDX=0
ANG_INDX=0
AWRSaveResults
+ VOLTAGES 6 1 2 3 4 5 6
+ CURRENTS 14 ACVSN!V2,1 ACVSN!V2,2 CAP!C1,1 CAP!X1,1 D3,1 DCVS!V1,1
DCVS!V1,2 IND!X1_U1,1 PORT!PORT_1,1 RES!R3,1
+ VCCS!U1,1 VCCS!U1,2 VCCS!U1,3 VCCS!U1,4
+ DCOPS
Sweep "AWR_INTERNAL_SWEEP" DC
EndSweep
$Netlist End
```

Appendix A5: PPA Simulation Set-up, Gain versus Various Bias Voltages

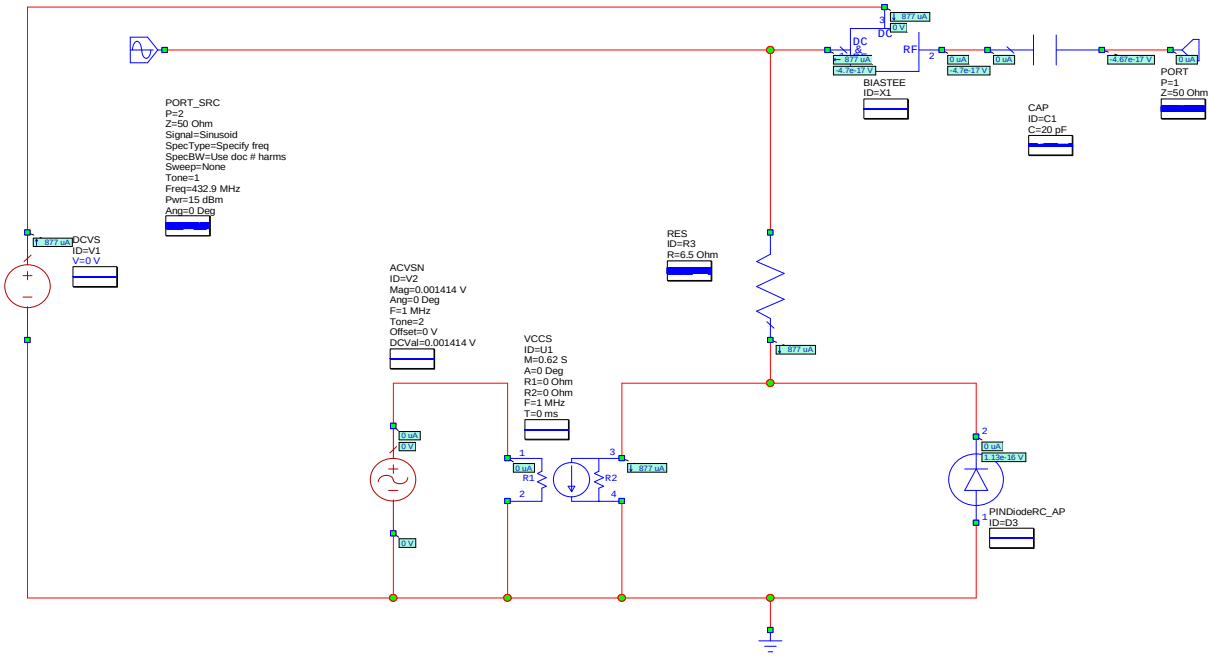


```
DIM
    RES  OH
    CAP  PF
    COND  /OH
    ANG  DEG
    FREQ  MHZ
    TIME  MS
    VOL  V
    CUR  UA
    IND  NH
    LNG  MM
    TEMP  C
CKT
RES 1 4 ID="R3" R=6.5
CAP 5 6 ID="C1" C=20
VCCS 2 0 1 0 ID="U1" M=0.62 A=0 R1=0 R2=0 F=1 T=0
ACVSN 2 0 ID="V2" Mag=0.001414 Ang=0 F=1 Tone=2 NHarm=0 &
    NSamp=1 Offset=0 DCVal=0.001414
BIASTEE 4 5 7 ID="X1"
DCVS 7 0 ID="V1" V\0
PINDiodeRC_AP 0 1 ID="D3" SCRIPT={""} B=3 BV=30 CJ=72 &
    CPACK=0 FC=0.5 IBV=0.0001 IF=0.1 IKF=6e-005 IKNEE=2000 &
    IS=3.5e-005 LBOND=0 M=0.45 MODEL_LEVEL=2 N=1.01 &
    REPI=0 RF=0.65 RHO=100000 RLIM=0.6 RP=1e+015 &
    RS=0 TAU=2e-008 VJ=0.552 W=0.006 WD=1e-007 TEMP=28
PORT 6 P=1 Z=50
PORT_SRC 4 P=2 Z=50 Signal=0 SpecType=1 SpecBW=0 Sweep=0 &
    Tone=1 Hint=0 NSamp=1 Freq=432.92 Pwr=15 Ang=0
DEF0P "PPAPINDiode"
```

```
$Visual System Simulator
```

```
$Version 8.04r build 4268 Rev1 (60469)
$Aplac netlist file
$Schematic Name: PPAPINDiode
#load "C:\\Program Files\\AWR\\AWR2008\\models\\ele_defs.dll"
type=awrmodel
Prepare
+ ADDDCPATH TAUDC=1e+008
+ ERR=0.001 ABS_ERR=1e-012 U=1 RMIN=1e-005 RMAX=1e+011 GMRES_M=100
ZEROPIVOT=1e-020
+ FNOM=0 TEMP=298.15 TNOM=298.15
VERSIONOPTION="tran0sourceonlyintrandc"
$*************** SUBCIRCUITS *****************
DefModel awr_subckt_1 2 1 2 PARAM 7 Mag Ang Offset DCVal ACMag ACAng
TRAN_F  GLOBAL_PARAM 1 AWR_SWP_INDX
Gyrator G1 1 2 3 0
Curr J_TR 3 0 SIN=[0,Mag,TRAN_F,0,0,Ang*180/PI] OFFSET=Offset
DC=DCVal NO_SS
Curr J_HB 3 0 TONE=[0,1] (Mag'Ang*180/PI-90) AC=(ACMag'ACAng*180/PI)
OFFSET=Offset NO_TRAN
EndModel
DefModel awr_subckt_2 1 1 PARAM 1 Z  GLOBAL_PARAM 1 AWR_SWP_INDX
Res R1 1 0 1 Z=Z NOISELESS
EndModel
DefModel awr_subckt_3 1 1 PARAM 4 Z TRAN_F PWR_INDX ANG_INDX
Gyrator G1 1 0 2 0
VECTOR Pwr0 0.502973
VECTOR Ang0 0
Curr J_TR 2 0
SIN=[0,Sqrt(Z)*Pwr0[PWR_INDX],TRAN_F,0,0,Ang0[ANG_INDX]*57.2958]
Res Y 2 0 1 Y=Z NOISELESS
EndModel
$*************** END SUBCIRCUITS *****************
Res RES!R3 6 2 6.5 TEMP=290
Cap CAP!C1 3 5 2e-011
LinearModel VCCS!U1 4 1 0 6 0
+ PARAM 6 T=0 M=0.62 A=0 R1=0 R2=0 F=1000000
awr_subckt_1 ACVSN!V2 1 0 Mag=0.001414 Ang=0 Offset=0 DCVal=0.001414
ACMag=0.001414 ACAng=0 TRAN_F=1000000
Cap CAP!X1 2 3 1e-005
Ind IND!X1_U1 4 2 0.001
Volt DCVS!V1 4 0 DC=0
PINDiodeRC D3 0 6 TEMP=301.15 WD=1e-007 B=3 BV=30 CJ=7.2e-011 CPACK=0
FC=0.5 IBV=1e-010 IF=1e-007 IKF=6e-011
+ IKNEE=0.002 IS=3.5e-011 LBOND=0 M=0.45 MODEL_LEVEL=2 N=1.01 REPI=0
RF=0.65 RHO=100000 RLIM=0.6
+ RP=1e+015 RS=0 TAU=2e-011 VJ=0.552 W=6e-006
awr_subckt_2 PORT!PORT_1 5 Z=(50, 0)
awr_subckt_3 PORT1_F!PORT_2 2 Z=(50, 0) TRAN_F=432920000 PWR_INDX=0
ANG_INDX=0
AWRSaveResults
+ VOLTAGES 6 1 2 3 4 5 6
+ CURRENTS 14 ACVSN!V2,1 ACVSN!V2,2 CAP!C1,1 CAP!X1,1 D3,1 DCVS!V1,1
DCVS!V1,2 IND!X1_U1,1 PORT!PORT_1,1 RES!R3,1
+ VCCS!U1,1 VCCS!U1,2 VCCS!U1,3 VCCS!U1,4
+ DCOPS
Sweep "AWR_INTERNAL_SWEEP" DC
EndSweep
```

Appendix A6: Curve Fitting

Gain ratio=(10^(normalized gain/20).

M	Fs power=64.22	Gain	Normalized Gain	Gain (ratio)
0	64.22	0	0	0
0.1	64.22	11.07	-13.61	0.208689
0.2	64.22	16.99	-7.69	0.412572
0.3	64.22	20.42	-4.26	0.61235
0.4	64.22	22.86	-1.82	0.810961
0.5	64.22	24.68	0	1
0.6	64.22	26.17	1.49	1.187135
0.7	64.22	27.43	2.75	1.372461
0.8	64.22	28.5	3.82	1.552387
0.9	64.22	29.44	4.76	1.729816
1	64.22	30.3	5.62	1.909853
1.1	64.22	31.02	6.34	2.074914
1.2	64.22	31.7	7.02	2.243882
1.3	64.22	32.31	7.63	2.407133
1.4	64.22	32.87	8.19	2.567438
1.5	64.22	33.38	8.7	2.722701
1.6	64.22	33.85	9.17	2.874088
1.7	64.22	34.29	9.61	3.023431
1.8	64.22	34.69	10.01	3.16592
1.9	64.22	35.06	10.38	3.303695
2	64.22	35.34	10.66	3.411929

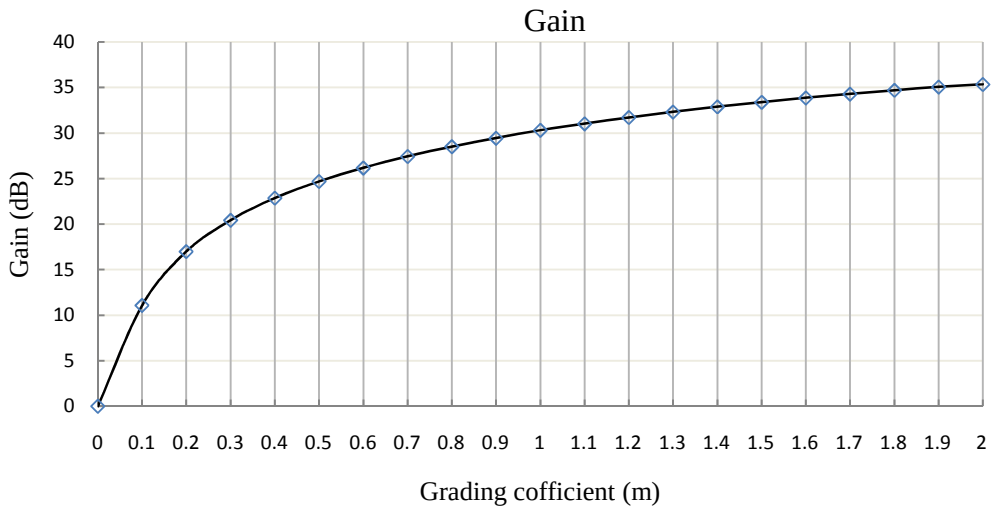

Gain Ratios at Various Grading Coefficient (m).

User-Selectable Polynomial

Coefficients

$y = a + bm + cm^2 + dm^3 + fm^4 + gm^5 + hm^6 + im^7$

Fitting target of sum of squared absolute error = 4.3253595042810687E-05
a = 3.8960985344577240E-04
b = 2.0600857376433175E+00
c = 2.5114593468130109E-01
d = -1.6286359450344763E+00
f = 2.6430596291788806E+00
g = -2.1327106934817333E+00
h = 8.4350596012622681E-01
i = -1.3054686027100060E-01

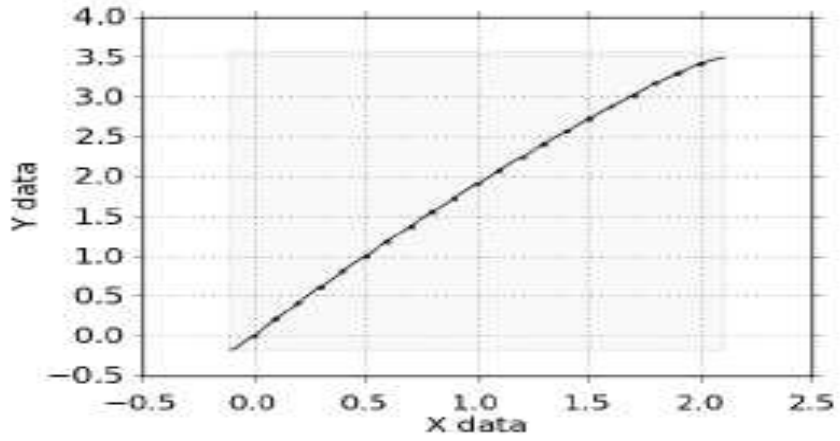

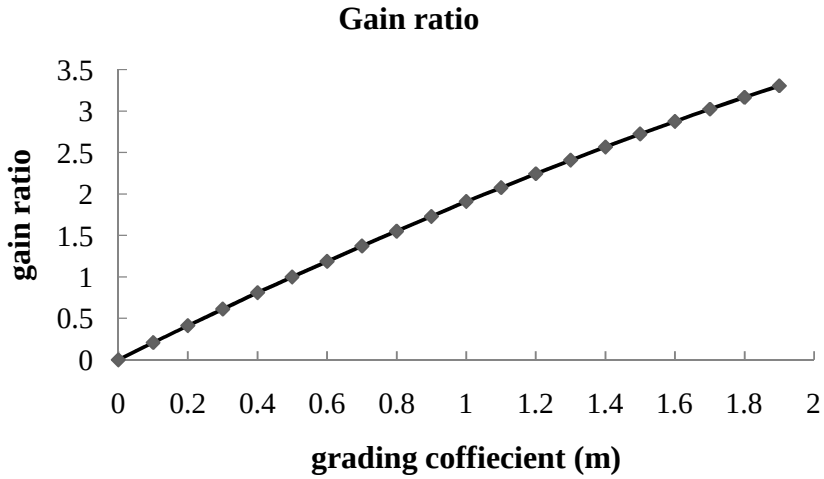

Normalized gain=Gian-(gain at m=0.5)= Gain-24.68

Appendix A7: DCHPPA Simulation Set-up

```
DIM
    RES  OH
    CAP  PF
    COND  /OH
    ANG  DEG
    FREQ  MHZ
    TIME  MS
    VOL  V
    CUR  UA
    IND  NH
    LNG  MM
    TEMP  C

CKT
RES 8 17 ID="R3" R=6.5
CAP 17 18 ID="C1" C=20
VCCS 7 0 8 0 ID="U1" M=0.62 A=0 R1=0 R2=0 F=1 T=0
ACVSN 7 0 ID="V2" Mag=0.001414 Ang=0 F=1 Tone=2 NHarm=0 &
    NSamp=1 Offset=0 DCVal=0.001414
PINDiodeRC_AP 0 8 ID="D3" SCRIPT={""} B=3 BV=30 CJ=72 &
    CPACK=0 FC=0.5 IBV=0.0001 IF=0.1 IKF=6e-005 IKNEE=2000 &
    IS=3.5e-005 LBOND=0 M=0.45 MODEL_LEVEL=2 N=1.01 &
    REPI=0 RF=0.65 RHO=100000 RLIM=0.6 RP=1e+015 &
    RS=0 TAU=2e-008 VJ=0.552 W=0.006 WD=1e-007 TEMP=28
SPLIT2 19 17 6 ID="P1" L21=3 L31=3 Z0=50
BPFB 18 15 ID="BPFB1" N=3 FP1=433.72 FP2=434.12 AP=4 &
    RS=50 RL=50 QU=7000
SDIODE 12 1 ID="SDiode1" IS=2.2e-005 JSW=0 MULT=1 AFAC=1 &
    PJFAC=0 RS=16 N=1 TT=0 CJ0=0.13 CJP=0 VJ=0.5 &
    PHP=0.8 M=0.5 MJSW=0.33 FC=0.5 FCS=0.5 BV=5 IBV=0 &
    IKF=0 IKR=0 EG=1.11 XTI=3 TEXT=26.85 T=27 KF=0 &
    AF=1 FFE=1 KB=0 AB=1 FB=1 NFLAG=1 DCAP=0 TLEV=0 &
    TLEVC=0 CTA=0 CTP=0 GAP1=0.000702 GAP2=1108 TCV=0 &
    TM1=0 TM2=0 TPB=0 TPHP=0 TRS=0 TTT1=0 TTT2=0 &
    IMAX=1e+006 COMPAT=1 TRS2=0 TGS=0 TGS2=0 CD=0 &
    TWONLBRANCHES=0 TWORESISTORS=0
SDIODE 3 2 ID="SDiode3" IS=2.2e-005 JSW=0 MULT=1 AFAC=1 &
    PJFAC=0 RS=16 N=1 TT=0 CJ0=0.13 CJP=0 VJ=0.5 &
    PHP=0.8 M=0.5 MJSW=0.33 FC=0.5 FCS=0.5 BV=5 IBV=0 &
    IKF=0 IKR=0 EG=1.11 XTI=3 TEXT=26.85 T=27 KF=0 &
    AF=1 FFE=1 KB=0 AB=1 FB=1 NFLAG=1 DCAP=0 TLEV=0 &
    TLEVC=0 CTA=0 CTP=0 GAP1=0.000702 GAP2=1108 TCV=0 &
    TM1=0 TM2=0 TPB=0 TPHP=0 TRS=0 TTT1=0 TTT2=0 &
    IMAX=1e+006 COMPAT=1 TRS2=0 TGS=0 TGS2=0 CD=0 &
    TWONLBRANCHES=0 TWORESISTORS=0
SDIODE 2 12 ID="SDiode4" IS=2.2e-005 JSW=0 MULT=1 AFAC=1 &
    PJFAC=0 RS=16 N=1 TT=0 CJ0=0.13 CJP=0 VJ=0.5 &
    PHP=0.8 M=0.5 MJSW=0.33 FC=0.5 FCS=0.5 BV=5 IBV=0 &
    IKF=0 IKR=0 EG=1.11 XTI=3 TEXT=26.85 T=27 KF=0 &
    AF=1 FFE=1 KB=0 AB=1 FB=1 NFLAG=1 DCAP=0 TLEV=0 &
    TLEVC=0 CTA=0 CTP=0 GAP1=0.000702 GAP2=1108 TCV=0 &
    TM1=0 TM2=0 TPB=0 TPHP=0 TRS=0 TTT1=0 TTT2=0 &
    IMAX=1e+006 COMPAT=1 TRS2=0 TGS=0 TGS2=0 CD=0 &
    TWONLBRANCHES=0 TWORESISTORS=0
SDIODE 1 3 ID="Sdiode2" IS=2.2e-005 JSW=0 MULT=1 AFAC=1 &
```

```
    PJFAC=0 RS=16 N=1 TT=0 CJ0=0.13 CJP=0 VJ=0.5 &
    PHP=0.8 M=0.5 MJSW=0.33 FC=0.5 FCS=0.5 BV=5 IBV=0 &
    IKF=0 IKR=0 EG=1.11 XTI=3 TEXT=26.85 T=27 KF=0 &
    AF=1 FFE=1 KB=0 AB=1 FB=1 NFLAG=1 DCAP=0 TLEV=0 &
    TLEVC=0 CTA=0 CTP=0 GAP1=0.000702 GAP2=1108 TCV=0 &
    TM1=0 TM2=0 TPB=0 TPHP=0 TRS=0 TTT1=0 TTT2=0 &
    IMAX=1e+006 COMPAT=1 TRS2=0 TGS=0 TGS2=0 CD=0 &
    TWONLBRANCHES=0 TWORESISTORS=0
XFMRTAP 0 14 12 13 3 ID="XF1" N1=1 N2=1
XFMRTAP 6 0 1 0 2 ID="XF2" N1=1 N2=1
CAP 0 13 ID="C2" C=78
CAP 0 5 ID="C3" C=245
CAP 0 16 ID="C4" C=78
IND 13 5 ID="L1" L=515
IND 5 16 ID="L2" L=515
BPFB 15 14 ID="BPFB2" N=3 FP1=433.72 FP2=434.12 AP=4 &
    RS=50 RL=50 QU=7000
PORT_SRC 19 P=2 Z=50 Signal=0 SpecType=1 SpecBW=0 Sweep=0 &
    Tone=1 Hint=0 NSamp=1 Freq=432.92 Pwr=18 Ang=0
PORT 16 P=1 Z=50
DEF0P "DCHPPA"
```

```
$Visual System Simulator
$Version 8.04r build 4268 Rev1 (60469)
$Aplac netlist file
$Schematic Name: DCHPPA
#load "C:\\Program Files\\AWR\\AWR2008\\models\\FilterMod.dll"
type=awrmodel
#load "C:\\Program Files\\AWR\\AWR2008\\models\\ele_defs.dll"
type=awrmodel
Prepare
+ ADDDCPATH TAUDC=1e+008
+ ERR=0.001 ABS_ERR=1e-012 U=1 RMIN=1e-005 RMAX=1e+011 GMRES_M=100
ZEROPIVOT=1e-020
+ TONE 2 9 BOX_AND_DIAMOND="1,1" HB_SAMPLING_METHOD=ONEDIM HB_MODE=1
HBSPECTRUMREL=0.001 INEXACT_NEWTON=1
+ FNOM=0 TEMP=298.15 TNOM=298.15
VERSIONOPTION="tran0sourceonlyintrandc;maxadm=1e6"

$*************** SUBCIRCUITS *****************
DefModel awr_subckt_1 2 1 2 PARAM 7 Mag Ang Offset DCVal ACMag ACAng
TRAN_F  GLOBAL_PARAM 1 AWR_SWP_INDX
Gyrator G1 1 2 3 0
Curr J_TR 3 0 SIN=[0,Mag,TRAN_F,0,0,Ang*180/PI] OFFSET=Offset
DC=DCVal NO_SS
Curr J_HB 3 0 TONE=[0,1] (Mag'Ang*180/PI-90) AC=(ACMag'ACAng*180/PI)
OFFSET=Offset NO_TRAN
EndModel
DefModel awr_subckt_2 2 1 2 GLOBAL_PARAM 1 AWR_SWP_INDX
Res RC 1 3 16 M=1
Res RB 3 4 0 M=1 TEMP=300.15 RESMODE=2
Diode DB 4 2 IS=2.2510844504e-011 N=1 TEMP=300.15 TNOM=300.15 NO_TEMP
+ EG=0 XTI=0 IKF=0 NBV=1 IBV=2.2510844504e-011
+ BV=5 CAPMOD=0 TT=0 CJO=1.3005413914e-013 M=0.5
+ VJ=0.49961354511 FC=0.5 KF=0 AF=1 MULT=1
Res RSW 3 5 0 M=0 TEMP=300.15 RESMODE=2
Diode DSW 5 2 IS=0 N=1 TEMP=300.15 TNOM=300.15 NO_TEMP
+ EG=0 XTI=0 IKF=0 NBV=1 IBV=0
```

```
+ BV=5 CAPMOD=0 TT=0 CJO=0 M=0.33
+ VJ=0.79976354511 FC=0.5 KF=0 AF=1 MULT=1
EndModel
DefModel awr_subckt_3 1 1 PARAM 4 Z TRAN_F PWR_INDX ANG_INDX
Gyrator G1 1 0 2 0
VECTOR Pwr0 0.710469
VECTOR Ang0 0
Curr J_TR 2 0
SIN=[0,Sqrt(Z)*Pwr0[PWR_INDX],TRAN_F,0,0,Ang0[ANG_INDX]*57.2958]
Res Y 2 0 1 Y=Z NOISELESS
EndModel
DefModel awr_subckt_4 1 1 PARAM 1 Z  GLOBAL_PARAM 1 AWR_SWP_INDX
Res R1 1 0 1 Z=Z NOISELESS
EndModel
$*************** END SUBCIRCUITS *****************
Res RES!R3 9 5 6.5 TEMP=290
Cap CAP!C1 5 2 2e-011
LinearModel VCCS!U1 4 1 0 9 0
+ PARAM 6 T=0 M=0.62 A=0 R1=0 R2=0 F=1000000
awr_subckt_1 ACVSN!V2 1 0 Mag=0.001414 Ang=0 Offset=0 DCVal=0.001414
ACMag=0.001414 ACAng=0 TRAN_F=1000000
PINDiodeRC D3 0 9 TEMP=301.15 WD=1e-007 B=3 BV=30 CJ=7.2e-011 CPACK=0
FC=0.5 IBV=1e-010 IF=1e-007 IKF=6e-011
+ IKNEE=0.002 IS=3.5e-011 LBOND=0 M=0.45 MODEL_LEVEL=2 N=1.01 REPI=0
RF=0.65 RHO=100000 RLIM=0.6
+ RP=1e+015 RS=0 TAU=2e-011 VJ=0.552 W=6e-006
LinearModel SPLIT2!P1 3 10 5 15
+ PARAM 3 Z0=50 L21=3 L31=3
LinearModel BPFB!BPFB1 2 2 3
+ PARAM 7 QU=7000 N=3 FP1=433720000 FP2=434120000 AP=4 RS=50 RL=50
awr_subckt_2 SDIODE!SDiode1 11 12
awr_subckt_2 SDIODE!SDiode3 13 14
awr_subckt_2 SDIODE!SDiode4 14 11
awr_subckt_2 SDIODE!Sdiode2 12 13
LinearModel XFMRTAP!XF1 5 0 4 11 6 13
+ PARAM 2 N2=1 N1=1
LinearModel XFMRTAP!XF2 5 15 0 12 0 14
+ PARAM 2 N2=1 N1=1
Cap CAP!C2 0 6 7.8e-011
Cap CAP!C3 0 7 2.45e-010
Cap CAP!C4 0 8 7.8e-011
Ind IND!L1 6 7 5.15e-007
Ind IND!L2 7 8 5.15e-007
LinearModel BPFB!BPFB2 2 3 4
+ PARAM 7 QU=7000 N=3 FP1=433720000 FP2=434120000 AP=4 RS=50 RL=50
awr_subckt_3 PORT1_F!PORT_2 10 Z=(50, 0) TRAN_F=432920000 PWR_INDX=0
ANG_INDX=0
awr_subckt_4 PORT!PORT_1 8 Z=(50, 0)
AWRSaveResults
+ VOLTAGES 15 1 2 3 4 5 6 7 8 9 10
+ 11 12 13 14 15
+ CURRENTS 38 ACVSN!V2,1 ACVSN!V2,2 BPFB!BPFB1,1 BPFB!BPFB2,1
CAP!C1,1 CAP!C2,1 CAP!C3,1 CAP!C4,1 D3,1 IND!L1,1
+ IND!L2,1 PORT!PORT_1,1 RES!R3,1 SDIODE!SDiode1,1 SDIODE!SDiode1,2
SDIODE!SDiode3,1 SDIODE!SDiode3,2 SDIODE!SDiode4,1 SDIODE!SDiode4,2
SDIODE!Sdiode2,1
+ SDIODE!Sdiode2,2 SPLIT2!P1,1 SPLIT2!P1,2 SPLIT2!P1,3 VCCS!U1,1
VCCS!U1,2 VCCS!U1,3 VCCS!U1,4 XFMRTAP!XF1,1 XFMRTAP!XF1,2
```

```
+ XFMRTAP!XF1,3 XFMRTAP!XF1,4 XFMRTAP!XF1,5 XFMRTAP!XF2,1
XFMRTAP!XF2,2 XFMRTAP!XF2,3 XFMRTAP!XF2,4 XFMRTAP!XF2,5
Sweep "AWR_INTERNAL_SWEEP"
+ HB FC=[4.3292e+008,1e+006]
EndSweep

$Netlist End
```

Appendix A8: Advanced DCHPPA Set-up

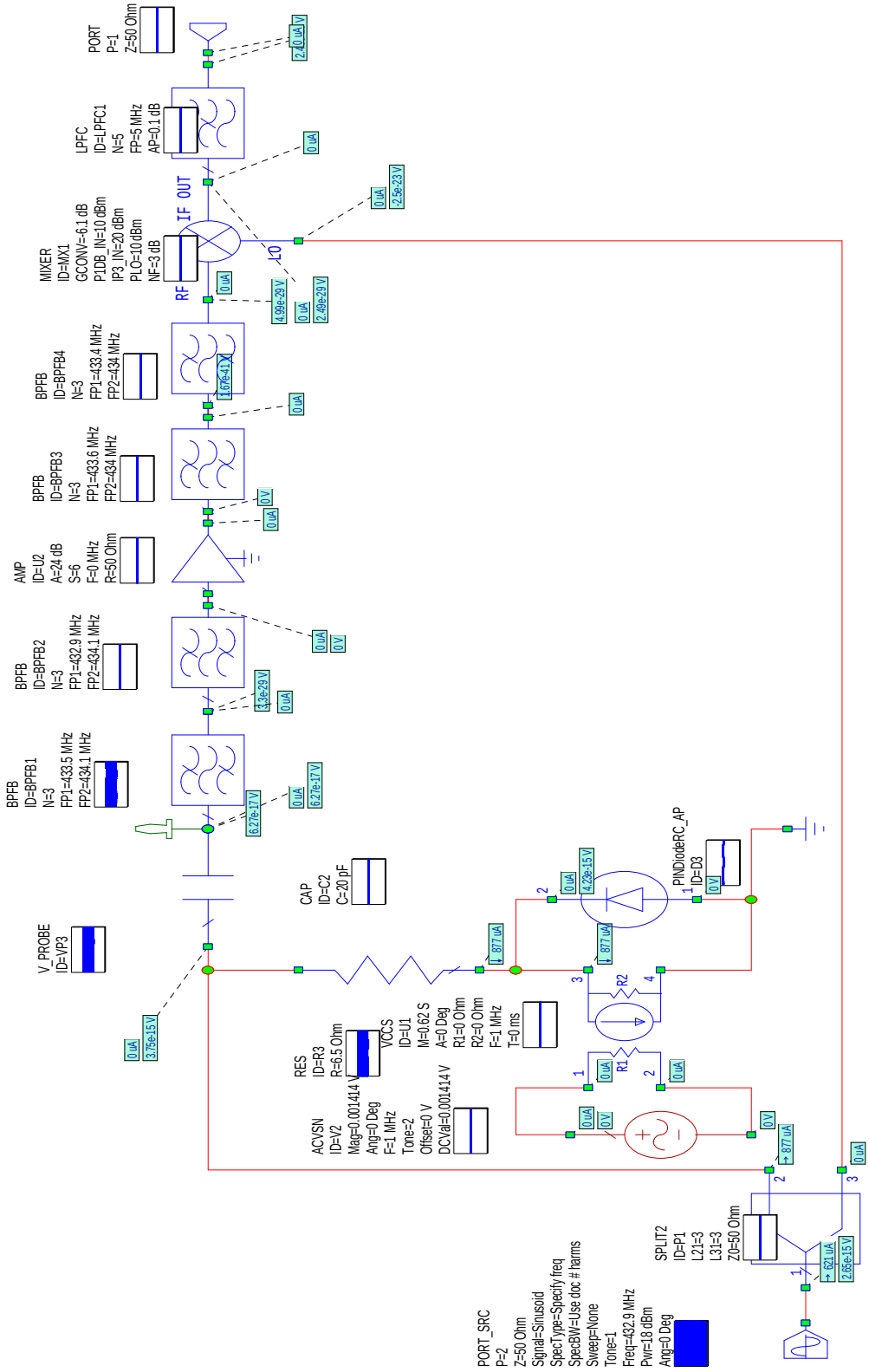

Appendix B

Appendix B1: PPA Up-converter Circuit

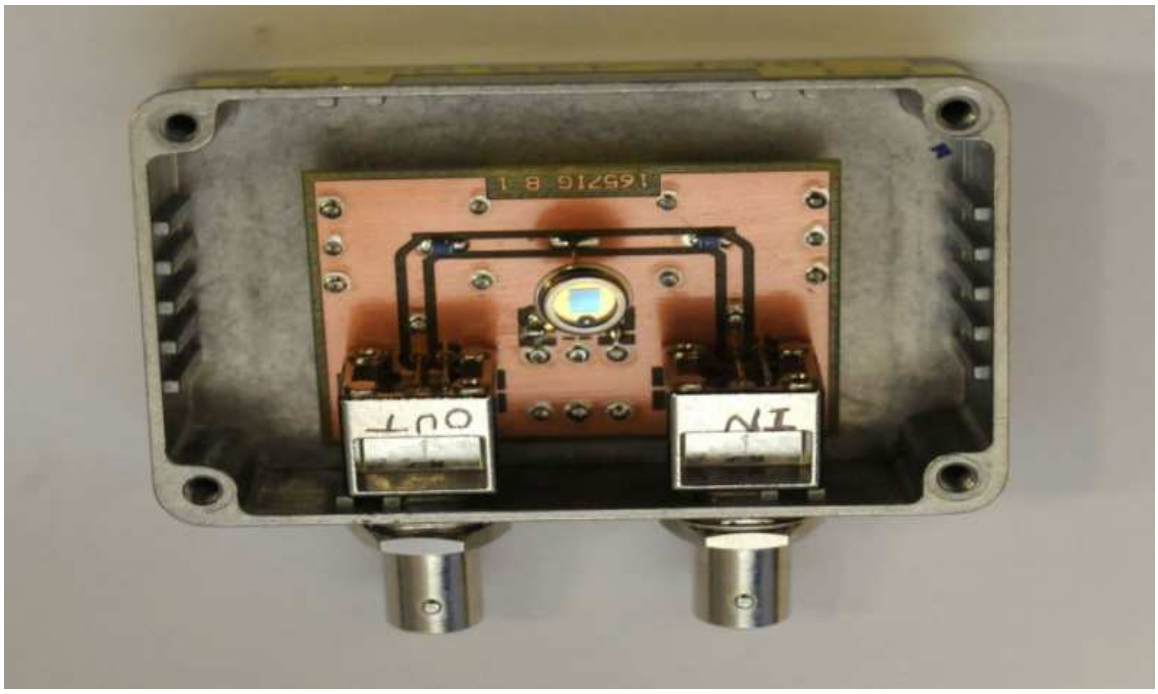

PPA PCB Circuit 1/2 (photodiode detector with tune circuits)

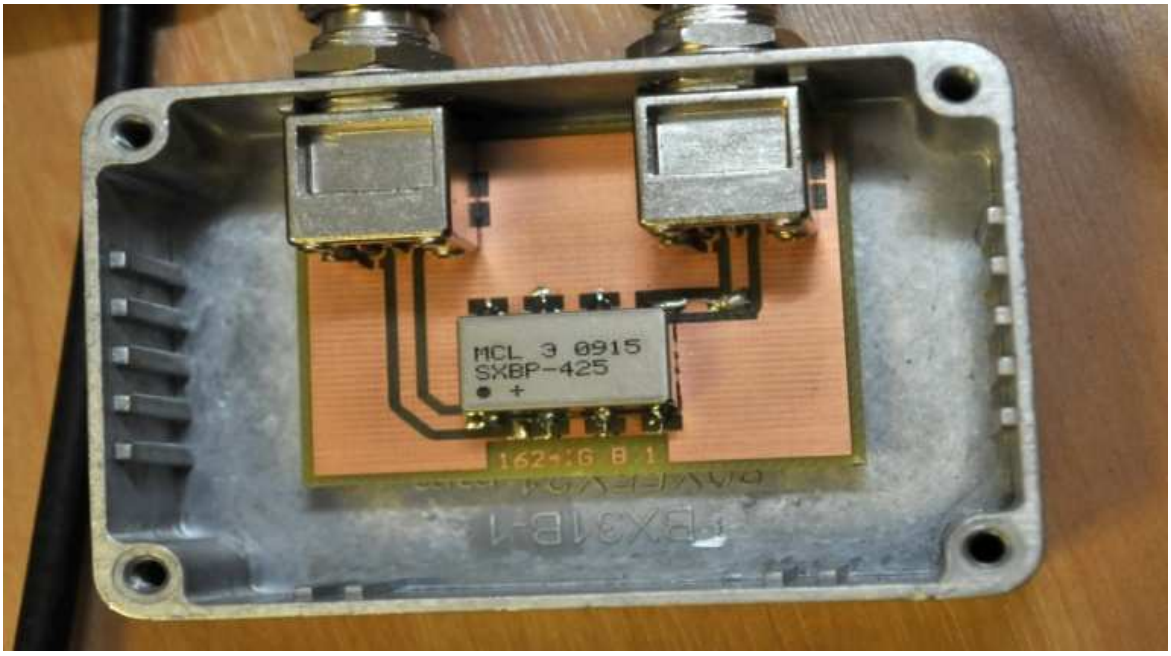

PPA PCB Circuit 2/2 (Band-pass filter, LC-SXBP-425MHz BPF)

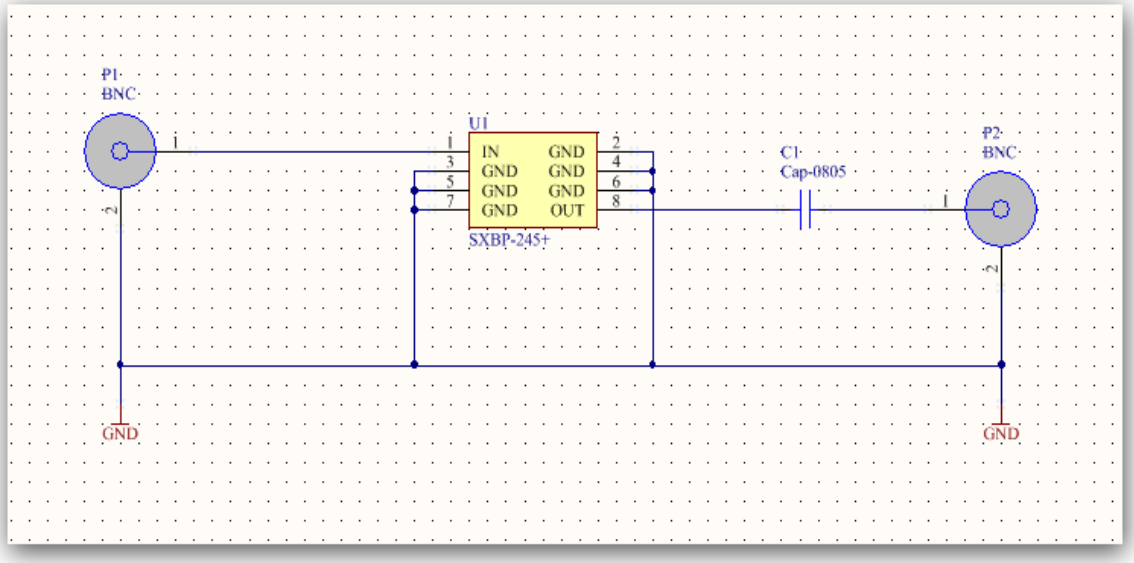

PPA PCB circuit 2/2 (Schematic Band-Pass filter, LC-SXBP-425MHz BPF)

Appendix B2: LED Drive Circuit

LED Drive Circuit

Appendix B3: DCHPPA Experiment Setup

DCHPPA Experiment Set-up

Appendix B4: PPA Up-converter Gain for Various Bias Voltages

Biasing Voltage	UHF Up-converter Gain	VHF Up-converter Gain
0	25.1	19.9
-0.5	21.1	16.1
-1	19.9	14.6
-1.5	16	11.9
-2	13.9	11
-2.5	11.1	8.7
-3	8.9	6.8
-3.5	5.9	4
-4	4.5	3.2
-4.5	3.5	2.1
-5	2.5	0.9

Appendix B5: PPA Circuit with RF Transformers Impedance

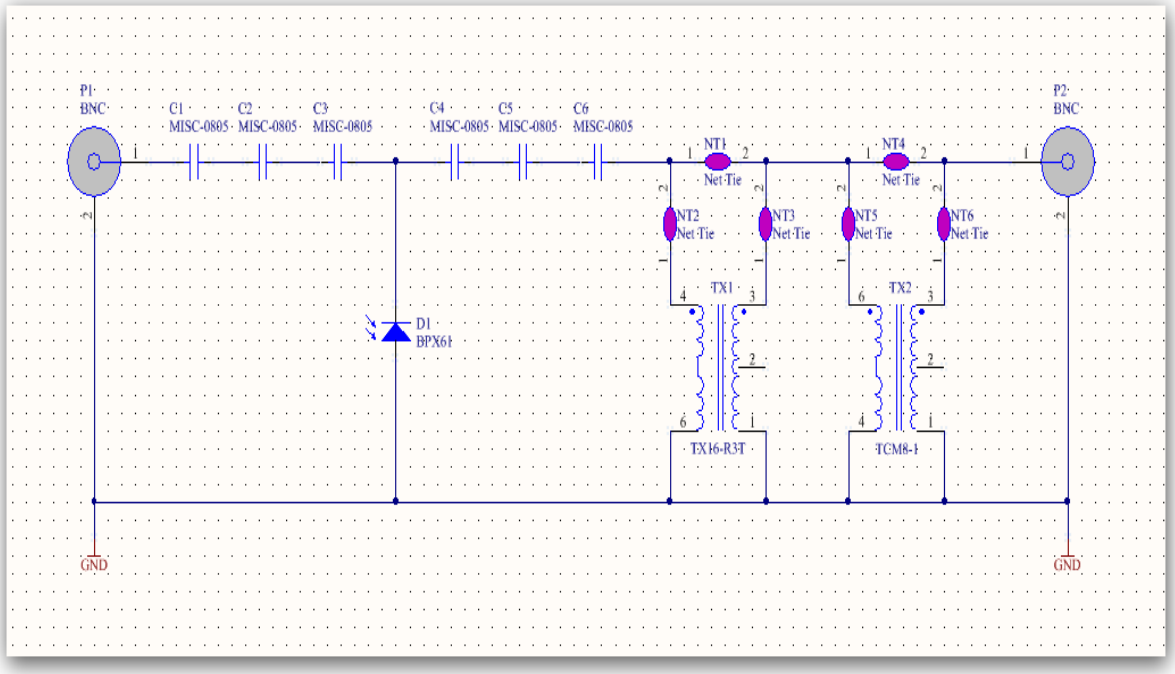

PPA Circuit with RF Transformers Impedance (i.e. TX16, TCM8)

Appendix B6: PPA Up-converter Gain for Various Pump Power

Pump Power dBm	UHF Up-converter Gain	VHF Up-converter Gain
27	26.1	
26	26.3	
25	26.6	
24	26	
23	25.2	
22	25.1	20
21	23.7	20.2
20	22.69	20.3
19	21.69	19.5
18	20.69	18.3
17	19.75	17.2
16	18.79	16.3
15	17.69	15.3
14	16.59	14.2
13	15.59	13.3
12	14.39	12.2
11	13.49	11.2
10	12.39	10.3
9	11.39	9.3
8	10.39	8.2
7	9.39	7.3
6	8.39	6.2
5	7.29	5.3
4	6.28	4.2
3	5.29	3.3
2	4.29	2.3
1	3.29	1.2
0	2.2	0.2
-1	1	-0.8
-2	0	-1.8
-3	-1.1	-2.7
-4	-2.2	-3.7

Appendix B7: Crystal filter FN-3809WS

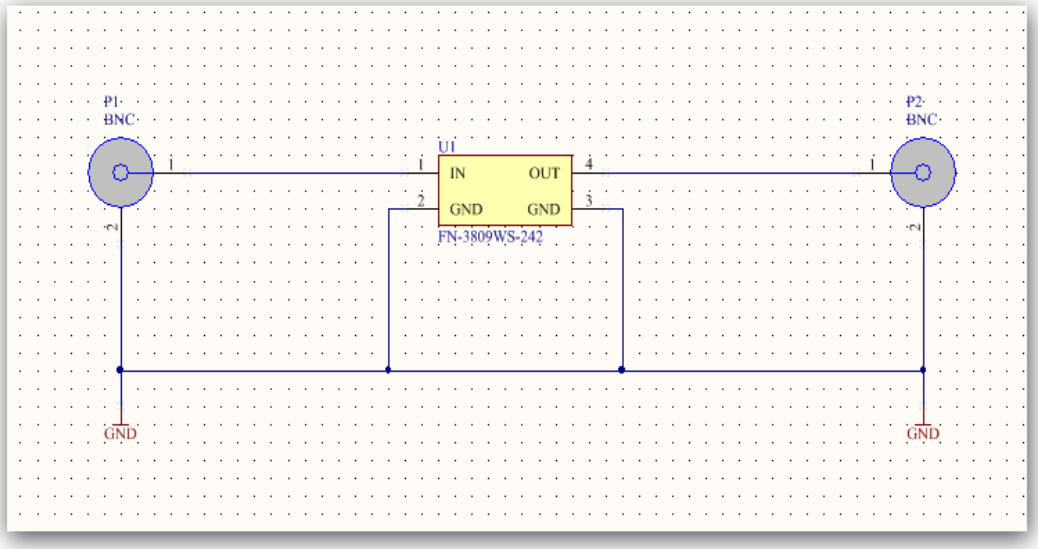

Crystal filter FN-3809WS (242MHz)

Appendix B8: SAW Band Pass Filter (B3760)

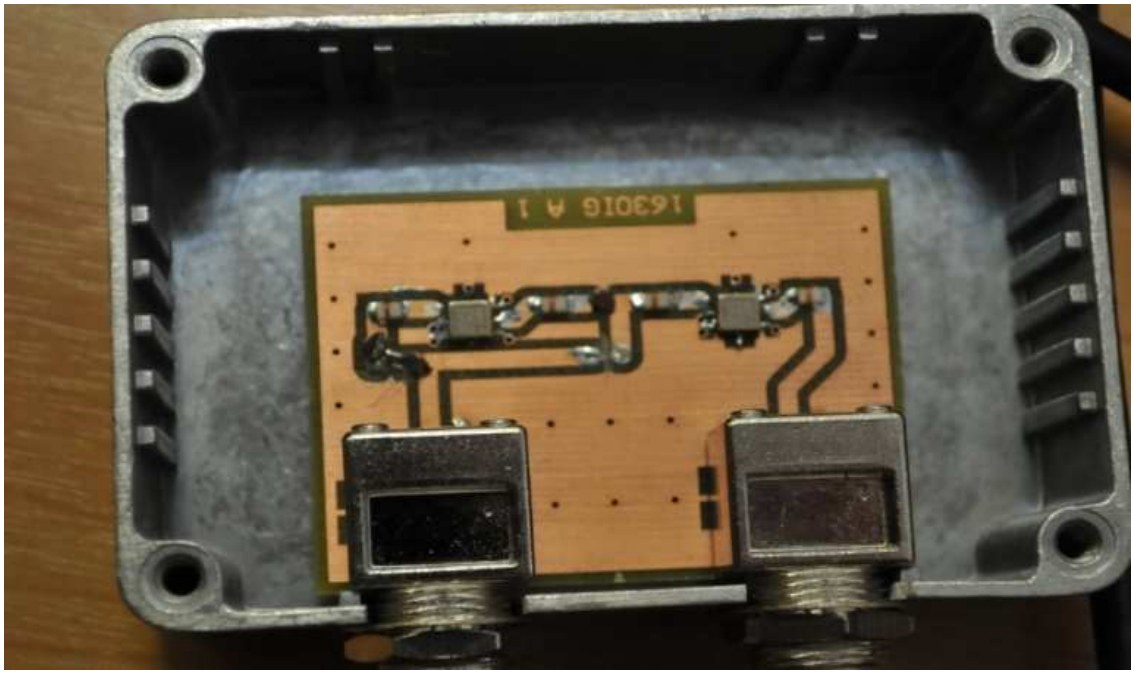

SAW-B3760 433.92Mhz BPF (cascade)

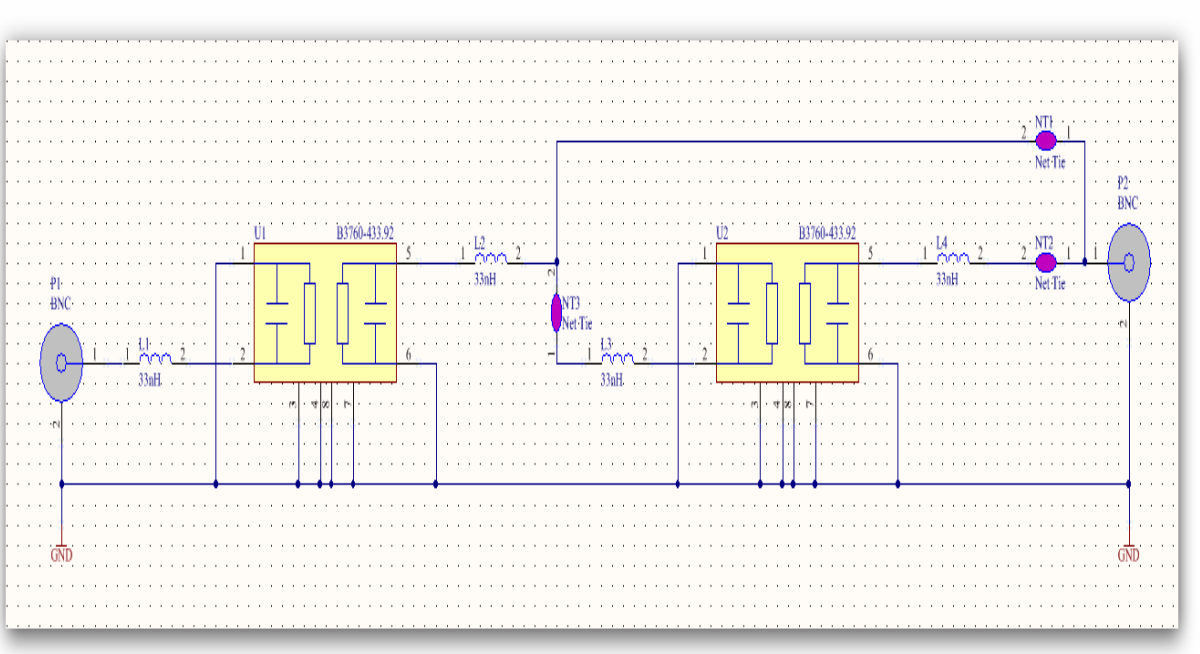

SAW-B3760 BPF 433.92MHz

Appendix B9: IF Amplifier

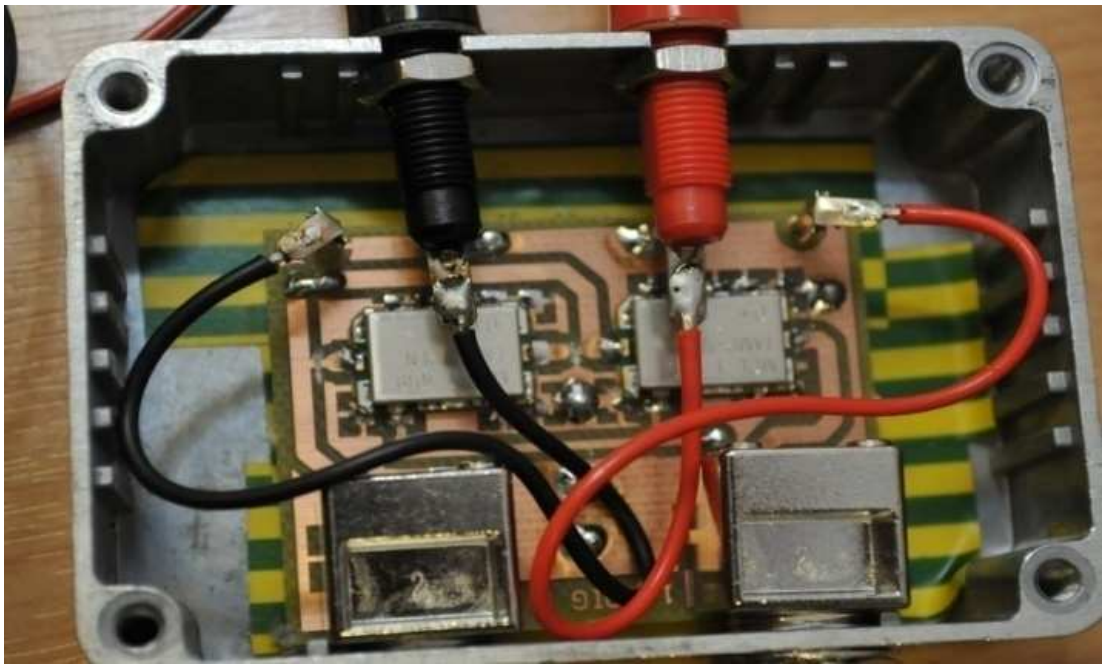

TAMP-72 LN Amplifiers

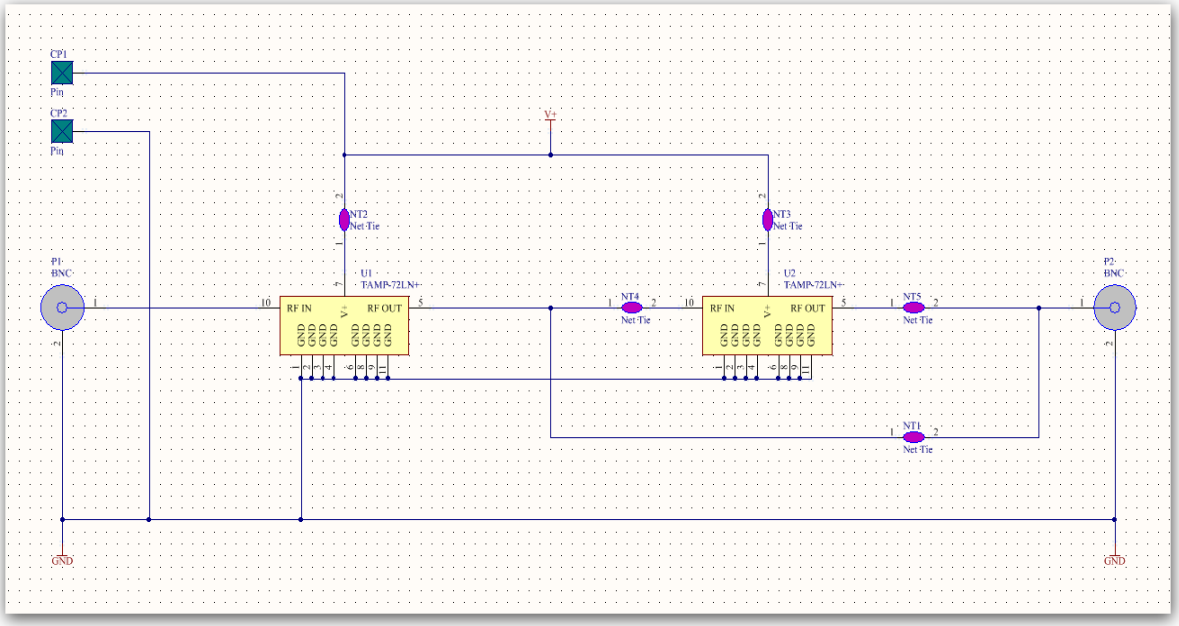

TAMP-72 LN Schematic Amplifier circuit

Appendix B10: SAW Band Pass Filter (B3790)

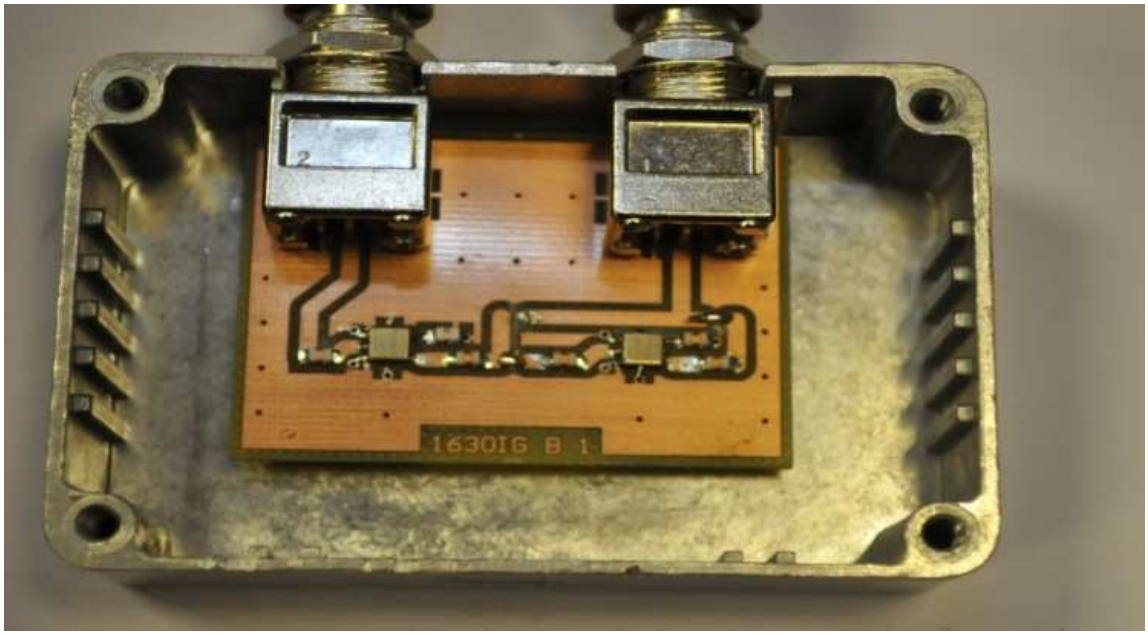

SAW-B3790 BPF 433.92MHz (Cascade)

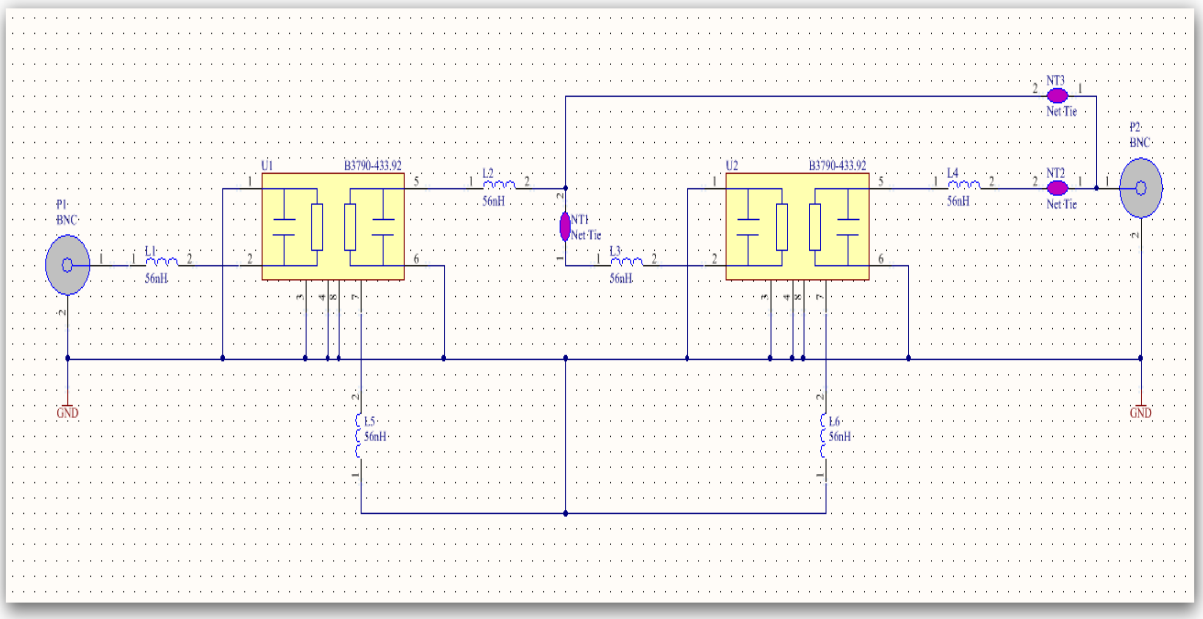

SAW-B3790 BPF 433.92MHz (Cascade)

Appendix B11: Active DB Mixer

Active DB Mixer

Appendix B12: Gain Chain DCHHPA Receiver

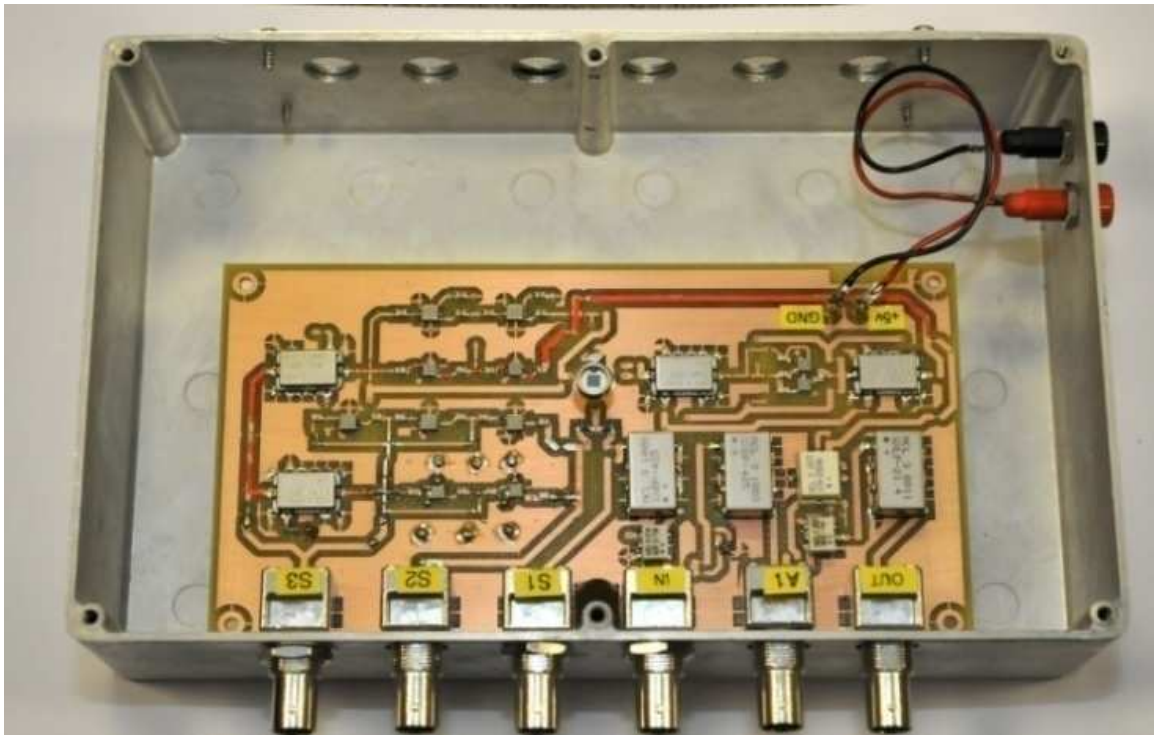

Gain chain DCHHPA receiver

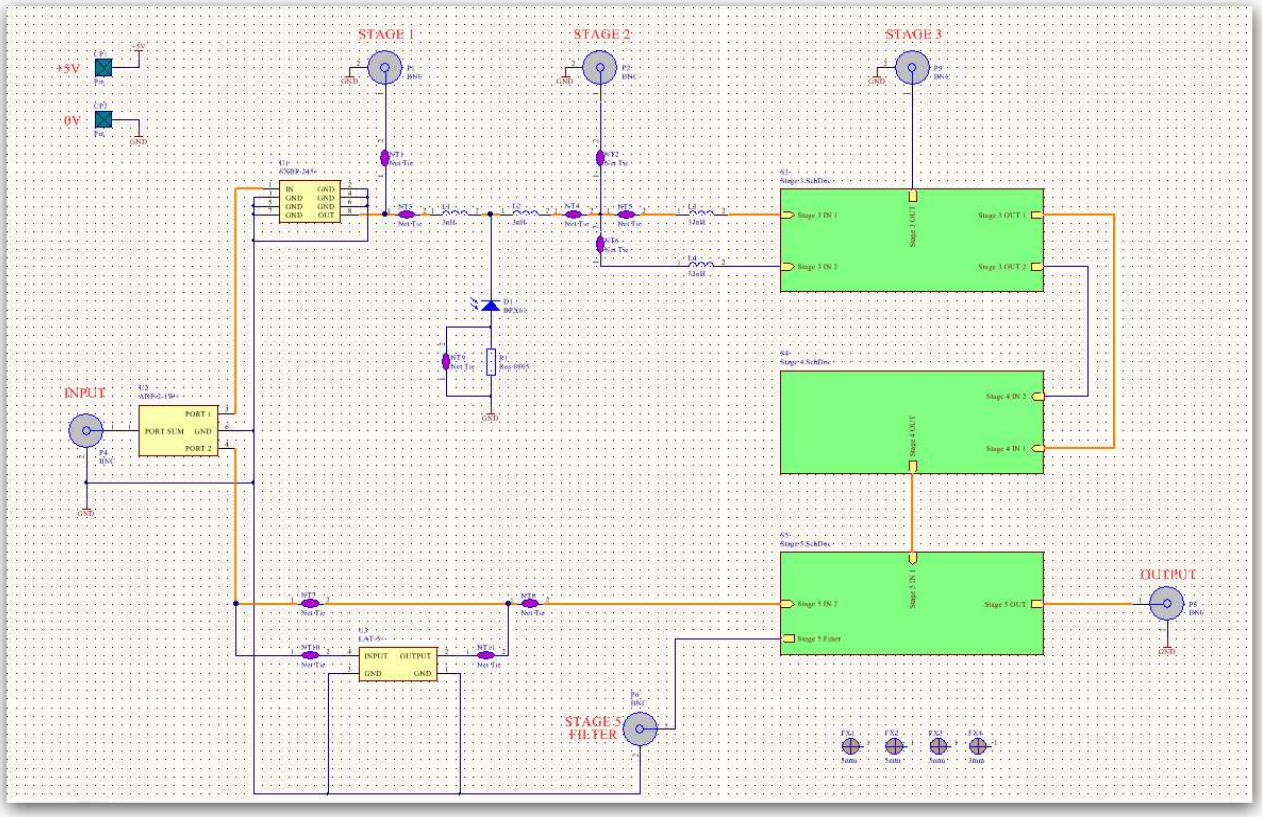

Gain Chain DHCPPA Complete Schematic Circuit

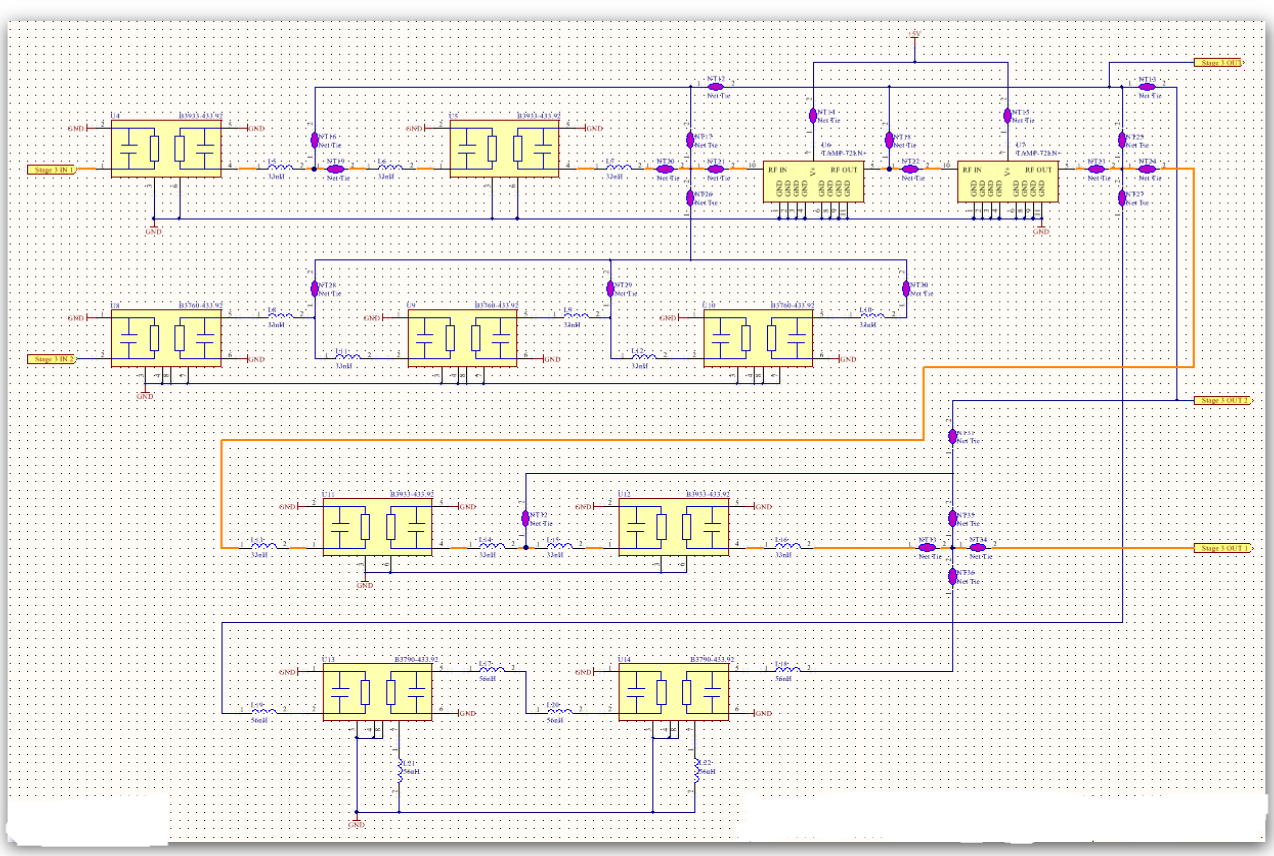

Gain Chain DHCPPA Subcircuit-1

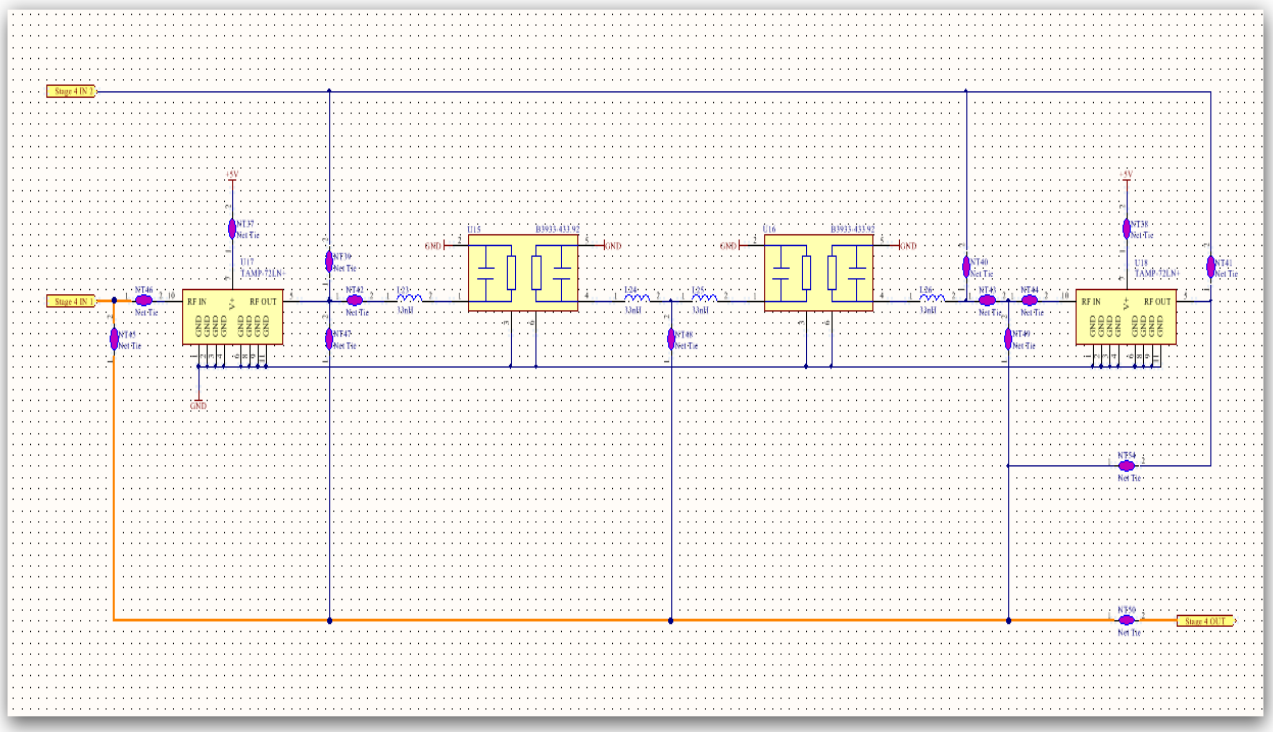

Gain Chain DHCPPA Subcircuit-2

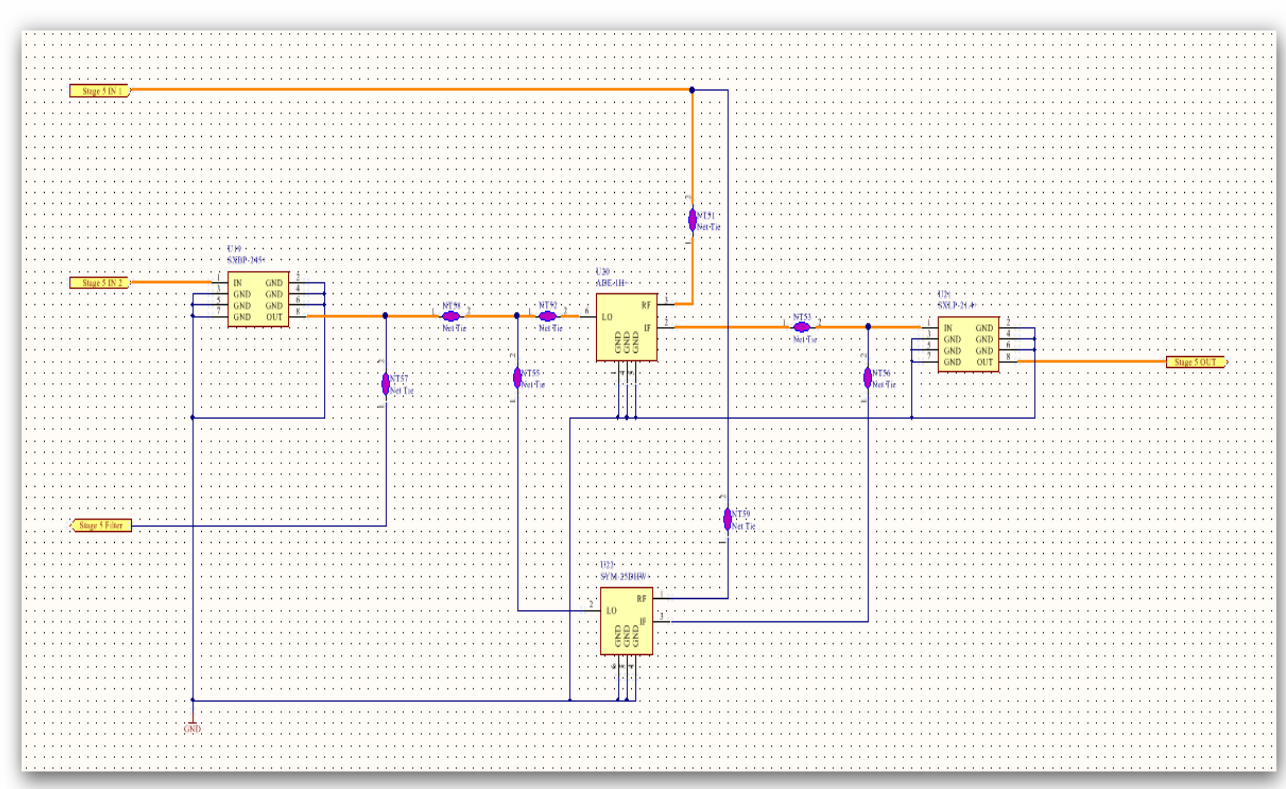

Gain Chain DHCPPA Subcircuit-3